# BROWNING AND WATERCORE DISORDERS IN ‘FUJI’ APPLES EXPLORED BY MEANS OF X-RAY COMPUTED TOMOGRAPHY (CT)

By

**Kenias Chigwaya**

*Dissertation presented for the degree of Doctor of Philosophy in the Faculty of AgriSciences (Department of Horticultural Science) at Stellenbosch University*

Supervisor: Dr EM Crouch

Co-supervisor: Dr IJ Crouch

December 2020

## DECLARATION

By submitting this dissertation electronically, I declare that the entirety of the work contained therein is my own, original work, that I am the sole author thereof (save to the extent explicitly otherwise stated) that reproduction and publication thereof by Stellenbosch University will not infringe any third party rights and that I have not previously in its entirety or in part submitted it for obtaining any qualification.

Date: December 2020

## SUMMARY

The Fuji apple cultivar occupies 9% of land under apple production in South Africa. To ensure all year-round fruit availability, 'Fuji' apples are stored for extended durations. However, 'Fuji' apples are prone to internal browning (IB) during storage. IB is characterized by patches of brown flesh in the apple tissue, which makes fruit unmarketable and causes financial losses. Browning symptoms that have been identified in apple cultivars include radial browning, diffuse browning, combination browning, $CO_2$ damage and core-flush. Techniques such as X-ray computed tomography (CT) that can evaluate IB disorders non-destructively are important. This study aimed to explore IB types and watercore in 'Fuji' apples quantitatively and qualitatively using X-ray CT.

Exposure of fruit to high $CO_2$ conditions for 3 days after harvest at 21 °C induced IB in the core region of fruit. The construction of porosity maps for intact fruit enabled characterization of tissue structure before and after disorder development. Porosity distribution of 'Fuji' was higher in the cortex region compared to the core region. High-resolution X-ray CT scans performed on IB affected and unaffected fruit tissue showed differences in microstructural properties such as porosity, pore size distribution and pore connectivity. Fruit size had a significant effect on the susceptibility of 'Fuji' apples to $CO_2$ stress-induced IB. Radial porosity profiles did not differ significantly between fruit that developed IB and fruit that did not develop IB. However, porosity along the axial profile was generally higher for fruit that did not develop IB, particularly in the region between the calyx end and the core region. This was the first X-ray CT study carried out on South African 'Fuji' apples to evaluate how fruit microstructural properties relate to the IB types identified under different storage conditions.

A further study was done to determine microstructural properties of watercore affected fruit tissue and the effects on storability of 'Fuji' apples. X-ray CT scans showed that fruit tissue with watercore had a significantly low porosity and connectivity of pores. This may have a

negative impact on respiratory gas diffusion in the fruit and could increase susceptibility to IB during storage. Furthermore, watercore affected tissue had significantly smaller cells due to plasmolysis.

For long-term storage experiments, it was found that regular atmosphere (RA) stored fruit had a significantly higher incidence of core-flush compared to fruit from controlled atmosphere (CA) and delayed controlled atmosphere (delayed CA) storage. Although CA and delayed CA were effective in reducing core-flush incidence, they both resulted in a significantly higher incidence of radial browning. Fruit with $CO_2$ damage and cavities were also evaluated in this study. $CO_2$ damage was associated with cell damage and increased pore sphericity. All IB types evaluated resulted in an increased tissue porosity and altering of pore sphericity, anisotropy and pore size distribution. IB after short-term exposure to $CO_2$ stress occurred only in the core region while IB types observed after long-term storage occurred in all fruit tissue regions. This study provided unique insights into the microstructural properties of different IB types occurring in ‘Fuji’ apples.

## OPSOMMING

Die appel kultivar Fuji beslaan 9% van die area onder appelproduksie in Suid-Afrika. Om die beskikbaarheid van vrugte regdeur die jaar te verseker, word 'Fuji' appels vir lang tydperke gestoor. 'Fuji'-appels is egter geneig tot interne verbruining (IV) tydens opberging. IV word gekenmerk deur areas van bruin vlees in die appelweefsel, maak vrugte onbemarkbaar en veroorsaak dus finansiële verliese.

Verbruiningstipes is geïdentifiseer in ander appelkultivars, naamlik radiale verbruining, diffuse verbruining, kombinasieverbruining, $CO_2$-skade en kernblos. Tegnieke soos X-straal-rekenaartomografie (CT) wat IV-afwykings nie vernietigend kan evalueer, is belangrik. Hierdie studie was daarop gemik om kwantitatief en kwalitatief IB-soorte en waterkern in 'Fuji'-appels te ondersoek met behulp van X-straal-CT.

Blootstelling aan vrugte aan hoë $CO_2$-vlakke gedurende 3 dae na oes by 21 °C, het IV in die kernweefsel van die vrug veroorsaak. Die opstel van porositeitskaarte vir ongeskonde vrugte, het karakterisering van weefselstruktuur moontlik gemaak voor en na die ontwikkeling van IV verbruining. Porositeitverdeling van 'Fuji' was hoër in die korteksstreek in vergelyking met die kernstreek. Hoë resolusie X-straal CT-skanderings wat op IV-aangetaste en onaangetaste vrugweefsel uitgevoer is, het verskille getoon in mikrostrukturele eienskappe soos porositeit, poriegrootteverdeling en porieverbinding. Vrugtegrootte het 'n beduidende uitwerking gehad op die vatbaarheid van 'Fuji' appels vir $CO_2$-stres geïnduseerde IV. Radiale porositeitsprofiele het nie beduidend verskil, tussen vrugte wat IV ontwikkel het en vrugte wat nie IV ontwikkel het nie. Porositeit langs die aksiale profiel was egter oor die algemeen hoër vir vrugte wat nie IV ontwikkel het nie, veral in die gebied tussen die kelkent en die kernweefsel. Dit is die eerste X-straal CT-studie wat op Suid-Afrikaanse 'Fuji'-appels uitgevoer is, met die doel om te evalueer hoe mikrostrukturele eienskappe van vrugte verband hou met die soorte IV wat onder verskillende bergingstoestande geïdentifiseer word.

‘n Verdere studie is gedoen om mikrostrukturele-eienskappe van waterkern voorkoms en berging van' Fuji 'appels te bepaal. X-straal CT-skanderings het getoon dat vrugteweefsel met waterkern 'n beduidende laer porositeit en konneksie van porieë het. Dit mag 'n beduidende impak hê op die verspreiding van gaswisseling in die vrugte en mag dus die vatbaarheid vir IV tydens opberging verhoog. Verder het weefsel wat deur waterkern aangetas is, aansienlik kleiner selle gehad as gevolg van plasmolise.

Vir langtermyn-opbergingseksperimente is gevind dat gewone atmosfeer (GA) gestoorde vrugte 'n beduidende hoër voorkoms van kernblos het in vergelyking met vrugte uit beheerde atmosfeer (BA) en vertraagde beheerde atmosfeer (vertraagde BA) opberging. Alhoewel BA en vertraagde BA effektief was om kernblos voorkoms te verminder, het albei gelei tot 'n aansienlike hoër voorkoms van radiale verbruining. Vrugte met $CO_2$-skade en holtes is ook in hierdie studie geëvalueer. $CO_2$-skade was geassosieer met selbeskadiging en verhoogde porie-sferisiteit. Al die IV-soorte wat geëvalueer is, het gelei tot 'n verhoogde weefselporeusheid en die verandering van porie-sferisiteit, anisotropie en poriegrootteverdeling. IV na korttermynblootstelling aan $CO_2$-stres het slegs in die kernstreek voorgekom, terwyl IV-tipes waargeneem na langtermynopberging in alle vrugteweefselstreke voorgekom het. Hierdie studie het unieke insigte gelewer oor die mikrostrukturele-eienskappe van verskillende verbruiningstipes wat in 'Fuji'-appels voorkom.

## DEDICATION

This dissertation is dedicated to my late mother Chipiwa Chigwaya who unfortunately did not see me finish this PhD. You are forever in my heart.

## LIST OF PUBLICATIONS AND SUBMITTED MANUSCRIPTS

1. Chigwaya, K., Schoeman, L., Fourie, W.J., Crouch, I., Viljoen, D. and Crouch, E.M., 2018. 'Fuji' apple internal browning explored via X-ray computed tomography (CT). Acta Hortic. 1201, 309-316. https://doi.org/10.17660/ActaHortic.2018.1201.42.

2. Chigwaya, K., du Plessis, A., Viljoen, D.W., Crouch, I.J., Crouch, E.M., 2021. Use of X-ray computed tomography and 3D image analysis to characterize internal browning in 'Fuji' apples after exposure to $CO_2$ stress. Sci. Hortic. 277, 1–10. https://doi.org/10.1016/j.scienta.2020.109840.

3. Chigwaya, K., Karuppanapandian, T., Schoeman, L., Viljoen, D.W., Crouch, I.J., Nugraha, B., Verboven, P., Nicolaï, B.M., Crouch, E.M. X-ray CT and porosity mapping to determine the effect of 'Fuji' apple morphological and microstructural properties on the incidence of $CO_2$ induced internal browning. Submitted in August 2020. Postharvest Biology & Technology.

## ACKNOWLEDGEMENTS

I would like to acknowledge the following organisations and individuals for their different roles in my PhD study:

The Stellenbosch University Department of Horticultural Sciences and HORTGRO Science for funding this study.

Dr Elke Crouch, my supervisor, for her guidance and advice throughout my PhD. Your unique leadership and wisdom helped to successfully complete my PhD. Thank you for believing in me and for giving me an opportunity to further my studies.

Dr Ian Crouch, my co-supervisor for always being there to assist whenever I needed help.

Dr Pieter Verboven and his MeBioS group (KU Leuven, Belgium) for their support and contribution during my stay in Belgium and for helping me understand the concepts of X-ray CT and image analysis.

Postdoctoral fellows at the Stellenbosch University Department of Horticultural Sciences (Dr Thirupathi Karuppanapandian and Dr Letitia Schoeman) for their help in reviewing my dissertation.

The staff at the Stellenbosch University CT scanner facility for assisting with my scanning work.

The staff at the Stellenbosch University Horticultural Sciences laboratory for help in carrying out fruit evaluations.

My work colleagues at ExperiCo (Agri-Research Solutions) for being welcoming when I joined them and for being a good and dependable family.

My colleagues in the PhD office for allowing me to share the challenges and difficulties of PhD life with them.

My close friends Tendai Mucheri and Tatenda Kawhena for their unconditional friendship and love.

Noxolo Sweetness Lukashe for the encouragement and for always being there for me.

My siblings, Caroline, Kudakwashe and Kudzaishe for their love and for cheering me up during my PhD and always. I love you guys.

My father, Pattison Chigwaya, for his love, encouragement and prayers. You have been there for me even through the toughest times. I love you Dad.

My whole extended family at large (Chigwaya and Tumbe families) for their love and prayers.

**This dissertation was finalised during a time that had difficulties brought about by the 2020 Coronavirus pandemic. I would like to thank the Almighty God for the gift of life and for allowing me to complete this PhD during such a time. Without Him, none of this would have been possible.**

**Psalms 37 vs 5 - Commit everything you do to the LORD. Trust Him, and He will help you.**

# TABLE OF CONTENTS

**NOTE:**

This dissertation was written according to the language and style required by the journal of Postharvest Biology and Technology. Each chapter represents an individual paper and some repetition between the chapters may occur.

# GENERAL INTRODUCTION AND OBJECTIVES

Fuji is one of the main apple cultivars globally and in South Africa. The popularity of 'Fuji' apples in South Africa and globally can be attributed to its distinctive juiciness, crispness and sweetness (Kweon et al., 2013). Fuji contributes 9% to the total area under apple production in South Africa and is the fifth most exported cultivar after Golden Delicious, Royal Gala, Granny Smith, and Cripps' Pink (HORTGRO, 2019). 'Fuji' apples have to be stored for extended durations to allow all year-round availability, which ensures off-season marketing. Controlled atmosphere (CA) storage is a commonly used storage technique for long-term fruit storage. CA storage utilizes an elevated $CO_2$ and low $O_2$ concentration to suppress fruit respiration and softening thereby increasing the storage life of the fruit (Volz et al., 1998; Gonzalez et al., 2001). 'Fuji' apples stored in CA sometimes develop internal browning (IB). IB is a physiological disorder characterized by brown patches with or without cavities that develop in the fruit flesh. Apples with IB have an aesthetically unpleasant internal appearance that is normally accompanied by off-flavors (Di Guardo et al., 2013). This drastically reduces the marketability and value of such fruit. Fuji is one of the apple cultivars that have IB problems during long-term storage (Argenta et al., 2000; Burke, 2010; Kweon et al., 2012; Chigwaya et al., 2018).

IB affects fruit quality and this causes significant financial losses as well as loss of international client confidence in the South African apple industry. It is important to investigate IB in 'Fuji' apples and to find solutions to mitigate the negative effects thereof. IB affects fruit microstructure and exploring IB incidence at a microstructural level can help shed more light on the different browning types and their causal as well as associated factors. Fruit microstructural features such as cells, intercellular spaces and cell walls can only be manifested in the micrometre and sub-micrometre ranges (Herremans, 2014). Techniques that can elucidate the microstructure of fruit are important in IB experiments because they help identify aeration and cell properties associated with IB incidence. Traditionally, imaging

methods such as light, electron and confocal microscopy are used to investigate fruit microstructure (Herremans et al., 2013). The problem with these methods is that they require destructive sampling, which means that samples cannot be studied in their natural states (Tanaka et al., 2018). Furthermore, sample preparation is required, and this is an arduous and time consuming exercise which is prone to a lot of errors and sample modification (Herremans et al., 2015). X-ray computed tomography (CT) is an innovative and non-destructive imaging technique that can be used in 3-dimensional (3D) imaging of fruit tissue at micrometre and nanometre resolutions (Schoeman et al., 2016). X-ray CT involves the use of absorption physics and reconstruction mathematics to produce 3D images of a scanned object (Bruyant, 2002). With X-ray CT, one is able to produce high quality images that show the arrangement of intercellular spaces and cells in the fruit tissue (Herremans et al., 2015). X-ray CT is useful in non-destructive fruit quality evaluations because it allows scanning of the same sample numerous times under different conditions (Schoeman et al., 2016). There is a need for more research on how IB affects the microstructure of ‘Fuji’ apples. While other studies have been done to determine how fruit microstructure is associated with IB of cultivars such as Braeburn (Herremans et al., 2013), such studies have not been comprehensively carried out for Fuji IB. The current study focused on the use of X-ray CT to evaluate IB disorders in ‘Fuji’ with the aim of unpacking how microstructural properties are related to the expression of the different IB types.

To fully encompass all aspects of this study, two literature reviews were carried out. The first literature review chapter focused on X-ray CT and its applicability to fruit microstructure evaluation. This review evaluated the basic principles of X-ray CT, followed by an overview of image processing as well as quantitative and qualitative image analysis. The applications of X-ray CT in fruit microstructure evaluations and modelling were also reviewed. In addition, the review assessed the advantages and limitations of using X-ray CT in fruit microstructure evaluation. The second literature review chapter focused on pre- and post-harvest factors that influence IB incidence in apples. Enzymatic processes as well as the role of fruit tissue porosity

during post-harvest storage were also reviewed. The two literature review chapters were followed by the first experimental chapter (Paper 1). The objective of this chapter was to compare microstructural properties of fruit tissue affected by $CO_2$ induced IB with unaffected fruit tissue, through the use of X-ray CT and 3D image analysis techniques. $CO_2$ is an important component of CA storage and this paper sought to elucidate how elevated levels of $CO_2$ may impact fruit tissue microstructure. Short-term exposure of 'Fuji' apples to induce and simulate browning disorders occurring during long-term CA storage has previously been explored by Argenta et al. (2002).

Gaseous exchange between apple fruit and their environment is important for physiological processes such as respiration which persist after harvest (Musse et al., 2010). Fruit tissue porosity is one of the factors affecting gaseous exchange and possibly IB incidence (Nugraha et al., 2019). Therefore, it is important to map the distribution of porosity within the entire fruit tissue and determine how this relates to IB incidence. The porosity of apple fruit generally increases in a radial direction from the core of the fruit towards the peel (Herremans et al., 2015). Low porosity and low pore connectivity regions within the fruit can restrict the movement of respiratory gases leading to the accumulation of $CO_2$, such regions may be at a higher risk of developing IB disorders during storage (Verboven et al., 2008; Ho et al., 2011; Nugraha et al., 2019). In addition to fruit tissue porosity, various microstructural and morphological properties may also affect the incidence of IB in 'Fuji' fruit. Thus, the objective of Paper 2 was to use X-ray CT and porosity mapping to determine the extent to which different morphological and microstructural properties influence the susceptibility of 'Fuji' apple to $CO_2$ induced IB. These properties included fruit size and density, radial and axial porosity profiles, and mean porosity.

The susceptibility of 'Fuji' apples to IB has also been found to be influenced by watercore incidence (Volz et al., 1998; Argenta et al., 2000). Watercore is characterized by water-soaked and glassy regions in some parts of the fruit tissue and is usually more apparent in over-mature apples (Herremans et al., 2014). Watercore affects the fruit microstructure through flooding of

the intercellular spaces with a sorbitol rich fluid. This has a negative impact on the fruit metabolism since intercellular spaces are important channels for facilitating gaseous exchange between the fruit and the storage environment (Argenta et al., 2002). Watercore in South African 'Fuji' apple has not been explored using X-ray CT as yet. Thus, Paper 3 was aimed at using X-ray CT to evaluate the watercore disorder in 'Fuji' apples. The specific objective of this chapter was to use X-ray CT and 3D image analysis to characterize microstructural properties of 'Fuji' fruit tissue affected by watercore and unaffected tissue.

Different types of browning are manifested during long-term storage of apples. Radial and diffuse browning have been identified in 'Cripps' Pink' apples, radial browning is a senescence related disorder which affects vascular tissue cells while diffuse browning is a result of the collapse of cortical cells (de Castro et al., 2007; James and Jobling, 2009). Core-flush is another type of browning that has been reported in different apple cultivars (Fan et al., 1999; Argenta et al., 2000). The causes of core-flush in apples have been attributed to senescent break down (Argenta et al., 2001) and chilling injury (Fan et al., 1999). $CO_2$ damage due to the elevated $CO_2$ concentration in CA storage is another common type of browning in apples (Lau, 1998). $CO_2$ damage is characterized by a brown discoloration that is sometimes accompanied by pits and cavities in the apple tissue (James and Jobling, 2009). To fully understand the different browning types in 'Fuji' apples, it is necessary to evaluate the fruit microstructure. Thus, Paper 4 aimed to use X-ray CT and 3D image analysis to quantify microstructural properties of different browning types that were observed after extended storage of 'Fuji' apples under different storage regimes.

**References**

Argenta, L., Fan, X., Mattheis, J., 2000. Delaying establishment of controlled atmosphere or $CO_2$ exposure reduces 'Fuji' apple $CO_2$ injury without excessive fruit quality loss. Postharvest Biol. Technol. 20, 221–229. https://doi.org/10.1016/S0925-5214(00)00134-4.

Argenta, L.C., Fan, X., Mattheis, J.P., 2001. Development of internal browning in 'Fuji' apples during storage, in: Washington Tree Fruit Postharvest Conference. Wenatchee, WA, pp. 1–4. http://ucce.ucdavis.edu/files/datastore/234-56.pdf.

Argenta, L., Fan, X., Mattheis, J., 2002. Impact of watercore on gas permeance and incidence of internal disorders in 'Fuji' apples. Postharvest Biol. Technol. 24, 113–122. https://doi.org/10.1016/S0925-5214(01)00137-5.

Bruyant, P.P., 2002. Analytic and iterative reconstruction algorithms in SPECT. J. Nucl. Med. 43, 1343–1358.

Burke, A., 2010. Quantifying flesh browning, polyphenoloxidase, total phenolic content and vitamin C in select apple varieties and progeny. PhD dissertation, Faculty of the Graduate School, Cornell University, United States of America.

Chigwaya, K., Schoeman, L., Fourie, W.J., Crouch, I., Viljoen, D. and Crouch, E.M., 2018. 'Fuji' apple internal browning explored via X-ray computed tomography (CT). Acta Hortic. 1201, 309-316. https://doi.org/10.17660/ActaHortic.2018.1201.42.

de Castro, E., Biasi, B., Mitcham, E., Tustin, S., Tanner, D., Jobling, J., 2007. Carbon dioxide-induced flesh browning in Pink Lady apples. Am. Soc. Hortic. 132, 713–719. https://doi.org/10.21273/JASHS.132.5.713.

Di Guardo, M., Tadiello, A., Farneti, B., Lorenz, G., Masuero, D., Vrhovsek, U., Costa, G., Velasco, R., Costa, F., 2013. A multidisciplinary approach providing new insight into fruit flesh browning physiology in apple (*Malus x domestica* Borkh.). PLoS One 8, e78004. https://doi.org/10.1371/journal.pone.0078004.

Fan, X., Mattheis, J.P., Blankenship, S., 1999. Development of apple superficial scald, soft scald, core flush, and greasiness is reduced by MCP. J. Agric. Food Chem. 47, 3063–3068. https://doi.org/10.1021/jf981176b.

Gonzalez, J.J., Valle, R.C., Bobroff, S., Biasi, W. V, Mitcham, E.J., McCarthy, M.J., 2001. Detection and monitoring of internal browning development in 'Fuji' apples using MRI. Postharvest Biol. Technol. 22, 179–188. https://doi.org/10.1016/S0925-5214(00)00183-6.

Herremans, E., Melado-Herreros, A., Defraeye, T., Verlinden, B., Hertog, M., Verboven, P., Val, J., Fernández-Valle, M.E., Bongaers, E., Estrade, P., Wevers, M., Barreiro, P., Nicolaï, B.M., 2014. Comparison of X-ray CT and MRI of watercore disorder of different apple cultivars. Postharvest Biol. Technol. 87, 42–50. https://doi.org/10.1016/j.postharvbio.2013.08.008.

Herremans, E., Verboven, P., Bongaers, E., Estrade, P., Verlinden, B.E., Wevers, M., Hertog, M.L.A.T.M., Nicolaï, B.M., 2013. Characterisation of 'Braeburn' browning disorder by means of X-ray micro-CT. Postharvest Biol. Technol. 75, 114–124. https://doi.org/10.1016/j.postharvbio.2012.08.008.

Herremans, E., Verboven, P., Verlinden, B.E., Cantre, D., Abera, M., Wevers, M., Nicolaï, B.M., 2015. Automatic analysis of the 3-D microstructure of fruit parenchyma tissue using X-ray micro-CT explains differences in aeration. BMC Plant Biol. 15, 1–14. https://doi.org/10.1186/s12870-015-0650-y.

Ho, Q.T., Verboven, P., Verlinden, B.E., Herremans, E., Wevers, M., Carmeliet, J., Nicolaï, B.M., 2011. A Three-Dimensional Multiscale Model for Gas Exchange in Fruit. Plant Physiol. 155, 1158–1168. https://doi.org/10.1104/pp.110.169391.

HORTGRO, 2019. Key Deciduous Fruit Statistics. Accessed 8 September 2020. https://www.hortgro.co.za/wp-content/uploads/docs/2020/07/key-deciduous-fruit-statistics-2019-1.pdf.

James, H.J., 2007. Understanding the flesh browning disorder of 'Cripps Pink' apples. PhD dissertation, Faculty of Agriculture, Food and Natural Resources, The University of Sydney, New South Wales, Australia.

James, H.J., Jobling, J.J., 2009. Contrasting the structure and morphology of the radial and diffuse flesh browning disorders and $CO_2$ injury of 'Cripps Pink' apples. Postharvest Biol. Technol. 53, 36–42. https://doi.org/10.1016/j.postharvbio.2009.02.001.

Kweon, H.J., Kim, M.J., Moon, Y.S., Lee, J.W., Choi, C., Choi, D.G., Lee, D.H., Kang, I.K., 2012. Relationship between Preharvest Factors and the Incidence of Storage Disorders in 'Fuji' Apples during CA Storage. Korean J. Hortic. Sci. Technol. 30, 50–55.

https://doi.org/10.7235/hort.2012.11049.

Kweon, H.J., Kang, I.K., Kim, M.J., Lee, J., Moon, Y.S., Choi, C., Choi, D.G., Watkins, C.B., 2013. Fruit maturity , controlled atmosphere delays and storage temperature affect fruit quality and incidence of storage disorders of 'Fuji ' apples. Sci. Hortic. 157, 60–64. https://doi.org/10.1016/j.scienta.2013.04.013.

Lau, O.L., 1998. Effect of growing season, harvest maturity, waxing, low $O_2$ and elevated $CO_2$ on flesh browning disorders in 'Braeburn' apples. Postharvest Biol. Technol. 14, 131–141. https://doi.org/10.1016/S0925-5214(98)00035-0.

Musse, M., De Guio, F., Quellec, S., Cambert, M., Challois, S., Davenel, A., 2010. Quantification of microporosity in fruit by MRI at various magnetic fields: Comparison with X-ray microtomography. Magn. Reson. Imaging 28, 1525–1534. https://doi.org/10.1016/j.mri.2010.06.028.

Nugraha, B., Verboven, P., Janssen, S., Wang, Z., Nicolaï, B.M., 2019. Non-destructive porosity mapping of fruit and vegetables using X-ray CT. Postharvest Biol. Technol. 150, 80–88. https://doi.org/10.1016/j.postharvbio.2018.12.016.

Saquet, A.A., Streif, J. and Bangerth, F., 2003. Reducing internal browning disorders in 'Braeburn' apples by delayed controlled atmosphere storage and some related physiological and biochemical changes. Acta Hortic. 628, 453-458 https://doi.org/10.17660/ActaHortic.2003.628.57.

Schoeman, L., Williams, P., du Plessis, A., Manley, M., 2016. X-ray micro-computed tomography (μCT) for non-destructive characterisation of food microstructure. Trends Food Sci. Technol. 47, 10-24. https://doi.org/10.1016/j.tifs.2015.10.016.

Tanaka, F., Nashiro, K., Obatake, W., Tanaka, F., Uchino, T., 2018. Observation and analysis of internal structure of cucumber fruit during storage using X-ray computed tomography. Eng. Agric. Environ. Food 11, 51–56. https://doi.org/10.1016/j.eaef.2017.12.004.

Verboven, P., Kerckhofs, G., Mebatsion, H.K., Ho, Q.T., Temst, K., Wevers, M., Cloetens, P., Nicolaï, B.M., 2008. Three-dimensional gas exchange pathways in pome fruit characterized by synchrotron X-ray computed tomography. Plant Physiol. 147, 518–527.

https://doi.org/10.1104/pp.108.118935.

Volz, R.K., Biasi, W. V., Grant, J.A., Mitcham, E.J., 1998. Prediction of controlled atmosphere-induced flesh browning in ‘Fuji’ apple. Postharvest Biol. Technol. 13, 97–107. https://doi.org/10.1016/S0925-5214(97)00080-X.

# LITERATURE REVIEW 1

## X-ray computed tomography (CT) and its application in fruit microstructure evaluation – A Review

**Abstract**

Microstructure plays a significant role in determining textural attributes and storability of fruit. X-ray computed tomography (CT) is an innovative and non-destructive imaging technique that can be used in 3-dimensional (3D) imaging of fruit tissue at micrometre (µm) and nanometre (nm) resolutions. X-ray CT uses absorption physics and reconstruction mathematics principles to produce 3D images of a scanned object. The objective of this review was to assess X-ray CT and its applicability in fruit microstructure evaluation and modelling. The review evaluated the background and basic principles of X-ray CT, followed by an overview of image processing as well as quantitative and qualitative image analysis. In addition, the review also assessed the advantages and limitations of using X-ray CT in fruit microstructure evaluation. The findings of this review showed that X-ray CT is increasingly being used in fruit microstructure evaluations. In fruit gas diffusion modelling studies, this technology produces 3D images that can provide an accurate representation of the geometric structure. The main advantages of X-Ray CT include 3D visualization capabilities, non-destructive nature and non-reliance on tedious sample preparation. However, limitations such as operator dependency and speed of of image acquisition still limit its use. Image artefacts such as beam hardening, cone beam artefact and phase contrast also present a challenge, however, most of these artefacts can be corrected using image reconstruction algorithms.

**Keywords:** 3-dimensional, artefacts, computed tomography, non-destructive, quantitative, qualitative

## 1. Introduction

The microstructure of fruit influences fruit textural attributes such as crispness and firmness which are important in determining the organoleptic satisfaction of consumers (Nicolaï et al., 2014). The study of fruit microstructure and how it influences fruit textural properties is thus important. Fruit microstructure plays a significant role in determining gas exchange and the extent to which gas concentrations can be upheld for long-term storage (Wang et al., 2020). Extended storage of fruit under controlled atmospheric conditions can lead to the development of internal physiological disorders such as internal browning. Different cultivars will require different storage conditions depending on their microstructure (Ting et al., 2013). Evaluating the microstructure of fruit allows for the development of appropriate storage protocols for the different fruit types and cultivars. To better understand the relationship between fruit tissue microstructure and fruit quality properties, it is necessary to obtain images of the tissue microstructure and to analyse them both qualitatively and quantitatively (Salvo et al., 2010).

Traditionally, imaging methods such as light, electron and confocal microscopy were used to investigate the microstructure of fruit (Herremans et al., 2013). The problem with these methods is that they require destructive sampling to investigate the microstructure, meaning that samples cannot be studied in their natural states. Furthermore, sample preparation is an arduous and time-consuming exercise and is prone to a lot of errors. X-ray computed tomography (CT) is an innovative and non-destructive imaging technique that can be used in 3D imaging of fruit tissue at micrometre (µm) and nanometre (nm) resolutions (Schoeman et al., 2016). X-ray CT involves the use of absorption physics and reconstruction mathematics to produce 3D images of a scanned object (Landis andKeane, 2010). With X-ray CT, one can produce high quality images that show the arrangement of intercellular spaces and cells in fruit tissue (Herremans et al., 2015b). Low-resolution X-ray CT is important in non-destructive fruit quality evaluations because it allows repeated measurements when the same sample is scanned numerous times under different conditions (Schoeman et al., 2016). However, for

high-resolution X-ray CT, this is only possible for small sized samples which will fit in the field-of-view of the X-ray CT scanner, for larger samples, sub-sampling will need to be performed. This is particularly important in storage experiments when the same fruit needs to be scanned at different times during the storage period in order to determine how the microstructure changes with storage duration. An intact fruit can be scanned with low-resolution X-ray CT or a small tissue sample can be obtained from the apple cortex and scanned with high-resolution X-ray CT to give more detailed microstructural information but is then destructive.

X-ray CT is a promising technology and is increasingly being used in fruit research to evaluate fruit microstructure. X-ray CT has been used several times to evaluate fruit internal disorders such as mealiness in pears (Muziri et al., 2016), internal browning in apples (Herremans et al., 2013; Chigwaya et al., 2018), watercore in apples (Herremans et al., 2014a) and broken stones in Japanese plums (Kritzinger et al., 2017). All this research has helped explain how internal disorders affect fruit microstructure and how these disorders can be avoided. Cantre et al. (2014a) used X-ray CT to evaluate the microstructure of the epidermal and sub-epidermal tissue in kiwi fruit, while Ting et al. (2013) were able to determine the microstructures of different apple cultivars using X-ray CT. Brecht et al. (1991) used X-ray CT to non-destructively determine the maturity of green tomatoes, whilst Magwaza and Opara (2014) used X-ray CT to non-destructively quantify and characterize the internal structure of intact pomegranate fruit. More recently, the distribution of thermo-physical properties such as porosity and thermal conductivity were determined in Japanese apricot using X-ray CT (Karmoker et al., 2019). A non-destructive method for automated internal quality grading of pear fruit using X-ray CT was investigated by Van De Looverbosch et al. (2020). Janssen et al. (2020) also used X-ray CT to evaluate the 3-dimensional (3D) pore structure of ‘Braeburn’ apples. Furthermore, X-ray CT has been successfully used in fruit modelling studies to explain the gas transport properties of fruit and to construct equations that explain the exchange of

respiratory gases between fruit and the storage atmosphere (Ho et al., 2011; Verboven et al., 2013; Herremans et al., 2015a).

This review assesses X-ray CT and its applicability to fruit microstructure evaluation and modelling with the first section focussing on the background and basic principles of X-ray CT, followed by an overview of image processing as well as quantitative and qualitative image analysis. In addition, the review also assesses the advantages and limitations of using X-ray CT in fruit microstructure evaluation.

## 2. Principles of X-ray CT

Generally, the principle of computed tomography involves quantifying the spatial distribution of a physical object from different directions and then computing 3D images from the data (Kalender, 2011). According to Landis and Keane (2010), the two most important aspects of X-ray CT are absorption physics, which is relevant to the production of 2-dimensional (2D) images, and reconstruction mathematics, which allows the production of 3D volumes. The process of producing images with CT is based on the fundamental principle that different tissues have different densities when exposed to X-ray photons (Kelkar, 2013). This means that X-rays can penetrate a material only to a certain extent. Compared to other radiation types, X-rays have a higher frequency and quantum energy (Fig. 1), and this gives them a penetration ability which allows for the inspection of the 3D spatial arrangement of thick samples such as fruit tissue (Herremans et al., 2015b). The relative transparency of X-rays through a material is known as the radiodensity; X-ray CT is based on the fact that different materials have different radiodensities (Kelkar, 2013). X-ray CT creates images based on X-ray attenuation within a sample (Cantre et al., 2014a). The differences in X-ray attenuation among different materials arises from the fact that different materials have different densities and atomic compositions (Chawanji et al., 2012).

X-ray attenuation through homogenous materials is calculated based on Beer's law:

$$\frac{I}{I0} = e^{-\mu x} \quad (1)$$

In equation 1, $\frac{I}{I0}$ is the attenuation of X-ray intensity per unit length of a given material, *x* is the thickness of the material and μ is the attenuation coefficient (Iassonov et al., 2009).

Attenuation of X-rays passing through a sample allows for the generation of high-resolution 3D volumes and 2D cross-sectional radiographs of materials being scanned (Iassonov et al., 2009). During X-ray CT scanning, a sample is placed on a stage that can rotate 360°. As the sample is rotating, X-rays produced by an X-ray source will pass through the sample with some being absorbed or fully attenuated while some are partially attenuated and transmitted through the sample, these transmitted X-rays are then detected by a detector which generates 2D radiographs based on information from the attenuated X-rays (du Plessis et al., 2016).

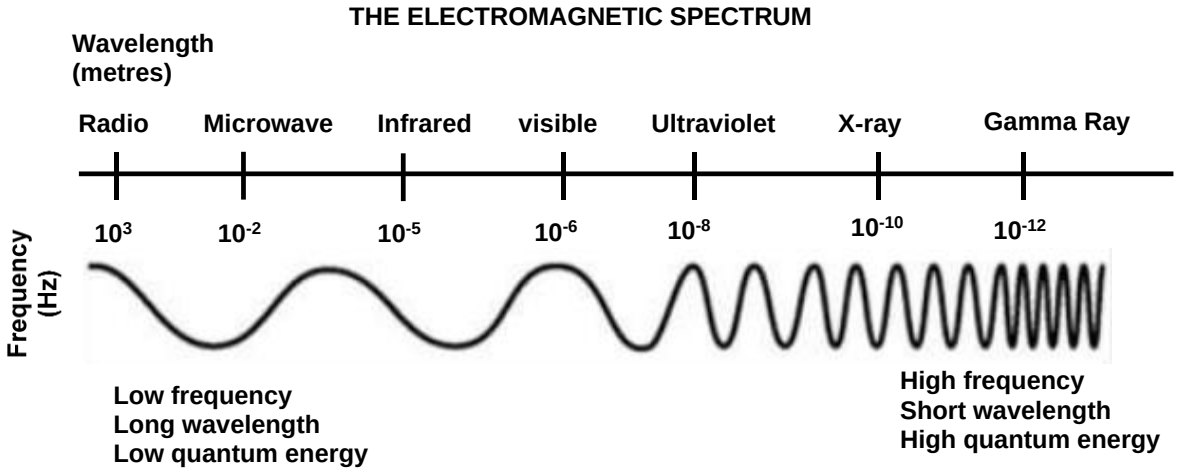


**Fig. 1.** Electromagnetic spectrum showing different radiation types, their characteristic wavelength and frequency. X-rays have a higher frequency, short wavelength and high quantum energy.

### 3. Hardware for X-ray CT

As suggested by its name, a modern computer system is a critical component of an X-ray CT set-up (Fig. 2). The computer system is involved in controlling the X-ray system,

acquisition of projection data, reconstruction, display and manipulation of tomographic images (Kotwaliwale et al., 2014). Other important components of the X-ray system are X-ray tubes, collimators and detectors. X-ray sources in laboratory CT are generally microfocus tubes with an electron beam focused on an anode target (Bultreys et al., 2016). The anode should be made up of a material with a high melting point (e.g. tungsten) because electrons release 99% of their energy as heat when they hit the anode target; thereby generating a lot of heat (Herremans, 2014). The X-ray source is the main limitation in the ability of laboratory CT to acquire images at a faster rate and this is due to power being dissipated when an electron beam hits the anode target, resulting in longer acquisition times (Bultreys et al., 2016). Most scanners use bremsstrahlung X-ray tubes as the radiation source (Kotwaliwale et al., 2014). To control scattered radiation and to adjust the beam to the required size, X-ray systems are also fitted with collimators at two points, one close to the X-ray tube and the other one close to the detector (Bultreys et al., 2016).

Another important component of an X-ray system are the detectors. The first X-ray detector was used by Roentgen in 1895 and it consisted of a sheet of paper that was coated with barium platinocyanide (Haff and Toyofuku, 2008). Detectors measure the quantity of X-rays transmitted through a scanned sample (Kotwaliwale et al., 2014). According to Kotwaliwale et al. (2014), detectors used in X-ray systems must be highly efficient with a large dynamic range and should be stable with respect to time and should not be affected by temperature fluctuations. The intensities of X-rays being transmitted through an object are digitised and a mathematical algorithm is then used to reconstruct these 2D images into 3D volumes (Sinka et al., 2004; du Plessis et al., 2016). Image acquisition should be very efficient because of the limited X-ray flux achievable with conventional laboratory-based sources (Bultreys et al., 2016). Large-flat panel detectors with thick scintillators are usually used in laboratory conditions, these have been replaced in recent years by hybrid detectors which do not have scintillator screens (Bultreys et al., 2016). These hybrid detectors convert absorbed X-rays into electron-hole pairs, which allows for greater response speed and energy

discriminating possibilities (Bultreys et al., 2016). Furthermore, they allow for energy dispersive acquisition and a significant decrease in electronic noise (Bultreys et al., 2016).

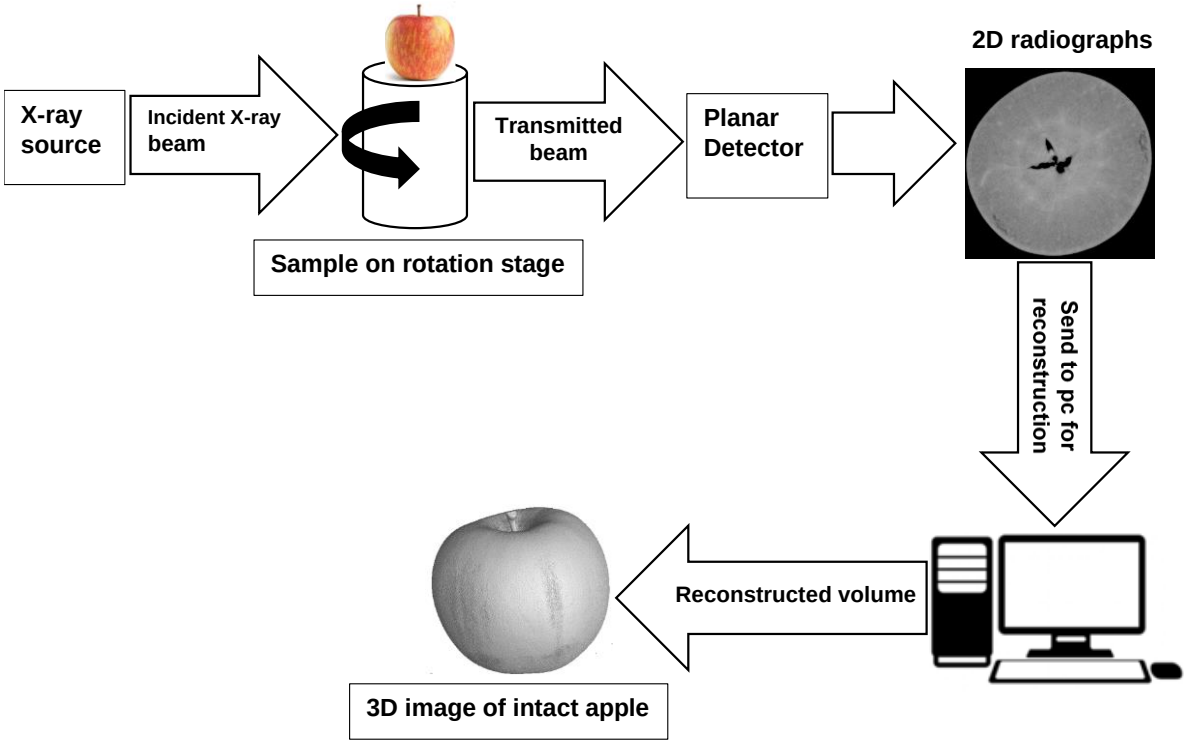


**Fig. 2.** Simple schematic illustration of an X-ray CT system. The X-ray source produces a beam of X-rays; some are absorbed by the sample while some pass through and are detected by a planar detector which produces 2D images (radiographs) which are then reconstructed into 3D volumes.

## 4. Image processing and analysis

### *4.1. Image reconstruction*

After the acquisition of 2D X-ray CT images, the next step would be to reconstruct these 2D radiographs into 3D volumes. Image reconstruction in X-ray CT is a mathematical process that generates tomographic images from X-ray projection data acquired at many different angles. Reconstruction of 3D volumes from a series of 2D images allows for the physical and physiological characterization of biological materials (Magwaza and Opara, 2014). Reconstruction software used include Octopus (Octopus Imaging Software. Ghent, Belgium), NRecon (Bruker microCT, Kontich, Belgium) and Phoenix Datos|x (GE Sensing & Inspection Technologies GmbH, Wunstorf, Germany). These reconstruction software have been used in

the reconstruction of projection images obtained from the scanning of fruit and vegetable samples (Arendse et al., 2016; Muziri et al., 2016; Nugraha et al., 2019; Wang et al., 2020). Nugraha et al. (2019) used Octopus software to reconstruct projection images from low-resolution scans while Phoenix Datos|x and NRecon were used to reconstruct projection images from high-resolution scans. Image reconstruction in CT can be classified into analytic reconstruction and iterative reconstruction (Bruyant, 2002). Analytic reconstruction methods, such as the filtered back-projection algorithm, are efficient and fast but they are unable to handle complicated factors such as scatter while on the other hand, iterative reconstruction algorithms are more versatile but less efficient (Bruyant, 2002). Currently, most reconstructions are performed using analytical filtered back-projection algorithms such as the Fieldmann-Davis-Kress (FDK) algorithm. This algorithm is simple and relatively fast (Bultreys et al., 2016). Reconstruction allows for the creation of a complete dataset which is composed of 3D pixels known as voxels.

### *4.2. Image segmentation*

Image segmentation is a process which involves the separation of an image into specific regions or voxel groups i.e. pores and cells (Herremans et al., 2013). Image segmentation is a very important step in image processing and analysis because it affects subsequent quantitative analysis and modelling procedures (Iassonov et al., 2009). Segmentation of CT images allows one to visualize and quantify morphological characteristics of a porous system from reconstructed X-ray CT data; this permits quantification of pore scale parameters such as porosity, connectivity, specific surface area and tortuosity (Iassonov et al., 2009). Thresholding is one of the most commonly used segmentation techniques due to its simplicity (Goh et al., 2018). Thresholding techniques can be separated into local and global thresholding (Zhang et al., 2017). Local thresholding uses grey level information to select multiple threshold values (Zhang et al., 2017), while global thresholding involves the defining of a single grey value to separate regions of interest based on analysis of the image histogram (Iassonov et al., 2009; Zhang et al., 2017). Voxels containing grey values lower than the

selected threshold value are regarded as background (pores), while those with grey values higher than the threshold value are regarded as sample material (Schoeman et al., 2016). Global thresholding is the most widely applied approach in X-ray CT segmentation, and it is easy to use. A commonly used method for selecting thresholds for general images is Otsu's method which maximises between class variance or minimises within class variance from an image histogram (Otsu, 1979; Zhang et al., 2017). Studies to demonstrate performance analysis has shown that the Otsu's method is simple to apply, robust and easily adaptable (Otsu, 1979; Goh et al., 2018).

Another commonly used tool for image segmentation is the watershed algorithm. This method favours the segmentation of regularly shaped spherical cells with touching and convex features (Herremans et al., 2015b). The watershed method is a powerful morphological tool for image segmentation. It derives its name from the geographical meaning of watershed, which refers to the ridge that divides areas drained by different river systems (Ruparelia, 2012). If you view the image as a landscape, the watershed lines determine boundaries which separates image regions (Ruparelia, 2012). For the visualization of the internal structures of various components to be possible, these internal structures should be significantly different to provide adequate contrast. If there is sufficient contrast, the morphology of these internal structures can be studied through virtual slicing of the 3D rendered volume (Baker et al., 2012).

### *4.3. Quantitative and qualitative image analysis*

Image reconstruction allows us to see a 3D volume of X-ray absorption. Different features of a material will have different X-ray absorption properties and they can therefore be easily distinguished from each other based on their grey values (Landis and Keane, 2010). One of the initial steps in quantitative and qualitative image analysis involves the selection of a region of interest (ROI). Although in some cases an entire X-ray CT dataset can be considered as a ROI, analysing an image in its original form can be an arduous and time-consuming exercise (Schoeman et al., 2016). In addition, there are usually other parts of the

dataset that are not part of the sample (e.g. background air and mounting material) and they need to be cropped out of the image. In high-resolution scans, the foam (used as mounting material) which holds the sample in position will need to be cropped out of the image and in low-resolution scans, the scanning reference which is used for density calculations should also be cropped out of the image. It is therefore important to select a ROI that is small enough to reduce analysis time but large enough to be statistically representative of the entire sample volume (Baker et al., 2012; Schoeman et al., 2016). According to Mendoza et al. (2007), such a ROI is usually referred to as a representative elementary (REV). Mendoza et al., (2007) estimated the minimum REV for apple cortical tissue to be 1.3 $mm^3$.

Smoothing of images by Gaussian or Median filters is necessary during image processing to remove random noise, smooth surfaces and to improve the appearance of CT images (Bassel, 2015; Schoeman et al., 2016). Image processing is generally applied to improve the quality of the image and it normally involves grey value modification and filtering (Maire et al., 2003). In fruit scans, the quality of the X-ray image produced depends on the selected tube voltage and current; this is due to the varying thickness, density and X-ray absorption properties of different fruit types (Kotwaliwale et al., 2014).

A large range of commercial and free access software are available for use in the extraction of qualitative and quantitative data from 3D volumes. Such software packages include ImageJ (Public domain: http://rsb.info.nih.gov/ij/), Avizo (Visualisation Science Group, Bordeaux, France), VGStudio Max (Volume Graphics GmbH, Heidelberg, Germany), CTAn (Bruker microCT, Kontich, Belgium) and Pore3D (SYRMEP, Trieste, Italy) (Maire et al., 2003). Initially, X-ray CT was mainly used as a method for acquiring 3D volumes from which visual observations and qualitative analysis could be made (Maire et al., 2003). However, with the advancing technology it has been possible to quantitatively extract key morphological and structural parameters (Maire et al., 2003). Specialized rendering software allow for the visual inspection of a 3D volume based on the linear attenuation coefficient (Cnudde and Boone, 2013). Qualitative analysis enables differentiation of anatomical and physiological

characteristics of a sample (Schoeman et al., 2016). CT images can also be quantitatively evaluated to determine densities within the image; similar grey values represent areas of similar densities. The advantage of X-ray CT is that image analysis is not limited to one image slice at a time but can be carried out in the whole volume in all three directions (Schoeman et al., 2016). Various morphological and microstructural parameters can be quantified from a 3D volume; these include pore connectivity, pore size distribution, porosity, pore geometry, tortuosity, network structure, wall thickness, pore sphericity, individual pore volume, dimensions and density information (Iassonov et al., 2009; Schoeman et al., 2016).

## 5. Application of X-ray CT in fruit microstructure evaluation

X-ray CT has become a common tool for evaluating fruit quality in recent years. In the field of horticulture, it is essential to make correlations between fruit properties and their microstructure in order to optimise handling and storage protocols. Table 1 summarizes some of the applications of X-ray CT in fruit microstructure evaluations. Tube voltage and current are important parameters which determine the ultimate spatial resolution obtained. Changing the tube current will affect the intensity of the X-rays while changing the tube voltage will change the X-ray spectrum (Herremans, 2014). In addition, the tube voltage also influences the attenuation of X-rays, which depends on the X-ray energy and properties (such as thickness) of the sample being scanned. As a result, no general guidelines can be given to optimize tube voltage and current settings, but these are optimized depending on the sample being scanned and the machine being used to ensure that X-rays are not completely absorbed or completely transferred by the object being scanned (Herremans, 2014).

**Table 1**

An overview of the applications of X-ray computed tomography in fruit microstructure evaluations

| Fruit type | Tube voltage and current | Spatial resolution | Application | Reference |
|---|---|---|---|---|
| Apple | 40 keV | 9.89 µm | Differentiation of microstructural parameters amongst different apple cultivars | Ting et al., 2013 |
| Apple | 85 keV and 58 keV | 82.6 µm, 4.8 µm | Multiscale modelling to understand respiration and fermentation | Herremans et al., 2014b |
| Apple | 80 keV, 100 µA and 49 keV, 201 µA | 4.8 µm | Comparison of X-ray CT and MRI to detect watercore disorder | Herremans et al., 2014a |
| Apple | 63 kV, 156 µA | 8.5 µm | Investigation of pore size distribution | Mendoza et al., 2010 |
| Apple | 58 keV | 4.8 µm | Characterization of Braeburn browning disorder | Herremans et al., 2013 |
| Apple | 240kV | 60 µm, 3 µm | Characterization of internal browning | Chigwaya et al., 2018 |
| Apple | 80 kV, 439 mA | | Assessment of bruise volumes | Diels et al., 2017 |
| Apple | 50 kV, 200 µA | 3.8 µm | Method developed to characterize the 3D microstructure of frozen apple | Vicent et al., 2017 |

| | | | | |
|---|---|---|---|---|
| Apple | 120 kV, 150 mA | | Detection of bitter pit progression in ‘Honeycrisp’ apples | Jarolmasjed et al., 2016 |
| Apple | 70 kV, 285 mA | 8.85 µm | Quantifying the changes in porosity, pore diameter, cell sphericity, cell diameter and cell elongation of apple parenchyma tissue during drying | Prawiranto et al., 2019 |
| Apple | 50 kV, 200 mA | 3.8 µm | Characterization of the 3D microstructure of frozen apple | Vicent et al., 2017 |
| Apple | 60kV, 175µA | 2.5µm | Effect of microstructure on light scattering properties of apple fruit | Wang et al., 2020 |
| Apple | 45–75 kV | 2.5 - 3.0 µm | Contrast enhanced 3D µCT of apple tissue using different impregnation techniques | Wang et al., 2017 |
| Apple | 44kV, 222 µA | 5 µm | Assessment of texture properties of different apple cultivars | Poles et al., 2020 |
| Apple | 90 kV, 140 kV, 60 kV, 500 µA, 220 µA, 170 µA | 45 µm, 100 µm, 5 µm | Pore network analysis of ‘Braeburn’ apples using X-ray CT | Janssen et al., 2020 |

| | | | | |
|---|---|---|---|---|
| Apple, pear, turnip, eggplant | 66kV,200 µA, 60kV, 167 µA | 132.2 µm, 2.60 µm, 4.00 µm, 4.87 µm | Non-destructive porosity mapping of fruit and vegetables | Nugraha et al., 2019 |
| Chestnut | 120 kV, 170mA | 1.42 µm, 2.52 µm | Postharvest non-invasive assessment of fresh chestnut internal decay | Donis-González et al., 2014 |
| Citrus | 75 kV, 468 mA | 128.9 µm, 99.6 µm | A segmentation and classification algorithm for online detection of internal disorders | Van Dael et al., 2016 |
| Cucumber | - | - | Characterization and quantification of the internal structure of cucumber fruit during storage | Tanaka et al., 2018b |
| Kiwi fruit | 60 kV, 167 µA | 4.87 µm | Microstructural characterization of commercial kiwifruit cultivars | Cantre et al., 2014a |
| Mango | 60 kV, 167 µA | 4.87 µm | Characterization of the 3D microstructure of mango | Cantre et al., 2014b |
| Mango | 150 keV, 3 mA | - | Relating X-ray absorption and quality characteristics of mango | Barcelon et al., 2000 |
| Pear | 180 kV | 58 µm | Microstructure analysis and detection of mealiness | Muziri et al., 2016 |

| | | | | |
|---|---|---|---|---|
| Pear | 53 kV, 0.21 mA | - | Study of spatial distribution of core breakdown | Lammertyn et al., 2003 |
| Pear | 80 kV, 120 mAh | - | CT imaging to determine pear bruise level due to external loads | Azadbakht et al., 2019 |
| Pear | 130 kV, 300 mA | 598.4 µm | Non-destructive Inspection of internal pear quality using X-ray CT | Van De Looverbosch et al., 2020 |
| Persimmon | 60 kV, 100 mA | 3.24µm | Modelling of the thermal diffusivity of persimmon flesh tissue using 3D structure based on X-ray CT | Tanaka et al., 2018a |
| Pineapple | 30KeV | - | Assessment of translucency in pineapple | Haff et al., 2006 |
| Plum | 160 kV, 120 µA | - | Study of stone hardening and broken stones in Japanese plums | Kritzinger et al., 2017 |
| Pomegranate | 200 kV, 100 µA | 71.4 µm | Non-destructive quantification and characterization | Magwaza and Opara, 2014 |
| Pomegranate | 245 kV, 300 µA | 71.4 µm | Characterization and volume estimation of pomegranate fruit external and internal morphological fractions | Arendse et al., 2016a |
| Pomegranate | 100kV, 200 µA | 71.4 µm | Estimation of the density of pomegranate fruit and their fractions | Arendse et al., 2016b |

## 6. Modelling of fruit dynamics using CT data

3D images obtained through X-ray CT can be used to extract an accurate representation of the geometric structure in fruit for modelling purposes (Maire and Withers, 2014). Modelling studies in fruit microstructure analysis can be done using segmented 3D volumes from image processing (Wang et al., 2018). From these volumes, one can construct transport equations that govern mass, heat and momentum transfer (Wang et al., 2018). The geometry of fruit microstructure is the basis of multiscale modelling of transport properties and it helps explain the interaction between the fruit and its environment (Ho et al., 2011). Multiscale modelling can solve diffusion equations over the 3D geometry which consists of void spaces and cells (Verboven et al., 2013).

Modelling of gas transport properties is important because transport processes play a vital role in fruit physiology. Gas transport refers to the transport of oxygen towards the mitochondria, removal of carbon dioxide and other metabolites such as ethanol from the mitochondria and distribution of plant hormones such as ethylene (Herremans et al., 2015a). Several studies have been done to explain the exchange of oxygen and carbon dioxide between fruit such as apples and the storage atmosphere. Ho et al. (2011) performed a study to investigate the exchange of oxygen and carbon dioxide in apple fruit using 3D microstructure images obtained by means of synchrotron radiation tomography. Through their work, they were able to determine that the susceptibility of fruit tissue to anoxia related physiological disorders may be due to the oxygen concentration in cells being much lower than what is estimated by simple macroscale models. This study further highlighted that the local oxygen concentration near the core of apple fruit was higher than the known estimated Michaelis-Menten constant of cytochrome c oxidase. This may explain why ‘Jonagold’ apples can be stored for extended durations without developing any storage related internal disorders.

In their studies to elucidate the occurrence of storage related disorders in 'Braeburn' apples, Herremans et al. (2014b) used multiscale modelling to evaluate changes in oxygen and carbon dioxide concentrations and how this affects respiration and fermentation rates, as well as disorder development during controlled atmosphere storage. Verboven et al. (2013) also utilized X-ray CT to determine the 3D assembly of void spaces inside the developing seed of *Brassica napus* and also performed modelling work to determine how oxygen moves into and within a seed. From their work, Verboven et al. (2013) determined that the size of voids and their connectivity are important parameters affecting the gas exchange properties of the seed and respiratory activity. Their modelling work also allowed them to estimate the quantity of oxygen present in various compartments of the seed either in gaseous or aqueous form. Tanaka et al. (2018a) used 3D images based on high-resolution X-ray CT to construct a heat transfer model for persimmon flesh tissue and their proposed method can be utilized as an effective tool for the evaluation of physiochemical properties and fruit quality.

## 7. Advantages of X-ray CT

### *7.1. 3D visualization and analysis*

One of the greatest advantages of using X-ray CT is the ability to perform non-destructive 3D imaging. The data acquired from 3D rendering and imaging is a 3D volume of the scanned sample comprising of numerous 2D slices (Schoeman et al., 2016). Each of these slices has a voxel that can be related to a Hounsfield Unit (HU) or CT number (Schoeman et al., 2016). The HU scale is a linear transformation of the original linear attenuation coefficient measurement into one in which the radiodensity of distilled water at standard pressure and temperature (STP) is defined as zero Hounsfield units (HU), while the radiodensity of air at STP is defined as -1000 HU (Kalender, 2011). CT numbers represent the attenuation capabilities of a sample and changes in physical density are reflected in changes in the CT numbers, where low density materials have a low HU, while high density materials have a high HU (Schoeman et al., 2016). 3D analysis allows

the extraction of qualitative and quantitative information from an image and this helps in defining the structure and morphology of a sample.

Numerous parameters can be obtained from a 3D model, these include anisotropy, connectivity, pore volume, pore diameter, length and cell wall thickness (Lim and Barigou, 2004; Schoeman et al., 2016). In fruit evaluations, X-ray CT is useful because it allows for the determination of porosity, pore size distribution and pore connectivity. All these parameters have a significant influence on the gas transport properties of the fruit and this affects the storability of fruit and the incidence of internal disorders during storage (Ting et al., 2013; Cantre et al., 2014a; Warning et al., 2014; Herremans et al., 2015b). 2D imaging on the other hand only allows a limited amount of information to be extracted from an image. In 2D imaging, only one image is acquired per sample as compared to 3D imaging which allows more than one 2D projection image to be obtained at various angles in order to be reconstructed into a 3D volume. This allows more detailed and precise information to be obtained about the sample (Lim and Barigou, 2004).

*7.2. Non-destructive technique*

The non-destructive nature of X-ray CT allows one to study the interior of an object or material without sacrificing or destroying it. The non-destructive aspect of X-ray CT is very important in the fruit industry because it allows one to visualize internal quality parameters without having to destroy the fruit. X-ray CT offers a reliable, non-destructive technique for sorting and isolating fruit with internal disorders such as browning, watercore and mealiness from consignments (Franck et al., 2007). In addition, X-ray CT allows for the same sample to be studied under different conditions due to its non-destructive nature. This is particularly useful in the fruit industry when repeated measurements need to be done on the same batch of fruit. Thus, the internal quality of the same fruit can be measured at harvest, after cold-storage and after shelf-life to see how storage and other factors under study affect the internal quality of the fruit at

different stages. Since X-ray CT is a non-destructive technique, it means that minimal sample preparation is needed before commencement of scanning. In high-resolution X-ray CT, the only sample preparation needed is to extract a tissue sample using a cork-borer and then wrap the sample in parafilm before securing it on a sample holder in the scanning machine. This saves time since sample preparation can be an arduous, tedious and time-consuming process. Furthermore, sample preparation can alter or damage the internal structure of a sample before scanning starts, leading to biased results.

## 8. Limitations of X-ray CT

### *8.1. Noise*

Like all other imaging techniques, X-ray CT is subject to noise. In general, noise refers to some part of the image signal that is not present in the original sample (Herremans, 2014). Noise is a random occurrence during X-ray CT scanning and can be a result of several unpredictable processes which occur during scanning. Such processes include the number of photons that leave the X-ray source, the number of photons that pass unaffected through the object and the number of photons that get captured by the detector (Cnudde and Boone, 2013). Noise is introduced during X-ray generation and then traverses as the X-ray moves along until it reaches the detector (Wang et al., 2008). Noise propagation through the calibration process is a complicated; however, noise distribution at the initial X-ray generation stage can be expressed as a Poisson function (Wang et al., 2008). Image noise is affected by many parameters and is more prominent when a scintillator is used (Cnudde and Boone, 2013).

### *8.2. Operator dependency*

No generally accepted protocols exist for X-ray CT scanning and this is due to variabilities in sample size, shape and composition (Cnudde and Boone, 2013). As a result of this, parameters

which influence the result and image quality must be chosen arbitrarily. Such parameters include tube voltage, total exposure time and beam filtering (Cnudde and Boone, 2013). The fact that different X-ray CT systems produce different results, coupled with the idea that there are no generally accepted calibration procedures for X-ray CT equipment, means that reliable comparison of results obtained in different X-ray CT set-ups is difficult (Cnudde and Boone, 2013). Obtaining quantitative results from a 3D volume is a very important step in X-ray CT and this is usually done using 3D analysis software. Segmentation is an important aspect of this analysis and is done based on grey value thresholding, which is extremely operator dependent due to effects such as partial volume and image noise (Baveye et al., 2010; Cnudde and Boone, 2013).

*8.3. Speed of image acquisition and processing*

The speed of image acquisition, reconstruction and image analysis limits the commercial applicability of X-ray CT. In studies on pears, Lammertyn et al. (2003) found that the X-ray CT measurement of a single pear, including reconstruction typically lasted for 10 mins. The time required to scan a cylindrical apple tissue sample at 9.89 µm was 33 mins (Ting et al., 2013). In studies on the browning of 'Braeburn' apples, Herremans et al. (2013) provided that the scanning time for each sample was 20 mins. For pineapples, Haff et al. (2006) found that each fruit needed an exposure time of 3 mins to get a complete X-ray CT volume. X-ray CT scans of intact fruit needed a total scan time of 25 mins in studies of watercore disorder (Herremans et al., 2014a). In their X-ray CT and porosity mapping studies of intact 'Jonagold' apple samples, Nugraha et al. (2019) provided that each scan lasted approximately 30 mins. The long acquisition time for X-ray CT present a challenge for its commercial implementation in fruit quality evaluation on sorting lines. Therefore, for X-ray CT to be successful as a commercial detector of internal fruit quality on the sorting line, the speed of image acquisition, reconstruction and image analysis will have to be substantially increased. The times discussed in this section vary greatly depending on the properties of the sample being scanned, the type of machine being used, and settings used.

However, the important point to note is that the speed of image acquisition, reconstruction and image analysis still needs to be improved to ensure commercial applicability. With advancing technology, development of faster computers and production of more advanced X-ray detectors, the speed of X-ray CT imaging is expected to greatly increase.

## 9. Image artefacts

### *9.1. Beam hardening*

Polychromacity gives rise to one of the most prevalent imaging artefacts in X-ray CT, i.e. beam hardening (Cnudde and Boone, 2013). Polychromatic X-rays have photons of varying energy, ranging from 0 eV to 100 keV (Kotwaliwale et al., 2014). X-ray sources that produce polychromatic beams affect the achievable image resolution, field of view and image quality (Nicolaï et al., 2014). X-rays with low energy (below 5 – 10 keV) are referred to as soft X-rays, while those with high energy (above 5 – 10 keV) are referred to as hard X-rays. A polychromatic beam is made up of a mixture of soft and hard X-rays. The soft X-rays are absorbed by the sample more easily than the hard X-rays, this results in a beam with more hard X-rays being transmitted through the sample, hence the name beam hardening. The linear attenuation coefficient is energy dependent, which means that low energy X-rays have a higher probability of being absorbed as compared to high energy X-rays (Cnudde and Boone, 2013). Beam hardening is the preferential attenuation of low energy X-rays, resulting in biased density gradients (Kelkar, 2013). On the other hand, synchotron radiation sources produce very intense monochromatic X-ray beams with a high flux resulting in good contrast and resolution (Nicolaï et al., 2014). The use of synchrotron radiation sources results in the production of 3D images which are free of artefacts such as beam hardening. The only challenge is that this can only be achieved at a few large synchotron facilities. A synchrotron source can provide high intensity X-rays with natural collimation and a small source size, making it possible to produce highly monochromatic X-rays using monochromators (Wei et al., 2013). Beam hardening can be corrected by using mathematical correction algorithms such

as the FDK (Feldkamp, Davis and. Kress) algorithm. These correction methods can attain good results for most samples but may fail for complex samples consisting of a variety of materials (Cnudde and Boone, 2013; Kelkar, 2013).

### *9.2. Cone beam artefact*

Another image artefact experienced during laboratory X-ray CT scanning is the cone beam effect. The cone beam effect results in slices which are far from the source suffering severe artefacts due to incomplete sampling of the 3D Radon space (De Witte, 2010). This artefact can be corrected by using a helical scanning trajectory and other iterative reconstruction methods (De Witte, 2010).

### *9.3. Phase contrast*

Phase contrast arises from temporal or spatial coherence of the X-ray beam (Cnudde and Boone, 2013). The basis of X-ray CT is the difference in X-ray absorption of materials to provide information about the internal structure of a sample. However, materials also interact with X-rays in other ways, such as introducing a phase shift in the X-ray beam. The contribution of the phase signal to the projection image when scanning at low-resolution is low, however, when moving to high-resolution scanning of small samples the absorption signal becomes small and contribution of phase signal to the projection image becomes significant (De Witte et al., 2009). Although phase contrast can be favourable for visual contrast since it gives rise to edge enhancement, it often hinders segmentation if left uncorrected. Very high-resolution and low sample attenuation are the main causes for the phase contrast artefact (Cnudde and Boone, 2013). A method known as Bronnikov Aided Correction (BAC) is a phase-correcting algorithm that prevents phase contrast by applying filtering operations on the projection images (De Witte et al., 2009). Wernersson et

al. (2014) proposed a post-processing filter that can be used to reduce phase contrast on reconstructed images without having to access the projection images.

### *9.4. Ring artefact*

The ring artefact is another common artefact that is encountered in X-ray CT. Ring artefacts appear as concentric rings around the centre of rotation and are mainly caused by uncorrected variations in the detector, as well as detector sensitivity (Vågberg et al., 2017). The appearance of ring artefacts is mostly problematic in 3D X-ray CT that is based on a 2D X-ray detector and a divergent X-ray beam (Eldib et al. 2017). The scan time for a 2D X-ray detector is generally longer because 2D flat-panel detectors (FPDs) are smaller than detectors used in typical medical CT. This makes it difficult to correct the non-uniformity of the detector sensitivity as it fluctuates during the scan (Eldib et al., 2017). Ring artefacts are usually caused by the pixels with deviating behaviour compared to neighbouring pixels. The data corruptions caused by ring artefacts make it difficult to extract accurate qualitative and quantitative data from these images (Wei et al., 2013). Vågberg et al. (2017) suggested that the use of a proper flat-field correction should be able to remove ring artefacts, but ring artefacts can persist after the flat-field correction due to imperfections or non-linear behaviour. Most published methods for removing ring artefacts are based on post scan image processing (Münch et al., 2009; Hasan et al., 2012; Rashid et al., 2012). The disadvantage of such methods is that some true features of the scanned object can be classified as artefacts and removed and false features may be introduced into the image (Vågberg et al., 2017). Vågberg et al. (2017) proposed a method for removing ring artefacts by addressing the true physical cause of ring artefacts, which are a result of scintillator variations.

In general, most artefacts are best countered by reconstruction methods since only reconstructed images are guaranteed to be consistent with projection data (Wernersson et al., 2014). Other forms of artefacts arise due to sample movement during scanning, thus secure

sample mounting should be performed. Examples of these artefacts are motion artefacts, angle artefacts and streak artefacts (Cnudde and Boone, 2013; Schoeman et al., 2016).

## 10. Conclusion

X-ray CT is a very important tool that has helped overcome several challenges in fruit microstructure evaluation. X-ray CT allows for the non-invasive 3D characterization of fruit tissue and this can assist in maintaining fruit quality during long-term storage. In addition, it also allows for the non-destructive detection of internal disorders such as internal browning, mealiness, core rot and broken stones. However, there is need for the development of a fast and reliable X-ray CT based method for online sorting of fruit to detect internal physiological disorders. Currently, no accurate method exists for predicting and detecting internal disorders such as internal browning at commercial speeds. Internal browning symptoms are not usually visible from the exterior of the fruit, thus an accurate method for identifying fruit with this disorder will be a huge benefit to the fruit industry. With continuous improvements in technology, imaging instruments and computing power, it is expected that X-ray CT can be fully implemented on the sorting line to categorize fruit based on maturity and internal quality. It is anticipated that technological and research advancements will allow for the development of reconstruction techniques and image processing algorithms that will achieve fast and affordable inline X-ray CT sorting systems for quality evaluation.

## References

Arendse, E., Fawole, O.A., Magwaza, L.S., Opara, U.L., 2016a. Non-destructive characterization and volume estimation of pomegranate fruit external and internal morphological fractions using X-ray computed tomography. J. Food Eng. 186, 42–49. https://doi.org/10.1016/j.jfoodeng.2016.04.011.

Arendse, E., Fawole, O.A., Magwaza, L.S., Opara, U.L., 2016b. Estimation of the density of pomegranate fruit and their fractions using X-ray computed tomography calibrated with polymeric materials. Biosyst. Eng. 148, 148–156. https://doi.org/10.1016/j.biosystemseng.2016.06.009.

Azadbakht, M., Vahedi Torshizi, M., Mahmoodi, M.J., 2019. The use of CT scan imaging technique to determine pear bruise level due to external loads. Food Sci. Nutr. 7, 273–280. https://doi.org/10.1002/fsn3.882.

Baker, D.R., Mancini, L., Polacci, M., Higgins, M.D., Gualda, G.A.R., Hill, R.J., Rivers, M.L., 2012. An introduction to the application of X-ray microtomography to the three-dimensional study of igneous rocks. Lithos 148, 262–276. https://doi.org/10.1016/j.lithos.2012.06.008.

Barcelon, E.G., Tojo, S., Watanabe, K., 2000. Relating X-ray Absorption and Some Quality Characteristics of Mango Fruit (*Mangifera indica* L.). J. Agric. Food Chem. 47, 3822–3825. https://doi.org/10.1021/jf980690e.

Baveye, P.C., Laba, M., Otten, W., Bouckaert, L., Dello Sterpaio, P., Goswami, R.R., Grinev, D., Houston, A., Hu, Y., Liu, J., Mooney, S., Pajor, R., Sleutel, S., Tarquis, A., Wang, W., Wei, Q., Sezgin, M., 2010. Observer-dependent variability of the thresholding step in the quantitative analysis of soil images and X-ray microtomography data. Geoderma 157, 51–63. https://doi.org/10.1016/j.geoderma.2010.03.015.

Brecht, J.K., Shewfelt, R.L., Garner, J.C., Tollner, E.W., 1991. Using X-ray-computed tomography to nondestructively determine maturity of green tomatoes. HortScience 26, 45–47. https://doi.org/10.21273/HORTSCI.26.1.45.

Bruyant, P.P., 2002. Analytic and iterative reconstruction algorithms in SPECT. J. Nucl. Med. 43, 1343–1358.

Bultreys, T., Boone, M.A., Boone, M.N., De Schryver, T., Masschaele, B., Van Hoorebeke, L., Cnudde, V., 2016. Fast laboratory-based micro-computed tomography for pore-scale research: Illustrative experiments and perspectives on the future. Adv. Water Resour. 95,

341–351. https://doi.org/10.1016/j.advwatres.2015.05.012.

Cantre, D., East, A., Verboven, P., Araya, X.T., Herremans, E., Nicolaï, B.M., Pranamornkith, T., Loh, M., Mowat, A., Heyes, J., 2014a. Microstructural characterisation of commercial kiwifruit cultivars using X-ray micro computed tomography. Postharvest Biol. Technol. 92, 79–86. https://doi.org/10.1016/j.postharvbio.2014.01.012.

Cantre, D., Herremans, E., Verboven, P., Ampofo-Asiama, J., Nicolaï, B., 2014b. Characterization of the 3-D microstructure of mango (*Mangifera indica* L. cv. Carabao) during ripening using X-ray computed microtomography. Innov. Food Sci. Emerg. Technol. 24, 28–39. https://doi.org/10.1016/j.ifset.2013.12.008.

Chawanji, A.S., Baldwin, A.J., Brisson, G., Webster, E., 2012. Use of X-ray micro tomography to study the microstructure of loose-packed and compacted milk powders. J. Microsc. 248, 49–57. https://doi.org/10.1111/j.1365-2818.2012.03649.x.

Chigwaya, K., Schoeman, L., Fourie, W.J., Crouch, I., Viljoen, D. and Crouch, E.M., 2018. 'Fuji' apple internal browning explored via X-ray computed tomography (CT). Acta Hortic. 1201, 309-316. https://doi.org/10.17660/ActaHortic.2018.1201.42.

Cnudde, V., Boone, M.N., 2013. High-resolution X-ray computed tomography in geosciences: A review of the current technology and applications. Earth-Science Rev. 123, 1–17. https://doi.org/10.1016/j.earscirev.2013.04.003.

De Witte, Y., 2010. Improved and practically feasible reconstruction methods for high resolution X-ray tomography. PhD dissertation, Faculty of Sciences, Ghent University, Ghent, Belgium.

De Witte, Y., Boone, M., Vlassenbroeck, J., Dierick, M., Masschaele, B., Van Hoorebeke, L., Cnudde, V., 2009. Correcting phase contrast artefacts in X-ray CT imaging, in: 2009 IEEE International Symposium on Biomedical Imaging: From Nano to Macro. IEEE, pp. 574–577. https://doi.org/10.1109/ISBI.2009.5193112.

Diels, E., Dael, M. Van, Keresztes, J., Vanmaercke, S., Verboven, P., Nicolaï, B., Saeys, W.,

Ramon, H., Smeets, B., 2017. Assessment of bruise volumes in apples using X-ray computed tomography. Postharvest Biol. Technol. 128, 24–32. https://doi.org/10.1016/j.postharvbio.2017.01.013.

Donis-González, I.R., Guyer, D.E., Fulbright, D.W., Pease, A., 2014. Postharvest noninvasive assessment of fresh chestnut (*Castanea spp*.) internal decay using computer tomography images. Postharvest Biol. Technol. 94, 14–25. https://doi.org/10.1016/j.postharvbio.2014.02.016.

du Plessis, A., le Roux, S.G., Guelpa, A., 2016. The CT Scanner Facility at Stellenbosch University: An open access X-ray computed tomography laboratory. Nucl. Instruments Methods Phys. Res. Sect. B Beam Interact. with Mater. Atoms 384, 42–49. https://doi.org/10.1016/j.nimb.2016.08.005.

Eldib, M.E., Hegazy, M., Mun, Y.J., Cho, Myung Hye, Cho, Min Hyoung, Lee, S.Y., 2017. A ring artifact correction method: validation by micro-CT imaging with flat-panel detectors and a 2D photon-counting detector. Sensors 17, 1–11. https://doi.org/10.3390/s17020269.

Franck, C., Lammertyn, J., Ho, Q.T., Verboven, P., Verlinden, B., Nicolaï, B.M., 2007. Browning disorders in pear fruit. Postharvest Biol. Technol. 43, 1–13. https://doi.org/10.1016/j.postharvbio.2006.08.008.

Goh, T.Y., Basah, S.N., Yazid, H., Safar, M.J.A., Saad, F.S.A., 2018. Performance analysis of image thresholding: Otsu technique. Meas. J. Int. Meas. Confed. 114, 298–307. https://doi.org/10.1016/j.measurement.2017.09.052.

Haff, R.P., Slaughter, D.C., Sarig, Y., Kader, A., 2006. X-ray assessment of translucency in pineapple. J. Food Process. Preserv. 30, 527–533. https://doi.org/10.1111/j.1745-4549.2006.00086.x.

Haff, R.P., Toyofuku, N., 2008. X-ray detection of defects and contaminants in the food industry. Sens. Instrum. Food Qual. Saf. 2, 262–273. https://doi.org/10.1007/s11694-008-9059-8.

Hasan, M.K., Sadi, F., Lee, S.Y., 2012. Removal of ring artifacts in micro-CT imaging using

iterative morphological filters. Signal, Image Video Process. 6, 41–53. https://doi.org/10.1007/s11760-010-0170-z.

Herremans, E., 2014. X - ray CT to detect internal structures in apple fruit. From high-resolution 3D microstructure imaging towards fast screening tools. PhD dissertation, Division of MeBioS, KU Leuven, Leuven, Belgium.

Herremans, E., Melado-Herreros, A., Defraeye, T., Verlinden, B., Hertog, M., Verboven, P., Val, J., Fernández-Valle, M.E., Bongaers, E., Estrade, P., Wevers, M., Barreiro, P., Nicolaï, B.M., 2014a. Comparison of X-ray CT and MRI of watercore disorder of different apple cultivars. Postharvest Biol. Technol. 87, 42–50. https://doi.org/10.1016/j.postharvbio.2013.08.008.

Herremans, E., Verboven, P., Bongaers, E., Estrade, P., Verlinden, B.E., Wevers, M., Hertog, M.L.A.T.M., Nicolaï, B.M., 2013. Characterisation of 'Braeburn' browning disorder by means of X-ray micro-CT. Postharvest Biol. Technol. 75, 114–124. https://doi.org/10.1016/j.postharvbio.2012.08.008.

Herremans, E., Verboven, P., Defraeye, T., Rogge, S., Ho, Q.T., Hertog, M.L.A.T.M., Verlinden, B.E., Bongaers, E., Wevers, M., Nicolaï, B.M., 2014b. X-ray CT for quantitative food microstructure engineering: The apple case. Nucl. Instruments Methods Phys. Res. Sect. B Beam Interact. with Mater. Atoms 324, 88–94. https://doi.org/10.1016/j.nimb.2013.07.035.

Herremans, E., Verboven, P., Hertog, M.L.A.T.M., Cantre, D., Van Dael, M., de Schryver, T., van Hoorebeke, L., Nicolaï, B.M., 2015a. Spatial development of transport structures in apple (*Malus* × *domestica* Borkh.) fruit. Front. Plant Sci. 6, 1–14. https://doi.org/10.3389/fpls.2015.00679.

Herremans, E., Verboven, P., Verlinden, B.E., Cantre, D., Abera, M., Wevers, M., Nicolaï, B.M., 2015b. Automatic analysis of the 3-D microstructure of fruit parenchyma tissue using X-ray micro-CT explains differences in aeration. BMC Plant Biol. 15, 1–14. https://doi.org/10.1186/s12870-015-0650-y.

Ho, Q.T., Verboven, P., Verlinden, B.E., Herremans, E., Wevers, M., Carmeliet, J., Nicolaï, B.M., 2011. A three-dimensional multiscale model for gas exchange in fruit. Plant Physiol. 155, 1158–1168. https://doi.org/10.1104/pp.110.169391.

Iassonov, P., Gebrenegus, T., Tuller, M., 2009. Segmentation of X-ray computed tomography images of porous materials: A crucial step for characterization and quantitative analysis of pore structures. Water Resour. Res. 45, 1–12. https://doi.org/10.1029/2009WR008087.

Janssen, S., Verboven, P., Nugraha, B., Wang, Z., Boone, M., Josipovic, I., Nicolaï, B.M., 2020. 3D pore structure analysis of intact 'Braeburn' apples using X-ray micro-CT. Postharvest Biol. Technol. 159, 111014. https://doi.org/10.1016/j.postharvbio.2019.111014.

Jarolmasjed, S., Espinoza, C.Z., Sankaran, S., Khot, L.R., 2016. Postharvest bitter pit detection and progression evaluation in 'Honeycrisp' apples using computed tomography images. Postharvest Biol. Technol. 118, 35–42. https://doi.org/10.1016/j.postharvbio.2016.03.014.

Kalender, W.A., 2011. Computed tomography: fundamentals, system technology, image quality, applications. John Wiley & Sons.

Karmoker, P., Obatake, W., Tanaka, F, Tanaka, F, 2019. Visualization of porosity and thermal conductivity distributions of Japanese apricot and pear during storage using X-ray computed tomography. Eng. Agric. Environ. Food 12, 505–510. https://doi.org/https://doi.org/10.1016/j.eaef.2019.11.002.

Kelkar, S.M., 2013. Using X-ray Imaging Techniques to Determine Density of Foods. PhD dissertation, Purdue University, Indiana, United States of America.

Kotwaliwale, N., Singh, K., Kalne, A., Jha, S.N., Seth, N., Kar, A., 2014. X-ray imaging methods for internal quality evaluation of agricultural produce. J. Food Sci. Technol. 51, 1–15. https://doi.org/10.1007/s13197-011-0485-y.

Kritzinger, I., Lötze, E., Jooste, M., 2017. Stone hardening and broken stones in Japanese plums

(*Prunus salicina Lindl.*) evaluated by means of computed tomography scans. Sci. Hortic. 221, 1–9. https://doi.org/10.1016/j.scienta.2017.04.008.

Lammertyn, J., Dresselaers, T., Van Hecke, P., Jancsok, P., Wevers, M., Nicolaï, B.M., 2003. MRI and X-ray CT study of spatial distribution of core breakdown in 'Conference' pears. Magn. Reson. Imaging 21, 805–815. https://doi.org/10.1016/S0730-725X(03)00105-X.

Landis, E.N., Keane, D.T., 2010. X-ray microtomography. Mater. Charact. 61, 1305–1316. https://doi.org/10.1016/j.matchar.2010.09.012.

Lim, K.S., Barigou, M., 2004. X-ray micro-computed tomography of cellular food products. Food Res. Int. 37, 1001–1012. https://doi.org/10.1016/j.foodres.2004.06.010.

Magwaza, L.S., Opara, L.U., 2014. Investigating non-destructive quantification and characterization of pomegranate fruit internal structure using X-ray computed tomography. Postharvest Biol. Technol. 95, 1–6. https://doi.org/10.1016/j.postharvbio.2014.03.014.

Maire, E., Fazekas, A., Salvo, L., Dendievel, R., Youssef, S., Cloetens, P., Letang, M.J., 2003. X-ray tomography applied to the characterization of cellular materials . Related finite element modeling problems. Compos. Sci. Technol. 63, 2431–2443. https://doi.org/10.1016/S0266-3538(03)00276-8.

Maire, E., Withers, P.J., 2014. Quantitative X-ray tomography. Int. Mater. Rev. 59, 1–43. https://doi.org/10.1179/1743280413Y.0000000023.

Mendoza, F., Verboven, P., Ho, Q.T., Kerckhofs, G., Wevers, M., Nicolaï, B., 2010. Multifractal properties of pore-size distribution in apple tissue using X-ray imaging. J. Food Eng. 99, 206–215. https://doi.org/10.1016/j.jfoodeng.2010.02.021.

Mendoza, F., Verboven, P., Mebatsion, H.K., Kerckhofs, G., Wevers, M., Nicolaï, B., 2007. Three-dimensional pore space quantification of apple tissue using X-ray computed microtomography. Planta 226, 559–570. https://doi.org/10.1007/s00425-007-0504-4.

Münch, B., Trtik, P., Marone, F., Stampanoni, M., 2009. Stripe and ring artifact removal with

combined wavelet-Fourier filtering. Opt. Express 17, 8567–8591. https://doi.org/10.1364/oe.17.008567.

Muziri, T., Theron, K.I., Cantre, D., Wang, Z., Verboven, P., Nicolaï, B.M., Crouch, E.M., 2016. Microstructure analysis and detection of mealiness in 'Forelle' pear (*Pyrus communis* L.) by means of X-ray computed tomography. Postharvest Biol. Technol. 120, 145–156. https://doi.org/10.1016/j.postharvbio.2016.06.006.

Nicolaï, B.M., Defraeye, T., Ketelaere, B. De, Herremans, E., Hertog, M.L.A.T.M., Saeys, W., Torricelli, A., Vandendriessche, T., Verboven, P., 2014. Nondestructive measurement of fruit and vegetable quality. Annu. Rev. Food Sci. Technol. 5, 285–312. https://doi.org/10.1146/annurev-food-030713-092410.

Nugraha, B., Verboven, P., Janssen, S., Wang, Z., Nicolaï, B.M., 2019. Non-destructive porosity mapping of fruit and vegetables using X-ray CT. Postharvest Biol. Technol. 150, 80–88. https://doi.org/10.1016/j.postharvbio.2018.12.016.

Otsu, N., 1979. A threshold selection method from gray-level histograms. IEEE Trans. Syst. Man Cybern. 9, 62–66.

Poles, L., Gentile, A., Giuffrida, A., Valentini, L., Endrizzi, I., Aprea, E., Gasperi, F., Distefano, G., Artioli, G., La Malfa, S., Costa, F., Lovatti, L., Di Guardo, M., 2020. Role of fruit flesh cell morphology and MdPG1 allelotype in influencing juiciness and texture properties in apple. Postharvest Biol. Technol. 164, 111161. https://doi.org/10.1016/j.postharvbio.2020.111161.

Prawiranto, K., Defraeye, T., Derome, D., Bühlmann, A., Hartmann, S., Verboven, P., Nicolaï, B., Carmeliet, J., 2019. Impact of drying methods on the changes of fruit microstructure unveiled by X-ray micro-computed tomography. RSC Adv. 9, 10606–10624. https://doi.org/10.1039/C9RA00648F.

Rashid, S., Lee, S.Y., Hasan, M.K., 2012. An improved method for the removal of ring artifacts in high resolution CT imaging. J. Adv. Signal Process. 2012, 1–18.

https://doi.org/10.1186/1687-6180-2012-93.

Ruparelia, S., 2012. Implementation of Watershed Based Image Segmentation Algorithm in FPGA. Master's thesis, Department of Parallel Systems, University of Stuttgart, Stuttgart, Germany.

Salvo, L., Suéry, M., Marmottant, A., Limodin, N., Bernard, D., 2010. 3D imaging in material science : Application of X-ray tomography. Comptes Rendus Phys. 11, 641–649. https://doi.org/10.1016/j.crhy.2010.12.003.

Schoeman, L., Williams, P., du Plessis, A., Manley, M., 2016. X-ray micro-computed tomography (μCT) for non-destructive characterisation of food microstructure. Trends Food Sci. Technol. 47, 10-24. https://doi.org/10.1016/j.tifs.2015.10.016.

Sinka, I.C., Burch, S.F., Tweed, J.H., Cunningham, J.C., 2004. Measurement of density variations in tablets using X-ray computed tomography. Int. J. Pharm. 271, 215–224. https://doi.org/10.1016/j.ijpharm.2003.11.022.

Tanaka, F, Imamura, K., Tanaka, F, Uchino, T., 2018a. Determination of thermal diffusivity of persimmon flesh tissue using three-dimensional structure model based on X-ray computed tomography. J. Food Eng. 221, 151–157. https://doi.org/10.1016/j.jfoodeng.2017.10.021.

Tanaka, F, Nashiro, K., Obatake, W., Tanaka, F., Uchino, T., 2018b. Observation and analysis of internal structure of cucumber fruit during storage using X-ray computed tomography. Eng. Agric. Environ. Food 11, 51–56. https://doi.org/10.1016/j.eaef.2017.12.004.

Ting, V.J.L., Silcock, P., Bremer, P.J., Biasioli, F., 2013. X-ray micro-computer tomographic method to visualize the microstructure of different apple cultivars. J. Food Sci. 78, E1735–E1742. https://doi.org/10.1111/1750-3841.12290

Vågberg, W., Larsson, J.C., Hertz, H.M., 2017. Removal of ring artifacts in microtomography by characterization of scintillator variations. Opt. Express 25, 23191–23198. https://doi.org/10.1364/OE.25.023191.

Van Dael, M., Lebotsa, S., Herremans, E., Verboven, P., Sijbers, J., Opara, U.L., Cronje, P.J., Nicolaï, B.M., 2016. A segmentation and classification algorithm for online detection of internal disorders in citrus using X-ray radiographs. Postharvest Biol. Technol. 112, 205–214. https://doi.org/10.1016/j.postharvbio.2015.09.020.

Van De Looverbosch, T., Rahman Bhuiyan, M.H., Verboven, P., Dierick, M., Van Loo, D., De Beenbouwer, J., Sijbers, J., Nicolaï, B., 2020. Nondestructive internal quality inspection of pear fruit by X-ray CT using machine learning. Food Control 113, 107170. https://doi.org/10.1016/j.foodcont.2020.107170.

Verboven, P., Herremans, E., Borisjuk, L., Helfen, L., Ho, Q.T., Tschiersch, H., Fuchs, J., Nicolaï, B.M., Rolletschek, H., 2013. Void space inside the developing seed of Brassica napus and the modelling of its function. New Phytol. 199, 936–947. https://doi.org/10.1111/nph.12342.

Vicent, V., Verboven, P., Ndoye, F.T., Alvarez, G., Nicolaï, B., 2017. A new method developed to characterize the 3D microstructure of frozen apple using X-ray micro-CT. J. Food Eng. 212, 154–164. https://doi.org/10.1016/j.jfoodeng.2017.05.028.

Wang, J., Lu, H., Liang, Z., Eremina, D., Zhang, G., Wang, S., Chen, J., Manzione, J., 2008. An experimental study on the noise properties of X-ray CT sinogram data in Radon space. Phys. Med. Biol. 53, 3327–3341. https://doi.org/10.1088/0031-9155/53/12/018.An.

Wang, Z., Herremans, E., Janssen, S., Cantre, D., Verboven, P., Nicolaï, B., 2018. Visualizing 3D food microstructure using tomographic methods: Advantages and disadvantages. Annu. Rev. Food Sci. Technol. 9, 323–343. https://doi.org/10.1146/annurev-food-030117-012639.

Wang, Z., Van Beers, R., Aernouts, B., Watté, R., Verboven, P., Nicolaï, B., Saeys, W., 2020. Microstructure affects light scattering in apples. Postharvest Biol. Technol. 159, 110996. https://doi.org/10.1016/j.postharvbio.2019.110996.

Wang, Z., Verboven, P., Nicolaï, B., 2017. Contrast-enhanced 3D micro-CT of plant tissues using different impregnation techniques. Plant Methods 13, 1–16. https://doi.org/10.1186/s13007-017-0256-5.

Warning, A., Verboven, P., Nicolaï, B., Van Dalen, G., Datta, A.K., 2014. Computation of mass transport properties of apple and rice from X-ray microtomography images. Innov. Food Sci. Emerg. Technol. 24, 14–27. https://doi.org/10.1016/j.ifset.2013.12.017.

Wei, Z., Wiebe, S., Chapman, D., 2013. Ring artifacts removal from synchrotron CT image slices. J. Instrum. 8, C06006. https://doi.org/10.1088/1748-0221/8/06/C06006.

Wernersson, E.L.G., Boone, M.N., Van Den Bulcke, J., Van Hoorebeke, L., Hendriks, C.L.L., 2014. Understanding phase contrast artefacts in micro computed absorption tomography, in: SSBA Symposium Proceedings. Swedish Society for Automated Image Analysis (SSBA).

Zhang, P, Lu, S., Li, J., Zhang, Ping, Xie, L., Xue, H., Zhang, J., 2017. Multi-component segmentation of X-ray computed tomography (CT) image using multi-Otsu thresholding algorithm and scanning electron microscopy. Energy Explor. Exploit. 35, 281–294. https://doi.org/10.1177/0144598717690090.

# LITERATURE REVIEW 2

## Factors influencing the incidence of internal browning in apples – A Review

**Abstract**

Apples are important to the South African economy and it is important to ensure that fruit of high quality are available for the local and export market all year round. The long-term storage of apples is limited by the incidence of internal browning (IB). IB is a physiological disorder characterized by brown patches with or without cavities that develop in the fruit flesh. Apples with IB have an aesthetically unpleasant internal appearance that is normally accompanied by off-flavors and this drastically reduces their marketability. IB types include radial, diffuse, $CO_2$ damage and core-flush browning. The objective of this literature study was to review different pre- and post-harvest factors that affect the incidence of IB in apples. This review also looked at how fruit microstructure (porosity) affects the storability of apples. IB symptoms arise from the activity of polyphenol oxidase (PPO) which oxidises phenols to brown coloured polymers. Pre-harvest factors reviewed in this literature study include cultivar differences, climate, mineral composition and watercore incidence. Even though IB is not visible at harvest, pre-harvest factors influence the expression of IB during post-harvest storage. The effect of fruit maturity at harvest on the expression of IB was also reviewed. Different storage regimes such as controlled atmosphere (CA) and delayed CA storage are used in post-harvest storage of fruit and their effects on IB incidence were also reviewed. Fruit tissue microstructure affects the diffusivity of metabolic gases and so this review also looked at the role of microstructure on fruit quality and IB expression during storage.

**Keywords:** Apples, controlled atmosphere, internal browning, polyphenol oxidase, post-harvest, pre-harvest.

## 1. Introduction

Apples are important to the South African agricultural sector with over 35 million trees planted on 24 970 hectares as of 2019, the major cultivars being Golden Delicious, Royal Gala and Granny Smith (HORTGRO, 2019). In terms of export volumes, 423 394 tonnes of apples were passed for export in 2019, predominantly to Far Eastern, Asian and African markets (HORTGRO, 2019). To ensure all year availability, fruit must be stored for extended periods of time under controlled environments such as controlled atmosphere (CA) storage. CA storage utilizes an elevated $CO_2$ and low $O_2$ concentration to suppress fruit respiration and fruit softening thereby increasing the storage life of the fruit (Volz et al., 1998; Gonzalez et al., 2001). Although beneficial in many ways, CA storage can result in fruit developing internal disorders such as internal browning (IB). IB is characterized by brown patches with or without cavities in the fruit flesh (Fig. 1). Apples with IB have an aesthetically unpleasant internal appearance that is normally accompanied by off-flavors and this drastically reduces the marketability and value of such apples (Di Guardo et al., 2013).

Different IB types occur in apples and they vary depending on their location within the apple tissue and severity. Radial and diffuse browning have been identified in ‘Cripps’ Pink’ apples (de Castro et al., 2007; James and Jobling, 2009). Radial browning has been identified as a senescence related disorder which is a result of fractured cell walls in the vascular tissue, while diffuse browning is a result of the collapse of cortical cells (de Castro et al., 2007; James and Jobling, 2009). As a result, radial browning mainly affects the vascular tissue while diffuse browning normally affects the cortical fruit tissue (James and Jobling, 2009). IB in apples has been attributed to the activity of the metalloenzyme polyphenol oxidase (PPO). Membrane damage due to the creation of hypoxic or anoxic conditions within the fruit and loss of compartmentalization results in the mixing of oxidative enzymes located in the plastids and

phenolic substrates located in the vacuole, a series of oxidation reactions and the production of brown coloured polymers in the apple flesh (Mellidou et al., 2014).

Many factors affect the incidence of IB in ‘Fuji’ apples. These can be classified into pre- and post-harvest factors. Type of apple cultivar is an important factor affecting browning. Some cultivars have been found to be more prone to IB as compared to others, and this is dependent upon phenolic content, activity of PPO and microstructural properties such as porosity (Hatoum et al., 2016). Climatic factors such as humidity, solar radiation and temperature during growth have a significant impact on the development of IB in apples (Rogers, 2014). Mineral nutrition is also a major determinant for browning incidence (Telias et al., 2006). In particular, calcium deficiency has been shown to be involved in a number of post-harvest disorders such as bitter pit and IB, this can be attributed to its role in the stability of cell membranes (Telias et al., 2006; de Freitas et al., 2010; Falchi et al., 2017). To achieve optimum quality and colour, ‘Fuji’ apples are sometimes harvested at advanced maturity, this has a negative impact of making fruit more susceptible to IB during storage (Argenta et al., 2001; Kweon et al., 2013). Storage conditions after harvest such as CA and delayed CA also affect IB incidence (Argenta et al., 2002b; Kweon et al., 2012).

The objective of this literature study was to review different pre- and post-harvest factors that affect the incidence of IB in apples. This review also looks at how fruit microstructure (porosity) affects the storability of apples.

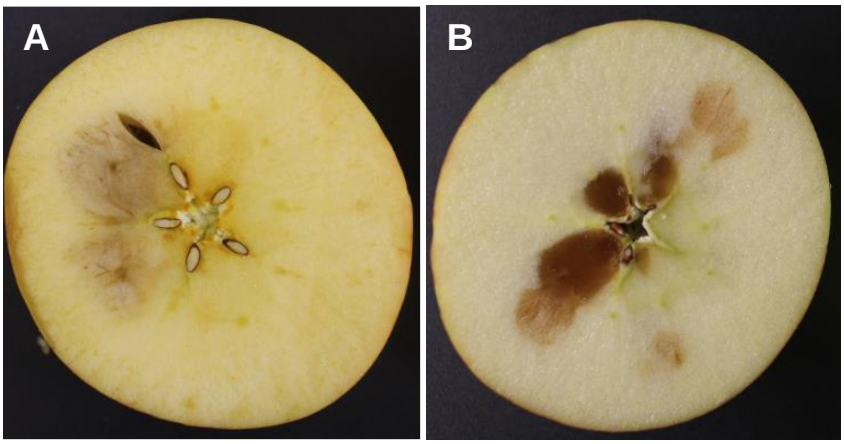


**Fig. 1.** 'Fuji' apples affected by internal browning (IB) with cavities (A) and without cavities (B).

## 2. Enzymatic browning

Enzymatic browning in apples can be classified into functional browning or adventitious browning (Hopfinger et al., 1984). Functional browning refers to browning reactions such as browning of seed coats which occurs during normal fruit development while adventitious browning which occurs during post-harvest storage as a result of cellular disruption is of greater concern to post-harvest physiologists (Hopfinger et al., 1984). Phenolic compounds are the most important secondary metabolites in fruit and vegetables, and they are responsible for colour, flavour and nutritional qualities (Holderbaum et al., 2010). Although the aetiology of IB in apples is not fully understood, the activity of PPO makes the IB symptoms visible. Enzymatic browning can be defined as the oxidation of polyphenols to quinones and is mainly associated with the activity of PPO (Hopfinger et al., 1984; Veltman, 2002; de Castro et al., 2008; Ma et al., 2015). PPO is a metalloenzyme with two copper-binding domains, CuA and CuB, which interact with molecular $O_2$ and phenolic substances (Di Guardo et al., 2013). Quinones are highly reactive and undergo further polymerisation and oxidation to form insoluble brown pigments known as melanins inside the fruit cortex (Nicolas et al., 1994; Veltman, 2002). Phenolic compounds are stored in the vacuole whereas PPO is stored in the plastids, loss of compartmentalization causes the mixing of PPO and the phenolic compounds leading to oxidation reactions (Fig. 2; Holderbaum et al.,

2010; Di Guardo et al., 2013). De-compartmentalization occurs when cells undergo low oxygen stress such that they are rendered incapable of repairing damage to membranes caused by reactive oxygen species (ROS; Hatoum et al., 2016). ROS are normally produced as by-products in cellular respiration.

The control of enzymatic browning is very critical to the horticultural industry because it affects quality attributes of fruit and vegetables. A study conducted by Holderbaum et al. (2010) to determine the phenolic composition of four different apple cultivars (Aori27, Elstar, Fuji, and Mellow) showed that Fuji apples had the highest phenolic content at harvest as compared to the other apple cultivars used in the study. This may be the reason why 'Fuji' apples are more prone to develop IB as compared to other apple cultivars. The susceptibility of different apple cultivars to IB is determined by the phenolic content, chlorogenic acid content as well as activity of PPO (Amiot et al., 1992). Amiot et al. (1992) further highlighted that apple cultivars with a low content of chlorogenic acid are at a lower risk of developing IB during long-term storage. Chlorogenic acid is a natural substrate of PPO and its oxidation gives rise to pigments that are able to co-oxidise many other substances (Amiot et al., 1992). The activity of PPO has also been shown to be increased by 1-Methylcyclopropene (1-MCP). A study by Hatoum et al. (2014) showed that the use of 1-MCP treatments on apples increased the activity of PPO which is responsible for enzymatic browning. This may be because 1-MCP inhibits ethylene production which in turn reduces the respiration rate and results in lower energy levels in cells, reducing their ability to maintain cellular integrity, this often happens when fruit are harvested too early (Hatoum et al., 2014). In their research on 'Empire' apples, Ma et al. (2015) found that the application of 1-MCP significantly increased the manifestation of IB and the disorder was more pronounced in the stem-end as compared to the calyx-end of the fruit. A study by Lafer (2006) on 'Golden Delicious' apples showed that overripe apples treated with 1-MCP had significantly higher levels of IB.

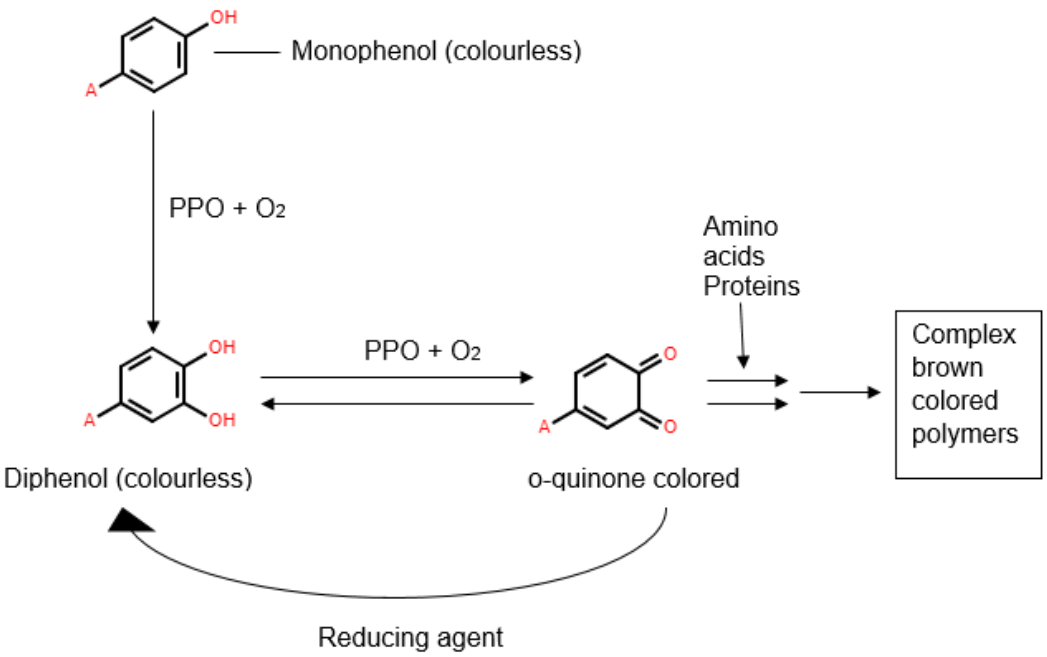


**Fig. 2.** Simple schematic representation of an enzymatic browning reaction (Based on Veltman, 2002).

## 3. Pre-harvest factors

### *3.1. Cultivar*

The incidence of IB in apples has been shown to be genotype specific and varies depending on the cultivar (Hatoum et al., 2016). In studies done by Hatoum et al. (2016), it was found that 'Jonagold' apples did not develop IB under the different pre- and post-harvest treatment combinations, whereas 'Braeburn' apples subjected to those same treatment combinations developed IB. The resistance of 'Jonagold' apples to developing IB during long-term storage has also been reported by Saquet et al. (2000). The susceptibility of different apple cultivars to IB has been found to be correlated to the level of phenolic compounds and activity of PPO, which is a catalyst of the browning reaction (Milani and Hamedi, 2005). According to research by Milani and Hamedi (2005), 'Red Delicious' apples had the highest polyphenol content and the highest rate of IB incidence (Milani and Hamedi, 2005).

A study by Holderbaum et al. (2010) in four different apple cultivars showed that there are varietal differences in terms of susceptibility to IB. The study which was done on 'Elstar', 'Fuji', 'Mellow' and 'Aori27' showed that 'Fuji' apples had the highest phenolic content at harvest and were more susceptible to IB incidence (Holderbaum et al., 2010). As a result of the high phenolic content, 'Fuji' is more suitable for fresh consumption while 'Aori27' is more suitable for fruit processing due to its low risk of enzymatic browning resulting from the low phenolic content and low PPO activity (Holderbaum et al., 2010).

Another factor that may affect susceptibility of different apple cultivars to browning is the structure of the intercellular air spaces (pores). Differences in the porosity of different apple cultivars has been investigated by Ting et al. (2013). The study which was done on 'Fuji', 'Scifresh' (Jazz$^{TM}$), 'Golden Delicious' and 'Braeburn' showed that 'Scifresh' (Jazz$^{TM}$) apples had the least porosity (17%) in the outer cortex region, this low porosity may make 'Scifresh' (Jazz$^{TM}$) more susceptible to cortical browning because pores are important channels for the movement of respiratory gases. The study also found that 'Fuji' apples contained a high number of small intercellular spaces, these small intercellular air spaces may have a negative effect on the gas transport properties of 'Fuji' making it susceptible to IB during long-term storage (Ting et al., 2013). This maybe the reason why 'Fuji' is more susceptible to IB as compared to other cultivars. However, this relationship between porosity and IB incidence still needs to be quantitatively ascertained.

*3.2. Climate*

Climatic factors such as humidity, solar radiation and temperature during growth have a significant impact on the development of IB in apples (Rogers, 2014). James et al. (2010) highlighted that climatic conditions during growth and development of 'Cripps' Pink' apples is

related to the expression of either diffuse or radial flesh browning during long-term storage. A major climatic factor that influences the incidence of IB is the accumulation of growing degree days (GDD) above 10 °C or accumulated heat units over the season (Bergman et al., 2012; Butler, 2015). Different types of IB as influenced by growing degree days have been identified in 'Cripps' Pink' apples in Australia. Diffuse browning in Australia occurs in cooler areas and is related to chilling injury (Bergman et al., 2012). Rogers (2014) highlighted that diffuse browning mainly occurs in regions where less than 1100 GDD above 10 °C are accumulated between full bloom and harvest. Cooler growing regions have also been found to increase the incidence of internal cavities in 'Braeburn' apples. A study by Lau (1998) showed that storing fruit in CA conditions after cool growing seasons increased the incidence of 'Braeburn' browning disorder and internal cavities. Research by Tong et al. (2016) showed that low temperatures at approximately 60 days after full bloom (DAFB) when 'Honeycrisp' fruit cells are actively growing (early cell expansion) were positively correlated with post-harvest diffuse browning incidence. They attributed this to the disruption of normal fruit growth by these low temperatures rendering the fruit incapable of acclimating normally to low temperatures during storage resulting in diffuse browning incidence.

According to Rogers (2014), radial flesh browning occurs in regions where between 1100 to 1700 GDD above 10 °C are accumulated between full bloom and harvest, and fruit grown in regions which accumulate more than 1700 GDD above 10 °C are not at risk of developing either diffuse or radial browning. Butler (2015) also identified another type of IB in 'Cripps' Pink' apples which exhibited patterns of both diffuse and radial browning. This type of browning was referred to as combination browning, Butler (2015) highlighted that combination browning was influenced by fruit size and not pre-harvest temperature. In their study on 'Cripps' Pink' apples to compare the incidence of IB of two climatically different apple production regions in South Africa, Butler (2015) found that diffuse browning was the main type of browning found in both growing regions, both growing regions accumulated more than 1500 GDD above 10 °C. These findings are in

contrast to the Australian flesh browning model by James (2007) which suggest that South African conditions do not promote the incidence of diffuse flesh browning. The diffuse browning observed seems to be more related to lower storage temperatures. The study by Butler (2015) showed that no radial browning occurred in the warmer season while it occurred in the cooler season. A better understanding of climatic conditions that predispose fruit to different browning types would allow farmers to better forecast IB incidence and optimize storage conditions (Tong et al., 2016).

### *3.3. Mineral composition (calcium and potassium)*

Mineral elements are crucial for fruit development and the incidence of IB in apples is affected by the mineral composition (James, 2007). As highlighted by James (2007), minerals of specific importance in apples include boron, calcium, copper, iron, magnesium, manganese, phosphorus, potassium and zinc. However, calcium seems to play a much bigger role in determining post-harvest quality of apples due to its role in membrane integrity and stability (Bergman et al., 2012). The influence of low calcium on the incidence of bitter pit in apples has been extensively studied (Telias et al., 2006; de Freitas et al., 2010; Falchi et al., 2017). A study by Telias et al. (2006) showed that calcium sprays were effective in reducing the incidence of bitter pit in ‘Honeycrisp’ apple. Low calcium content within the fruit has been linked to the increased incidence of IB during CA storage (Argenta et al., 2001; Corrêa et al., 2017). High levels of magnesium, potassium and nitrogen within the fruit have been shown to increase the incidence of IB in apples (Miqueloto et al., 2014). However, Butler (2015) found that ‘Cripps’ Pink’ fruit with higher levels of potassium and magnesium had lower IB incidence. Additionally, older trees with high potassium and magnesium levels exhibited less IB (Butler, 2015). Potassium is known to compete with calcium for uptake from the soil (Danner et al., 2015) and so high potassium content in the soil may lead to low calcium uptake and increased risk of IB incidence (Hatoum et al., 2016). High levels of potassium and magnesium coupled with satisfactory amounts of calcium within the fruit may induce physiological disorders during cold storage of fruit (Brackmann and Ribeiro,

1992). Magnesium and potassium compete with calcium for binding sites in the cell and so their increased availability may limit the availability of calcium (Falchi et al., 2017).

Calcium is an indispensable component of cell walls and the middle lamella and hence it influences post-harvest quality and storability of fruit (Brackmann and Ribeiro, 1992). The rate of calcium transport is highly dependent on the rate of xylem water mass flow and therefore most of the calcium is accumulated during the fruit set phase when transpiration is at its peak (Hocking et al., 2016). In addition, there is loss of xylem functionality during fruit growth and this has been associated with an increase in number and elongation of parenchyma cells, which raptures the xylem vessels without affecting the phloem vessels (Miqueloto et al., 2014). This results in low levels of calcium in the fruit because the phloem does not translocate enough calcium (Brackmann and Ribeiro, 1992). As a result, calcium concentration within the fruit is diluted as the fruit continues to increase in size. This may explain why bigger fruit are more likely to develop IB as compared to smaller fruit. In addition, calcium normally accumulates in the vacuoles of plant cells and this can trigger localized depletion of apoplastic calcium ions leading to increased membrane leakage and plasmolysis (de Freitas et al., 2010). Shortage of calcium leads to increased membrane permeability and this promotes de-compartmentalization which increases the risk of IB (Brackmann and Ribeiro, 1992). A study by Shirzadeh et al. (2011) to determine if calcium dips were effective in improving quality maintenance in ‘Jonagold’ apples showed that calcium reduced respiration rate and improved firmness of the apples. de Castro et al. (2007) found that increased calcium content in ‘Cripps’ Pink’ apples reduced the risk of fruit developing IB during storage. A study by Neuwald et al. (2013) on organically grown ‘Santana’ apples in Germany showed that weekly calcium sprays starting from June drop until harvest, significantly reduced IB incidence during CA storage. ‘Fuji’ apples with IB have been found to contain lower levels of calcium as compared to non-brown fruit (Corrêa et al., 2017). In their study, Corrêa et al. (2017) found that calcium was the only mineral with a close relationship to the incidence of IB

in ‘Fuji’ during storage. They further highlighted that ‘Fuji’ apples with a low calcium content are at a higher risk of developing IB during long-term storage. Boron is also an important mineral that affects incidence of IB, boron helps in stabilizing both the cell wall and the cell membrane (de Castro et al., 2008).

*3.4. Impact of watercore on IB incidence*

Watercore is a physiological disorder that occurs whilst fruit are still on the tree and is characterized by hard and water-soaked areas in the fruit flesh (Bowen and Watkins, 1997; Argenta et al., 2002a; Neuwald et al., 2012). Watercore has generally been associated with late harvested fruit, a dramatic increase in watercore percentage was observed as the fruit weight and percentage soluble solids increased (Bowen and Watkins, 1997). The disorder occurs in different apple cultivars but the variation in its incidence from one season to the next makes it a difficult disorder to study (Bowen and Watkins, 1997). Watercore has also been found to occur in pears. The incidence of watercore in Japanese pear ‘Niitaka’ was significantly increased when temperatures around the fruit were increased during fruit maturation (Hayama et al., 2014). High temperatures influence processes such as photosynthesis, respiration, transpiration and nutrient absorption, these factors can interact with each other to cause watercore (Hayama et al., 2004). Factors causing the development of watercore at high temperatures remain poorly understood. The increased incidence of watercore due to an increase in air temperature to above 30 °C during fruit growth was also reported in ‘Tsugaru’ Apples (Yamada et al., 1998). However, Yamada et al. (2004) found that watercore in ‘Fuji’ apples mostly developed at low temperatures of between 7 and 10 °C and did not occur at 25 °C. Low temperatures reduce evapotranspiration and this increases the water status of the fruit causing water-soaked conditions in the fruit tissue (Yamada et al., 2004). Ferguson et al. (1999) identified two types of watercore (early and late) and both were related to sink issues in phloem unloading. The intercellular spaces in watercored apples

are flooded with water that has a high sorbitol and sucrose concentration and low glucose and fructose concentration (Argenta et al., 2002a).

Although watercore is desired by some Japanese customers as a sign of full ripeness, it can potentially lead to the development of IB during storage (Kasai and Arakawa, 2010). The flooding of intercellular spaces renders them unable to efficiently execute their role of facilitating gaseous exchange within the fruit and results in the development of stress conditions (Argenta et al., 2002a). Such stress conditions within the fruit can lead to the onset of anaerobic respiration and development of internal disorders such as IB. According to Argenta et al. (2002a), severe watercore of 'Jonathan' apples at harvest is linked to anaerobic respiration and accumulation of ethanol, acetaldehyde and ethyl acetate possibly leading to internal breakdown of fruit during long-term CA storage. A study by Kweon et al. (2012) on Korean 'Fuji' apples showed that watercore incidence increased in late harvested fruit and that watercore was correlated to the development of flesh browning during CA storage.

Oxidative stress is an important aspect in the development of IB, this is shown by the reduced incidence of IB as a result of the application of diphenylamine (DPA) before long-term CA storage (de Castro et al., 2008). A study by Kasai and Arakawa (2010), in 'Fuji' apples showed that anti-oxidant levels were reduced, and hydrogen peroxide levels were always higher in watercored tissue as compared to non-watercored tissue. The increased resistance to gas diffusion in watercored tissue leads to an increased $pCO_2$ and onset of hypoxic conditions which inhibit alternative oxidase (AOX) and stimulates the production of hydrogen peroxide (Kasai and Arakawa, 2010; Rhoads et al., 2006).

The plant electron transport chain consists of two terminal oxidases, cytochrome c oxidase (COX) which reduces $O_2$ in the cytochrome pathway, and the alternative oxidase (AOX) involved in ubiquinone reduction (Rhoads et al., 2006). If the activities of these two oxidases are reduced,

ROS activity may increase leading to the development of IB, although the relationship is not clear-cut (Kasai and Arakawa, 2010). Kasai and Arakawa (2010) found that most of the watercore in 'Fuji' apples dissipated after 5 months of CA storage, however, the antioxidant levels in cells previously affected by watercore remained low even after the complete dissipation of watercore. Storage of 'Fuji' apples at a low $CO_2$ partial pressure (<1 kPa) increases the rate of disappearance of watercore, although this may have a negative impact on other fruit quality attributes (Kweon et al., 2013). In addition, Kasai and Arakawa (2010) suggested that the enhanced activity of the enzyme ascorbate peroxidase in watercored tissue consumes anti-oxidants such as ascorbic acid and this results in low levels of antioxidants and increased susceptibility to IB incidence. Kasai and Arakawa (2010) further highlighted that since watercore develops whilst fruit is still on the tree, the activity of ascorbate peroxidase as well as production of hydrogen peroxide may also be increased before harvest in watercored tissues. This means that the antioxidant levels in watercored tissue is already low at harvest and this predisposes watercored fruit to IB incidence.

## 4. Post-harvest factors

### *4.1. Fruit maturity (picking date)*

Harvest maturity is considered an important aspect in the susceptibility of 'Fuji' apples to IB during CA storage (Argenta et al., 2001; Kweon et al., 2013). Kweon et al. (2013) found that both watercore and flesh browning incidence increased with advancing maturity. According to the study, IB incidence increased with fruit maturity after 180 DAFB, it is therefore recommended that 'Fuji' apples should not be harvested later than 180 DAFB (Kweon et al., 2013). Kweon et al. (1998) found that over-mature 'Fuji' apples still exhibited IB during CA storage even though the establishment of CA storage was delayed for 4 weeks. Research done by Grant et al. (1996) has shown that 'Fuji' apples harvested earlier than 180 DAFB developed very little IB even when stored at elevated $CO_2$ concentration (1.5 and 3% $CO_2$). In addition, Volz and Mitcham (1997) also found that $CO_2$ induced IB incidence in 'Fuji' apples increased with advancing maturity. A

study by Parker and Guerra (2008) showed that mature 'Fuji' apples have clumps of small, elongated and branched cells known as callus hairs which fill the airspaces and hinder gas exchange in late harvested 'Fuji' apples. This helps explain why late harvested 'Fuji' apples are at a higher risk of developing IB. Research on South African 'Cripps' Pink' apples have shown a direct link between IB incidence and apple maturity at harvest (Bergman et al., 2012). The study by Bergman et al. (2012) pointed out to the higher IB incidence observed in fruit harvested at an advanced maturity as compared to fruit harvested at optimum maturity. Majoni (2012) found that the total ascorbate and glutathione levels, and the poly-unsaturated fatty acid to the mono-unsaturated fatty acid ratio in 'Cripps' Pink' was much lower at post-optimum maturity compared to fruit harvest at optimum maturity.

In a three year study on IB incidence in 'Fuji' apples, Grant et al. (1996) found that the incidence of IB varied from year to year but was strongly influenced in each year by harvest maturity and $CO_2$ concentration in the storage atmosphere. Grant et al. (1996) attributed this to greater resistance to gas diffusion in the tissue of more mature fruit, possibly due to the increased presence of callus hairs. 'Fuji' apples must develop a minimum amount of external red colour for them to be acceptable and competitive on the export market. However, 'Fuji' apples normally attain optimum internal quality before sufficient red colour develops, this results in producers delaying harvest so that sufficient red colour is attained. In Korea, 'Fuji' apples are typically harvested at advanced maturity so that they meet required quality characteristics such as red colouration and high soluble solute concentration (Kweon et al., 2013). The late harvesting of fruit has the negative impact of predisposing fruit to developing IB during CA storage (Grant et al., 1996).

The relationship between late harvest and IB incidence has also been reported in other apple cultivars. In a study on 'Braeburn' apples, Elgar et al. (1999), found that late harvested fruit from low cropping trees had a moderate to high risk of developing IB during CA storage. A study

by Kittemann et al. (2015) in Kanzi® apples showed that the sensitivity of the apples to IB significantly increased with later harvest dates. Lau (1998) found an increase in both IB and internal cavities for 'Braeburn' apples harvested at advanced maturity, they attributed this to increased respiration rate, increased tissue and skin resistance to gas exchange and increased sensitivity to CA storage conditions. Paul and Pandey (2014) highlighted that the resistance of fruit tissue to $CO_2$ diffusion is dependent upon fruit variety, size and harvest maturity. Gong et al. (2001) found a higher browning incidence in over-mature Braeburn apples and he attributed this to low activity of superoxide dismutase. Superoxide dismutase is important for the protection of cells from damage by superoxide anions. A study by Lentheric et al. (1999) on pear fruit showed that the activity of superoxide dismutase fell about five times when fruit were picked more mature. The concentration of ROS is usually higher in more mature fruit because of changes in enzymatic and non-enzymatic antioxidants, this may explain why more mature fruit are more prone to damage, leading to IB during storage (Lentheric et al., 1999).

A study on 'Cripps' Pink' apples to determine IB susceptibility showed a lot of variation in the relationship between IB and harvest date. There was a high IB incidence for later harvested fruit in one season while the following season had a lower IB for later harvested fruit (de Castro et al., 2007). This shows the erratic and unpredictable nature of IB incidence. In another study on 'Cripps' Pink' apples, Butler (2015) found that fruit maturity affected diffuse browning while it did not seem to influence radial browning. Attainment of sufficient blush development is one of the reasons why fruit is left on the tree beyond the optimum maturity date, whilst leaving fruit on the tree for longer may have a positive impact on blush development, it predisposes fruit to IB problems during long-term CA storage (Butler, 2015). According to Brown et al. (2003), Tasmanian 'Cripps' Pink' apples harvested one week after the commercial harvest date had 28% more IB compared to apples harvested on the commercial harvest date.

### *4.2. Storage regime*

#### *4.2.1. CA storage*

Apples are produced during a certain time of the year and therefore they need to be stored for extended periods to ensure that they are available all year-round. To reduce respiration rates and delay ripening and senescence, fruit are stored at low temperature and in modified gas conditions. CA storage refers to the storage of fruit under controlled levels of $O_2$, $CO_2$, $N_2$, temperature and humidity (DeEll et al., 2016). One of the earliest reports of the capabilities of extending storage life of apples through modifying the storage conditions was published by Kidd and West in 1927, since then the CA technology has greatly developed (Kweon et al., 1998). Refinement of CA storage has produced a number of other specialised storage techniques such as dynamic CA, initial low oxygen stress storage, ultra-low oxygen CA and the stepwise increase of $CO_2$ concentration (Kweon et al., 2013; DeEll et al., 2016).

Under CA, fruit are stored at a low $O_2$ partial pressure and an elevated $CO_2$ partial pressure (Buts et al., 2015). In South Africa, 'Fuji' apples can be stored for 7-8 months in a storage environment with 1.5% $O_2$, 0.5% $CO_2$ at -0.5 °C (Findlay and Combrink, 2013). Although the storage life of apples is increased by CA storage, physiological problems such as IB can also occur as a result of the modified gas conditions (Kittemann et al., 2015). IB in 'Fuji' apples has been found to occur during long-term CA storage. The susceptibility of 'Fuji' apples to developing IB during long-term CA storage has been reported by several researchers (Volz and Mitcham, 1997; Argenta et al., 2001, 2000; Argenta et al., 2002b; Chung et al., 2005; Holderbaum et al., 2010; Kweon et al., 2012; Kweon et al., 2013; Ma et al., 2015).

#### *4.2.2. Delayed CA storage*

In most cases, the rapid establishment of CA is encouraged to obtain maximum quality and firmness retention, however, increased IB incidence has been associated with rapid establishment of CA (DeEll and Ehsani-Moghaddam, 2012). Delaying the establishment of CA storage after harvest can be a good storage protocol to reduce the incidence of IB during long-term storage of apples (DeEll et al., 2016). Several researchers have looked into the effectiveness of delayed CA in reducing IB in apples (Argenta et al., 2000; DeEll et al., 2016). The results obtained by Argenta et al. (2000) indicated that the susceptibility of 'Fuji' apples to $CO_2$ injury is highest during the first few weeks after harvest and that delaying CA establishment for a few weeks after harvest is effective in reducing the incidence of IB. Although other quality attributes of the fruit such as firmness and titratable acidity (TA) were affected by delayed CA, this was not sufficiently high to offset the benefits of delayed CA in reducing IB (Argenta et al., 2000). Since the susceptibility of fruit to IB varies from season to season, the required duration of the delay in establishing CA also varies from season to season and may be determined each season by exposing fruit to high $CO_2$ concentration for 3 days after harvest (Argenta et al., 2000).

Although the mechanism by which delayed CA reduces IB is not yet fully understood, it has been found that fruit subjected to delayed CA contained higher ATP levels, presumably because these fruit have higher respiration rates and subsequently a higher energy status (Franck et al., 2007). In addition to this, browning disorders in 'Conference' pears have been related low ATP levels and to a low ATP:ADP ratio during CA storage (Saquet et al., 2003). This suggests that low ATP levels may be an important factor in explaining the incidence of IB in apples and pears (Saquet et al., 2003). Low levels of ATP have been shown to affect lipid synthesis and desaturation of acyl chains and this can lead to decompartmentalization, which results in IB (Saquet et al., 2003). The reduction of ATP levels and respiration rates in fruit which was not subjected to delayed CA was also explained by Lammertyn et al. (2003) using a respiration-diffusion model in 'Conference' pears, they found that establishment of CA storage immediately

after harvest resulted in very high internal $CO_2$ levels, these conditions can induce membrane damage and IB. This observation was not made in fruit subjected to delayed CA.

Other apple cultivars have also been shown to respond well to delayed CA. DeEll and Ehsani-Moghaddam (2012) found that delayed CA was effective in reducing both $CO_2$ injury and other IB types in 'Empire' apples, however, the use of 1-MCP to reduce softening was required to make the delayed CA more beneficial. Delaying the establishment of CA for 2 - 4 weeks was found to be effective in reducing IB in 'Cripps' Pink' apples (de Castro et al., 2007). The benefits of delayed CA were also reported by DeEll et al. (2016) on 'Honeycrisp' apples, they found that IB was consistently reduced by delayed CA although in some years the benefits of delayed CA were compromised by other disorders such as lenticel breakdown and greasiness. The period of delayed CA required to lower IB was reduced when 1-MCP was used (DeEll et al., 2016). Carbon dioxide injury was reduced in 'Bramley's Seedling' apples when the establishment of CA conditions were delayed for 10 days. The beneficial effects of delayed CA have also been reported in 'Conference' pears; fruit stored without delayed CA had a very high incidence of IB while fruit stored with delayed CA had very low incidence of IB and cavities (Saquet et al., 2003).

*4.3. Role of porosity in gaseous exchange during post-harvest storage*

Apples are climacteric fruit, and they continue to undergo respiration after harvest during long-term storage. It is important for the fruit to have sufficient $O_2$ at all times to support respiration and avoid hypoxic or anoxic conditions which can lead to fermentation and incidence of IB. Diffusivity values for both $O_2$ and $CO_2$ are higher in air than in water and this implies that both $CO_2$ and $O_2$ are predominantly transported through the pores (Ho et al., 2011). Intercellular spaces (pores) are the main pathways through which $O_2$ is transported to the respiring cells and $CO_2$ is transported away from the respiring cells. Gaseous $O_2$ is absorbed by the fruit via diffusion through the stomata or lenticels, from there the $O_2$ enters the pores which is the main pathway for

$O_2$ transport, tissues with high porosity are able to efficiently transport oxygen as compared to tissues with lower porosity (Cukrov, 2018). From the pores, the $O_2$ then diffuses through the cell membrane into the cytoplasm before reaching the mitochondria where respiration takes place (Cukrov, 2018). Lower porosity or smaller pores restrict the movement of gases leading to low $O_2$ levels and increased $CO_2$ levels in fruit tissue, conditions which promote anaerobic respiration (Verboven et al., 2008; Nugraha et al., 2019). The porosity of apple fruit increases gradually from the core of the fruit towards the peel of the fruit (Herremans et al., 2015a). A study by Chigwaya et al. (2018) on Fuji apples showed that the core of apple fruit, which is reported to have a lower porosity as compared to the cortex region (Nugraha et al., 2019), developed IB after fruit were stressed with 50% $CO_2$ for 3 days, while the cortex region remained unaffected. A combination of low diffusivity of metabolic gases coupled with high respiratory activity causes hypoxic or anoxic conditions in low porosity regions of the fruit, this causes cell death, tissue damage and IB (Herremans et al., 2015a).

Microstructural properties of pores such as volume, length, sphericity and surface area differ amongst apple cultivars (Mendoza et al., 2007). A study by Ting et al. (2013) to determine the microstructure of different apple cultivars showed that 'Scifresh' (Jazz$^{TM}$) apples had the lowest porosity in the cortex region (17%) as compared to Golden Delicious (29.8%), Fuji (29.3%) and Braeburn (25.3%). The study also showed that 'Fuji' apples are made up of many small pores which as a sum were comparable to the volume of pores in 'Golden Delicious' apples which is made up of a small number of large pores (Ting et al., 2013). The small size of the pores in 'Fuji' may restrict gas diffusion, and this may be responsible for the higher susceptibility of 'Fuji' to IB disorders during long-term CA storage.

Physiological disorders such as watercore which reduce the porosity of fruit tissue have been shown to predispose fruit to the development of IB during long-term storage (Argenta et al., 2002b; Herremans et al., 2014). In addition to the porosity, other properties of the pores such as

connectivity, anisotropy and tortuosity also have an impact on the gas transport properties and development of IB during long-term storage. Connectivity is important because more connected pores are able to transport respiratory gases more efficiently than less connected pores (Warning et al., 2014). According to Mendoza et al. (2007), the connectivity of pores has a great influence on transport properties such as permeability and is important to the understanding of the relationship between microstructure and transport properties. Connectivity determines the tortuosity of the pore channels. Tortuosity accounts for the fact that the transport of gases follows a meandering network of pores rather than a straight path and is calculated as the effective path followed by the molecules divided by the shortest path (Salvo et al., 2010; Herremans et al., 2015b). Anisotropy is a measure of how the pores are aligned and it also affects the effectiveness of the pores in gas transport (Wevers et al., 2012; Cantre et al., 2014).

## 5. Conclusion

The erratic and unpredictabile nature of different IB types makes them difficult disorders to manage. Although the disorder is manifested during post-harvest storage, it is important to try and mitigate the disorder by starting to look at pre-harvest factors that may make the fruit more susceptible to IB during storage. Mineral nutrition is one of the important pre-harvest factors that should be carefully monitored. Due to its role in membrane integrity and stability, it is important to make sure that trees are supplied with sufficient nutrients during fruit growth and development. It is important to harvest ‘Fuji’ apples at an acceptable maturity, prefferably not more than 180 DAFB to limit the risk of IB during storage. Although CA storage is important for the maintanance of quality during long-term storage, it is important to maintain the $O_2$ levels in CA storage above the lower oxygen limit (which varies depending on the cultivar) to avoid a shift in the metabolic pathway from respiration to fermentation. Delaying the establishment of CA conditions has also been shown to have a positive effect on reducing IB incidence in ‘Fuji’. However, more research still needs to be done to confirm the effectiveness of delayed CA in reducing IB. The role of

porosity in the incidence of IB should also be considered, low tissue porosity restricts movement of respiratory gases and this may make the fruit more susceptible to IB. Non-destructive imaging techniques which quantify the porosity of intact fruit may be helpful in efforts to substantiate the link between microstructure (porosity) and the susceptibility of fruit to IB. Non-destructive techniques to detect IB in intact apples can also be very useful in detection and preventing fruit with IB from being sold to consumers. Such techniques include X-ray computed tomography which utilizes gray value and density differences in fruit tissue have the potential to identify and isolate fruit with IB.

**References**

Amiot, M.J., Tacchini, M., Aubert, S., Nicolas, J., 1992. Phenolic composition and browning susceptibility of various apple cultivars at maturity. J. Food Sci. 57, 958–962. https://doi.org/10.1111/j.1365-2621.1992.tb14333.x.

Argenta, L., Fan, X., Mattheis, J., 2000. Delaying establishment of controlled atmosphere or $CO_2$ exposure reduces 'Fuji' apple $CO_2$ injury without excessive fruit quality loss. Postharvest Biol. Technol. 20, 221–229. https://doi.org/10.1016/S0925-5214(00)00134-4.

Argenta, L., Fan, X., Mattheis, J., 2001. Development of IB in 'Fuji' apples during storage, in: Washington Tree Fruit Postharvest Conference. Wenatchee, WA, pp. 1–4. http://ucce.ucdavis.edu/files/datastore/234-56.pdf.

Argenta, L., Fan, X., Mattheis, J., 2002a. Impact of watercore on gas permeance and incidence of internal disorders in 'Fuji' apples. Postharvest Biol. Technol. 24, 113–122. https://doi.org/10.1016/S0925-5214(01)00137-5.

Argenta, L.C., Fan, X., Mattheis, J.P., 2002b. Responses of 'Fuji' apples to short and long duration exposure to elevated $CO_2$ concentration. Postharvest Biol. Technol. 24, 13–24. https://doi.org/10.1016/S0925-5214(01)00120-X.

Bergman, H., Crouch, E., Crouch, I., Jooste, M., Majoni, J., 2012. Update on the possible causes and management strategies of flesh browning disorders in ‘Cripps’ Pink’ apples. SA fruit J. 11, 56–59.

Bowen, J.H., Watkins, C.B., 1997. Fruit maturity, carbohydrate and mineral content relationships with watercore in ‘Fuji’ apples. Postharvest Biol. Technol. 11, 31–38. https://doi.org/10.1016/S0925-5214(97)01409-9.

Brackmann, A., Ribeiro, D.N., 1992. Physiological disorders in apples related with calcium deficiency and its control. Ciência Rural 22, 247–253. http://dx.doi.org/10.1590/S0103-84781992000200021.

Brown, G., Schimanski, L. and Jennings, D., 2003. Investigating internal browning of Tasmanian 'Pink Lady' apples. Acta Hortic. 628, 161-166. https://doi.org/10 17660/ActaHortic.2003.628.19.

Butler, L., 2015. Internal flesh browning of ‘Cripps Pink’ apple (*Malus domestica* Borkh.) as influenced by pre-harvest factors and the evaluation of near infrared reflectance spectroscopy as a non-destructive method for detecting browning. Master’s thesis, Department of Horticultural Sciences, Faculty of AgriSciences, Stellenbosch University, Stellenbosch, South Africa.

Buts, K., Hatoum, D., Hertog, M.L.A.T.M., Nicolaï, B.M. and Carpentier, S., 2015. Browning of apple cortex during CA storage: A proteomics approach. Acta Hortic. 1071, 373-379. https://doi.org/10.17660/ActaHortic.2015.1071.48.

Cantre, D., Herremans, E., Verboven, P., Ampofo-Asiama, J., Nicolaï, B., 2014. Characterization of the 3-D microstructure of mango (*Mangifera indica* L. *cv.* Carabao) during ripening using X-ray computed microtomography. Innov. Food Sci. Emerg. Technol. 24, 28–39. https://doi.org/10.1016/j.ifset.2013.12.008.

Chigwaya, K., Schoeman, L., Fourie, W.J., Crouch, I., Viljoen, D. and Crouch, E.M., 2018. 'Fuji' apple internal browning explored via X-ray computed tomography (CT). Acta Hortic. 1201,

309-316. https://doi.org/10.17660/ActaHortic.2018.1201.42.

Chung, H., Moon, K., Chung, S., Choi, J., 2005. Control of IB and quality improvement of 'Fuji' apples by stepwise increase of $CO_2$ level during controlled atmosphere storage. J. Sci. Food Agric. 85, 883–888. https://doi.org/10.1002/jsfa.1867.

Corrêa, T.R., Steffens, C.A., do Amarante, C.V.T., Miqueloto, A., Brackmann, A., Ernani, P.R., 2017. Multivariate analysis of mineral content associated with flesh browning disorder in 'Fuji' apples produced in Southern Brazil. Bragantia 76, 327–334. https://doi.org/10.1590/1678-4499.127.

Cukrov, D., 2018. Progress toward Understanding the Molecular Basis of Fruit Response to Hypoxia. Plants 7, 78. https://doi.org/10.3390/plants7040078.

Danner, M.A., Scariotto, S., Citadin, I., Penso, G.A., Cassol, L.C., 2015. Calcium sources applied to soil can replace leaf application in 'Fuji' apple tree. Pesqui. Agropecuária Trop. 45, 266–273. https://doi.org/10.1590/1983-40632015v4534457

de Castro, E., Biasi, B., Mitcham, E., Tustin, S., Tanner, D., Jobling, J., 2007. Carbon Dioxide-induced Flesh Browning in Pink Lady Apples. Am. Soc. Hortic. 132, 713–719. https://doi.org/10.21273/JASHS.132.5.713.

de Castro, E., Barrett, D.M., Jobling, J., Mitcham, E.J., 2008. Biochemical factors associated with a $CO_2$ -induced flesh browning disorder of Pink Lady apples. Postharvest Biol. Technol. 48, 182–191. https://doi.org/10.1016/j.postharvbio.2007.09.027.

de Freitas, S.T., do Amarante, C.V.T., Labavitch, J.M., Mitcham, E.J., 2010. Cellular approach to understand bitter pit development in apple fruit. Postharvest Biol. Technol. 57, 6–13. https://doi.org/10.1016/j.postharvbio.2010.02.006.

DeEll, J.R., Ehsani-Moghaddam, B., 2012. Delayed controlled atmosphere storage affects storage disorders of 'Empire' apples. Postharvest Biol. Technol. 67, 167–171. https://doi.org/10.1016/j.postharvbio.2012.01.004.

DeEll, J.R., Lum, G.B., Ehsani-Moghaddam, B., 2016. Effects of delayed controlled atmosphere

storage on disorder development in ‘Honeycrisp’ apples. Can. J. Plant Sci. 96, 621–629. https://doi.org/10.1139/cjps-2016-0031.

Di Guardo, M., Tadiello, A., Farneti, B., Lorenz, G., Masuero, D., Vrhovsek, U., Costa, G., Velasco, R., Costa, F., 2013. A Multidisciplinary Approach Providing New Insight into Fruit Flesh Browning Physiology in Apple (*Malus x domestica* Borkh.). PLoS One 8, e78004. https://doi.org/10.1371/journal.pone.0078004.

Elgar, H.J., Lallu, N., Watkins, C.B., 1999. Harvest Date and Crop Load Effects on a Carbon Dioxide–related Storage Injury of ‘Braeburn’ Apple. HortScience. 34, 305–309. https://doi.org/10.21273/hortsci.34.2.305.

Falchi, R., D’Agostin, E., Mattiello, A., Coronica, L., Spinelli, F., Costa, G., Vizzotto, G., 2017. ABA regulation of calcium-related genes and bitter pit in apple. Postharvest Biol. Technol. 132, 1–6. https://doi.org/10.1016/j.postharvbio.2017.05.017.

Ferguson, I., Volz, R., Woolf, A., 1999. Preharvest factors affecting physiological disorders of fruit. Postharvest Biol. Technol. 15, 255–262.

Findlay, J.S., Combrink, J.C., 2013. South African controlled atmosphere storage operator’s manual. SA Apple and Pear Producers’ Association. Paarl, South Africa.

Franck, C., Lammertyn, J., Ho, Q.T., Verboven, P., Verlinden, B., Nicolaï, B.M., 2007. Browning disorders in pear fruit. Postharvest Biol. Technol. 43, 1–13. https://doi.org/10.1016/j.postharvbio.2006.08.008.

Gong, Y., Toivonen, P.M.A., Lau, O.L., Wiersma, P.A., 2001. Antioxidant system level in 'Braeburn' apple is related to its browning disorder. Bot. Bull. Acad. Sin. 42, 259–264.

Gonzalez, J.J., Valle, R.C., Bobroff, S., Biasi, W. V, Mitcham, E.J., McCarthy, M.J., 2001. Detection and monitoring of IB development in ‘Fuji’ apples using MRI. Postharvest Biol. Technol. 22, 179–188. https://doi.org/10.1016/S0925-5214(00)00183-6.

Grant, J., Mitcham, B., Biasi, B., Chinchiolo, S., 1996. Late harvest, high $CO_2$ storage increase IB of ‘Fuji’ apples. Calif. Agric. 50, 26–29. https://doi.org/10.3733/ca.v050n03p26.

Hatoum, D., Buts, K., Hertog, M.L.A.T.M., Geeraerd, A.H., Schenk, A., Vercammen, J., Nicolaï, B.M., 2014. Effects of pre- and postharvest factors on browning in Braeburn. Hort. Sci. 41, 19–26. https://doi.org/10.17221/180/2013-HORTSCI.

Hatoum, D., Hertog, M.L.A.T.M., Geeraerd, A.H., Nicolaï, B.M., 2016. Effect of browning related pre- and postharvest factors on the 'Braeburn' apple metabolome during CA storage. Postharvest Biol. Technol. 111, 106–116. https://doi.org/10.1016/j.postharvbio.2015.08.004.

Hayama, H., Iwatani, A., Nishimoto, T., Oya, Y., Nakamura, Y., 2014. Watercore disorder in Japanese pear 'Niitaka' is increased by high fruit temperatures during fruit maturation. Sci. Hortic. 175, 27–32. https://doi.org/10.1016/j.scienta.2014.05.033.

Herremans, E, Verboven, P., Hertog, M.L.A.T.M., Cantre, D., van Dael, M., De Schryver, T., van Hoorebeke, L., Nicolaï, B.M., 2015a. Spatial development of transport structures in apple (*Malus* × *domestica* Borkh.) fruit. Front. Plant Sci. 6, 679. https://doi.org/10.3389/fpls.2015.00679.

Herremans, E, Verboven, P., Verlinden, B.E., Cantre, D., Abera, M., Wevers, M., Nicolaï, B.M., 2015b. Automatic analysis of the 3-D microstructure of fruit parenchyma tissue using X-ray micro-CT explains differences in aeration. BMC Plant Biol. 15, 1–14. https://doi.org/10.1186/s12870-015-0650-y.

Herremans, E., Melado-Herreros, A., Defraeye, T., Verlinden, B., Hertog, M., Verboven, P., Val, J., Fernández-Valle, M.E., Bongaers, E., Estrade, P., Wevers, M., Barreiro, P., Nicolaï, B.M., 2014. Comparison of X-ray CT and MRI of watercore disorder of different apple cultivars. Postharvest Biol. Technol. 87, 42–50. https://doi.org/10.1016/j.postharvbio.2013.08.008.

Ho, Q.T., Verboven, P., Verlinden, B.E., Herremans, E., Wevers, M., Carmeliet, J., Nicolaï, B.M., 2011. A three-dimensional multiscale model for gas exchange. Plant Physiol. 155, 1158–1168. https://doi.org/10.1104/pp.110.169391.

Hocking, B., Tyerman, S.D., Burton, R.A., Gilliham, M., 2016. Fruit calcium: Transport and physiology. Front. Plant Sci. 7, 1–17. https://doi.org/10.3389/fpls.2016.00569.

Holderbaum, D.F., Kon, T., Kudo, T., Guerra, M.P., 2010. Enzymatic Browning, Polyphenol Oxidase Activity, and Polyphenols in Four Apple Cultivars: Dynamics during Fruit Development. HortScience 45, 1150–1154. https://doi.org/10.21273/HORTSCI.45.8.1150.

Hopfinger, J.A., Poovaiah, B.W., Patterson, M.E., 1984. Calcium and magnesium interactions in browning of 'Golden Delicious' apples with bitter pit. Sci. Hortic. 23, 345–351. https://doi.org/10.1016/0304-4238(84)90031-1.

HORTGRO, 2019. Key Deciduous Fruit Statistics. Accessed 8 September 2020. https://www.hortgro.co.za/wp-content/uploads/docs/2020/07/key-deciduous-fruit-st atistics-2019-1.pdf.

James, H., Jobling, J., Tanner, D., Tustin, S., Wilkinson, I., 2010. Climatic conditions during growth relate to risk of Pink Lady™ apples developing flesh browning during storage. Acta Hortic. 857, 197–204. https://doi.org/10.17660/ActaHortic.2010.857.22.

James, H.J., 2007. Understanding the flesh browning disorder of 'Cripps Pink' apples. PhD dissertation, Faculty of Agriculture, Food and Natural Resources, The University of Sydney, New South Wales, Australia.

James, H.J., Jobling, J.J., 2009. Contrasting the structure and morphology of the radial and diffuse flesh browning disorders and $CO_2$ injury of 'Cripps Pink' apples. Postharvest Biol. Technol. 53, 36–42. https://doi.org/10.1016/j.postharvbio.2009.02.001.

Kasai, S., Arakawa, O., 2010. Antioxidant levels in watercore tissue in 'Fuji' apples during storage. Postharvest Biol. Technol. 55, 103–107. https://doi.org/10.1016/j.postharvbio.2009.08.008

Kittemann, D., Neuwald , D.A. and Streif , J., 2015. Internal browning in 'Kanzi®' Apple – Reasons and Possibilities to reduce the disorder. Acta Hortic. 1079, 409-414. https://doi.org/10.17660/ActaHortic.2015.1079.52.

Kweon, H.J, Kim, H.Y., Ryu, O.H., Park, Y.M., 1998. Effects of CA Storage Procedures and

Storage Factors on the Quality and the Incidence of Physiological Disorders of 'Fuji' Apples. Hortic. Environ. Biotechnol. 39, 35–39.

Kweon, H.J., Kim, M.J., Moon, Y.S., Lee, J.W., Choi, C., Choi, D.G., Lee, D.H., Kang, I.K., 2012. Relationship between Preharvest Factors and the Incidence of Storage Disorders in 'Fuji' Apples during CA Storage. Korean J. Hortic. Sci. Technol. 30, 50–55. https://doi.org/10.7235/hort.2012.11049.

Kweon, H.J., Kang, I.K., Kim, M.J., Lee, J., Moon, Y.S., Choi, C., Choi, D.G., Watkins, C.B., 2013. Fruit maturity, controlled atmosphere delays and storage temperature affect fruit quality and incidence of storage disorders of 'Fuji' apples. Sci. Hortic. 157, 60–64. https://doi.org/10.1016/j.scienta.2013.04.013.

Lafer, G., 2006. Storability and fruit quality of 'Golden Delicious' as affected by harvest date, AVG and 1-MCP treatments. J. Fruit Ornam. Plant Res. 14, 203-212.

Lammertyn, J., Scheerlinck, N., Jancsók, P., Verlinden, B.E., Nicolaï, B.M., 2003. A respiration-diffusion model for 'Conference' pears II. Simulations and relation to core breakdown. Postharvest Biol. Technol. 30, 43–55. https://doi.org/10.1016/S0925-5214(03)00062-0.

Lau, O.L., 1998. Effect of growing season, harvest maturity, waxing, low $O_2$ and elevated $CO_2$ on flesh browning disorders in 'Braeburn' apples. Postharvest Biol. Technol. 14, 131–141. https://doi.org/10.1016/S0925-5214(98)00035-0.

Lentheric, I., Pinto, E., Vendrell, M., Larrigaudiere, C., 1999. Harvest date affects the antioxidative systems in pear fruits. J. Hortic. Sci. Biotechnol. 74, 791–795. https://doi.org/10.1080/14620316.1999.11511190.

Majoni, T.J., 2012. Physiology and biochemistry of 'Cripps' Pink' apple (*Malus domestica* Borkh.) ripening and disorders with special reference to postharvest flesh browning. Master's thesis, Department of Horticultural Sciences, Faculty of AgriSciences, Stellenbosch University, Stellenbosch, South Africa.

Mendoza, F., Verboven, P., Mebatsion, H.K., Kerckhofs, G., Wevers, M. and Nicolaï, B., 2007.

Three-dimensional pore space quantification of apple tissue using X-ray computed microtomography. Planta 226, 559–570. https://doi.org/10.1007/s00425-007-0504-4.

Mellidou, I., Buts, K., Hatoum, D., Ho, Q.T., Johnston, J.W., Watkins, C.B., Schaffer, R.J., Gapper, N.E., Giovannoni, J.J., Rudell, D.R., Hertog, M.L.A.T.M., Nicolaï, B.M., 2014. Transcriptomic events associated with IB of apple during postharvest storage. BMC Plant Biol. 14, 1–17. https://doi.org/10.1186/s12870-014-0328-x.

Milani, J. and Hamedi, M., 2005. Susceptibility of five apple cultivars to enzymatic browning. Acta Hortic. 682, 2221-2226. https://doi.org/10.17660/ActaHortic.2005.682.303.

Miqueloto, A., do Amarante, C.V.T., Steffens, C.A., dos Santos, A., Mitcham, E., 2014. Relationship between xylem functionality, calcium content and the incidence of bitter pit in apple fruit. Sci. Hortic. 165, 319–323. https://doi.org/10.1016/j.scienta.2013.11.029.

Neuwald, D.A., Kittemann , D., Streif, J. and Andrade, C.A.W., 2012. Watercore dissipation in ‘Fuji’ apples by postharvest temperature conditioning treatments. Acta Hortic. 934, 1097-1102. https://doi.org/10.17660/ActaHortic.2012.934.147.

Neuwald, D.A., Streif , J. and Kittemann, D., 2015. Postharvest IB during CA Storage of ‘Santana’ Apples – Reasons and Possibilities to Reduce the Disorder. Acta Hortic. 1071, 597-601. https://doi.org/10.17660/ActaHortic.2015.1071.77.

Nicolas, J.J., Richard-Forget, F.C., Goupy, P.M., Amiot, M., Aubert, S.Y., 1994. Enzymatic browning reactions in apple and apple products. Crit. Rev. Food Sci. Nutr. 34, 109–157. https://doi.org/10.1080/10408399409527653.

Nugraha, B., Verboven, P., Janssen, S., Wang, Z., Nicolaï, B.M., 2019. Non-destructive porosity mapping of fruit and vegetables using X-ray CT. Postharvest Biol. Technol. 150, 80–88. https://doi.org/10.1016/j.postharvbio.2018.12.016.

Parker, M.L., Guerra, W., 2008. Occurrence and implications for postharvest quality of intercellular callus hair growth in the outer cortex of apples of ‘Fuji’ and ‘Fuji’ sports. Postharvest Biol. Technol. 48, 192–198. https://doi.org/10.1016/j.postharvbio.2007.10.007.

Paul, V., Pandey, R., 2014. Role of internal atmosphere on fruit ripening and storability — a review. J. Food Sci. Technol. 51, 1223–1250. https://doi.org/10.1007/s13197-011-0583-x.

Rhoads, D.M., Umbach, A.L., Subbaiah, C.C., Siedow, J.N., 2006. Mitochondrial reactive oxygen species . contribution to oxidative stress and interorganellar signaling. Plant Physiol. 141, 357–366. https://doi.org/10.1104/pp.106.079129.ROS.

Rogers, G., 2014. Managing the risk of flesh browning for 'Cripps Pink' apples using a climate model. Applied Horticultural Research Pty Ltd, Horticulture Australia. https://doi.org/ISBN 0 7341 3327 8.

Salvo, L., Suéry, M., Marmottant, A., Limodin, N., Bernard, D., 2010. 3D imaging in material science : Application of X-ray tomography. Comptes Rendus Phys. 11, 641–649. https://doi.org/10.1016/j.crhy.2010.12.003.

Saquet, A. A., Streif, J., Bangerth, F., 2003. Energy metabolism and membrane lipid alterations in relation to brown heart development in 'Conference' pears during delayed controlled atmosphere storage. Postharvest Biol. Technol. 30, 123–132. https://doi.org/10.1016/S0925-5214(03)00099-1.

Saquet, A.A., Streif, J., Bangerth, F., 2000. Changes in ATP, ADP and pyridine nucleotide levels related to the incidence of physiological disorders in 'Conference' pears and 'Jonagold' apples during controlled atmosphere storage. J. Hortic. Sci. Biotechnol. 75, 243–249. https://doi.org/10.1080/14620316.2000.11511231.

Shirzadeh, E., Rabiei, V., Sharafi, Y., 2011. Effect of calcium chloride ($CaCl_2$) on postharvest quality of apple fruits. African J. Agric. Res. 6, 5139–5143. https://doi.org/10.5897/AJAR11.1189.

Telias, A., Hoover, E., Rosen, C., Bedford, D., Cook, D., 2006. The effect of calcium sprays and fruit thinning on bitter pit incidence and calcium content in 'Honeycrisp' apple. J. Plant Nutr. 29, 1941–1957. https://doi.org/10.1080/01904160600927492.

Ting, V.J.L., Silcock, P., Bremer, P.J., Biasioli, F., 2013. X-ray micro-computer tomographic

method to visualize the microstructure of different apple cultivars. J. Food Sci. 78, E1735–E1742. https://doi.org/10.1111/1750-3841.12290.

Tong, C.B.S., Chang, H.Y., Boldt, J.K., Ma, Y.B., DeEll, J.R., Moran, R.E., Bourgeois, G., Plouffe, D., 2016. Diffuse flesh browning in 'Honeycrisp' apple fruit is associated with low temperatures during fruit growth. HortScience. 51, 1256–1264. https://doi.org/10.21273/HORTSCI11179-16.

Veltman, R.H., 2002. On the origin of IB in pears (*Pyrus communis* L. *cv* Conference). PhD dissertation, Wageningen University, Wageningen, Netherlands. ISBN 90-5808-636-4.

Verboven, P., Kerckhofs, G., Mebatsion, H.K., Ho, Q.T., Temst, K., Wevers, M., Cloetens, P., Nicolaï, B.M., 2008. Three-dimensional gas exchange pathways in pome fruit characterized by synchrotron X-Ray computed comography. Plant Physiol. 147, 518–527. https://doi.org/10.1104/pp.108.118935.

Volz, R., Mitcham, B., 1997. Internal browning in 'Fuji' Apples. Perish. Handl. Newsl. 6. Accessed 2 December 2019. http://ucce.ucdavis.edu/files/datastore/234-56.pdf.

Volz, R.K., Biasi, W. V., Grant, J.A., Mitcham, E.J., 1998. Prediction of controlled atmosphere-induced flesh browning in 'Fuji' apple. Postharvest Biol. Technol. 13, 97–107. https://doi.org/10.1016/S0925-5214(97)00080-X.

Warning, A., Verboven, P., Nicolaï, B., van Dalen, G., Datta, A.K., 2014. Computation of mass transport properties of apple and rice from X-ray microtomography images. Innov. Food Sci. Emerg. Technol. 24, 14–27. https://doi.org/10.1016/j.ifset.2013.12.017.

Wevers, M., Kerckhofs, G., Pyka, G., Herremans, E., Van Ende, A., Hendrickx, R., Verstrynge, E., Mariën, A., Valcke, E., Pareyt, B., Wilderjans, E., 2012. X-ray computed tomography for non-destructive testing, in: Proceedings ICT 2012, International Conference on Industrial Computed Tomography. pp. 1–10.

Yamada, H., Hasegawa, Y., Mito, K., 1998. Watercore Induced by preharvest high fruit temperature in watercore-resistant 'Tsugaru' Apples. Environ. Control Biol. 36, 209–216.

https://doi.org/10.2525/ecb1963.36.209.

Yamada, H., Takechi, K., Hoshi, A., Amano, S., 2004. Comparison of water relations in watercored and non-watercored apples induced by fruit temperature treatment. Sci. Hortic. 99, 309–318. https://doi.org/10.1016/S0304-4238(03)00104-3.

## PAPER 1

# Use of X-ray computed tomography (CT) and 3D image analysis to characterize internal browning in 'Fuji' apples after exposure to $CO_2$ stress

**Abstract**

In this study X-ray computed tomography (X-ray CT) was used to determine microstructural differences between 'Fuji' apple tissue affected by internal browning (IB) and unaffected tissue after short-term exposure (3 days) to a storage atmosphere with 0.1% $O_2$ and 50% $CO_2$. The incidence of IB disorders observed were concentrated in the core region of the fruit. IB developed in 31% of fruit at varying degrees of severity. X-ray CT scanning was able to give pore and cell microstructural information such as porosity, length, sphericity, connectivity, equivalent diameter and anisotropy. High-resolution X-ray CT scans showed that fruit tissue with IB had a lower total porosity and pore connectivity compared to unaffected fruit tissue, likely due to membrane damage and flooding of intercellular spaces with cellular fluids. Image analysis showed that pores in affected brown tissue were significantly more spherical compared to the other tissue types. Low porosity in the fruit core region might restrict respiratory gas diffusivity and this may predispose the core region to $CO_2$ induced IB. The study showed that $CO_2$ induced IB disorders in 'Fuji' can be evaluated at a microstructural level using X-ray CT. This work expands knowledge from previous studies which showed that IB disorders in 'Fuji' apples caused by low $O_2$ and high $CO_2$ atmospheres are associated with changes in microstructural properties. It is important to ensure that gas levels in controlled atmosphere (CA) storage environments are properly maintained to avoid IB disorders.

**Keywords**: Internal browning, controlled atmosphere, high-resolution X-ray CT, Low-resolution scans, *Malus domestica*, porosity

## 1. Introduction

Long-term storage of 'Fuji' apples has been made possible by the use of controlled atmosphere (CA) storage techniques (Argenta et al., 2000; Tanaka et al., 2018). CA storage utilises an elevated $CO_2$ and low $O_2$ concentration to reduce respiration and this extends the storage life of fruit (Pedreschi et al., 2009a). Although CA storage has the capacity to maintain quality during long-term storage, it can also result in the incidence of storage disorders such as internal browning (IB) especially when $CO_2$ levels are too high (Lau, 1998; Elgar et al., 1999). To mimic the IB types such as $CO_2$ damage which occur during long-term CA storage, 'Fuji' apples are sometimes stored at high $CO_2$ levels for short durations. Short-term exposure of 'Fuji' apples to high $CO_2$ levels has previously been used as an accurate predictor of fruit susceptibility to CA-induced IB (Argenta et al., 2002). IB is characterized by patches of brown flesh with or without cavities that develop in the apple tissue (Argenta et al., 2002).

Because of diffusion limitations in fruit tissue, reduced $O_2$ and elevated $CO_2$ levels within the storage atmosphere can result in the establishment of a concentration gradient within the apple tissue which causes a decrease of the $O_2$ partial pressure and an increase of $CO_2$ partial pressure towards the core of the fruit (Ho et al., 2013). This can result in a change of the fruit metabolic pathway from the normal respiration to fermentation (Saquet et al., 2003; Mellidou et al., 2014). Metabolomics and proteomic studies have confirmed the impairment of the oxidative pathway and a shift to the fermentation pathway when fruit is stored under extreme CA (Pedreschi et al., 2008, 2009a, 2009b). The shift to the fermentation pathway will result in less available energy to maintain membrane integrity and this causes membrane damage by reactive oxygen species leading to loss of compartmentalisation and onset of IB (Mellidou et al., 2014). Responses of 'Fuji' apples after short-term exposure to elevated $CO_2$ levels have been investigated by Argenta et al. (2002). They found that the severity of the $CO_2$ injury was higher in fruit exposed to 20 kPa $CO_2$ after harvest than in fruit exposed to 20 kPa $CO_2$ after 8 months of CA storage. Ke et

al. (1990) found that 'Bartlett' pears exposed to 50% $CO_2$ had a higher incidence of IB disorders compared to those exposed to 80% $CO_2$.

To fully understand what happens at the microstructural level as a result of $CO_2$ induced browning, it is necessary to evaluate the fruit microstructure. Traditionally, light and confocal microscopy have been used to evaluate fruit microstructure (Schotsmans et al., 2004, Pieczywek and Zdunek, 2012). However, these methods are limited in their penetration depth and reliance on destructive analysis of thin 2D sections to estimate volumetric measurements of 3D structures (Herremans et al., 2013), potentially missing important information. A method for isolating and measuring the shape and size of apple cells from 2D images was proposed by McAtee et al. (2009), however, this method still provides limited 3D geometric information. X-ray computed tomography is an innovative imaging technique that can be utilised in the acquisition of 3D spatial data from intact fruit samples (Ting et al., 2013). X-ray CT has been gaining popularity due to its non-destructive nature and the ability to image 3D structures. It has a high penetration depth and does not require tedious sample preparation as some other methods (Vicent et al., 2017). The use of X-ray CT in apple fruit microstructure evaluations has been explored by different researchers. Ting et al. (2013) used this technique to evaluate microstructural properties of different apple cultivars while Herremans et al. (2013) used it in the characterization of 'Braeburn' browning disorder, a form of $CO_2$ damage which occurs during CA storage of 'Braeburn' apples. Diels et al. (2017) explored its use in the assessment of bruising in apples, bruising occurs during post-harvest handling and is characterized by flattening and discoloration of the fruit tissue. Using X-ray CT, Poles et al. (2020) investigated the interactions between cell morphology and texture-juiciness properties of fourteen apple cultivars, which included Fuji. Their study showed that 'Fuji' apples had the highest fraction of small pores, this property may increase the susceptibility of 'Fuji' to IB symptoms during CA storage since small pores may be limited in their gas transport capacity.

The objective of this present study was to compare microstructural properties of fruit tissue affected by $CO_2$ induced IB with unaffected fruit tissue by using X-ray CT and 3D image analysis techniques.

## 2. Materials and Methods

### *2.1. Fruit material*

'Fuji' apples were harvested in March 2018 from Wakkerstroom farm (33°17'47.1"S 19°14'54.8"E) located in the Koue Bokkeveld area in the Western Cape Province, South Africa. The fruit were harvested at shoulder height from each tree, from either side of the canopy. Fruit were randomly mixed and not separated according to the different canopy positions. Fruit were harvested into lug boxes and transported to the fruit evaluation lab at the Department of Horticultural Sciences, Stellenbosch University, South Africa. Maturity indexing was done on arrival at the lab to determine the maturity status of the fruit at harvest.

### *2.2. Fruit quality evaluations at harvest*

To determine fruit maturity at harvest, fruit were evaluated for diameter, mass, height, ground peel colour, blush percentage, flesh firmness, titratable acidity (TA), total soluble solutes (TSS) and starch breakdown. TA and TSS were measured on pooled samples of 20 fruit whereas the other parameters were determined on each of 40 fruit. Fruit diameter, mass and height were measured using a Cranston gauge and electronic balance (FTA 2007, Guss, Strand, South Africa). Ground peel colour of fruit were rated from 0.5 (green) to 5 (yellow), using the South African Industry colour chart for apples and pears (Unifruco Research Services, Bellville, South Africa). The blush percentage was determined by a trained reviewer who estimated the percentage of the fruit surface covered by a red blush (0% for no red blush and 100% for full red blush). Fruit firmness was measured equatorially on opposite sides of the fruit on a peeled surface

using a universal fruit texture analyser (FTA 2007, Guss, Strand, South Africa), fitted with a 7.9 mm diameter probe. Titratable acidity was measured by titration of fruit juice using an automated titrator (Metrohm AG 760. Harison, Switzerland). Total soluble solutes content was measured on a drop of expressed fruit juice using a hand-held digital refractometer (Atago Digital-Refractometer PR-32, Tokyo, Japan). Percentage starch conversion was estimated using the iodine test with a starch conversion chart (Unifruco Research Services, Bellville, South Africa) with a scale of 0% to 100%, where 0% was totally stained and 100% was totally unstained.

*2.3. High $CO_2$/low $O_2$ stress treatment*

After harvesting, 400 fruit were subjected to a storage atmosphere with 0.1% $O_2$ and 50% $CO_2$ for 3 days at room temperature (21 °C). This was done by placing the fruit in a tightly closed Janny MT bin and then pumping in $CO_2$ until the controlled atmosphere bin comprised of 50% $CO_2$. The level of $O_2$ in the Janny MT bin after $CO_2$ enrichment was 0.1%. The level of gases inside the controlled atmosphere bin was measured using a handheld gas analyser (ICA 350 Dual Analyser, Storage Control Systems, Inc. UK). The level of $CO_2$ inside the bin was maintained at 50% throughout the duration of the experiment. At the end of the 3 days, all the fruit were taken out of the bin and each of the fruit were cut to evaluate the incidence of IB.

*2.4. Intensity of browning incidence*

To quantify the IB incidence, the intensity index chart in Fig. 1 was used after each of the fruit were cut into two halves at the equator. An intensity index of 0 was used if the core of the apple did not have any IB incidence. An intensity index of 1 was used if up to 20% of the apple core was affected by IB. An intensity index of 2 was used if up to 40% of the apple core was affected by IB. If 60% of the apple core was affected by IB, an intensity index of 3 was given to such fruit. Fruit in which the core was between 60 and 80% affected by IB was given an index of

4. In severe cases were the entire fruit core was affected by IB, an intensity index of 5 was given. After evaluation and scoring of fruit, 20 fruit with IB and 20 fruit without IB were randomly selected for low-resolution and high-resolution X-ray CT scanning. Before low-resolution whole fruit scans, the two cut halves had to be carefully placed back on top of each other and secured with a cling wrap to secure the fruit for scanning.

*2.5. Low-resolution micro-CT (whole fruit scans)*

To determine grey values and tissue density, low-resolution micro-CT scanning was done on 40 whole apples at the Stellenbosch University Central Analytical Facility. Twenty of the fruit had core IB while 20 did not have core IB. The V|Tome|X L240 micro-CT scanner (GE Sensing & Inspection Technologies GmbH, Wunstorf, Germany) contains two X-ray tubes, one with a reflection-type target and the other with a transmission target (du Plessis et al., 2016). The average time per scan was 30 min and 2300 projection images were captured. The samples were scanned at a voltage of 100 kV and a current of 100 µA, these parameters were able to give a voxel size of 60 µm. A series of 2D X-ray projection images were obtained and these were reconstructed using reconstruction software Datos|x®2.1 (GE Sensing & Inspection Technologies GmbH, Wunstorf, Germany) to generate virtual 3D volumes.

*2.6. High-resolution micro-CT*

Cylindrical samples for high-resolution micro-CT were obtained using a cork-borer of 5 mm diameter. Each sample had a diameter of 5 mm and was 15 mm long. For apples with core browning, 2 samples were scanned, one from the brown region and another from a white region without browning (Fig. 2). For apples without any form of browning, one sample was taken from the apple core. The samples from the non-brown apples were used as control samples. In total, 60 samples were scanned at high-resolution, 20 brown samples from fruit with IB, 20 white

samples from fruit with IB and 20 white samples from unaffected fruit. The cylindrical tissue samples were cut on either end to about 15 mm length and wrapped in parafilm to avoid dehydration during scanning. The samples were then loaded individually onto the Nanotom S instrument (GE Sensing & Inspection Technologies GmbH, Wunstorf, Germany) at the Stellenbosch University Central Analytical Facility for scanning. Various system settings were tested to optimize the scan quality. A series of 2600 projection images were obtained as the sample was rotated 360°. The samples were scanned at a voltage of 60 kV and a current of 240 µA giving a voxel size of 3 µm. The average scan time was 45 min-per sample. A series of 2D X-ray projection images were obtained and these were reconstructed into 3D volumes using reconstruction software Datos|x®2.1 (GE Sensing & Inspection Technologies GmbH, Wunstorf, Germany) to generate virtual 3D images.

*2.7. Image analysis*

To extract suitable quantitative information from X-ray CT images, it is necessary to perform 3D image analysis. Image analysis was done on 3D volumes generated after reconstruction. The polychromacity of the X-ray beam gives rise to the beam hardening effect (du Plessis et al., 2020). As a result, beam hardening correction of level 2 (software specific value) had to be applied to correct this artefact. The beam hardening effect causes the appearance of artefacts, i.e., continuous variation in grey values within the reconstructed volume depending on the variation of object thickness at different positions (Boas and Fleischmann, 2012). Analysing the whole image in its entirety can be an arduous and time-consuming exercise, hence it was necessary to select a region of interest (ROI) from the original image (Schoeman et al., 2016). Although a ROI is smaller in size compared to the original image, it was important to ensure that the selected ROI was large enough to be statistically representative of the whole sample. In this study a ROI cube

measuring 2.5 x 2.5 x 2.5 mm was used. This volume of 15.625 $mm^3$ was larger than the lower limit for a representative volume element of 1.3 $mm^3$ that was proposed by Mendoza et al. (2007).

After this, it was necessary to remove random noise that occurs during scanning. Filtering was done using a median filter for cell analysis in Avizo 2019.1 (VSG, Bordeaux, France) and an adaptive gauss filter for pore analysis in VGStudio Max 3.2 (Volume Graphics GmbH, Heidelberg, Germany). After filtering, the image was segmented into the constituent cells and pores so that subsequent analysis procedures could be carried out. Automatic thresholding using Otsu's method was done to create a binary image consisting of only cells and pores (Otsu, 1979). Otsu's thresholding involves the defining of a single grey value to separate regions of the image based on analysis of the image histogram (Otsu, 1979; Iassonov et al., 2009; Zhang et al., 2017). Voxels containing grey values lower than this threshold value are regarded as background while those with grey values higher than the threshold value are regarded as sample material (Schoeman et al., 2016). Segmentation of X-ray CT images using Otsu method has been used by Herremans et al. (2013) in Braeburn apples, Muziri et al. (2016) in Forelle pears and Ting et al. (2013) in determination of differences in microstructural properties of different apple cultivars. After image thresholding, 3D image analysis was then done, and various microstructural properties determined (Table 1). 3D image analysis was done using Avizo 2019.1 (VSG, Bordeaux, France), CTAn 1.18.0.0 (Bruker microCT, Kontich, Belgium) and VGStudio Max 3.2 (Volume Graphics GmbH, Heidelberg, Germany).

*2.8. Cell isolation*

Automatic segmentation of individual cells was not possible due to insufficient contrast between cytoplasm and cell wall. Hence, segmentation of individual cells was done using the watershed separation algorithm (Wang et al., 2020). The 3D region that was identified as cells after segmentation needed to be further segmented into individual cells to allow for the

quantification of individual cell properties. This was implemented using the “separate objects” module in Avizo 2019.1. The watershed method is a powerful morphological tool for image segmentation. It derives its name from the geographical meaning of watershed, which refers to a ridge that divides areas drained by different river systems (Ruparelia, 2012). If you view the image as a landscape, the watershed lines determine boundaries which separates image regions (Ruparelia, 2012).

The algorithm works by calculating the chamfer distance map of the binary image, in which greyscales represent the distance from that pixel to the nearest black (background) pixel, regardless of direction. The chamfer distance map which computes the distance as a discrete approximation produces a mountain peak at the centre of each of the cells. In this study, the Separate objects/Chamfer Conservative module in Avizo 2019.1 was used to compute watershed lines on the binary image. All cells that intersected the dataset borders after watershed separation were removed in order to exclude incomplete individual cells from cell measurements (Fig. 3). After watershed separation, some cells were not fully separated, and such cells had to be excluded from the image since they give rise to inaccurate results. A virtual sieve was used to remove incorrectly segmented cells and unseparated clumps of cells (Fig. 3). Based on literature, all individual objects with a length larger than 400 µm and a sphericity index (quantified using Avizo 2019.1) lower than 0.75 were removed from the 3D model (Herremans et al., 2015; Wang et al., 2020). This allowed the 3D model of the image to comprise of only the correctly segmented cells. This protocol was validated by Herremans et al. (2015) by manually segmenting individual cells and they found no significant differences in this method and manually segmented individual cells. Failure of the watershed algorithm to detect cell boundaries in affected tissue samples proved that there was disruption of cellular structure in brown affected tissue (Fig. 4).

*2.9. Calculation of tissue density*

To enable calculation of the densities of different tissue regions in the apple tissue, a reference of known density (2.21 $gcm^{-3}$) was scanned together with the apple during low-resolution (whole fruit) scanning. This made it possible to calculate the density of a given region of interest (ROI) based on the density of the reference using equation 1. The tissue density was determined for white unaffected fruit tissue, white tissue from affected fruit and brown affected fruit tissue. The density calibration was developed and validated by Guelpa et al. (2015) in maize (*Zea mays L.*) kernels.

$$\text{Relative density} = \frac{\text{Mean grey value of ROI}}{\text{Mean grey value of reference}} \times 2.21\ \text{gcm}^{-3} \qquad (1)$$

*2.10. Data analysis*

To determine if there were differences between the different browning scores, the data was first transformed using logit transformation and ANOVA was done on the transformed data using STATISTICA Version 13.1 (StatSoft Inc., Tulsa, USA). The data was analysed as a completely randomised design (CRD) to compare the differences amongst the different browning scores. Data for pore and cell properties was analysed as a completely randomised design and mean separations were done using Fisher's Least Significance Difference (LSD) test at a significance level of 5% using STATISTICA Version 13.1.

## 3. Results

*3.1. Fruit maturity at harvest*

Table 2 presents the maturity parameters of 'Fuji' apples that were used in this study. The apples used in this study were harvested during the commercial harvest period in 2018 and the maturity indices show that the apples were at an advanced maturity at the time of harvest (starch breakdown = 81 ± 19.5%; Firmness = 7.7 ± 0.6 kg; TA = 0.31 ± 0.02%).

*3.2. Browning intensity index*

The results in Table 3 show that 69 ± 6% of the fruit had an intensity index of 0, meaning that they did not have any IB symptoms. 11 ± 2% of the fruit had an intensity index of 1, showing that 20% of the core was affected by IB in this fruit. 7 ± 2% of the fruit had an intensity index of 2, meaning that up to 40% of the core was affected by IB. 6 ± 2% of the fruit had a browning intensity index of 3, meaning that up to 60% of the core region was affected by IB. 4 ± 1% of the fruit had up to 80% of their core being affected by IB and 3 ± 2% of the fruit had their entire core region affected by IB.

*3.3. Morphometric parameters of pores*

Table 4 represents the 3D morphometric parameters of pores. The number of closed pores was not significantly different amongst the tissue samples. Affected brown samples had a closed porosity of 3.1% which was significantly lower than the closed porosity of white samples from affected fruit (5.1%) and unaffected samples (5.9%). Affected brown samples had an open porosity of 0.9% which was significantly lower than the open porosity of white samples from affected fruit (6.2%) and unaffected samples (6.4%). The total porosity, which is a sum of the open and closed porosity was significantly lower in affected brown samples (4.0%) and significantly higher in white samples from affected fruit samples (10.9%) and unaffected samples (11.9%; Fig. 5). The connectivity of the pores was significantly higher in unaffected samples (745.7) and white samples from affected fruit (705.6) compared to affected brown samples which had a connectivity of just 52.2. In terms of length, pores from unaffected samples and white samples from affected fruit were significantly longer with lengths of 120.07 µm and 128.65 µm, respectively. Pores from affected brown samples had a significantly smaller average length of only 95.43 µm. Pores from affected brown tissue had a significantly high sphericity of 0.882

compared to pores in white samples from affected fruit (0.828) and unaffected tissue samples (0.849). Sphericity is the measure of how closely the shape of an object approaches that of a mathematically perfect sphere. Pore anisotropy was significantly lower in affected brown tissue (0.765) as compared to white tissue samples from affected fruit (0.811) and unaffected tissue samples (0.792). Anisotropy refers to the existence of a preferential alignment of the pores and is calculated by performing a mean intercept length analysis. Most pores in all tissue types had an equivalent diameter of less than 160 µm (Fig. 6). In general, for all the pore parameters evaluated the white tissue samples (white tissue from affected fruit and unaffected tissue) did not differ significantly but differed significantly from the brown tissue samples. Pore parameters such as porosity, pore connectivity, number of closed pores and pore length were significantly higher in the white samples compared to the brown samples (Table 4).

*3.4. Morphometric parameters of cells*

Table 5 represents the 3D morphometric parameters of cells. The length and thickness of the cells did not differ significantly amongst the different tissue samples. There was a significant difference amongst the different tissue types in terms of the width of the cells. Cells from brown affected core tissue samples had the largest width (174.32 µm) as compared to cells from white unaffected core tissue samples (162.74 µm) and white tissue samples from affected fruit (160.86 µm). The surface area of the cells from the different tissue samples also differed significantly. Cells from brown affected tissue samples had the largest surface area (0.155 $mm^2$) as compared to cells from unaffected tissue samples (0.139 $mm^2$) and white tissue samples from affected fruit (0.139 $mm^2$). There was a significant difference amongst the different tissue types in terms of the euler connectivity of the cells. Cells from brown affected tissue samples had the lowest Euler3D (0.637) compared to cells from white unaffected tissue samples (0.921) and white tissue samples from affected fruit (0.902). Euler number indicates the connectedness of 3D structures; higher values indicate poorly connected structures while lower values indicate highly

connected structures. The different tissue types did not differ significantly in terms of anisotropy and EqDiameter. The sphericity of cells in brown affected tissue samples was significantly lower (0.688) as compared to the sphericity of cells in white tissue samples from affected fruit (0.767) and unaffected tissue samples (0.773). Due to disruption of cellular structure, cell boundaries in affected brown samples were destroyed and could not be detected by the watershed algorithm (Fig. 4). This resulted in only a few cells being able to be properly segmented for cell analysis.

### *3.5. Tissue density*

Fruit were scanned at low-resolution with a reference of known density and this made it possible to calculate the densities of the different regions of interest within the fruit tissue based on the measured grey values of the fruit tissue and known density of the reference. The density of fruit tissue affected by IB (1.278 ± 0.005 g/cm$^3$) did not differ significantly from that of unaffected tissue (1.268 ± 0.006 g/cm$^3$). The only differences were seen in the contrasting greyscale intensities between fruit tissue affected by IB and fruit tissue without IB. Fruit tissue with IB was characterized by a light grey colour (Fig. 7).

## 4. Discussion

Short-term exposure of ‘Fuji’ apples to high $CO_2$ levels has been used as a reliable method to predict susceptibility of ‘Fuji’ apples to IB incidence during long-term storage (Argenta et al., 2002). The results of this study showed that there was incidence of IB to varying degrees after short-term exposure to high $CO_2$, however, all the browning occurred in the core region of the fruit (Fig. 7). The reason for the high incidence of IB in the core is unclear but it might be due to the low porosity and low respiratory gas diffusivity in the core region compared to the cortex region and the long radial distance of the core region from the fruit surface (Herremans et al., 2015). However, the link between porosity and IB incidence still need to be conclusively ascertained and

experiments that can directly and quantitatively address this relationship are crucial. Because of the difficulties associated with manipulating porosity, controlled experiments cannot be carried out to control this feature and so work linking IB incidence to low porosity has not directly ascertained the relationship. Nugraha et al. (2019) conducted experiments on spatial porosity distribution in 'Jonagold' apple and found that the core region of 'Jonagold' apple fruit is made up of dense tissue with a porosity of 3 - 12% while the cortex region is relatively more porous (12 - 35%), in this study the porosity of healthy core region tissue was 10.9%. Ting et al. (2013) reported a porosity of 29.3% in the cortex of 'Fuji' apples. According to Herremans et al. (2013), the inner cortex of apples has a low porosity, and the pores are poorly connected, these microstructural properties may hinder gaseous exchange in the core region of the fruit. The interaction of these factors may cause insufficient movement of $CO_2$ in the core region leading to its accumulation, onset of fermentation processes and incidence of IB. In their studies on the effect of $CO_2$ partial pressure on blueberry fruit (which is also climacteric), Beaudry (1993) found that a $CO_2$-induced elevation in the respiratory quotient (RQ) was due to $CO_2$-induced fermentation which is linked to the development of off-flavours and tissue damage. In this current study, the tissue damage resulted in IB of the core region of 'Fuji' apples.

A study by Yearsley et al. (1996) on 'Cox's Orange Pippin' apples (stored for 86 – 90 hours at 24 °C in external $O_2$ ranging from 0 to <30 kPa) showed that anaerobic $CO_2$ production increased markedly as the internal $O_2$ concentration decreased below 2.0 kPa and reached a maximum at the lowest internal $O_2$ concentration. Their study further highlighted that the variance in internal atmospheres of apples with the same external $O_2$ concentration (0.1% in the current study) showed a preference to decrease as the internal $O_2$ approached the lower oxygen limit (LOL) and then increased as it fell below the LOL. $CO_2$ related disorders may develop at internal $O_2$ and $CO_2$ levels above the onset of fermentation through the reduction of mitochondrial function (Yearsley et al., 1997). The high $CO_2$/low $O_2$ (50% $CO_2$/0.1% $O_2$) concentrations used in this study

may have induced an internal atmosphere that is conducive for the onset of fermentation. Therefore, it is important to quantify internal gas concentration because the $CO_2$ and $O_2$ concentrations to which fruit tissue readily responds to is that in the call-sap (Dadzie et al., 1996; Yearsley et al., 1996).

In this study, the internal $CO_2$ concentrations would have been at most 54% in the core and 52% in the cortex, this small difference between the $CO_2$ levels is unlikely to be the cause of IB preferentially developing in the core. The small difference in gas composition between sub-epidermal and core tissue was also highlighted by Dadzie et al. (1996) in their studies on 'Cox's Orange Pippin' and 'Granny Smith' apples. Variation in the composition of the internal atmosphere between different apple cultivars is due to differences in respiration rate, peel permeance, and fruit surface area to mass ratio (Banks et al., 1993; Yearsley et al., 1996). In this present study, it is unlikely that differences in internal $CO_2$ concentration between the core and the cortex contributed to the development of IB in the core region. Peel permeance is also another factor contributing to the internal atmosphere, in their study, Yearsley et al. (1997) found that ‘Braeburn’ had a higher average internal $CO_2$ (0.7 kPa) and lower $O_2$ (1.0 kPa) at 20 °C in air compared to 'Cox's Orange Pippin', probably resulting from the lower peel permeance of ‘Braeburn’. Determination of peel permeance of ‘Fuji’ may help in efforts to quantify internal atmosphere levels that are problematic.

Even though IB observed in this paper was restricted to the core region, $CO_2$ induced IB during long-term CA storage usually occurs in both the core and cortex region and is sometimes accompanied by pits and cavities, susceptible cultivars include Braeburn, Kanzi, Elstar, Santana and Fuji (de Freitas and Pareek, 2019). This highlights the complex nature of IB symptoms and mechanisms. IB observed in commercially stored South African ‘Fuji’ apples occurs in all regions of the fruit tissue and is not limited to only the core region.

While low porosity may be a factor contributing to IB incidence (Herremans et al., 2015), it is also an after-effect of short-term $CO_2$ induced IB since affected fruit tissue is characterized by reduced porosity (Chigwaya et al., 2018). This present study looked at the closed porosity, open porosity and total porosity, in all instances the porosity was significantly lower in brown affected tissue samples. The 3D pore models clearly showed the reduced porosity (4%) in brown affected tissue samples (Fig. 5). This reduced porosity due to IB can be attributed to the damage of cells and membrane leakage leading to cellular fluids filling up the intercellular air spaces and rendering them unable to efficiently execute their role of respiratory gas transport (Herremans et al., 2013; Mellidou et al., 2014). During long-term cold storage, the cellular fluids and free water that floods the intercellular air spaces as a result of $CO_2$ induced membrane damage will diffuse out of the fruit as storage time progresses leaving large cavities in the affected tissue (Lau, 1998). However, this study presented an acute response to high external $CO_2$ levels and not a chronic response, which is due to low $CO_2$ concentrations slowly inducing the disorder over time.

In addition to the reduced total porosity, affected brown tissue also had low pore connectivity. The poor pore connectivity coupled with low porosity of affected tissue further aggravated the disorder (Schotsmans et al., 2004; Herremans et al., 2013). Connectivity looks at the connectedness of the pores and low pore connectivity indicates low capacity of the pores to efficiently transport respiratory gases (James and Jobling, 2009; Mebatsion et al., 2009; Verboven et al., 2013). In terms of size, the pores in brown affected dead tissue had a significantly smaller length and this shows that as the flooding of intercellular spaces progressed, the larger pores were eliminated first leaving behind smaller pores which are limited in their capacity to efficiently transport respiratory gases (Herremans et al., 2013). The sphericity of affected brown tissue was significantly higher meaning that the pores in the affected tissue were more spherical than pores from unaffected tissue. The pores in apples fruit are normally randomly shaped with a less defined shape (Ting et al., 2013). The spherical shape of pores in affected tissue is a clear sign that the

fruit microstructure was altered by IB. Low-resolution scans done on the fruit did not show significant differences in the tissue density of affected and unaffected tissue. However, differences in greyscale intensity were seen from the light grey colour of fruit tissue affected by IB as compared to the dark grey colour of tissue not affected by IB (Fig. 7). Pore anisotropy was low in brown affected tissue samples and this indicates loss of oriented structures as the browning progresses (Herremans et al., 2013).

Changes in cellular structure of the fruit tissue was associated with IB. The effect of cellular structure damage on IB incidence has been highlighted by several (Argenta et al., 2000; de Castro et al., 2007, 2008). When the watershed segmentation algorithm was applied to images from unaffected tissue samples, the cell-to-cell boundaries were clearly defined, however, this was not the case in images from tissue samples with IB. The cellular structure in brown affected tissue was severely disrupted to such an extent that neighbouring cells could not be distinguished from each other with the watershed separation method (Fig. 4). The failure of the watershed algorithm to detect the cell-to-cell boundaries shows that the cellular structure was severely disrupted, resulting in IB symptoms. As a result, only a few cells were properly isolated and obtainable for analysis. Cells from affected tissue had a smaller width and surface area compared to cells from unaffected tissue. The cells from affected tissue also had a significantly lower sphericity compared to cells from unaffected tissue, this can be attributed to cell damage due to loss of membrane integrity and membrane leakage (Saquet et al., 2000; Mellidou et al., 2014).

## 5. Conclusion

'Fuji' apples exposed to a storage atmosphere with 0.1% $O_2$ and with 50% $CO_2$ for 3 days after harvest at ambient temperature developed varying degrees of IB that was concentrated around the core region of the fruit. 3D image analysis showed that brown affected fruit tissue had significantly lower porosity and lower connectivity of pores, probably due to filling of pore spaces

with cellular fluids released after cell damage caused by the high $CO_2$ and low $O_2$ concentration. The sphericity of pores in brown tissue was significantly higher which points out to changes of fruit microstructure and cellular structure possibly leading to IB development. Low porosity in specific regions of the fruit may play a role in predisposing fruit to localised development of $CO_2$ induced IB. Determination of microstructural parameters in relation to IB incidence will add value to the comprehensive understanding of postharvest handling and storage of 'Fuji' apples. Internal manipulation of respiratory gases may be explored as a way to ascertain the relationship between porosity and IB incidence directly and quantitatively. If the levels of $CO_2$ in the low porosity regions (core) can be quantified, replication of these concentrations in the larger pore regions (cortex) of the fruit can help determine the relationship between porosity and IB incidence.

**Acknowledgements**

The authors would like to thank the South African Apple and Pear Producer's Association and HORTGRO Science for funding this research.

## References

Argenta, L., Fan, X., Mattheis, J., 2000. Delaying establishment of controlled atmosphere or $CO_2$ exposure reduces 'Fuji' apple $CO_2$ injury without excessive fruit quality loss. Postharvest Biol. Technol. 20, 221–229. https://doi.org/10.1016/S0925-5214(00)00134-4.

Argenta, L.C., Fan, X., Mattheis, J.P., 2002. Responses of 'Fuji' apples to short and long duration exposure to elevated $CO_2$ concentration. Postharvest Biol. Technol. 24, 13–24. https://doi.org/10.1016/S0925-5214(01)00120-X.

Banks, N.H., Dadzie, B.K., Cleland, D.J., 1993. Reducing gas exchange of fruits with surface coatings. Postharvest Biol. Technol. 3, 269–284. https://doi.org/10.1016/0925-5214(93)90062-8

Beaudry, R.M., 1993. Effect of carbon dioxide partial pressure on blueberry fruit respiration and respiratory quotient. Postharvest Biol. Technol. 3, 249–258. https://doi.org/10.1016/0925-5214(93)90060-G

Boas, F.E., Fleischmann, D., 2012. CT artifacts: causes and reduction techniques. Imaging Med. 4, 229–240.

Chigwaya, K., Schoeman, L., Fourie, W.J., Crouch, I., Viljoen, D. and Crouch, E.M., 2018. 'Fuji' apple internal browning explored via X-ray computed tomography (CT). Acta Hortic. 1201, 309-316. https://doi.org/10.17660/ActaHortic.2018.1201.42.

Dadzie, B.K., Banks, N.H., Cleland, D.J., Hewett, E.W., 1996. Changes in respiration and ethylene production of apples in response to internal and external oxygen partial pressures. Postharvest Biol. Technol. 9, 297–309. https://doi.org/10.1016/S0925-5214(96)00030-0.

de Castro, E., Barrett, D.M., Jobling, J., Mitcham, E.J., 2008. Biochemical factors associated with a $CO_2$-induced flesh browning disorder of Pink Lady apples. Postharvest Biol. Technol. 48, 182–191. https://doi.org/10.1016/j.postharvbio.2007.09.027.

de Castro, E., Biasi, B., Mitcham, E., Tustin, S., Tanner, D., Jobling, J., 2007. Carbon Dioxide-induced Flesh Browning in Pink Lady Apples. Am. Soc. Hortic. 132, 713–719. https://doi.org/10.21273/JASHS.132.5.713.

de Freitas, S.T. and Pareek, S. eds., 2019. Postharvest physiological disorders in fruits and vegetables. CRC Press. https://doi.org/10.1201/b22001.

Diels, E., Dael, M. Van, Keresztes, J., Vanmaercke, S., Verboven, P., Nicolaï, B., Saeys, W., Ramon, H., Smeets, B., 2017. Assessment of bruise volumes in apples using X-ray computed tomography. Postharvest Biol. Technol. 128, 24–32. https://doi.org/10.1016/j.postharvbio.2017.01.013.

du Plessis, A., le Roux, S.G., Guelpa, A., 2016. The CT Scanner Facility at Stellenbosch University: An open access X-ray computed tomography laboratory. Nucl. Instruments Methods Phys. Res. Sect. B Beam Interact. with Mater. Atoms 384, 42–49.

https://doi.org/10.1016/j.nimb.2016.08.005.

du Plessis, A., Tshibalanganda, M., le Roux, S.G., 2020. Not all scans are equal: X-ray tomography image quality evaluation. Mater. Today Commun. 22, 100792. https://doi.org/10.1016/j.mtcomm.2019.100792.

Elgar, H.J., Lallu, N., Watkins, C.B., 1999. Harvest Date and Crop Load Effects on a Carbon Dioxide–related Storage Injury of 'Braeburn' Apple. HortScience 34, 305–309. https://doi.org/10.21273/hortsci.34.2.305.

Guelpa, A., Plessis, A., Kidd, M., Manley, M., 2015. Non-destructive Estimation of Maize (*Zea mays L.*) Kernel Hardness by Means of an X-ray Micro-computed Tomography (µCT) Density Calibration 1419–1429. https://doi.org/10.1007/s11947-015-1502-3.

Herremans, E., Verboven, P., Bongaers, E., Estrade, P., Verlinden, B.E., Wevers, M., Hertog, M.L.A.T.M., Nicolaï, B.M., 2013. Characterisation of 'Braeburn' browning disorder by means of X-ray micro-CT. Postharvest Biol. Technol. 75, 114–124. https://doi.org/10.1016/j.postharvbio.2012.08.008.

Herremans, E., Verboven, P., Verlinden, B.E., Cantre, D., Abera, M., Wevers, M., Nicolaï, B.M., 2015. Automatic analysis of the 3-D microstructure of fruit parenchyma tissue using X-ray micro-CT explains differences in aeration. BMC Plant Biol. 15, 1–14. https://doi.org/10.1186/s12870-015-0650-y.

Ho, Q.T., Verboven, P., Verlinden, B.E., Schenk, A., Nicolaï, B.M., 2013. Controlled atmosphere storage may lead to local ATP deficiency in apple. Postharvest Biol. Technol. 78, 103–112. https://doi.org/10.1016/j.postharvbio.2012.12.014.

Iassonov, P., Gebrenegus, T., Tuller, M., 2009. Segmentation of X-ray computed tomography images of porous materials: A crucial step for characterization and quantitative analysis of pore structures. Water Resour. Res. 45, 1–12. https://doi.org/10.1029/2009WR008087.

James, H.J., Jobling, J.J., 2009. Contrasting the structure and morphology of the radial and diffuse flesh browning disorders and $CO_2$ injury of 'Cripps Pink' apples. Postharvest Biol.

Technol. 53, 36–42. https://doi.org/10.1016/j.postharvbio.2009.02.001.

Ke, D., van Gorsel, H., Kader, A.A., 1990. Physiological and Quality Responses of `Bartlett' Pears to Reduced $O_2$ and Enhanced $CO_2$ Levels and Storage Temperature. J. Am. Soc. Hortic. Sci. 115, 435–439. https://doi.org/10.21273/jashs.115.3.435.

Lau, O.L., 1998. Effect of growing season, harvest maturity, waxing, low $O_2$ and elevated $CO_2$ on flesh browning disorders in 'Braeburn' apples. Postharvest Biol. Technol. 14, 131–141. https://doi.org/10.1016/S0925-5214(98)00035-0.

McAtee, P.A., Hallett, I.C., Johnston, J.W., Schaffer, R.J., 2009. A rapid method of fruit cell isolation for cell size and shape measurements. Plant Methods 5, 1–7. https://doi.org/10.1186/1746-4811-5-5.

Mebatsion, H.K., Verboven, P., Endalew, A.M., Billen, J., Ho, Q.T., Nicolaï, B.M., 2009. A novel method for 3-D microstructure modeling of pome fruit tissue using synchrotron radiation tomography images. J. Food Eng. 93, 141–148. https://doi.org/10.1016/j.jfoodeng.2009.0 1.00 8.

Mellidou, I., Buts, K., Hatoum, D., Ho, Q.T., Johnston, J.W., Watkins, C.B., Schaffer, R.J., Gapper, N.E., Giovannoni, J.J., Rudell, D.R., Hertog, M.L.A.T.M., Nicolaï, B.M., 2014. Transcriptomic events associated with internal browning of apple during postharvest storage. BMC Plant Biol. 14, 1–17. https://doi.org/10.1186/s12870-014-0328-x.

Mendoza, F., Verboven, P., Mebatsion, H.K., Kerckhofs, G., Wevers, M., Nicolaï, B., 2007. Three-dimensional pore space quantification of apple tissue using X-ray computed microtomography. Planta 226, 559–570. https://doi.org/10.1007/s00425-007-0504-4.

Muziri, T., Theron, K.I., Cantre, D., Wang, Z., Verboven, P., Nicolaï, B.M., Crouch, E.M., 2016. Microstructure analysis and detection of mealiness in 'Forelle' pear (*Pyrus communis L .*) by means of X-ray computed tomography. Postharvest Biol. Technol. 120, 145–156. https://doi.org/10.1016/j.postharvbio.2016.06.006.

Nugraha, B., Verboven, P., Janssen, S., Wang, Z., Nicolaï, B.M., 2019. Non-destructive porosity

mapping of fruit and vegetables using X-ray CT. Postharvest Biol. Technol. 150, 80–88. https://doi.org/10.1016/j.postharvbio.2018.12.016.

Otsu, N., 1979. A threshold selection method from gray-level histograms. IEEE Trans. Syst. Man Cybern. 9, 62–66.

Pedreschi, R., Franck, C., Lammertyn, J., Erban, A., Kopka, J., Hertog, M., Verlinden, B., Nicolaï, B., 2009a. Metabolic profiling of 'Conference' pears under low oxygen stress. Postharvest Biol. Technol. 51, 123–130. https://doi.org/10.1016/j.postharvbio.2008.05.019.

Pedreschi, R., Hertog, M., Robben, J., Lilley, K.S., Karp, N.A., Baggerman, G., Vanderleyden, J., Nicolaï, B., 2009b. Gel-based proteomics approach to the study of metabolic changes in pear tissue during storage. J. Agric. Food Chem. 57, 6997–7004. https://doi.org/10.1021/jf901432h.

Pedreschi, R., Hertog, M., Robben, J., Noben, J.P., Nicolaï, B., 2008. Physiological implications of controlled atmosphere storage of 'Conference' pears (*Pyrus communis L.*): A proteomic approach. Postharvest Biol. Technol. 50, 110–116. https://doi.org/10.1016/j.postharvbio.2008.04.0 04.

Pieczywek, P.M., Zdunek, A., 2012. Automatic classification of cells and intercellular spaces of apple tissue. Comput. Electron. Agric. 81, 72–78. https://doi.org/10.1016/j.compag.2011.11.006.

Poles, L., Gentile, A., Giuffrida, A., Valentini, L., Endrizzi, I., Aprea, E., Gasperi, F., Distefano, G., Artioli, G., La Malfa, S., Costa, F., Lovatti, L., Di Guardo, M., 2020. Role of fruit flesh cell morphology and MdPG1 allelotype in influencing juiciness and texture properties in apple. Postharvest Biol. Technol. 164, 111161. https://doi.org/10.1016/j.postharvbio.2020.111161.

Ruparelia, S., 2012. Implementation of Watershed Based Image Segmentation Algorithm in FPGA. Master's thesis, Department of Parallel Systems, University of Stuttgart, Stuttgart, Germany.

Saquet, A.A., Streif, J., Bangerth, F., 2000. Changes in ATP, ADP and pyridine nucleotide levels

related to the incidence of physiological disorders in ‘Conference’ pears and ‘Jonagold’ apples during controlled atmosphere storage. J. Hortic. Sci. Biotechnol. 75, 243–249. https://doi.org/10.1080/14620316.2000.11511231.

Saquet, A.A., Streif, J., Bangerth, F., 2003. Energy metabolism and membrane lipid alterations in relation to brown heart development in ‘Conference’ pears during delayed controlled atmosphere storage. Postharvest Biol. Technol. 30, 123–132. https://doi.org/10.1016/S0925-5214(03)00099-1.

Schoeman, L., Williams, P., du Plessis, A., Manley, M., 2016. X-ray micro-computed tomography (μCT) for non-destructive characterisation of food microstructure. Trends Food Sci. Technol. https://doi.org/10.1016/j.tifs.2015.10.016.

Schotsmans, W., Verlinden, B.E., Lammertyn, J., Nicolaï, B.M., 2004. The relationship between gas transport properties and the histology of apple. J. Sci. Food Agric. 84, 1131–1140. https://doi.org/10.1002/jsfa.1768.

Tanaka, F., Tatsuki, M., Matsubara, K., Okazaki, K., Yoshimura, M., Kasai, S., 2018. Methyl ester generation associated with flesh browning in ‘Fuji’ apples after long storage under repressed ethylene function. Postharvest Biol. Technol. 145, 53–60. https://doi.org/10.1016/j.postharvbio.2018.06.002.

Ting, V.J.L., Silcock, P., Bremer, P.J., Biasioli, F., 2013. X-ray micro-computer tomographic method to visualize the microstructure of different apple cultivars. J. Food Sci. 78, E1735–E1742. https://doi.org/10.1111/1750-3841.12290.

Verboven, P., Herremans, E., Borisjuk, L., Helfen, L., Ho, Q.T., Tschiersch, H., Fuchs, J., Nicolaï, B.M., Rolletschek, H., 2013. Void space inside the developing seed of Brassica napus and the modelling of its function. New Phytol. 199, 936–947. https://doi.org/10.1111/nph.12342.

Vicent, V., Verboven, P., Ndoye, F.T., Alvarez, G., Nicolaï, B., 2017. A new method developed to characterize the 3D microstructure of frozen apple using X-ray micro-CT. J. Food Eng. 212, 154–164. https://doi.org/10.1016/j.jfoodeng.2017.05.028.

Wang, Z., Van Beers, R., Aernouts, B., Watté, R., Verboven, P., Nicolaï, B., Saeys, W., 2020. Microstructure affects light scattering in apples. Postharvest Biol. Technol. 159, 110996. https://doi.org/10.1016/j.postharvbio.2019.110996.

Yearsley, C.W., Banks, N.H., Ganesh, S., Cleland, D.J., 1996. Determination of lower oxygen limits for apple fruit. Postharvest Biol. Technol. 8, 95–109. https://doi.org/10.1016/0925-5214(96)00064-6.

Yearsley, C.W., Banks, N.H., Ganesh, S., 1997. Effect of carbon dioxide on the internal lower oxygen limits of apple fruit. Postharvest Biol. Technol. 12, 1–13. https://doi.org/10.1016/S0925-5214(97)00044-6.

Zhang, P, Lu, S., Li, J., Zhang, P, Xie, L., Xue, H., Zhang, J., 2017. Multi-component segmentation of X-ray computed tomography (CT) image using multi-Otsu thresholding algorithm and scanning electron microscopy. Energy Explor. Exploit. 35, 281–294. https://doi.org/10.1177/0144598717690090.

**Table 1**

Morphometric parameters used to describe 3D micro-CT images, based on Herremans et al. (2013), with modifications.

| **Microstructural parameter** | **Unit** | **Description** |
|---|---|---|
| Volume | $mm^3$ | Volume of object |
| Area | $mm^2$ | Area of the object boundary |
| Length | µm | Maximum of the ferret diameters used over a range of angles |
| Width | µm | Minimum of the ferret diameters used over a range of angles |
| Anisotropy | - | Measure of preferential alignment of structures. This value is scaled from 0 for total isotropy to 1 for total anisotropy |
| Euler number | - | It gives information about the connectivity of a 3D structure. Higher values indicate poorly connected structures and lower values for better connected structures |
| Connectivity | - | The number of connections between matrix structures per unit volume, based on Euler number |
| Total Porosity | % | Pore volume divided by the total volume |
| Closed porosity | % | The connected assemblage of space (black) voxels that is fully surrounded on all sides in 3D by solid (white) voxels. |
| Open porosity | % | Any space located within a solid object or between solid objects with connection in 3D space with outside space. |
| Sphericity | - | measures the ratio of the surface area of a sphere with the same volume as the cell/pore to its surface area |

**Table 2**

Physiochemical properties (± standard deviation) of 'Fuji' apples used in this study at harvest.

| Parameter | Value |
|---|---|
| Diameter (mm) | 71.7 ± 6.1 |
| Mass (g) | 166.1 ± 27.0 |
| Height (mm) | 61.9 ± 4.6 |
| Background peel colour (Chart value) | 3.3 ± 0.3 |
| Blush percentage (%) | 48.0 ± 19.0 |
| Firmness (kg) | 7.7 ± 0.6 |
| #TA (%) | 0.31 ± 0.02 |
| ^TSS (%) | 13.6 ± 0.8 |
| Starch breakdown (%) | 81.0 ± 19.5 |

#Titratable acidity
^Total soluble solutes

**Table 3**

Browning intensity index of fruit after the high $CO_2$/low $O_2$ stress treatment (50% $CO_2$/0.1% $O_2$). Number of apples at each browning intensity index was expressed as a percentage of the total number of fruit ± standard error.

| Browning intensity index | 0 | 1 | 2 | 3 | 4 | 5 |
|---|---|---|---|---|---|---|
| Percentage of total fruit (%) | 69 ± 6 a | 11 ± 2 b | 7 ± 2 bc | 6 ± 2 bc | 4 ± 1 c | 3 ± 2 c |
| *P-value* | | | *< 0.0001* | | | |
| *LSD (after logit transformation)* | | | *0.92* | | | |

Data was first transformed using logit transformation before statistical analysis was carried out.

**Table 4**

Three dimensional morphometric parameters of the pores of fruit core tissue (affected brown tissue, white tissue from affected fruit and unaffected tissue) obtained from X-ray CT images of 'Fuji' apples after the high $CO_2$/low $O_2$ stress treatment (50% $CO_2$/0.1% $O_2$). 3D indicates that the measurements were done on 3-dimensional images.

| | Surface area ($\mu m^2$) | Surface area/ volume ratio ($\mu m^{-1}$) | Number of closed pores | Closed porosity (%) | Open porosity (%) | Total porosity (%) | Connectivity | Length3D (µm) | Sphericity | Anisotropy |
|---|---|---|---|---|---|---|---|---|---|---|
| Affected brown tissue | 79.53 b | 5.34 b | 1666 ns | 3.1 b | 0.9 b | 4.0 b | 52.2 b | 95.43 b | 0.882 a | 0.765 b |
| White tissue from affected fruit | 176.96 a | 12.80 a | 2987 | 5.1 a | 6.2 a | 10.9 a | 705.6 a | 128.65 a | 0.828 c | 0.811 a |
| Unaffected tissue | 188.37 a | 13.69 a | 3390 | 5.9 a | 6.4 a | 11.9 a | 745.7 a | 120.07 a | 0.849 b | 0.792 a |
| *Pr > F(Model)* | *< 0.0001* | *< 0.0001* | *0.121* | *< 0.0001* | *< 0.0001* | *< 0.0001* | *< 0.0001* | *0.002* | *0.000* | *0.001* |
| *LSD value* | *15.25* | *1.206* | *1433* | *0.881* | *1.604* | *1.933* | *101.609* | *15.337* | *0.02* | *0.02* |

Results are indicated as mean values. Different letters for the same parameter indicate significant differences according to Fishers LSD at $p<0.05$. ns represents non-significant differences.

**Table 5**

Three dimensional morphometric parameters of the cells of core region fruit tissue (affected brown tissue, white tissue from affected fruit and unaffected tissue) obtained from X-ray CT images of 'Fuji' apples after the high $CO_2$/low $O_2$ stress treatment. 3D indicates that the measurements were done on 3-dimensional images.

| | Length3D (µm) | Thickness3D (µm) | Width3D (µm) | Area3D ($mm^2$) | Euler3D | Volume3D ($mm^3$) | Anisotropy | EqDiameter (µm) | Sphericity |
|---|---|---|---|---|---|---|---|---|---|
| Affected brown tissue | 295.73 ns | 167.61 ns | 174.32 a | 0.155 a | 0.637 b | 0.0035 ns | 0.682 ns | 178.82 ns | 0.688 b |
| White tissue from affected fruit | 285.92 | 157.75 | 160.86 b | 0.139 b | 0.902 a | 0.0035 | 0.686 | 177.56 | 0.767 a |
| Unaffected tissue | 287.24 | 159.88 | 162.74 b | 0.139 b | 0.921 a | 0.0035 | 0.682 | 180.00 | 0.773 a |
| *Pr > F(Model)* | *0.277* | *0.062* | *0.004* | *0.002* | *< 0.0001* | *0.935* | *0.927* | *0.818* | *< 0.0001* |
| *LSD value* | *11.225* | *7.285* | *6.926* | *0.0086* | *0.039* | *0.0004* | *0.024* | *7.536* | *0.012* |

Results are indicated as mean values. Different letters for the same parameter indicate significant differences according to Fisher's LSD at $p<0.05$. ns represents non-significant difference.

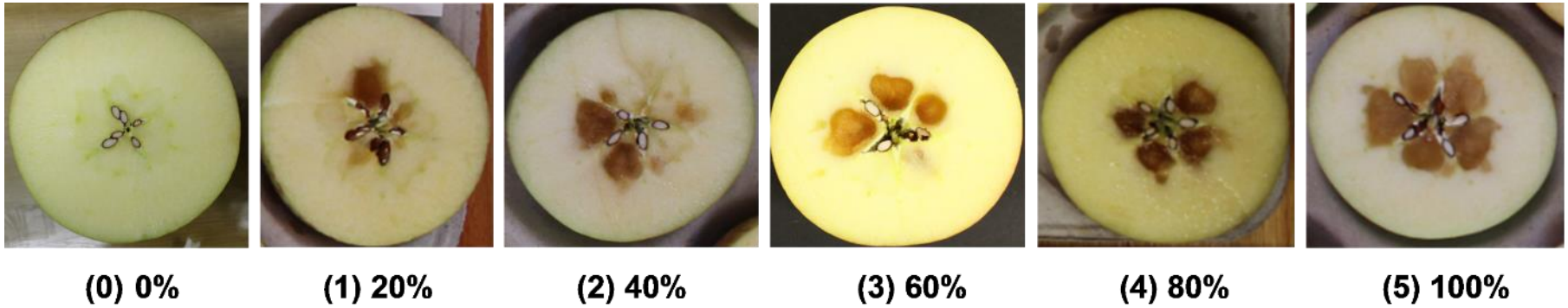


**Fig. 1.** Reference used for internal browning (IB) intensity index. Fruit with a score of 0 did not show any IB in the core while fruit with an intensity index of 5 had a 100% IB coverage of the core region.

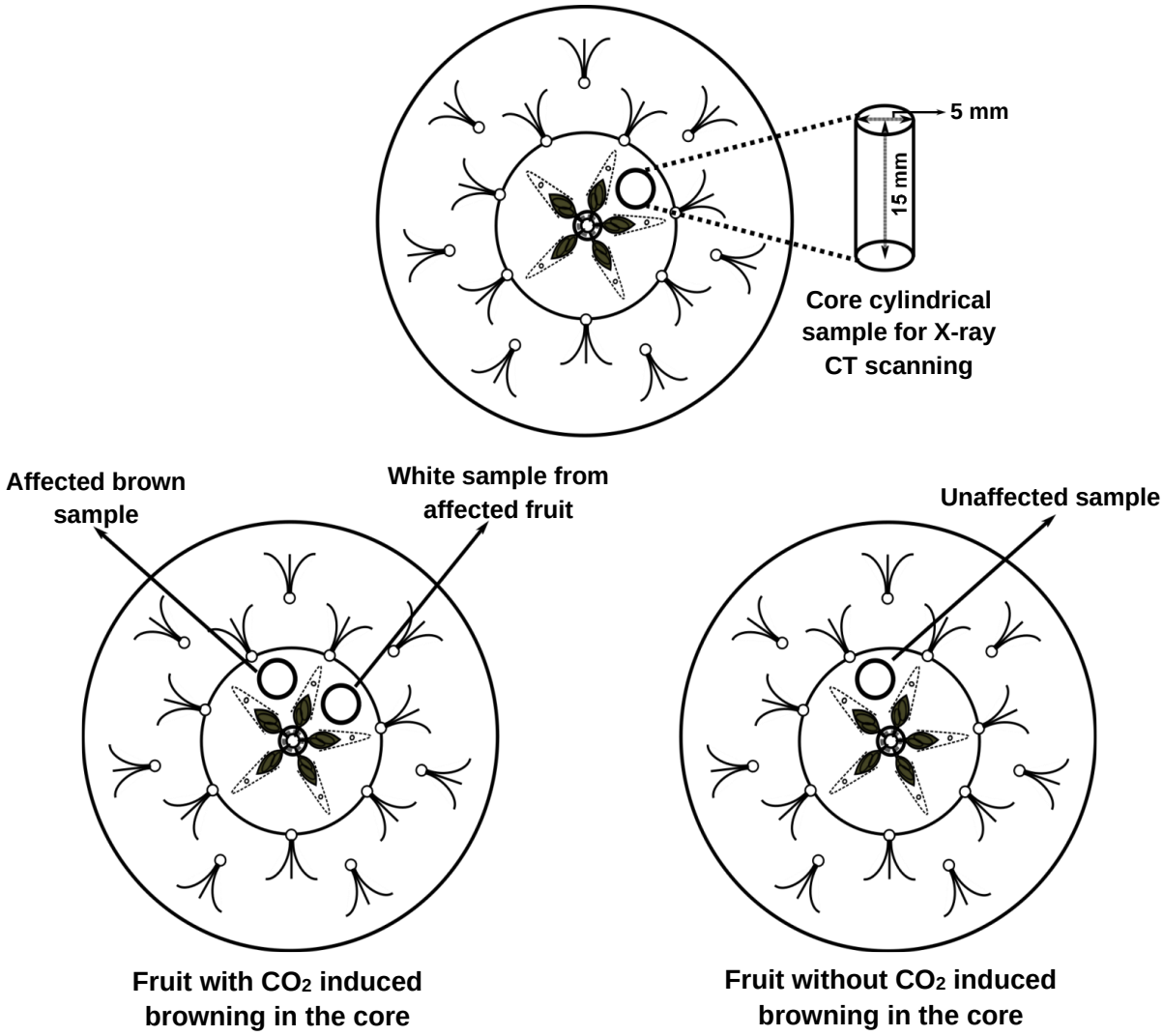


**Fig. 2.** Schematic presentation for the sampling positions from fruit with $CO_2$ induced browning in the core and fruit without $CO_2$ induced browning. Cylindrical samples with a diameter of 5 mm and length of 15 mm were obtained from fruit tissue using a cork-borer.

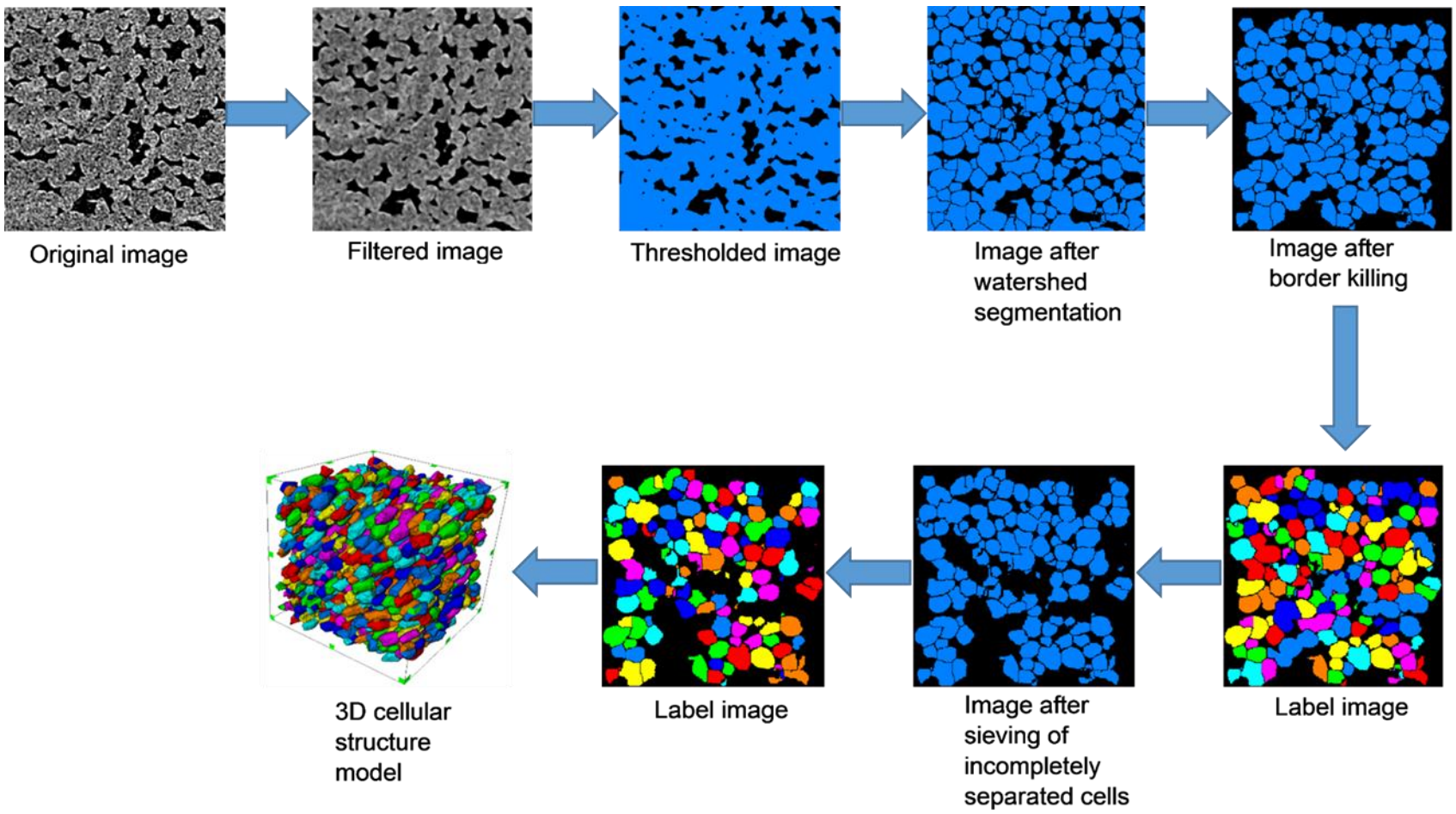


**Fig. 3.** Schematic representation of the procedure followed for the isolation of individual cells and measurement of individual cell parameters using Avizo 2019.1.

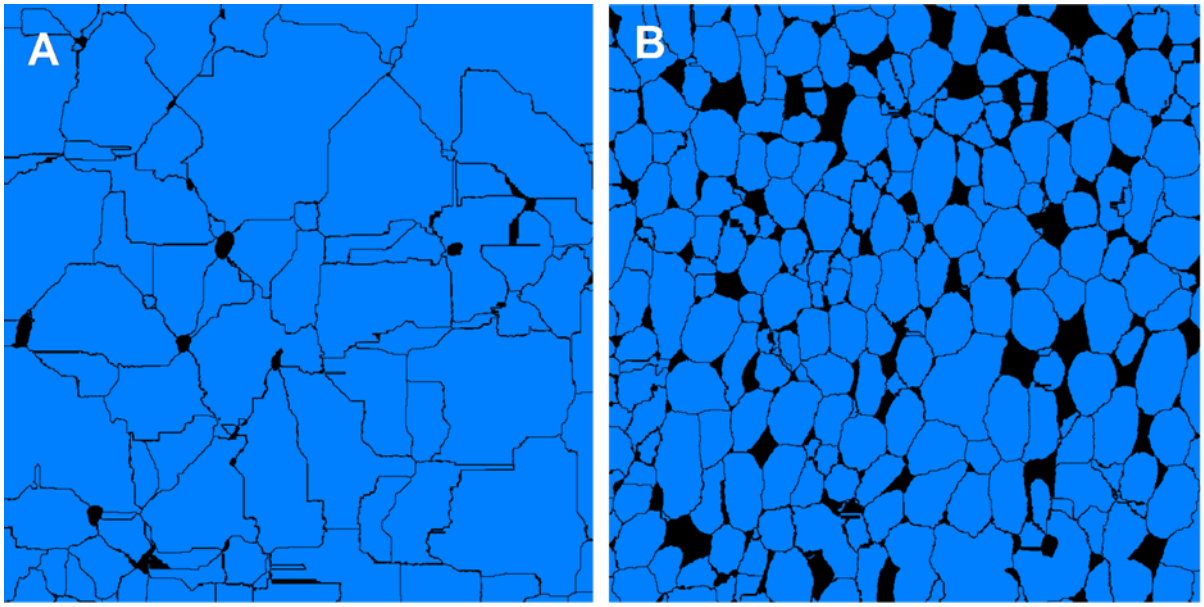


**Fig. 4.** Thresholded 2D binary images of A – Brown affected core region tissue sample and B – unaffected core region tissue sample after application of the 'separate objects' module in Avizo 2019.1. The separate objects module computes watershed lines to separate n neighbouring cells. The cells are in blue and the pores are in black. Tissue samples were obtained from 'Fuji' apples. The volume of the region of interest was 15.625 $mm^3$ (2.5 x 2.5 x 2.5 mm).

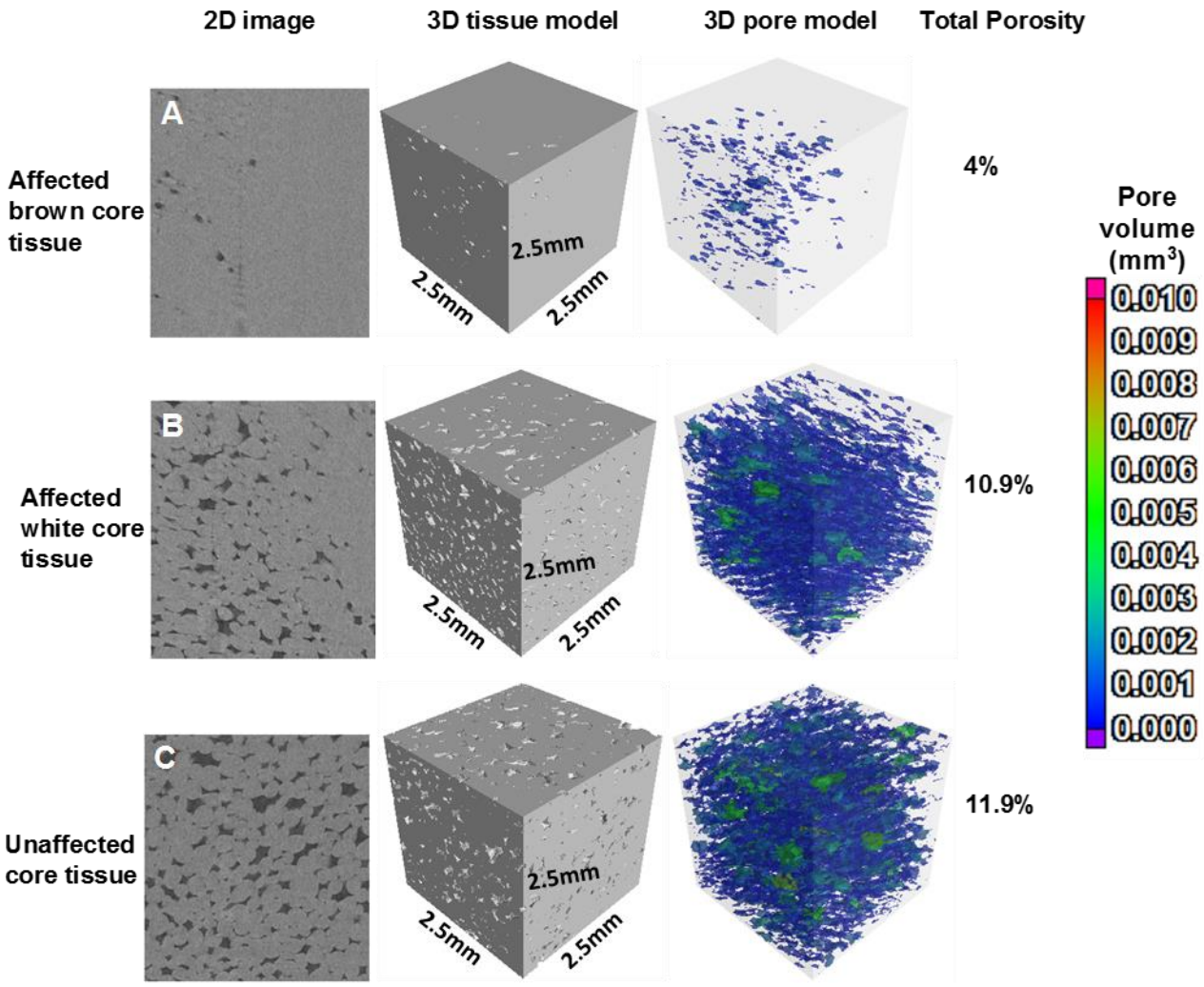


**Fig. 5.** 2D images after surface determination, 3D tissue models and 3D pore models of A - affected brown core tissue, B - white core tissue adjacent to affected brown tissue and C - unaffected core tissue of 'Fuji' apples after X-ray CT scanning and 3D image analysis of fruit tissue obtained from fruit after the high $CO_2$/low $O_2$ stress treatment. Pores are dark grey and fruit tissue is light grey. Different colours in the 3D pore models represent different pore volumes as shown in the scale.

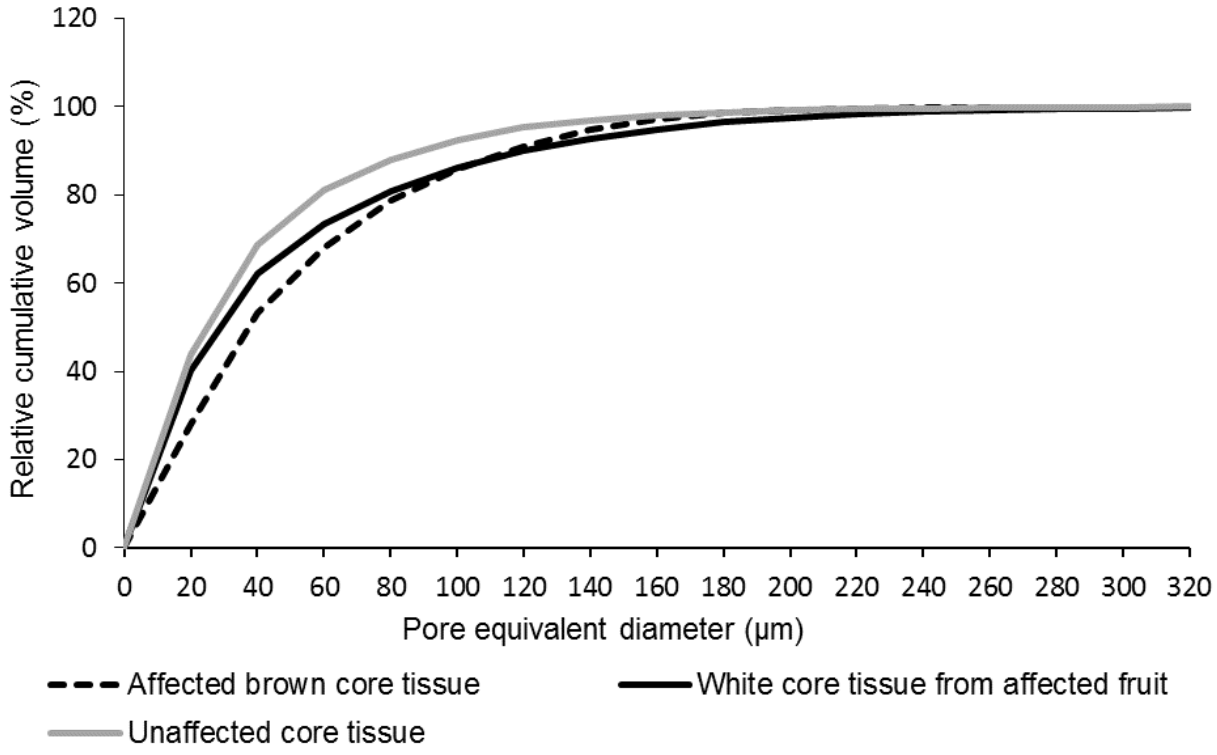


**Fig. 6.** Normal curve of distribution for individual pores in function of the equivalent diameter (µm) for affected brown core tissue, white core tissue from affected fruit and unaffected core tissue.

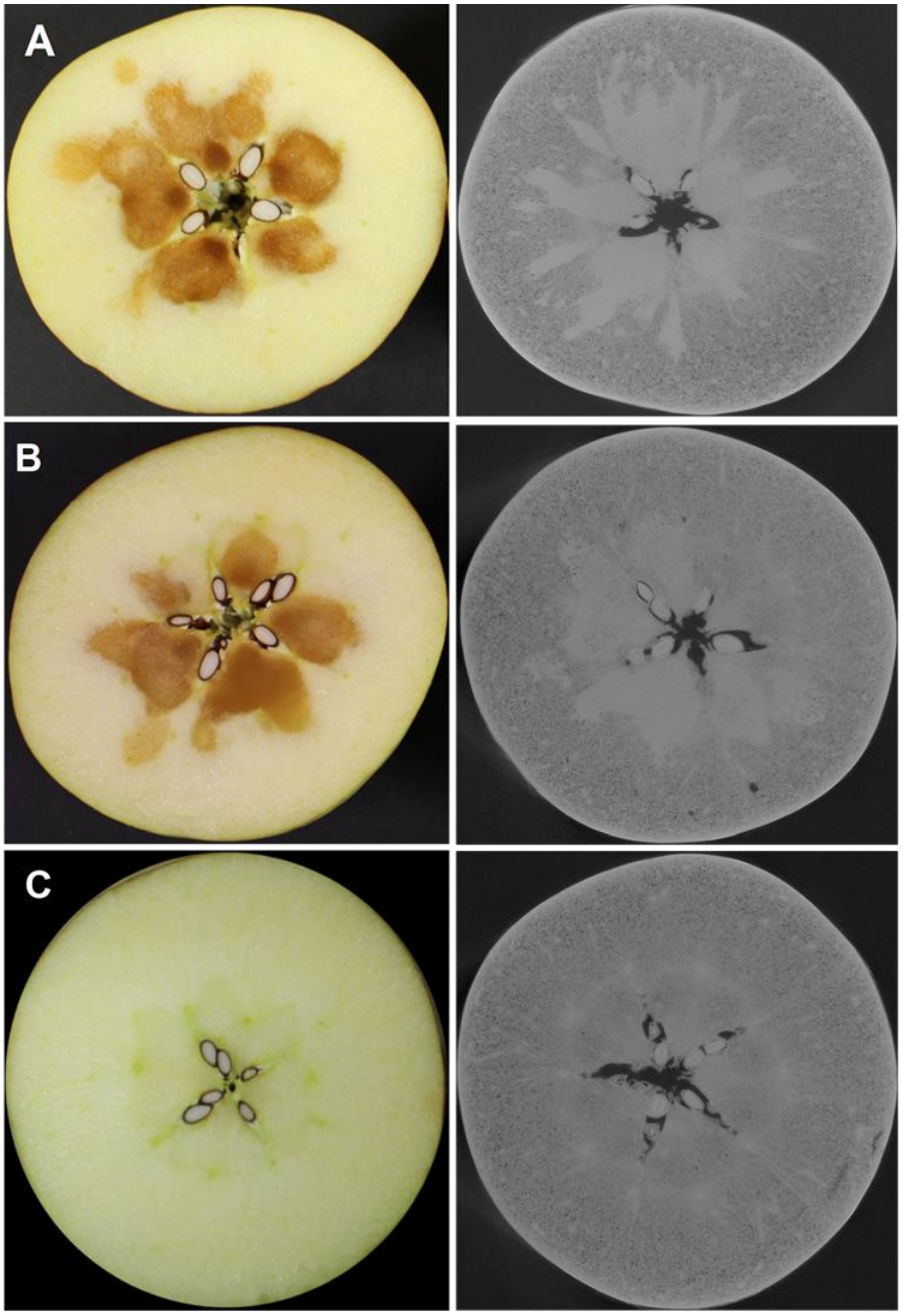


**Fig. 7.** Original images and corresponding greyscale images (of same fruit) for A and B - fruit with IB in the core region and C - a fruit without IB in the core region. Low-resolution scans were done at a resolution of 60 µm on whole fruit after the high $CO_2$/low $O_2$ stress treatment (50% $CO_2$/0.1% $O_2$).

**PAPER 2**

# X-ray CT and porosity mapping to determine the effect of 'Fuji' apple morphological and microstructural properties on the incidence of $CO_2$ induced internal browning


## Abstract

The objective of this study was to use X-ray computed tomography (CT) to map the porosity of 'Fuji' apple and help determine the extent to which different fruit morphological and microstructural properties influence the susceptibility of the fruit to $CO_2$ stress-induced internal browning (IB). There is considerable variability in the distribution of porosity within each fruit, hence non-destructive methods to map porosity of the entire fruit are important for the determination of porosity profiles and porosity variation. Morphological and microstructural properties evaluated included fruit size and density, radial and axial porosity profiles, and mean porosity. X-ray CT based porosity mapping and high-resolution X-ray CT were used to determine porosity changes in fruit tissue following exposure to an atmosphere enriched with 50% $CO_2$ at room temperature (21 °C) for 3 days after harvest. Low-resolution X-ray CT scans enabled the construction of porosity maps for intact fruit based on a grey value porosity correlation and a juice scan which acted as a 0% porosity reference. Short-term exposure of fruit to a high level of $CO_2$ markedly induced IB in the core region of the fruit. Axial porosity profiles showed that porosity along the axial plane was usually lower in fruit that developed IB after the stress treatment. Larger sized fruit were significantly ($P = 0.0001$) more susceptible to the $CO_2$ stress induced IB disorder. The porosity in the IB affected fruit tissue significantly declined ($P = 0.0276$) from 8.6 to 5.4% following the $CO_2$ stress treatment. It is recommended to avoid the storage of larger fruit for long durations and to ensure that levels of $CO_2$ and $O_2$ in the controlled atmosphere (CA) storage environment are carefully controlled to minimize the risk of high $CO_2$/low $O_2$ stress conditions and IB incidence.


**Keywords**: Axial porosity profile; computed tomography; $CO_2$ stress; fruit size

## 1. Introduction

Apples are climacteric fruit and the gaseous exchange between fruit and their environment is important for a physiological process such as respiration, which persists after harvest and during storage in controlled atmosphere (CA) conditions (Musse et al., 2010). CA environments generally use low levels of $O_2$ and increased concentrations of $CO_2$ combined with low temperatures to minimize respiration related metabolic changes in the fruit. Respiration of fruit after harvest depends on the availability of $O_2$ and it follows Michaelis-Menten kinetics (Ho et al., 2011). Diffusivity values for both $O_2$ and $CO_2$ are higher in the air than in water and this implies that both respiratory gases are predominantly transported through intercellular spaces (Kuroki et al., 2004; Ho et al., 2011). The microstructure of apple fruit consists of parenchyma cells, vascular tissue, and intercellular spaces (Mendoza et al., 2007). Intercellular spaces are the main channel through which $O_2$ is diffused into the respiring tissues and $CO_2$ is transported away (Cukrov, 2018). Intercellular spaces are also referred to as pores and porosity represents the pore volume as a fraction of the total sample volume (Mendoza et al., 2007).

The distribution of porosity in apple fruit is heterogeneous and varies at different locations within the same fruit (Nugraha et al., 2019). Herremans et al. (2015a) noted that the porosity of fruit tissue increases gradually in a radial direction from the core region towards the surface (peel) of the fruit. Regions in the fruit that have low porosity and low pore connectivity may have a negative effect on the movement of respiratory gases, leading to an accumulation of $CO_2$ and reduced internal $O_2$ concentration (Verboven et al., 2008; Nugraha et al., 2019). This may then cause localised development of hypoxic (very low $O_2$) or anoxic (no $O_2$) conditions depending on the fruit tissue microstructure (Pedreschi et al., 2009; Boeckx et al., 2019). The occurrence of hypoxic and anoxic conditions can result in the incidence of several post-harvest disorders such as internal browning (IB) in fruit (Cukrov, 2018).

IB is one of the most problematic post-harvest disorders in apples. ‘Fuji’ apples are especially prone to IB and this has been highlighted by several researchers (Volz et al., 1998; Argenta et al., 2000; Kweon et al., 2012, 2013). IB in ‘Fuji’ occasionally occurs in CA storage conditions and this disorder is affected by the size and maturity of fruit at harvest (Argenta et al., 2000). The use of very high $CO_2$ atmospheres (20 and 50% $CO_2$) to simulate IB disorders, which occur during CA storage of ‘Fuji’, has been proposed by Volz et al. (1998). They found strong positive correlations between flesh browning after CA storage and that which occurred after short-term exposure to high $CO_2$ levels.

To fully understand the browning of apples, it is necessary to study the morphological and microstructural properties of fruit such as size, density, and porosity profiles. Non-destructive methods such as X-ray computed tomography (CT) have been used previously in several studies to determine tissue porosity of apple and pears (Ting et al., 2013; Herremans et al., 2015a,b; Muziri et al., 2016; Nugraha et al., 2019; Janssen et al., 2020). However, porosity is generally determined from high-resolution X-ray CT scanning of a small tissue sample and does not allow scanning of the entire apple. Thus, this methodology is not adequate to describe the heterogeneity of porosity in the whole fruit (Nugraha et al., 2019). Although a low-resolution X-ray CT scan is sufficient to narrate the grey value variations in a complete fruit, it needs further processing to show porosity variations (Nugraha et al., 2019). Porosity mapping is based on the principle that different regions in an apple have different grey values due to differences in X-ray attenuation and tissue density. Determination of whole fruit porosity by X-ray CT has been recently performed for persimmon (Tanaka et al., 2018) and apple, pear, eggplant and turnip (Nugraha et al., 2019).

The present study aimed to use X-ray CT and porosity mapping to determine the extent to which different morphological and microstructural properties influence the susceptibility of ‘Fuji’ apple to $CO_2$ induced IB. The study also sought to use X-ray CT based porosity mapping and

high-resolution X-ray CT to determine porosity changes in the fruit after a $CO_2$ stress treatment was applied.

## 2. Materials and methods

### *2.1. Fruit material*

'Fuji' apples (*Malus x domestica* Borkh.) were harvested during the 3rd week of March 2019 (week 11) from Wakkerstroom farm (33°17'47.1"S 19°14'54.8"E) located in the Koue Bokkeveld area in the Western Cape Province, South Africa. Fruit of optimum harvest maturity were picked during the commercial harvest window for South African 'Fuji' apples. Fruit were harvested at shoulder height, from random positions around the tree canopy. The harvested fruit were placed into a lug box that was transported to the fruit evaluation laboratory at the Department of Horticultural Sciences, Stellenbosch University, Stellenbosch, South Africa. Figure 1 schematically describes the process of methodology development.

### *2.2. Low-resolution X-ray CT scanning of whole fruit and the radial cylindrical tissue sample*

Thirty-four (n = 34) intact fruit were scanned at a resolution of 132.2 µm using the V|Tome|X L240 micro-CT (µCT) scanner (GE Sensing & Inspection Technologies GmbH, Wunstorf, Germany), before being subjected to a $CO_2$ stress treatment. The V|Tome|X L240 µCT scanner contains two X-ray tubes, one with a reflection-type target and the other with a transmission target (du Plessis et al., 2016). The average time per scan was 5 min and 567 projection images were captured. The samples were scanned at a voltage of 120 kV and a current of 200 µA. These settings were not able to show individual pores, but they were capable of visualizing variations in grey value distributions. In addition to the whole fruit samples, a radial cylindrical tissue sample with a diameter of 5 mm (Fig. 2) was excised from the equator of the apple and scanned at the same settings as the intact apples. An additional apple was juiced and placed in a small plastic

tube and scanned under the same settings as the intact apples to act as a 0% porosity reference for each sample (Nugraha et al., 2019). Each sample was scanned with a plastic reference standard for density calibration. Since scanning time was very short (5 min), it was assumed that there were no variations and that scans were relatively uniform and consistent.

### *2.3. $CO_2$ stress treatment and evaluation of IB incidence in 'Fuji' fruit*

After low-resolution X-ray CT scanning, all fruit (n = 34) were subjected to a $CO_2$ stress treatment for 3 days at room temperature (21 °C). Fruit were placed in a Janny MT CA bin (JMT US, LLC, Okemos, USA) that consisted of an atmosphere enriched with 50% $CO_2$, this was achieved by pumping in $CO_2$ until the required level of $CO_2$ was achieved. The concentration of $O_2$ was 9.7% after the $CO_2$ enrichment. The level of gases in the CA bin were measured using a handheld gas analyser (F-950 Three Gas Analyser, Felix Instruments Inc., USA). The excess level of $CO_2$ was pumped out from the CA bin and replaced with $N_2$ to maintain 50% $CO_2$ throughout the experimental period. At the end of the 3 days, the fruit were taken out of the bin and each fruit was cut into two halves to evaluate the incidence of IB.

### *2.4. High-resolution X-ray CT scanning cylindrical tissue samples*

High-resolution X-ray CT was carried out to determine the porosity in fruit after exposure to $CO_2$ stress. Scanning was performed on cylindrical tissue samples (diameter: 5 mm; length: 15 mm) excised from the core region of seven fruit with IB incidence (Fig. 2). Four cylindrical core samples were also scanned to determine the porosity changes in fruit that did not develop IB. The high-resolution scans were performed at a resolution of 4 µm, using the Phoenix Nanotom S instrument (GE Sensing & Inspection Technologies GmbH, Wunstorf, Germany). Various system settings were tested to optimize scan quality. A series of 2600 projection images were obtained as the sample was rotated 360°. The samples were scanned at a voltage of 60 kV and a current

of 240 µA. Porosity, from porosity maps taken before the $CO_2$ stress treatment, and porosity from high-resolution X-ray CT after the treatment, allowed for the determination of porosity changes due to the $CO_2$ stress treatment. The data obtained from the radial cylindrical sample scanned at low- and high-resolution X-ray CT was used to model a greyscale intensity – porosity correlation, according to Nugraha et al. (2019). The correlation model was used in the construction of porosity maps. A multiple scan mode was used to scan the radial tissue sample because the sample was larger than the field of view of the X-ray detector. This mode divided the sample into four equal parts and eventually a complete structure of the sample was obtained after 4 hours of scanning.

*2.5. Reconstruction of low and high-resolution scans*

Both the low- and high-resolution scans were reconstructed into 3D volumes using Datos|x® 2.1 software (GE Sensing and Inspection Technologies GmbH, Wunstorf, Germany). The projection images from low-resolution X-ray CT scans were reconstructed into 8-bit 3D volumes. To remove the beam hardening effect, which is caused by polychromacity of the X-ray beam, beam hardening correction level 2 (software specific value) was applied. The beam hardening effect causes the appearance of artefacts, i.e., continuous variation in grey values within the reconstructed volume, depending on the variation of object thickness at different positions (Boas and Fleischmann, 2012). Ideally, an object consisting of analogous material should have homogenous grey values after reconstruction and should be used to determine the optimal correction level (Nugraha et al., 2019). The low-resolution radial scans and the high-resolution nano-CT scans were also reconstructed into 3D volumes using the same software and settings as for the intact fruit.

*2.6. Image analysis of intact apples*

VGStudio Max 3.3 (Volume Graphics GmbH, Heidelberg, Germany) software was used to extract the intact apple images from the low-resolution whole fruit scans. This had to be done to exclude background objects such as the sample holder and scanning reference from the image. The resulting image, which consisted of only the intact apple was saved as a 2-D 8-bit image stack, which was then uploaded to Matlab 9.4 (The Mathworks, Natick, MA, USA) to generate the porosity map of the whole apple. Porosity maps were used to determine the porosity profiles of fruit that developed IB and fruit that did not develop IB. Radial porosity profiles were constructed in Matlab 9.4 by determining the radial distance of different points from the fruit surface, starting from a distance of 2 mm from the fruit surface towards the centre of the apple. To determine the axial porosity profiles, a calyx to pedicel end axial sample was extracted from the low-resolution image of each apple using Amira-Avizo 2019.1 (Visualization Sciences Group (VSG), Bordeaux, France). The axial porosity profiles were determined on this axial sample by applying the moving average principle using a 3.2 mm cubic representative element volume (Nugraha et al., 2019).

Density was also calculated on the intact apples; this was made possible because each apple was scanned with a plastic reference of known density. Density was calculated based on equation 1.

$$\text{relative density} = \frac{\text{Mean grey value of ROI}}{\text{Mean grey value of reference}} \times 2.21\ \text{gcm}^{-3} \qquad (1)$$

*2.7. Image analysis for high-resolution CT scans*

After reconstruction, the 3-dimensional (3D) volumes were loaded into VGStudio Max 3.3 for image analysis and porosity determination. Analysing the whole image in its entirety can be an arduous and time-consuming exercise. As a result, it was necessary to select a smaller region of interest (ROI) from the original image (Schoeman et al., 2016). Although a ROI is smaller in

size compared to the original image, it is important to ensure that the selected ROI is large enough to be statistically representative of the whole sample. In this study a ROI cube measuring 2.5 x 2.5 x 2.5 mm was used. This volume of 15.625 $mm^3$ was larger than the recommended lower limit for a representative volume element of 1.3 $mm^3$ that was proposed for apple tissue by Mendoza et al. (2007).

After selection of the ROI, it was necessary to remove random noise in the selected ROI for subsequent analysis to be performed accurately. An adaptive gauss filter was used. This filter allows blurring of the selected data set, without destroying relevant structures in the image. A smoothing level of 1.5 was used, with an edge threshold set at 0.3 and 10 iterations. Smoothing specifies the amount of smoothing applied, while the edge threshold specifies to which amount edges are protected from the smoothing process. Iterations specify how many times the filter should be executed to determine the value of a voxel. After filtering, the image was segmented into its constituent pores and cells using automatic thresholding which employs Otsu's method (Otsu, 1979). Automatic thresholding allows for the determination of the background peak and the material peak in the histogram and then calculates the grey value of the material boundary. The background signifies the pores, while the material represents the cells. The result of automatic thresholding was a binary greyscale image consisting of pores (0) and cells (1). The total porosity of the sample was calculated by quantifying the volume of the pores and expressing it as a percentage of the total ROI volume. Foam structure analysis was also carried out in VGStudio Max 3.3 and this enabled quantification of the individual pore volumes within the entire ROI volume.

*2.8. Greyscale intensity and porosity correlation*

VGStudio Max 3.3 was used for the calculation of grey values and actual porosity of different ROIs in the radial sample. This made it possible to do a correlation analysis between greyscale

values and porosity to create porosity maps of the whole fruit (Nugraha et al., 2019). The correlation model was applied to the low-resolution whole fruit images, allowing the construction of a porosity map of each fruit before $CO_2$ stress treatment was applied. The measured porosity of a cylindrical sample after exposure to $CO_2$ stress was compared to the initial porosity at the approximate same position on the porosity map of fruit before $CO_2$ stress treatment. The difference between the high-resolution X-ray CT porosity and porosity from the porosity maps was then calculated.

### *2.9. Measurement of fruit height and diameter*

Fruit height was measured on 3D volumes of scanned fruit in VGStudio Max 3.3 using the calliper instrument to measure the distance from the calyx end of the apple to the pedicel end. Fruit diameter was determined using the same calliper instrument by measuring the radial distance from one end to the other in the middle region of the fruit (longest radial distance from one end of the apple to the other end).

### *2.10. Statistical analysis*

Regression analysis was performed to determine the relationship between grey values from the low-resolution scans and porosity from the high-resolution scans of the radial sample. A dependent sample *t*-test was performed to determine the changes in porosity in IB affected and unaffected fruit after $CO_2$ stress treatment. Independent sample *t*-tests were carried out to determine statistical differences for diameter, height, density and mean porosity. All statistical analyses were performed at a 5% significance level using STATISTICA version 13 (StatSoft, Inc., Tulsa, USA).

## 3. Results

### *3.1. Regression analysis between greyscale intensity and porosity of fruit tissue*

Construction of porosity maps was made possible by the correlation model between greyscale intensity and porosity of fruit tissue. In the present study, greyscale intensity values from the low-resolution CT scan of a radial tissue sample were plotted against the actual porosity determined from the high-resolution nano-CT scan of the same radial sample (Fig. 3A). The corresponding ROIs were chosen on the low- and high-resolution scans (Fig. 3B). Fourteen ROIs, each with a volume of 6 $mm^3$ were used for the correlation analysis. The greyscale intensity correlated well with the actual porosity of 'Fuji' apple ($R^2$ = 0.96; Fig. 3A). A juice sample which was used as a 0% porosity reference was also included in the regression analysis.

*3.2. Porosity maps of 'Fuji' fruit*

Greyscale X-ray CT images of 'Fuji' fruit were converted into porosity maps based on the greyscale intensity – porosity correlation model. Porosity distributions in horizontal cross-sectional images of larger fruit that developed IB in the core region and smaller fruit that did not develop IB after the $CO_2$ stress treatment were constructed and are demonstrated in Fig. 4A and B. The porosity maps were able to visualize the 3D distribution of the porosity within the entire fruit. The porosity was lower in the core region of the fruit, having an average porosity of 8% - 12%, whereas the cortex region had a higher porosity of 15% - 20% (Fig. 4A, B). A very low porosity region of less than 5% was localized in the region immediately under the peel of the 'Fuji' fruit (Fig. 4A, B). In the current study, a significant difference ($P = 0.0001$) in the diameter of 'Fuji' fruit that developed IB and fruit that did not develop IB was observed (Fig. 5A). Fruit that developed IB and fruit that did not develop IB had an average diameter of 82.3 ± 0.9 mm and 75.8 ± 0.9 mm, respectively (Fig. 5A). The height of 'Fuji' fruit did not differ significantly ($P = 0.2186$) between the two fruit categories (developed IB and no development of IB; Fig. 5A). The initial whole fruit mean porosity and the whole fruit density did not differ significantly between the two categories of 'Fuji' fruit (Fig. 5B), even though a slightly lower mean porosity and slightly higher density of whole fruit

tissue was noticed in the fruit that developed IB (Fig. 5B). Fruit that developed IB and fruit with no IB development had a whole fruit mean porosity of 13.1 and 14.2% respectively, and a density of 0.65 g/cm$^3$ and 0.61 g/cm$^3$, respectively (Fig. 5B).

*3.3. Mean radial and axial porosity profiles of whole fruit*

Radial porosity profiles describe a change in tissue porosity in a radial direction from the peel towards the centre of the apple on the equatorial plane (Fig. 6A). The porosity profiles were modelled for the two fruit groups i.e. fruit that developed IB and fruit that did not develop IB. The same pattern of changes in the mean radial porosity profiles were recorded for both fruit groups of fruit i.e. a decrease in porosity from the peel towards the centre of the fruit (Fig. 6A). There was no marked difference in the porosity profile pattern that was noticed along the radius of fruit from both categories. The only difference being that the fruit that developed IB had a longer radial porosity profile due to the larger fruit size (Fig. 6A). A comparable trend in the pattern of axial porosity distribution profiles was observed in both fruit groups, i.e. a higher porosity on the calyx end (0 mm) which decreased towards the core region of the fruit and then gradually rose/increased towards the pedicel end (Fig. 6B). The axial porosity profiles of 'Fuji' fruit that did not develop IB were generally higher and the highest porosity distribution was recorded in the region between the calyx end and the core region of the fruit (Fig. 6B).

*3.4. $CO_2$ stress-induced browning in 'Fuji' apple*

Figure 7A shows greyscale images of selected fruit before $CO_2$ stress treatment, while Figure 7B illustrates porosity maps of the same fruit before $CO_2$ stress treatment and Figure 7C presents cross-sectional images of the fruit after $CO_2$ stress treatment. IB observed after $CO_2$ stress treatment occurred in the core region of the fruit (Fig. 7C).

*3.5. $CO_2$ stress-induced porosity differences in affected and unaffected fruit*

For fruit that developed IB, the porosity of IB affected fruit tissue before $CO_2$ stress treatment was significantly higher compared to the porosity after $CO_2$ stress treatment (Fig. 8). There was a significant decrease (*P = 0.0276)* in porosity from 8.6% before $CO_2$ stress treatment to 5.4% after the application of the $CO_2$ stress treatment. Tissue samples obtained from unaffected fruit did not show a significant change in porosity (*P = 0.2410*). The initial porosity for unaffected fruit before the $CO_2$ stress treatment was 10.2% and the final porosity after the $CO_2$ stress treatment was 9.3% (Fig. 8).

The porosity after $CO_2$ stress treatment was as low as 0.5% in some of the samples. The size of the individual pores in IB affected fruit was also very small; most of the individual pores had a volume ranging between 0.000 $mm^3$ and 0.004 $mm^3$ (Fig. 9). This illustrates that all the larger pores were eliminated by the occurrence of IB, leaving behind only the smaller pores. In some of the samples, there were a few larger pores which had a volume higher than 0.008 $mm^3$.

## 4. Discussion

The X-ray CT results for the spatial distribution experiment demonstrate the potential of CT techniques to study the morphological and microstructural properties of IB disorder in ‘Fuji’ apple. In the current analysis, there was no significant difference in the radial porosity profiles that were constructed from the peel towards the centre of the fruit that developed IB and fruit that did not develop IB (Fig. 6A). The porosity distribution was relatively higher in the cortex region and decreased gradually towards the core region of fruit from both categories. Similar findings on the porosity distribution in various regions of fruit were previously reported for ‘Jonagold’ apple (Ho et al., 2011; Herremans et al., 2015a; Nugraha et al., 2019). The axial porosity profiles, measured from the calyx end towards the pedicel end, showed that the porosity in ‘Fuji’ fruit that did not develop IB was generally higher in comparison to the porosity of fruit that developed IB,

particularly in the region between the calyx end and the core. These differences in porosity distribution along the axial profile of fruit may help to explain why some of the fruit developed IB, whilst others did not develop IB. The higher porosity along the axial profile may have stimulated better gas diffusion, making fruit less susceptible to IB.

In fruit, the diffusivity of metabolic gases such as $O_2$ and $CO_2$ is highly dependent on the porosity distribution (Schotsmans et al., 2004). Herremans et al. (2015a) demonstrated that low porosity in the core region and regions leading to the core of fruit can limit the movement of respiratory gases through the fruit resulting in a buildup of $CO_2$ and $O_2$, possibly making the core region of fruit more susceptible to IB incidence. However, this relationship between low porosity and IB is associative and methods that can quantitatively and directly address this relationship are crucial. Ke et al. (1990) reported that a dark brown discolouration occurred in the middle region of 'Bartlett' pear fruit after short-term exposure to 50 and 80% $CO_2$ levels, similar to the results observed in this current study on 'Fuji' apples. Recently, Janssen et al. (2020) identified a zone of very low porosity and poor pore connectivity between the hypanthium and ovary region in 'Braeburn' apples stored at CA conditions that are not optimal (1 °C, 1 kPa $O_2$ and 3 kPa $CO_2$). In the current analysis, such a low porosity zone was not observed in 'Fuji' fruit tissue (Fig. 6A), thus it is anticipated that radial porosity distribution may not be a key factor contributing to the stimulation of IB incidence. Conversely, more prominent differences in the axial porosity profile were noticed between IB affected and unaffected 'Fuji' fruit (Fig. 6B).

In this present study, the initial mean porosities and relative densities of the whole 'Fuji' fruit did not differ significantly for fruit that developed IB compared to fruit that did not develop IB (Fig. 5B). This illustrated that differences in porosity in specific regions within the fruit play a bigger role in susceptibility to IB compared to overall fruit porosity. The higher porosity in the cortex region of the fruit may allow for better diffusivity of respiratory gases (Ho et al., 2010b; Janssen et al., 2020). This could be a possible reason why the cortex remained unaffected by IB in the current study.

Studies done on ‘Braeburn’ apples showed that a core region which has an $O_2$ concentration of 0.5%, is at a higher risk of developing oxidative stress and IB compared to the cortex region, which has an $O_2$ concentration of 1.5 – 2% (Mellidou et al., 2014). Previously, Ho et al. (2010a) highlighted that increasing respiration rate resulted in anoxia in the central region of ‘Conference’ pear fruit and this was more severe in large fruit than in smaller fruit. Analysis of internal gas concentration profiles inside fruit, while accounting for porosity maps, will allow us to verify the effect of spatial differences in porosity. Quantification of internal gas atmospheres was previously carried out for three apple cultivars (Kanzi, Jonagold, and Braeburn) by Ho et al. (2010b). Their measurements showed that the $O_2$ concentration in apple tissue was considerably lower than that of the ambient atmosphere (21 kPa $O_2$ and 0 kPa $CO_2$ at 20 °C). Additionally, the $O_2$ concentration decreased towards the core of the three apple cultivars and this points out to the existence of a $O_2$ concentration gradient from the surface to the core (Ho et al., 2010b). On the other hand, there is a increasing gradient in $CO_2$ concentrations from the fruit surface towards the core of the fruit (Paul and Pandey, 2014). Ho et al. (2010b) observed that diffusivity of both $O_2$ and $CO_2$ increased significantly with distance from the centre of the fruit, showing a possible relationship between porosity (high porosity in cortex and low porosity in the core) and diffusivity: high porosity facilitates gas exchange leading to a large diffusivity. A possible link between low porosity and low diffusivity was also highlighted by Yearsley et al. (1997) in their studies on post-climacteric ‘Cox’s Orange Pippin’ and ‘Braeburn’ apples, they provided that the lower porosity and higher density of ‘Braeburn’ may potentially reduce diffusivity of $O_2$ through the cortex and contribute to increased internal lower oxygen limit ($LOL^i$s) of 'Braeburn' compared to ‘Cox’s Orange Pippin’ fruit.

Fruit diameter also played a significant role in the incidence of IB. This was shown by the significantly higher susceptibility of larger fruit to $CO_2$ induced IB. In earlier studies, Meheriuk et al. (1994) highlighted that IB is more predominant in large fruit, as well as late harvested and

overmatured fruit. Lammertyn et al. (2000) found that large and heavy ‘Conference’ pears have a higher probability of developing IB disorders. Late harvesting of fruit usually results in the harvest of larger fruit, which are more susceptible to IB (Franck et al., 2007). A similar trend of larger fruit being more susceptible to IB was observed by Lammertyn et al. (2003) for ‘Conference’ pears, where it was reported that the percentage brown tissue per slice increased with increasing diameter. Ho et al. (2016) postulated that the risk of fermentation associated with IB incidence was higher in late harvested larger pear fruit. This was attributed to the increased $O_2$ minimal value as fruit size increases, which enhances the risk of fermentation related IB disorders. The $O_2$ minimal value refers to the lowest $O_2$ concentration below which fermentation, due to hypoxia, is more likely to occur (Ho et al., 2016).

In this study, there was a significant decrease in porosity of ‘Fuji’ fruit that developed IB after exposure to $CO_2$ stress treatment. The average porosity of core tissue samples before $CO_2$ stress treatment was 8.6%, while the average porosity after $CO_2$ stress treatment was 5.4%. Diffusion limitations in the fruit tissue and a high $CO_2$ concentration in the storage atmosphere can cause the establishment of a concentration gradient within the apple tissue which can result in decreasing $O_2$ partial pressure and increasing $CO_2$ partial pressure towards the core of the fruit (Ho et al., 2010b; 2013). The high $CO_2$ levels may result in the development of hypoxic or anoxic conditions within the fruit (Herremans et al., 2013; Cukrov, 2018). Furthermore, high levels of $CO_2$ have a negative effect on the $O_2$ consumption of several fruit and vegetables (Peppelenbos and van’t Leven, 1996). While it is difficult to determine how high $CO_2$ levels affect fruit $O_2$ consumption, it may be a result of competitive inhibition of $O_2$ by $CO_2$ (Fagundes et al., 2013). Competitive inhibition occurs when both the inhibitor ($CO_2$) and substrate ($O_2$) compete for the same active site of the enzyme (Peppelenbos and van’t Leven, 1996). In studies on ‘Gala’ apple slices, which were based on inhibition models, Fagundes et al. (2013) recognised a clear effect of high $CO_2$ on reduced $O_2$ consumption, indicating that competitive inhibition probably occurred.

Another possible explanation on the effect of high $CO_2$ levels on fruit metabolism would be its influence on cytoplasmic pH. Exposure of fruit to high $CO_2$ levels can cause the pH to drop due to dissociation of carbonic acid to bicarbonate and hydrogen ions (Mathooko, 1996). Such $CO_2$ mediated drop in pH may have a significant impact on various enzymes and enzymatic intermediates in fruit metabolic pathways (Ke et al., 1993; Mathooko, 1996). In addition, a shift in cytoplasmic pH can also lead to loss of compartmentalization and mixing of phenolic substrates with oxidative enzymes and subsequent formation of brown coloured polymers (Franck et al., 2007). Mathooko (1996) further reported that elevated concentrations of $CO_2$ in fruit storage environments may reduce the enzyme activity of phosphofructokinase, which suppresses the glycolytic pathway, while promoting fermentative metabolism and accumulation of fermentation metabolites such as acetaldehyde and ethanol. A shift from normal aerobic respiration to fermentative respiration has the adverse effect of generating less energy to maintain membrane integrity, which may lead to membrane damage, cellular decompartmentalization (causing the release of cellular fluids into intercellular spaces), and IB incidence in fruit (Franck et al., 2007).

Schotsmans et al. (2004) stated that the flooding of intercellular spaces with cellular fluids results in a reduction in porosity in apple fruit tissue and this phenomenon is similar to the results obtained in the current study (Fig. 8). Flooding of intercellular spaces and reduced porosity signifies the initial stages of $CO_2$ induced IB before the cellular fluids diffuse out of the fruit, leaving cavities in the fruit tissue. This can happen when fruit are stored for long durations in CA environments. In the present study, ‘Fuji’ apples were stored only for a short time (3 days) in high $CO_2$ conditions and this may not have allowed adequate time for cellular fluids to diffuse out of the fruit and as a result there were no voids or cavities observed within the fruit tissue.

## 5. Conclusion

'Fuji' apples stressed with 50% $CO_2$ at room temperature (21 °C) resulted in IB incidence in the core region of the fruit. A high correlation was established between the grey values and porosity, making it possible to construct porosity maps of intact fruit from low-resolution X-ray CT images. The porosity maps visualized the distribution of porosity in the entire fruit, indicating a low porosity in the core region and a high porosity in the cortex region. While the radial porosity profiles did not show major porosity differences between the two fruit categories (with and without IB development), the axial porosity profiles revealed that the porosity in fruit that did not develop IB was generally higher along the axial plane, particularly in regions close to the calyx end. High-resolution X-ray CT scans, performed after $CO_2$ stress treatment, allowed the determination of porosity changes that occurred as a result of $CO_2$ stress. There was a decrease in porosity for IB affected fruit tissue after the $CO_2$ stress treatment. Fruit size significantly influenced IB incidence, with larger fruit being more susceptible. Although there was a relationship between IB incidence and low porosity, it is important to find methods that can quantitatively and directly ascertain this connection. It is important to avoid long storage durations for larger fruit as they will be at a higher risk of developing IB. To avoid the production of excessively large fruit, it is important to carefully control pre-harvest factors such as crop load, nutrition and irrigation; which ultimately influence the final fruit size. This study presented the negative effects of high $CO_2$ levels in the CA storage atmosphere and the susceptibility of 'Fuji' apples to $CO_2$ induced IB disorders. Porosity mapping can be used in future studies to screen fruit for porosity differences, segregate and treat them with IB inducing storage conditions to further ascertain the relationship between porosity and IB.

## Acknowledgements

This study was financially supported by the South African Apple and Pear Producers' Association and HORTGRO Science.

## References

Argenta, L.C., Fan, X., Mattheis, J.P., 2000. Delaying establishment of controlled atmosphere or $CO_2$ exposure reduces 'Fuji' apple $CO_2$ injury without excessive fruit quality loss. Postharvest Biol. Technol. 20, 221–229. https://doi.org/10.1016/S0925-5214(00)00134-4.

Boas, F.E., Fleischmann, D., 2012. CT artifacts: causes and reduction techniques. Imaging Med. 4, 229–240.

Boeckx, J., Pols, S., Hertog, M.L.A.T.M., Nicolaï, B.M., 2019. Regulation of the central carbon metabolism in apple fruit exposed to postharvest low-oxygen stress. Front. Plant Sci. 10, 1384. https://doi.org/10.3389/fpls.2019.01384.

Cukrov, D., 2018. Progress toward understanding the molecular basis of fruit response to hypoxia. Plants 7, 78. https://doi.org/10.3390/plants7040078.

du Plessis, A., le Roux, S.G., Guelpa, A., 2016. The CT Scanner Facility at Stellenbosch University: An open access X-ray computed tomography laboratory. Nucl. Instrum. Methods Phys. Res., B 384, 42–49. https://doi.org/10.1016/j.nimb.2016.08.005.

Fagundes, C., Carciofi, B.A.M., Monteiro, A.R., 2013. Estimate of respiration rate and physicochemical changes of fresh-cut apples stored under different temperatures. Food Sci. Technol. (Campinas) 33, 60–67. http://dx.doi.org/10.1590/S0101-20612013005000023.

Franck, C., Lammertyn, J., Ho, Q.T., Verboven, P., Verlinden, B., Nicolaï, B.M., 2007. Browning disorders in pear fruit. Postharvest Biol. Technol. 43, 1–13. https://doi.org/10.1016/j.postharvbio.2006.08.008.

Herremans, E., Verboven, P., Bongaers, E., Estrade, P., Verlinden, B.E., Wevers, M., Hertog, M.L.A.T.M., Nicolaï, B.M., 2013. Characterisation of 'Braeburn' browning disorder by means of X-ray micro-CT. Postharvest Biol. Technol. 75, 114–124. https://doi.org/10.1016/j.postharvbio.2012.08.008.

Herremans, E., Verboven, P., Hertog, M.L.A.T.M., Cantre, D., van Dael, M., De Schryver, T., Van Hoorebeke, L., Nicolaï, B.M., 2015a. Spatial development of transport structures in apple

(*Malus* × *domestica* Borkh.) fruit. Front. Plant Sci. 6, 679. https://doi.org/10.3389/fpls.2015.00679.

Herremans, E., Verboven, P., Verlinden, B.E., Cantre, D., Abera, M., Wevers, M., Nicolaï, B.M., 2015b. Automatic analysis of the 3D microstructure of fruit parenchyma tissue using X-ray micro-CT explains differences in aeration. BMC Plant Biol. 15, 264. https://doi.org/10.1186/s12870-015-0650-y.

Ho, Q.T., Rogge, S., Verboven, P., Verlinden, B.E., Nicolaï, B.M., 2016. Stochastic modelling for virtual engineering of controlled atmosphere storage of fruit. J. Food Eng. 176, 77–87. https://doi.org/10.1016/j.jfoodeng.2015.07.003.

Ho, Q.T., Verboven, P., Verlinden, B.E., Herremans, E., Wevers, M., Carmeliet, J., Nicolaï, B.M., 2011. A three-dimensional multiscale model for gas exchange in fruit. Plant Physiol. 155, 1158–1168. https://doi.org/10.1104/pp.110.169391.

Ho, Q.T., Verboven, P., Verlinden, B.E., Nicolaï, B.M., 2010a. A model for gas transport in pear fruit at multiple scales. J. Exp. Bot. 61, 2071–2081. https://doi.org/10.1093/jxb/erq026.

Ho, Q.T., Verboven, P., Verlinden, B.E., Schenk, A., Delele, M.A., Rolletschek, H., Vercammen, J., Nicolaï, B.M., 2010b. Genotype effects on internal gas gradients in apple fruit. J. Exp. Bot. 61, 2745–2755. https://doi.org/10.1093/jxb/erq108

Ho, Q.T., Verboven, P., Verlinden, B.E., Schenk, A., Nicolaï, B.M., 2013. Controlled atmosphere storage may lead to local ATP deficiency in apple. Postharvest Biol. Technol. 78, 103–112. https://doi.org/10.1016/j.postharvbio.2012.12.014

Janssen, S., Verboven, P., Nugraha, B., Wang, Z., Boone, M., Josipovic, I., Nicolaï, B.M., 2020. 3D pore structure analysis of intact ‘Braeburn’ apples using X-ray micro-CT. Postharvest Biol. Technol. 159, 111014. https://doi.org/10.1016/j.postharvbio.2019.111014.

Ke, D., Mateos, M., Siriphanich, J., Li, C., Kader, A.A., 1993. Carbon dioxide action on metabolism of organic and amino acids in crisphead lettuce. Postharvest Biol. Technol. 3, 235–247. https://doi.org/10.1016/0925-5214(93)90059-C.

Ke, D., van Gorsel, H., Kader, A.A., 1990. Physiological and quality responses of 'Bartlett' pears to reduced $O_2$ and enhanced $CO_2$ levels and storage temperature. J. Am. Soc. Hortic. Sci. 115, 435–439. https://doi.org/10.21273/jashs.115.3.435.

Kuroki, S., Oshita, S., Sotome, I., Kawagoe, Y., Seo, Y., 2004. Visualization of 3D network of gas-filled intercellular spaces in cucumber fruit after harvest. Postharvest Biol. Technol. 33, 255–262. https://doi.org/10.1016/j.postharvbio.2004.04.002.

Kweon, H.J., Kang, I.K., Kim, M.J., Lee, J., Moon, Y.S., Choi, C., Choi, D.G., Watkins, C.B., 2013. Fruit maturity, controlled atmosphere delays and storage temperature affect fruit quality and incidence of storage disorders of 'Fuji' apples. Sci. Hortic. 157, 60–64. https://doi.org/10.1016/j.scienta.2013.04.013.

Kweon, H.J., Kim, M.J., Moon, Y.S., Lee, J., Choi, C., Choi, D.G., Lee, D.H., Kang, I.K., 2012. Relationship between preharvest factors and the incidence of storage disorders in 'Fuji' apples during CA storage. Korean J. Hortic. Sci. Technol. 30, 50–55. https://doi.org/10.7235/hort.2012.11049.

Lammertyn, J., Aerts, M., Verlinden, B.E., Schotsmans, W., Nicolaï, B.M., 2000. Logistic regression analysis of factors influencing core breakdown in 'Conference' pears. Postharvest Biol. Technol. 20, 25–37. https://doi.org/10.1016/S0925-5214(00)00114-9.

Lammertyn, J., Dresselaers, T., Van Hecke, P., Jancsok, P., Wevers, M., Nicolaï, B.M., 2003. MRI and X-ray CT study of spatial distribution of core breakdown in 'Conference' pears. Magn. Reson. Imaging 21, 805–815. https://doi.org/10.1016/S0730-725X(03)00105-X.

MacDaniels, L.H., 1940. The morphology of the apple and other pome fruits. Mem. Cornell Agric. Exp. Stn. 230, 32.

Mathooko, F.M., 1996. Regulation of respiratory metabolism in fruits and vegetables by carbon dioxide. Postharvest Biol. Technol. 9, 247–264. https://doi.org/10.1016/S0925-5214(96)00019-1.

Meheriuk, M., Prange, R.K. Lidster, P.D., Porritt, S.W., 1994. Postharvest disorders of apples and pears. Agriculture Canada Publication 1737E. Communications Branch, Agriculture Canada Ottawa, Ont. 66.

Mellidou, I., Buts, K., Hatoum, D., Ho, Q.T., Johnston, J.W., Watkins, C.B., Schaffer, R.J., Gapper, N.E., Giovannoni, J.J., Rudell, D.R., Hertog, M.L.A.T.M., Nicolaï, B.M., 2014. Transcriptomic events associated with internal browning of apple during postharvest storage. BMC Plant Biol. 14, 1–17. https://doi.org/10.1186/s12870-014-0328-x.

Mendoza, F., Verboven, P., Mebatsion, H.K., Kerckhofs, G., Nicolaï, B., 2007. Three-dimensional pore space quantification of apple tissue using X-ray computed microtomography. Planta 226, 559–570. https://doi.org/10.1007/s00425-007-0504-4.

Musse, M., De Guio, F., Quellec, S., Cambert, M., Challois, S., Davenel, A., 2010. Quantification of microporosity in fruit by MRI at various magnetic fields: comparison with X-ray microtomography. Magn. Reson. Imaging 28, 1525–1534. https://doi.org/10.1016/j.mri.2010.06.028.

Muziri, T., Theron, K.I., Cantre, D., Wang, Z., Verboven, P., Nicolaï, B.M., Crouch, E.M., 2016. Microstructure analysis and detection of mealiness in ‘Forelle’ pear (*Pyrus communis L*.) by means of X-ray computed tomography. Postharvest Biol. Technol. 120, 145–156. https://doi.org/10.1016/j.postharvbio.2016.06.006.

Nugraha, B., Verboven, P., Janssen, S., Wang, Z., Nicolaï, B.M., 2019. Non-destructive porosity mapping of fruit and vegetables using X-ray CT. Postharvest Biol. Technol. 150, 80–88. https://doi.org/10.1016/j.postharvbio.2018.12.016.

Otsu, N., 1979. A threshold selection method from gray-level histograms. IEEE Trans. Syst. Man Cybern. 9, 62–66.

Paul, V., Pandey, R., 2014. Role of internal atmosphere on fruit ripening and storability - a review. J. Food Sci. Technol. 51, 1223–1250. https://doi.org/10.1007/s13197-011-0583-x

Pedreschi, R., Franck, C., Lammertyn, J., Erban, A., Kopka, J., Hertog, M., Verlinden, B., Nicolaï,

B., 2009. Metabolic profiling of ‘Conference’ pears under low oxygen stress. Postharvest Biol. Technol. 51, 123–130. https://doi.org/10.1016/j.postharvbio.2008.05.019.

Peppelenbos, H.W., van’t Leven, J., 1996. Evaluation of four types of inhibition for modelling the influence of carbon dioxide on oxygen consumption of fruits and vegetables. Postharvest Biol. Technol. 7, 27–40. https://doi.org/10.1016/0925-5214(96)80995-1.

Schoeman, L., Williams, P., du Plessis, A., Manley, M., 2016. X-ray micro-computed tomography (μCT) for non-destructive characterisation of food microstructure. Trends Food Sci. Technol. 47, 10–24. https://doi.org/10.1016/j.tifs.2015.10.016.

Schotsmans, W., Verlinden, B.E., Lammertyn, J., Nicolaï, B.M., 2004. The relationship between gas transport properties and the histology of apple. J. Sci. Food Agric. 84, 1131–1140. https://doi.org/10.1002/jsfa.1768.

Tanaka, F., Imamura, K., Tanaka, F., Uchino, T., 2018. Determination of thermal diffusivity of persimmon flesh tissue using three-dimensional structure model based on X-ray computed tomography. J. Food Eng. 221, 151–157. https://doi.org/10.1016/j.jfoodeng.2017.10.021.

Ting, V.J.L., Silcock, P., Bremer, P.J., Biasioli, F., 2013. X-ray micro-computer tomographic method to visualize the microstructure of different apple cultivars. J. Food Sci. 78, E1735–E1742. https://doi.org/10.1111/1750-3841.12290

Verboven, P., Kerckhofs, G., Mebatsion, H.K., Ho, Q.T., Temst, K., Wevers, M., Cloetens, P., Nicolaï, B.M., 2008. Three-dimensional gas exchange pathways in pome fruit characterized by synchrotron X-ray computed tomography. Plant Physiol. 147, 518–527. https://doi.org/10.1104/pp.108.118935.

Volz, R.K., Biasi, W.V., Grant, J.A., Mitcham, E.J., 1998. Prediction of controlled atmosphere-induced flesh browning in ‘Fuji’ apple. Postharvest Biol. Technol. 13, 97–107. https://doi.org/10.1016/S0925-5214(97)00080-X.

Yearsley, C.W., Banks, N.H., Ganesh, S., 1997. Effect of carbon dioxide on the internal lower oxygen limits of apple fruit. Postharvest Biol. Technol. 12, 1–13. https://doi.org/10.1016/S0925-5214(97)00044-6

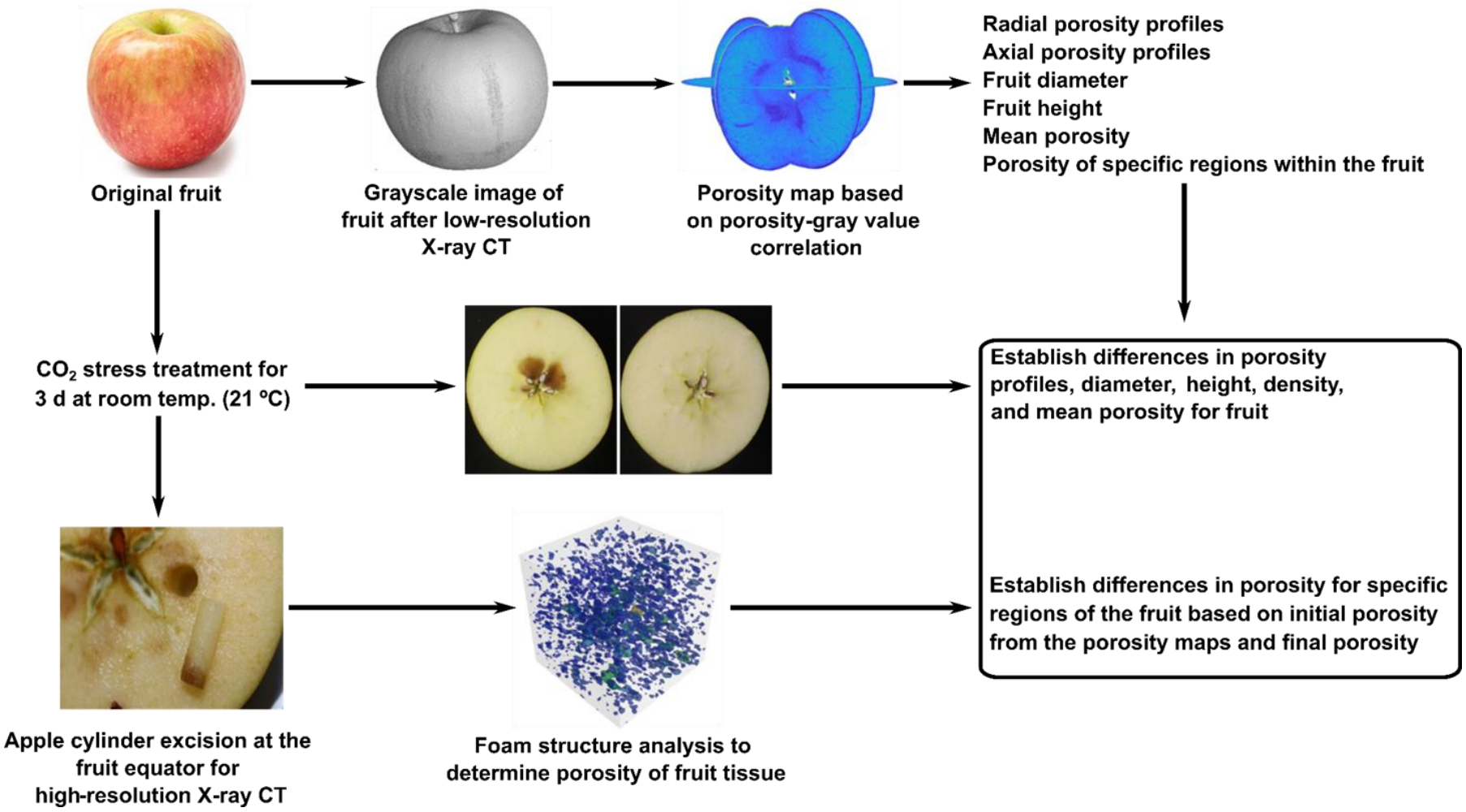


**Fig. 1.** A schematic representation of the experimental procedure followed in this study. Fruit were scanned at low-resolution (132.2 µm) before being subjected to a $CO_2$ stress treatment and porosity maps of each fruit were created. High-resolution scans (4 µm) of small cylindrical samples from selected fruit was done after the stress treatment, this allowed for determination of porosity changes.

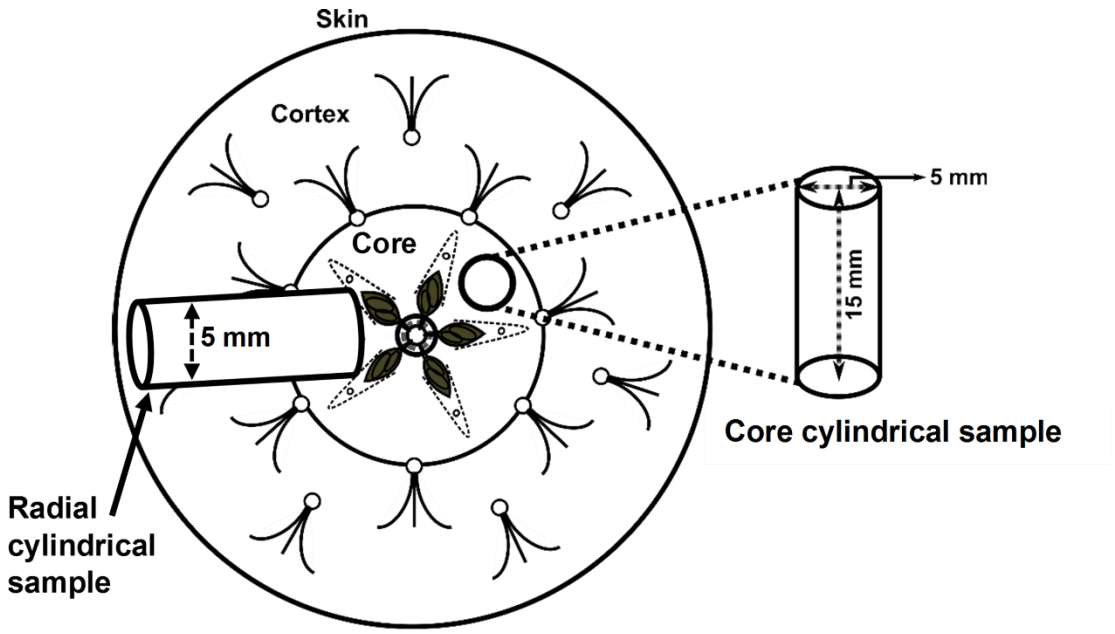


**Fig. 2.** A schematic diagram of the excision of radial and core the cylindrical samples from the core region of a 'Fuji' apple used for X-ray nano-CT scanning after the $CO_2$ stress treatment (modified from MacDaniels, 1940).

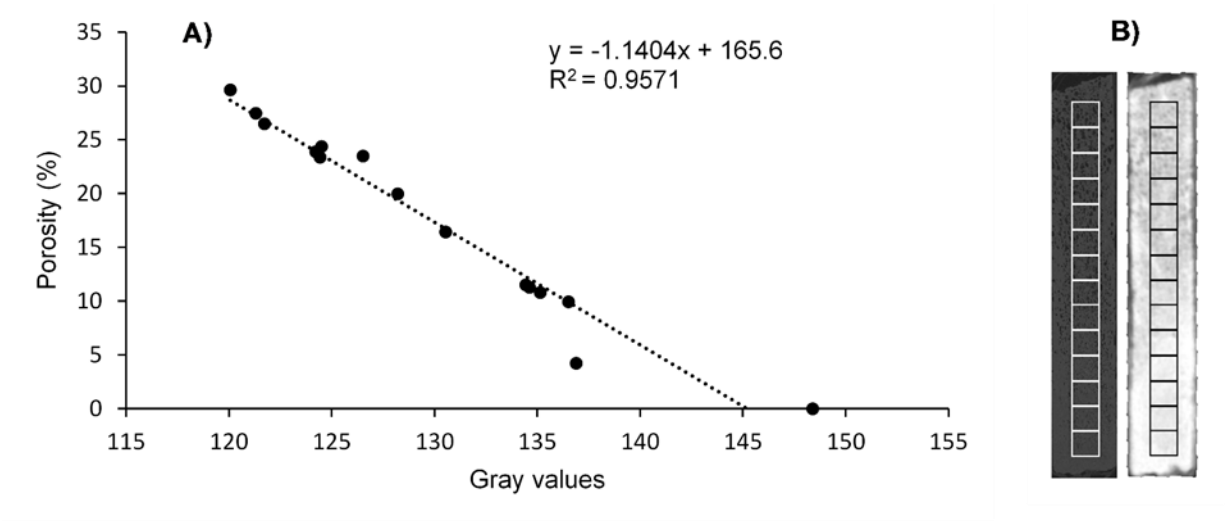


**Fig. 3.** Regression analysis between grey values of a low-resolution X-ray CT scan of a radial tissue sample and actual porosity obtained from a high-resolution X-ray CT scan of the same radial sample (A). Fourteen regions of interest (ROIs) were taken at approximately the same positions on the high-(left) and low-(right) resolution CT image (B) and used for correlation analysis. The grey value for the juice scan which acted as a 0% porosity reference was included in the correlation.

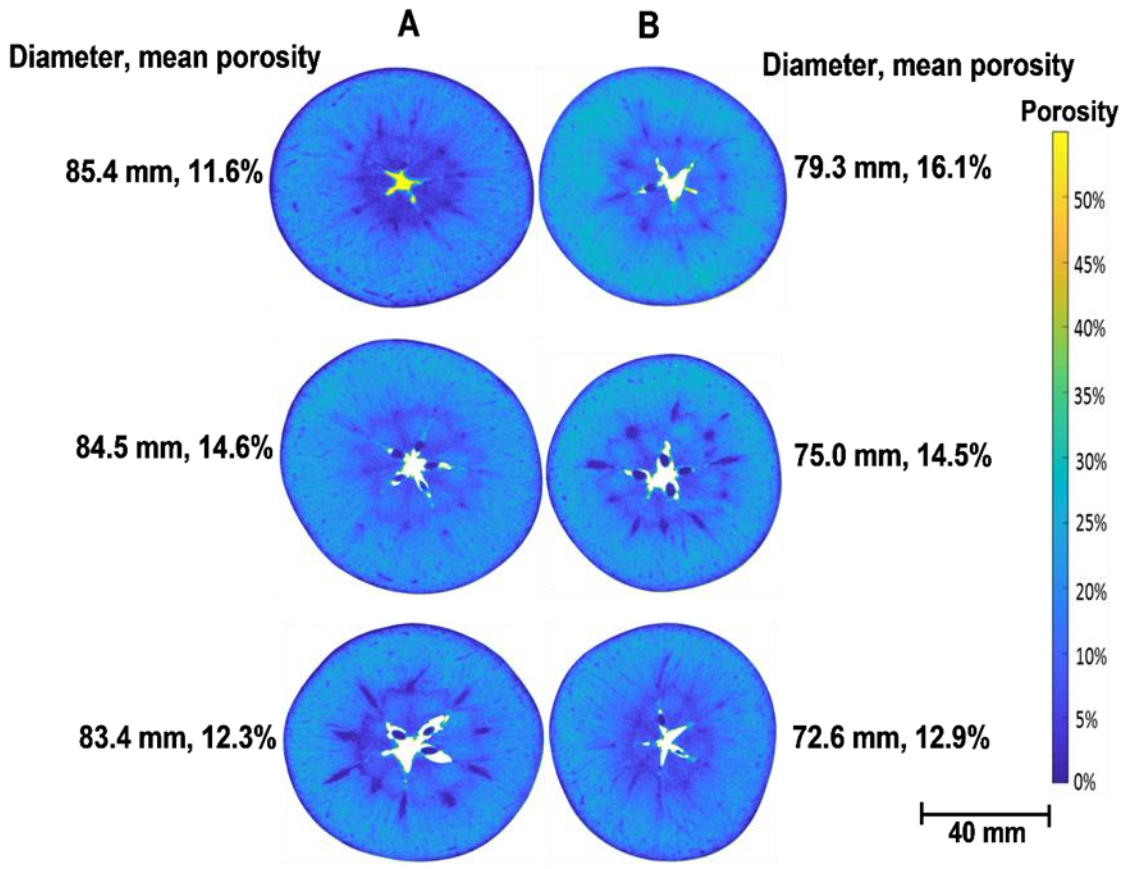


**Fig. 4.** Coronal (X-Z) slices of porosity maps for selected larger 'Fuji' fruit that developed core region internal browning (IB) (A) and selected smaller fruit that did not develop core region IB (B) after $CO_2$ stress treatment.

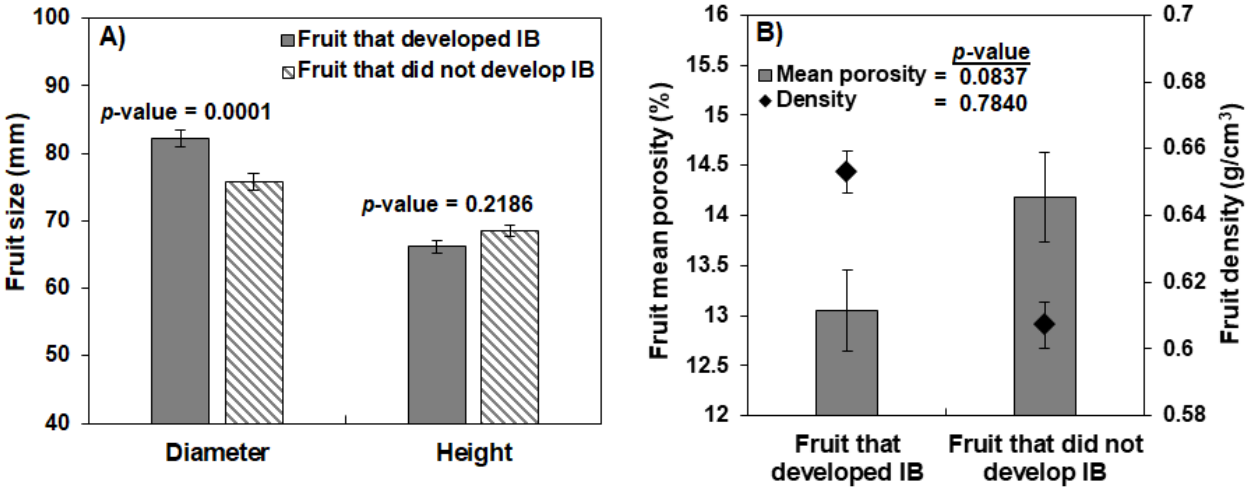


**Fig. 5.** Initial diameter, height (A), initial whole fruit mean porosity and whole fruit density (B) of 'Fuji' fruit that developed internal browning (IB) and fruit that did not develop IB after exposure to $CO_2$ stress treatment. Error bars indicate the SE of eight independent measurements.

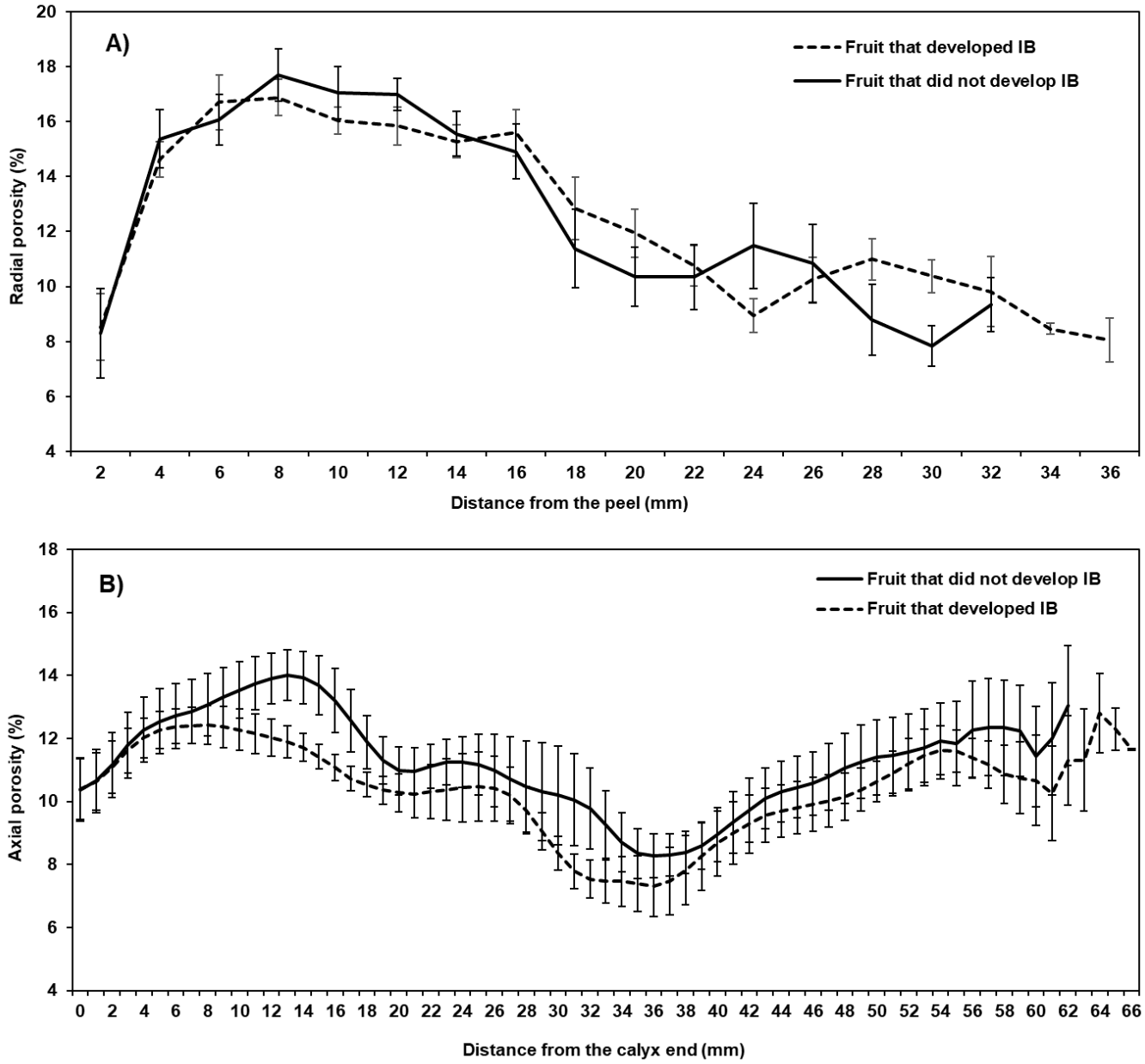


**Fig. 6.** Initial mean radial (A) and axial (B) porosity profiles of 'Fuji' apples with and without internal browning (IB) development. Radial porosity was plotted as a function of radial distance from the fruit peel (0 mm) towards the centre of the apple, whereas axial porosity was plotted as the axial distance from the calyx end (0 mm) towards the pedicel end. Error bars indicate the SE of eight independent measurements.

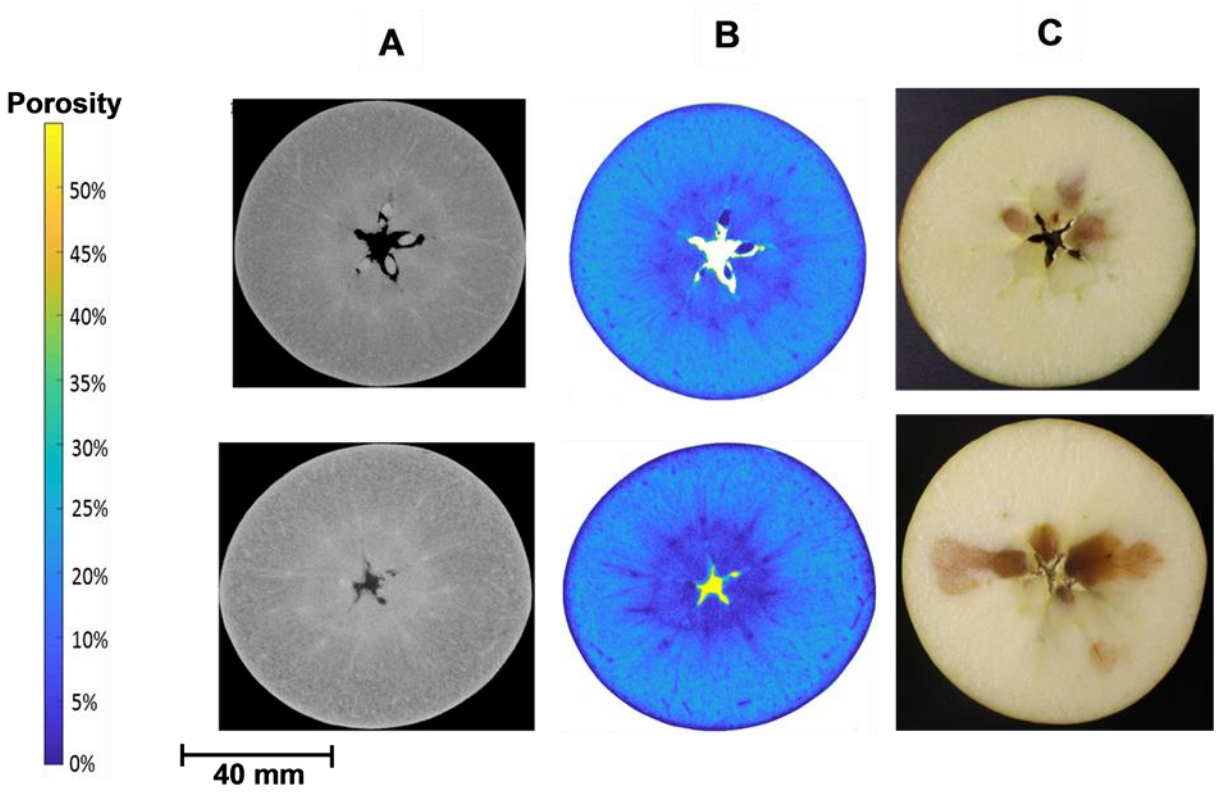


**Fig. 7.** Typical IB observed after exposure of 'Fuji' fruit to a storage environment enriched with 50% $CO_2$. This Figure visualizes the greyscale image (A) and porosity map (B) of the same fruit before $CO_2$ stress treatment, as well as the photographed image (C) after $CO_2$ stress treatment.

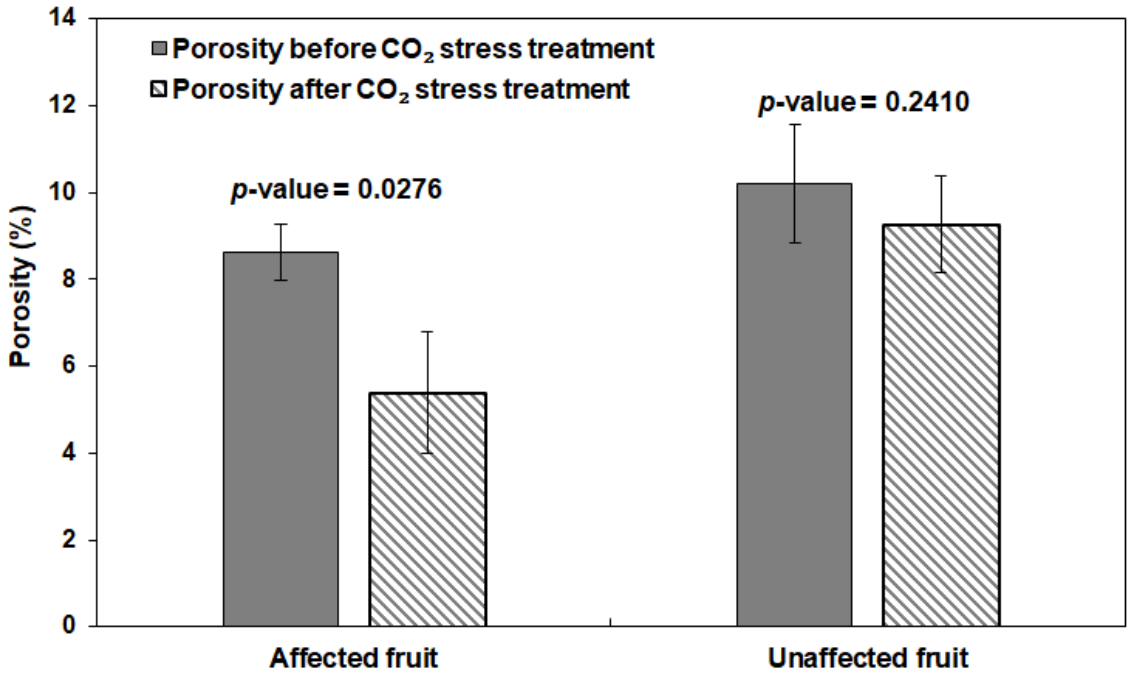


**Fig. 8.** The porosity of cylindrical samples in the core region generated from porosity maps of 'Fuji' fruit before the $CO_2$ stress treatment and porosity from high-resolution X-ray CT scans after $CO_2$ stress treatment: fruit affected with IB and unaffected fruit. Error bars indicate the SE of seven independent measurements for affected fruit and four independent measurements for unaffected fruit.

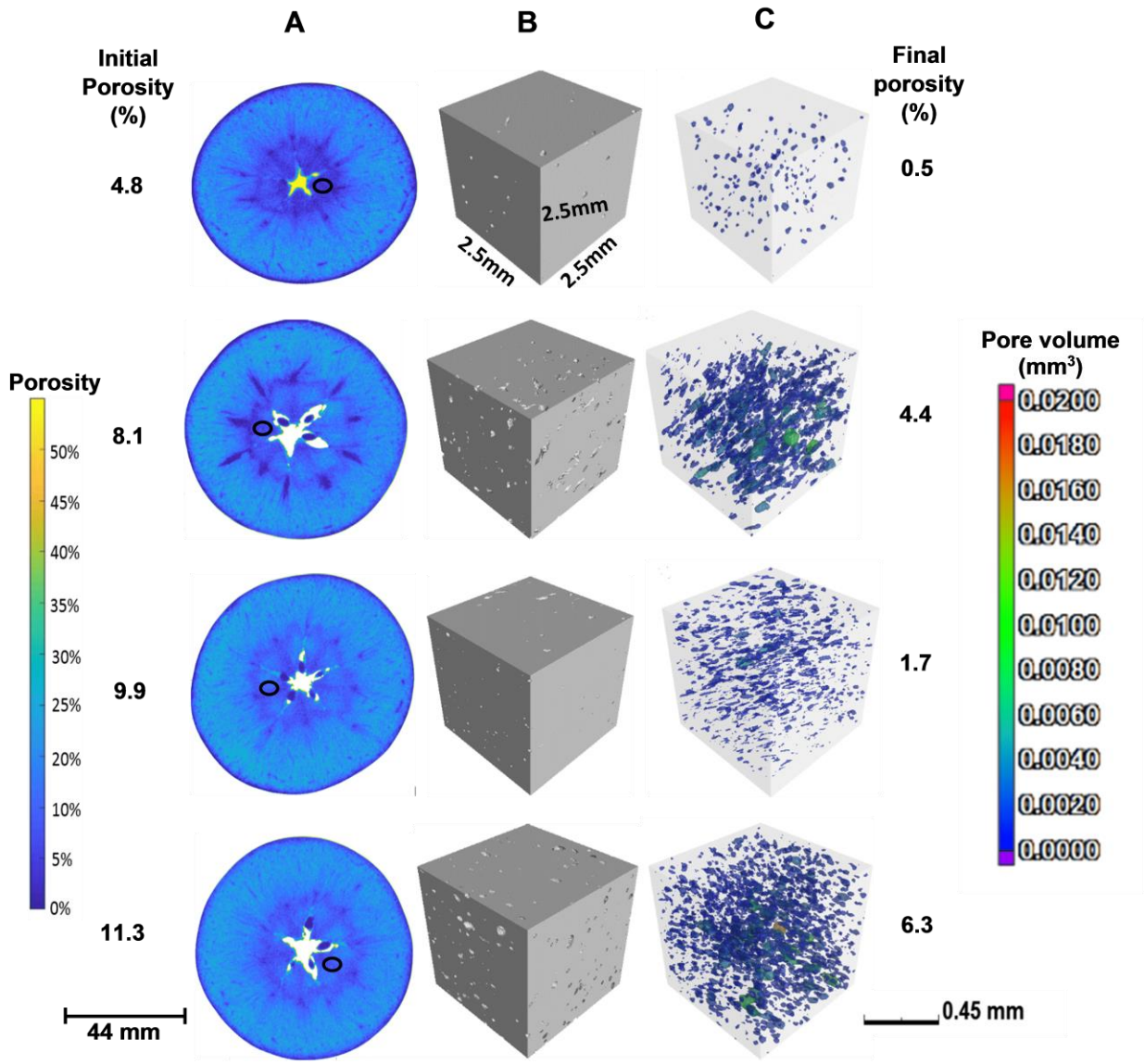


**Fig. 9.** Images of selected fruit showing porosity maps of 'Fuji' fruit before $CO_2$ stress treatment (A) and 3D tissue models (B) and 3D pore models (C) of core tissue samples affected with IB after $CO_2$ stress treatment (50% $CO_2$ / 9.7% $O_2$). The initial and final porosity values were determined from an affected region in the core of the fruit sample. The region where the core sample was excised is indicated by the black circle on the porosity maps (A). All 3D pore and tissue models were of equal volume.

**PAPER 3**

# Watercore disorder in 'Fuji' apples characterized by means of X-ray computed tomography (CT)


## Abstract

The objective of this study was to determine microstructural properties of 'Fuji' apple tissue affected by watercore and unaffected fruit vascular tissue by using X-ray computed tomography (CT) and 3D image analysis techniques. Low-resolution scans were done on whole fruit at a resolution of 60 µm while high-resolution scans were done at 3 µm resolution on affected and unaffected tissue samples obtained from the fruit vascular tissue. Results of low-resolution X-ray CT scans showed that fruit vascular tissue affected by watercore had a significantly higher tissue density compared to unaffected tissue. High-resolution scans showed that vascular tissue affected by watercore had significantly low total porosity (3.6%) and pore connectivity (111.7) compared to unaffected tissue, which had a total porosity of 10.7% and pore connectivity of 446.4. Low porosity and pore connectivity restrict movement of respiratory gases in affected tissue and this can lead to accumulation of $CO_2$ and anaerobic conditions which may cause internal browning (IB). Cellular structure was also affected by watercore, affected tissue had significantly smaller cells compared to unaffected tissue. This can be a result of shrinkage of cells due to diffusion of water molecules from the cells towards the intercellular spaces, which have a low water potential due to a high sorbitol concentration. The results of this study showed that watercore affects fruit microstructural properties such as porosity and connectivity of pores. These compromised microstructural properties may affect gas diffusion in affected 'Fuji' apples, possibly making the fruit more susceptible to IB development during long-term storage.


**Keywords**: Intercellular spaces, high-resolution, long-term storage, low-resolution, porosity, sorbitol rich fluid

## 1. Introduction

Fuji is an important apple cultivar globally due to its good eating quality, high market value and long-term storability (Veberic et al., 2007; Kasai and Arakawa, 2010). However, 'Fuji' apples sometimes develop watercore disorders whilst still on the tree. Watercore is characterized by water-soaked and glassy regions in some parts of the fruit flesh (Herremans et al., 2014). Extensive plantings of Fuji trees worldwide have triggered an interest into the research on watercore since the cultivar is known to be susceptible (Bowen and Watkins, 1997). 'Fuji' apples harvested with optimum colour and blush for market requirements are likely to have watercore (Bowen and Watkins, 1997). Watercore is usually more apparent in mature apples and is desired by customers in some parts of the world as an indicator of full ripeness (Harker et al., 1999; Kasai and Arakawa, 2010; Melado-Herreros et al., 2013). This is because the accumulated liquid is rich in sorbitol and this gives affected apples a sweet taste (Lu and Lu, 2017). In normal apples, sorbitol is translocated from the vascular phloem cells and is converted to fructose and glucose. In affected apples, sorbitol metabolism is inhibited, leading to its accumulation in the intercellular spaces (Lu and Lu, 2017). The development of watercore may be influenced by various pre-harvest factors such as water regime, temperature, and mineral nutrition (Yamada et al., 1998).

Yamada et al. (2004) found that watercore in 'Fuji' apples mostly developed at low temperatures of between 7 and 10 °C and did not occur at 25 °C. Low temperatures reduce evapotranspiration and sink demand causing an increase of the water status and water-soaked conditions in the fruit tissue (Yamada et al., 2004). Watercore normally starts in the vascular bundles around the core-line of the fruit and can spread to other regions of the fruit flesh where it is not visible from the exterior of the fruit and is thus classified as an internal disorder (Bowen and Watkins, 1997; Herremans et al., 2014). Clark et al. (1998) classified watercore into two groups namely block and radial watercore. Block watercore is characterized by a rectangular block of

affected tissue that covers the entire core area and extends into the flesh beyond the core area (Clark et al., 1998; Melado-Herreros et al., 2013). Radial watercore on the other hand affects carpellary bundles around the core-line and flesh that is adjacent to the affected vascular bundles (Clark et al., 1998; Melado-Herreros et al., 2013). Although apples with watercore are suitable for consumption at harvest, they may develop internal disorders such as internal browning (IB) during long-term storage and this limits their storability (Clark et al., 1998). In less severe cases, watercore may disappear during long-term storage (Clark et al., 1998), but in some severe cases, IB and tissue breakdown may occur as a result of watercore (Bennedsen and Peterson, 2005; Kasai and Arakawa, 2010).

Although the disorder has been extensively studied, it remains only partially understood. Research has shown that watercore affects the apple tissue at a microstructural level (Argenta et al., 2002). Watercore has been found to be associated with the flooding of intercellular spaces, higher sorbitol levels, higher sucrose levels as well as lower glucose and fructose concentrations (Bowen and Watkins, 1997; Argenta et al., 2002; Gao et al., 2005). Flooding of the intercellular airspaces has a negative impact on the fruit metabolism. The intercellular air spaces are important channels which facilitate gaseous exchange between the fruit and the storage environment (Argenta et al., 2002). Intercellular air spaces facilitate the diffusion of $O_2$ towards the respiring cells as well as the removal of $CO_2$ away from the respiring cells. Flooding of the intercellular air spaces will render them unable to efficiently execute their role in gaseous exchange (Herremans et al., 2014). This will result in the build-up of $CO_2$ within the apple tissue and onset of stress conditions as well as the conversion of the metabolic pathway from respiration to fermentation (Harker et al., 1999). This has a negative impact of producing less energy to support membrane integrity and may result in loss of compartmentalisation and incidence of IB disorders. Kasai and Arakawa (2010) found that watercore affected tissue had high levels of hydrogen peroxide and

low levels of the antioxidant ascorbic acid, this results in membrane damage and browning incidence.

Since watercore affects the fruit tissue at a microstructural level, imaging techniques that characterize fruit microstructure are useful in the study of watercore disorders. Marigheto and Hills (2005) used magnetic resonance imaging (MRI) as a potential on-line sensor of apple quality and found that watercore is easily detected by MRI due to a changed proton density. However, after doing experiments to compare the effectiveness of X-ray computed tomography (CT) and MRI as potential imaging techniques to detect watercore, Herremans et al. (2014) found that X-ray CT provided a clearer and superior visualization of the watercore disorder. The use of X-ray CT to evaluate the watercore disorder in South African grown 'Fuji' apples has not been carried out as yet. Such an investigation paves way for a better understanding of the watercore disorder in 'Fuji' apples and the potential of X-ray CT to be used on the sorting line to isolate watercore affected fruit.

Thus, the objective of this study was to characterize microstructural properties of 'Fuji' fruit affected by watercore and unaffected fruit using X-ray CT scanning and 3D image analysis techniques. Such information is important because it allows for the determination of the extent to which watercore will affect storability and disorder incidence of 'Fuji' during storage.

## 2. Materials and Methods

### *2.1. Fruit material*

Fruit were harvested in March 2018 from Wakkerstroom farm (33°17'47.1"S 19°14'54.8"E) located in the Koue Bokkeveld area in Western Cape Province, South Africa. The fruit were harvested at shoulder height from each tree, from random positions around the canopy during the commercial harvest period for South African 'Fuji' apples. Fruit were harvested into lug boxes and

transported to the fruit evaluation laboratory at the Department of Horticultural Sciences, Stellenbosch University, South Africa. Maturity indexing was done on arrival at the laboratory to determine the maturity status of the fruit at harvest. The fruit were then cut into two halves to determine the incidence of watercore, following which low- and high-resolution X-ray CT was carried out. Twenty fruit with watercore and twenty fruit without watercore were selected for X-ray-CT scanning. To enable whole fruit scanning of entire fruit, the cut halves were carefully placed back on top of each other and secured with clingwrap to reduce moisture loss during scanning.

*2.2. Maturity indexing at harvest*

To get a clear indication of the maturity status of the fruit at harvest, a sample of fruit were used to determine diameter, mass, height, background peel colour, blush percentage, flesh firmness, titratable acidity (TA), total soluble solutes (TSS) and starch breakdown. TA and TSS were measured on pooled samples of 20 fruit whereas the other parameters were done on single fruit. Fruit diameter, mass and height were measured using a Cranston gauge and electronic balance (FTA 2007, Güss, Strand, South Africa). Background colour of fruit were rated from 0.5 (green) to 5 (yellow), using the South African Industry colour chart for apples and pears (Unifruco Research Service, Bellville, South Africa). The blush percentage was determined by trained reviewers who estimated the percentage of the fruit surface covered by a red blush (0% for no red blush and 100% for full red blush). Fruit firmness was measured equatorially, on a peeled surface on opposite sides of the fruit, using a universal fruit texture analyser (FTA 2007, Güss, Strand, South Africa), fitted with a 7.9 mm diameter probe. TSS content was measured on a drop of expressed juice from a pooled sample of 20 fruit per replicate using a handheld digital refractometer (Atago Digital-Refractometer PR-32, Tokyo, Japan). TA was measured by titration of individual fruit juice from a pooled sample of 20 fruit per replicate using an automated titrator (Metrohm AG 760. Harison, Switzerland). Percentage starch conversion was estimated using the

iodine test with a starch conversion chart (Unifruco Research Services, Bellville) with a scale of 0% to 100%, where 0% was totally stained and 100% was totally unstained.

*2.3. Low-resolution micro-CT*

To determine grey values and tissue density, low-resolution micro-CT scanning was done on 15 whole fruit at the Stellenbosch University Central Analytical Facility. The V|Tome|X L240 micro-CT scanner (GE Sensing & Inspection Technologies GmbH, Wunstorf, Germany) contains two X-ray tubes, one with a reflection-type target and the other with a transmission target (du Plessis et al., 2016). The average time per scan was 30 min and 2300 projection images were captured. The samples were scanned at a voltage of 100 kV and a current of 100 µA, these parameters were able to give a voxel size of 60 µm. A series of 2D X-ray images were obtained, and these were reconstructed using reconstruction software Datos|x®2.1 (GE Sensing & Inspection Technologies GmbH, Wunstorf, Germany) to generate virtual 3D images.

*2.4. Calculation of tissue density*

To calculate the relative density of different tissue regions in the apple tissue, a reference of known density (2.21 $gcm^{-3}$) was scanned together with the apple during low-resolution scanning. This made it possible to calculate the density of a given region of interest (ROI) based on the density of the reference using equation 1:

$$\text{relative density} = \frac{\text{Mean grey value of ROI}}{\text{Mean grey value of reference}} \times 2.21\ \text{gcm}^{-3} \qquad (1)$$

Regions of interest (ROIs) were obtained from vascular bundle regions of fruit affected by watercore and some were obtained from the vascular bundle regions of fruit that was not affected by watercore.

*2.5. Sampling for high-resolution X-ray CT scanning*

Figure 1 shows the morphology of the apple fruit. Cylindrical samples for high-resolution X-ray CT scanning were obtained from fruit with watercore and fruit without watercore (Fig. 2). For fruit with watercore, one sample was obtained from a watercore affected region on the vascular bundle section of each of the twenty fruit and scanned at high-resolution. For fruit without watercore, one sample was obtained from the vascular bundle region of each of the 20 fruit. The samples were wrapped in parafilm before X-ray CT scanning to prevent dehydration during scanning.

*2.6. High-resolution X-ray CT scanning*

The samples were then loaded individually onto the Nanotom S instrument (GE Sensing & Inspection Technologies GmbH, Wunstorf, Germany) at the Stellenbosch University Central Analytical Facility for scanning. Various system settings were tested to optimize the scan quality. A series of 2600 projection images were obtained as the sample was rotated 360°. The samples were scanned at a voltage of 60 kV, current of 240 µA, and a voxel size of 3 µm. The average scan time was 45 mins per sample. A series of 2D X-ray images were obtained, and these were reconstructed using reconstruction software Datos|x®2.1 (GE Sensing & Inspection Technologies GmbH, Wunstorf, Germany) to generate virtual 3D images (du Plessis et al., 2016).

*2.7. Image analysis*

To extract suitable quantitative information from X-ray CT images, it is necessary to do 3D image analysis. The projection images produced during scanning were reconstructed into 3D volumes using Datos|x®2.1 (GE Sensing & Inspection Technologies GmbH, Wunstorf, Germany). The Polychromacity of the X-ray beam gives rise to the beam hardening effect. As a result, beam hardening correction of level 2 (machine specific value) had to be applied to correct this artefact.

Analysing the whole image in its entirety can be a very arduous and time-consuming exercise, hence it was necessary to select a ROI from the original image (Schoeman et al., 2016). Although a ROI is smaller in size compared to the original image, it is important to ensure that the selected ROI is large enough to be statistically representative of the whole sample. In this study a ROI measuring 2.5 x 2.5 x 2.5 mm was used, this representative volume of 15.625 $mm^3$ was larger than the lower limit for a representative volume element of 1.3 $mm^3$ that was suggested by Mendoza et al. (2007).

After this, random noise that occurs during scanning was removed by filtering using a median and gaussian filters. After the image was filtered, it was segmented into its constituent cells and pores so that subsequent analysis procedures can be carried out. Automatic thresholding using Otsu's method was done to create a binary image consisting of only cells and pores. Otsu's thresholding involves the defining of a single grey value to separate regions of the image on the basis of analysis of the image histogram (Otsu, 1979; Zhang et al., 2017). Voxels containing grey values lower than this threshold value are regarded as background (pores) while those with grey values higher than the threshold value are regarded as sample material (cells; Schoeman et al., 2016). Segmentation of X-ray CT images using Otsu method has been used by Herremans et al. (2013) in Braeburn apples, Muziri et al. (2016) in Forelle pears and Ting et al. (2013) in determination of differences in microstructural properties of different apple cultivars. After image thresholding, 3D image analysis was then done, and various microstructural properties were determined (Table 1). 3D image analysis was done using Avizo 2019.1 (VSG, Bordeaux, France), CTAn 1.18.0.0 (Bruker microCT, Kontich, Belgium) and VGSTUDIO MAX 3.2 (Volume Graphics GmbH, Heidelberg, Germany).

*2.8. Cell isolation*

Automatic segmentation of individual cells was not possible due to insufficient contrast between cytoplasm and cell wall (Cantre et al., 2014). The 3D region that was identified as cells after segmentation needed to be further segmented into individual cells to allow for the quantification of individual cell properties. To differentiate neighbouring cells in the binary image, a technique known as watershed separation was used (Meyer and Beucher, 1990). This was implemented using the separate objects module in Avizo 2019.1 (VSG, Bordeaux, France). The watershed method is a powerful mathematical morphological tool for image segmentation. If you view the image as a landscape, the watershed lines determine boundaries which separates image regions (Ruparelia, 2012). The algorithm works by calculating the Chamfer distance map of the binary image, in which greyscales represent the distance from that pixel to the nearest black (background) pixel, regardless of direction. The chamfer distance map which computes the distance as a discrete approximation can be seen as a height chart, producing a mountain peak at the centre of each of the cells. In this study, the Separate objects/Chamfer Conservative module in Avizo 2019.1 (VSG, Bordeaux, France) was used to compute watershed lines on the segmented binary image. All cells that intersected the dataset borders after watershed separation were removed to exclude incomplete individual cells from the later morphological calculations. After watershed separation, some cells were not fully separated, and such cells had to be excluded from the image since they will give rise to inaccurate results. A virtual sieve was used to remove incorrectly segmented cells and unseparated clumps of cells. Based on literature, all individual objects with a length larger than 400 µm and a sphericity index lower than 0.75 were removed from the 3D model (Herremans et al., 2015). This allowed the 3D model of the image to comprise of only the correctly segmented cells (Fig. 3). This protocol was validated by Herremans et al. (2015) by manually segmenting individual cells and they found no significant differences in this method and manually segmented individual cells.

*2.9. Data analysis*

To quantify differences amongst the pore and cell properties differences watercore affected and unaffected fruit vascular tissue, independent *t*-tests were performed using STATISTICA Version 13.1 (StatSoft Inc., Tulsa, USA). The means were compared at a significance level of 5%.

## 3. Results

### *3.1. Fruit maturity at harvest*

Table 2 presents the maturity parameters of 'Fuji' apples that were used in this study. The apples were harvested from a farm in the Koue Bokkeveld region of South Africa. Maturity at harvest is a very important factor that affects the quality and storage potential of apples. The quality and storage potential can be affected by either early harvest or late harvest especially when the fruit are intended for long-term storage. The apples used in this study were harvested during the commercial harvest period in 2018 and the maturity indices show that the apples were relatively over-mature at the time of harvest as shown by the very high starch breakdown (81 ± 19.5%). Of all the harvested fruit, 63% had varying degrees of radial watercore.

### *3.2. Pore properties*

Figure 4 presents the pore properties obtained after high-resolution scans done on watercore affected and unaffected vascular tissue. The total porosity was significantly higher ($P < 0.0001$) in unaffected vascular tissue (10.7%) as compared to affected vascular tissue (3.6%; Fig. 4A). The open porosity was also significantly higher ($P < 0.0001$) in unaffected vascular tissue (5%) as compared to watercore affected vascular tissue (1.6%; Fig. 4B). The pores in unaffected vascular tissue were significantly ($P < 0.0001$) more connected as compared to the pores in unaffected vascular tissue (Fig. 4C). In terms of length, the pores in unaffected vascular tissue were significantly ($P = 0.002$) longer (109.8 µm) as compared to the pores in watercore affected vascular tissue (69.5 µm; Fig. 4D). The pores in unaffected vascular tissue

were significantly (*P < 0.0001*) more anisotropic as compared to the pores in watercore affected vascular tissue (Fig. 4E). The pores in watercore affected vascular tissue were significantly (*P = 0.001*) more spherical with a higher sphericity (0.97) as compared to the pores in unaffected vascular tissue (0.86; Fig. 4F). The differences in porosity between watercore affected and unaffected vascular tissue were also clearly shown in the 2D and 3D images (Fig. 5). The 3D pore model for vascular tissue affected by watercore shows that the pores occupy a very small volume while the 3D pore model of fruit vascular tissue that does not have watercore show that the pores occupy a considerable volume. Pore space distributions show that 90% of the pores in watercore affected vascular tissue had an equivalent diameter of 60 µm or less while 82% of the pores in unaffected vascular tissue had an equivalent diameter of 60 µm or less (Fig. 6).

### *3.3. Cell properties*

Figure 7 presents the cell properties of fruit vascular tissue with watercore and unaffected vascular tissue. The sphericity of cells was significantly (*P = 0.001*) higher in watercore affected vascular tissue (0.88) as compared to unaffected fruit vascular tissue (0.76; Fig. 7A). In terms of equivalent diameter, the cells from unaffected vascular tissue had a significantly (*P = 0.001*) higher diameter (168.48 µm) as compared to watercore affected vascular tissue (116.65 µm; Fig. 7B). The cells from unaffected vascular tissue were significantly (*P = 0.004*) more anisotropic as compared to watercore unaffected vascular tissue (Fig. 7C). Cells from unaffected vascular tissue had a significantly (*P = 0.032*) larger volume as compared to cells from watercore affected vascular tissue (Fig. 7D). Unaffected vascular tissue had significantly (*P = 0.004*) thicker cells as compared to watercore affected vascular tissue (Fig. 7E). In addition to this, cells from unaffected vascular tissue had significantly (*P = 0.000*) longer cells (271.09 µm) as compared to cells from watercore affected vascular tissue (182.08 µm; Fig. 7F).

### *3.4. Tissue density*

Regions of interest taken from regions affected by watercore had a significantly (*P < 0.0001*) higher tissue density (1.30 $gcm^{-3}$) as compared to regions of interest obtained from regions without watercore (1.18 $gcm^{-3}$; Fig. 8). The greyscale cross sectional image of a fruit with watercore in Fig. 8 clearly shows the colour differences for sections of the fruit affected by watercore and unaffected fruit sections. The regions of the fruit affected by watercore are denser and are characterized by a light grey colour while those regions which are unaffected by watercore are less dense and are characterized by a slightly darker grey colour (Fig. 9).

## 4. Discussion

High-resolution X-ray CT scans done in this study showed that watercore affected vascular tissue had a significantly low total porosity as compared to unaffected vascular tissue. The open porosity was also significantly lower in watercore affected vascular tissue as compared to unaffected vascular tissue. The reduction in porosity as a result of flooding of the intercellular spaces with a sorbitol rich fluid has been highlighted by several researchers (Clark et al., 1998; Argenta et al., 2002; Yamada et al., 2004; Herremans et al., 2014). The accumulation of the sorbitol rich liquid in the intercellular spaces reduces the scattering of light passing through the tissue and this gives affected tissue a translucent appearance. In this study, watercore affected regions had a high tissue density as compared to watercore free regions and these differences were clearly visible in the low-resolution X-ray CT scans. The reduction in fruit porosity as a result of watercore has a significant impact on the gas transport properties of the fruit since pores are important channels for gas exchange within the fruit. Watercore compromises the efficiency of gas transport in affected apples and this reduces their storage potential. The incidence of internal disorders in apples harvested with watercore has been reported by several researchers (Fukuda, 1984; Argenta et al., 2002; Kweon et al., 2012). Argenta et al. (2002) found a relationship between watercore and $CO_2$ injury in ‘Fuji’ apples, their research highlighted the

accumulation of ethanol and acetaldehyde in watercore affected apples and this indicates the presence of anaerobic respiration. Research by Kweon et al. (2012) showed that 'Fuji' apples harvested later than 180 days after full bloom were prone to the development of watercore which was correlated to the incidence of IB during long-term CA storage. A study by Fukuda (1984) found a positive correlation between watercore at harvest and internal breakdown in 'Fuji' apples.

In addition to the porosity changes, various pore parameters were also affected by the incidence of watercore. The connectivity of the pores in watercore affected vascular tissue was significantly low as compared to that of unaffected vascular tissue. Connectivity is an important pore parameter since it affects the movement of respiratory gases within the fruit tissue. Connectivity has a significant impact on transport properties such as permeability and its quantification is important for microstructure-transport property relationships (Mendoza et al., 2007). The low connectivity of pores in watercore affected vascular tissue shows that the capacity of the affected vascular tissue to efficiently transport respiratory gases was severely compromised. This results in the onset of anaerobic conditions within the fruit, predisposing the fruit to internal disorders during long-term storage. The length of the pores was also affected, the length of the pores in watercore affected vascular tissue was significantly smaller as compared to that of unaffected tissue. This shows that larger pores were eliminated by being filled with the sorbitol rich fluid, this resulted in only smaller pores being available and these smaller pores have a limited capacity in terms of their gas transport capabilities. Watercore affected vascular tissue also had a lower anisotropy as compared to unaffected vascular tissue. Anisotropy is a measure of preferential alignment of structures, scaled from 0 for total isotropy to 1 for total anisotropy (Khan and Vincent, 1990; Cantre et al., 2014). The implications of pore anisotropy in apple fruit are wide ranging and it has been thought to have effects on the textural and transport properties of fruit (Mendoza et al., 2007). The pores in watercore affected vascular tissue were more spherical as compared to those in unaffected vascular tissue, this shows that

there were also some changes in the cell structure in watercore affected vascular tissue since the distribution and shape of cells influences the shape of the pores. The change in shape of pores also possibly had an effect on the gas transport properties of the pores.

In addition to the measured pore parameters, cell parameters in both watercore affected and unaffected vascular tissue were quantified. The results from cell quantification showed that there were significant differences in the cell properties of watercore affected and unaffected vascular tissue. Watercore affected fruit tissue cell properties such as sphericity, volume, thickness, and length. This shows that watercore had an effect on the cellular structure. Several researchers have alluded to the effect of watercore on the cellular structure, Kasai and Arakawa (2010) attributed these cellular changes in watercore affected tissue to the loss of membrane integrity via peroxidation of unsaturated fatty acid or denaturation of proteins by reactive oxygen species. Yamada et al. (2006) also highlighted changes in cellular properties as a result of watercore, they attributed this to membrane permeability changes and the movement of sorbitol between the cells and the intercellular spaces. The accumulation of the sorbitol rich fluid in the intercellular spaces may cause a reduction in the water potential in these intercellular spaces, resulting in water osmotically moving out of the cells towards the intercellular spaces thereby causing shrinkage and reduced size of the cells. The effect of watercore on both the pore and cell properties of affected fruit shows that watercore is an important disorder that affects the storability of ‘Fuji’ apples.

## 5. Conclusion

X-ray CT and 3D image analysis show that there are microstructural differences between watercore affected and unaffected vascular tissue. Watercore affected both cellular and pore structure. Fruit vascular tissue affected by watercore was characterized by low porosity as well as low connectivity of pores and this is expected to have a significant impact on the gas diffusion

properties of the pores. Watercore also resulted in smaller cells in affected vascular tissue as compared to unaffected vascular tissue, possibly due to the effect of differences in water potential between the cell and the intercellular spaces which may cause plasmolysis. Low-resolution scans showed clear tissue density differences between affected and unaffected vascular tissue. This shows that X-ray CT has the potential to be used for detection of watercore on the sorting line based on density differences between watercore affected and unaffected fruit. However, a lot of work still needs to be done to improve the speed of the data capturing process so that it can be feasible for usage at commercial speeds on the sorting line.

## Acknowledgments

This study was made possible by the financial support from the South African Apple and Pear Producer's Association and HORTGRO Science.

## References

Argenta, L., Fan, X., Mattheis, J., 2002. Impact of watercore on gas permeance and incidence of internal disorders in 'Fuji' apples. Postharvest Biol. Technol. 24, 113–122. https://doi.org/10.1016/S0925-5214(01)00137-5.

Bennedsen, B.S., Peterson, D.L., 2005. An optical method for detecting watercore and mealiness in apples. Trans. Am. Soc. Agric. Eng. 48, 1819–1826.

Bowen, J.H., Watkins, C.B., 1997. Fruit maturity, carbohydrate and mineral content relationships with watercore in 'Fuji' apples. Postharvest Biol. Technol. 11, 31–38. https://doi.org/10.1016/S0925-5214(97)01409-9.

Cantre, D., Herremans, E., Verboven, P., Ampofo-Asiama, J., Nicolaï, B., 2014. Characterization of the 3-D microstructure of mango (*Mangifera indica* L. cv. Carabao) during ripening using X-ray computed microtomography. Innov. Food Sci. Emerg. Technol. 24, 28–39.

https://doi.org/10.1016/j.ifset.2013.12.008.

Clark, C.J., MacFall, J.S., Bieleski, R.L., 1998. Loss of watercore from 'Fuji' apple observed by magnetic resonance imaging. Sci. Hortic. 73, 213–227. https://doi.org/10.1016/S0304-4238(98)00076-4.

du Plessis, A., le Roux, S.G., Guelpa, A., 2016. The CT Scanner Facility at Stellenbosch University: An open access X-ray computed tomography laboratory. Nucl. Instruments Methods Phys. Res. Sect. B Beam Interact. with Mater. Atoms 384, 42–49. https://doi.org/10.1016/j.nimb.2016.08.005.

Fukuda, H., 1984. Relationship of watercore and calcium to the incidence of internal storage disorders of 'Fuji' apple fruit. J. Japan. Soc. Hort. Sci 53, 298–302. https://doi.org/https://doi.org/10.1093/mnras/183.3.341.

Gao, Z., Jayanty, S., Beaudry, R., Loescher, W., 2005. Sorbitol transporter expression in apple sink tissues: Implications for fruit sugar accumulation and watercore development. J. Am. Soc. Hortic. Sci. 130, 261–268. https://doi.org/10.21273/jashs.130.2.261

Harker, F.R., Watkins, C.B., Brookfield, P.L., Miller, M.J., Reid, S., Jackson, P.J., Bieleski, R.L., Bartley, T., 1999. Maturity and regional influences on watercore development and its postharvest disappearance in 'Fuji' apples. J. Am. Soc. Hortic. Sci. 124, 166–172. https://doi.org/10.21273/JASHS.124.2.166.

Herremans, E., Melado-Herreros, A., Defraeye, T., Verlinden, B., Hertog, M., Verboven, P., Val, J., Fernández-Valle, M.E., Bongaers, E., Estrade, P., Wevers, M., Barreiro, P., Nicolaï, B.M., 2014. Comparison of X-ray CT and MRI of watercore disorder of different apple cultivars. Postharvest Biol. Technol. 87, 42–50. https://doi.org/10.1016/j.postharvbio.2013.08.008.

Herremans, E., Verboven, P., Verlinden, B.E., Cantre, D., Abera, M., Wevers, M., Nicolaï, B.M., 2015. Automatic analysis of the 3-D microstructure of fruit parenchyma tissue using X-ray micro-CT explains differences in aeration. BMC Plant Biol. 15, 1–14.

https://doi.org/10.1186/s12870-015-0650-y.

Kasai, S., Arakawa, O., 2010. Antioxidant levels in watercore tissue in 'Fuji' apples during storage. Postharvest Biol. Technol. 55, 103–107. https://doi.org/10.1016/j.postharvbio.2009.08.008

Khan, A.A., Vincent, J.F.V., 1990. Anisotropy of apple parenchyma. J. Sci. Food Agric. 52, 455–466. https://doi.org/10.1002/jsfa.2740520404.

Kweon, H.J., Kim, M.J., Moon, Y.S., Lee, J., Choi, C., Choi, D.G., Lee, D.H., Kang, I.K., 2012. Relationship between preharvest factors and the incidence of storage disorders in 'Fuji' apples during CA storage. Korean J. Hortic. Sci. Technol. 30, 50–55. https://doi.org/10.7235/hort.2012.11049.

Lu, Y., Lu, R., 2017. Non-destructive defect detection of apples by spectroscopic and imaging technologies: a review. Trans. ASABE 60, 1765–1790. https://doi.org/10.13031/trans.12431.

MacDaniels, L.H., 1940. The morphology of the apple and other pome fruits. Mem. Cornell Agric. Exp. Stn. 230, 32.

Marigheto, N., Hills, B., 2005. MRI as a potential on-line sensor of apple quality, in: Information and Technology for Sustainable Fruit and Vegetable Production FRUTIC 05. Montpellier France, pp. 12–16.

Melado-Herreros, A., Muñoz-García, M.A., Blanco, A., Val, J., Fernández-Valle, M.E., Barreiro, P., 2013. Assessment of watercore development in apples with MRI: Effect of fruit location in the canopy. Postharvest Biol. Technol. 86, 125–133. https://doi.org/10.1016/j.postharvbio.2013.06.030

Mendoza, F., Verboven, P., Mebatsion, H.K., Kerckhofs, G., Nicolaï, B., 2007. Three-dimensional pore space quantification of apple tissue using X-ray computed microtomography. Planta 226, 559–570. https://doi.org/10.1007/s00425-007-0504-4

Otsu, N., 1979. A threshold selection method from gray-level histograms. IEEE Trans. Syst. Man Cybern. 9, 62–66.

Ruparelia, S., 2012. Implementation of Watershed Based Image Segmentation Algorithm in FPGA. Master's thesis, Department of Parallel Systems, University of Stuttgart, Stuttgart, Germany.

Veberic, R., Zadravec, P., Stampar, F., 2007. Fruit quality of 'Fuji' apple (*Malus domestica* Borkh.) strains. J. Sci. Food Agric. 8, 593–599. https://doi.org/10.1002/jsfa.2726.

Yamada, H., Hasegawa, Y., Mito, K., 1998. Watercore induced by preharvest high fruit temperature in watercore-resistant 'Tsugaru' apples. Environ. Control Biol. 36, 209–216. https://doi.org/10.2525/ecb1963.36.209.

Yamada, H., Takechi, K., Hoshi, A., Amano, S., 2004. Comparison of water relations in watercored and non-watercored apples induced by fruit temperature treatment. Sci. Hortic. 99, 309–318. https://doi.org/10.1016/S0304-4238(03)00104-3.

Yamada, H., Kaga, Y., Amano, S., 2006. Cellular compartmentation and membrane permeability to sugars in relation to early or high temperature-induced watercore in apples. Sci. Hortic. 108, 29–34. https://doi.org/10.1016/j.scienta.2006.01.002.

**Table 1**

Morphometric parameters used to describe 3D high-resolution X-ray CT images, based on Herremans et al. (2013), with modifications.

| **Microstructural parameter** | **Unit** | **Description** |
|---|---|---|
| Volume | $mm^3$ | Volume of object |
| Area | $mm^2$ | Area of the object boundary |
| Length | µm | Maximum of the ferret diameters used over a range of angles |
| Width | µm | Minimum of the ferret diameters used over a range of angles |
| Equivalent diameter | µm | The diameter of a sphere of equivalent volume as the irregularly shaped object |
| Anisotropy | - | Measure of preferential alignment of structures. This value is scaled from 0 for total isotropy to 1 for total anisotropy |
| Connectivity | - | The number of connections between matrix structures per unit volume, based on Euler number |
| Total Porosity | % | Pore volume divided by the total volume |
| Open porosity | % | Any space located within a solid object or between solid objects with connection in 3D space with outside space. |
| Sphericity | - | measures the ratio of the surface area of a sphere with the same volume as the cell/pore to its surface area |

**Table 2**

Physiochemical properties of 'Fuji' apples used in this study at harvest.

| Parameter | Value |
|---|---|
| Diameter (mm) | 71.7 ± 6.1 |
| Mass (g) | 166.1 ± 27.0 |
| Height (mm) | 61.9 ± 4.6 |
| Background peel colour (Chart value) | 3.3 ± 0.3 |
| Blush percentage (%) | 48 ± 19.0 |
| Firmness (kg) | 7.7 ± 0.6 |
| #TA (%) | 0.31 ± 0.02 |
| ^TSS (%) | 13.6 ± 0.8 |
| Starch breakdown (%) | 81 ± 19.5 |

#Titratable acidity
^Total soluble solutes

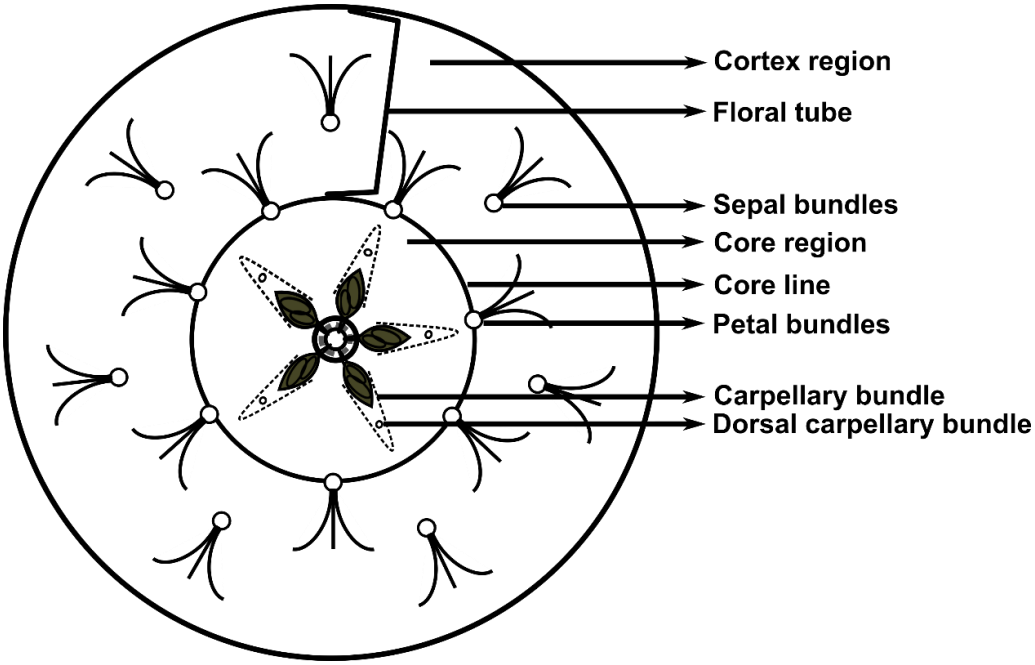


**Fig. 1.** Schematic presentation of the transverse section for apple showing gross morphology of the fruit (Based on MacDaniels, 1940).

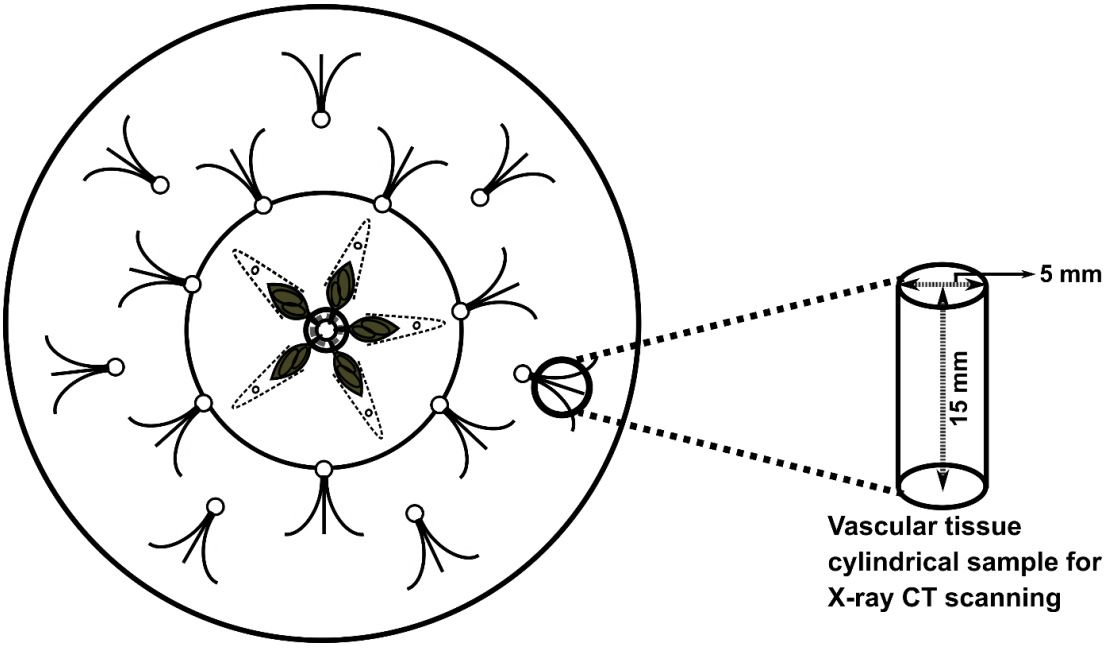


**Fig. 2.** Schematic presentation of the sampling position. The cylindrical samples were obtained from the vascular tissue region (sepal bundle) of the apple parenchyma.

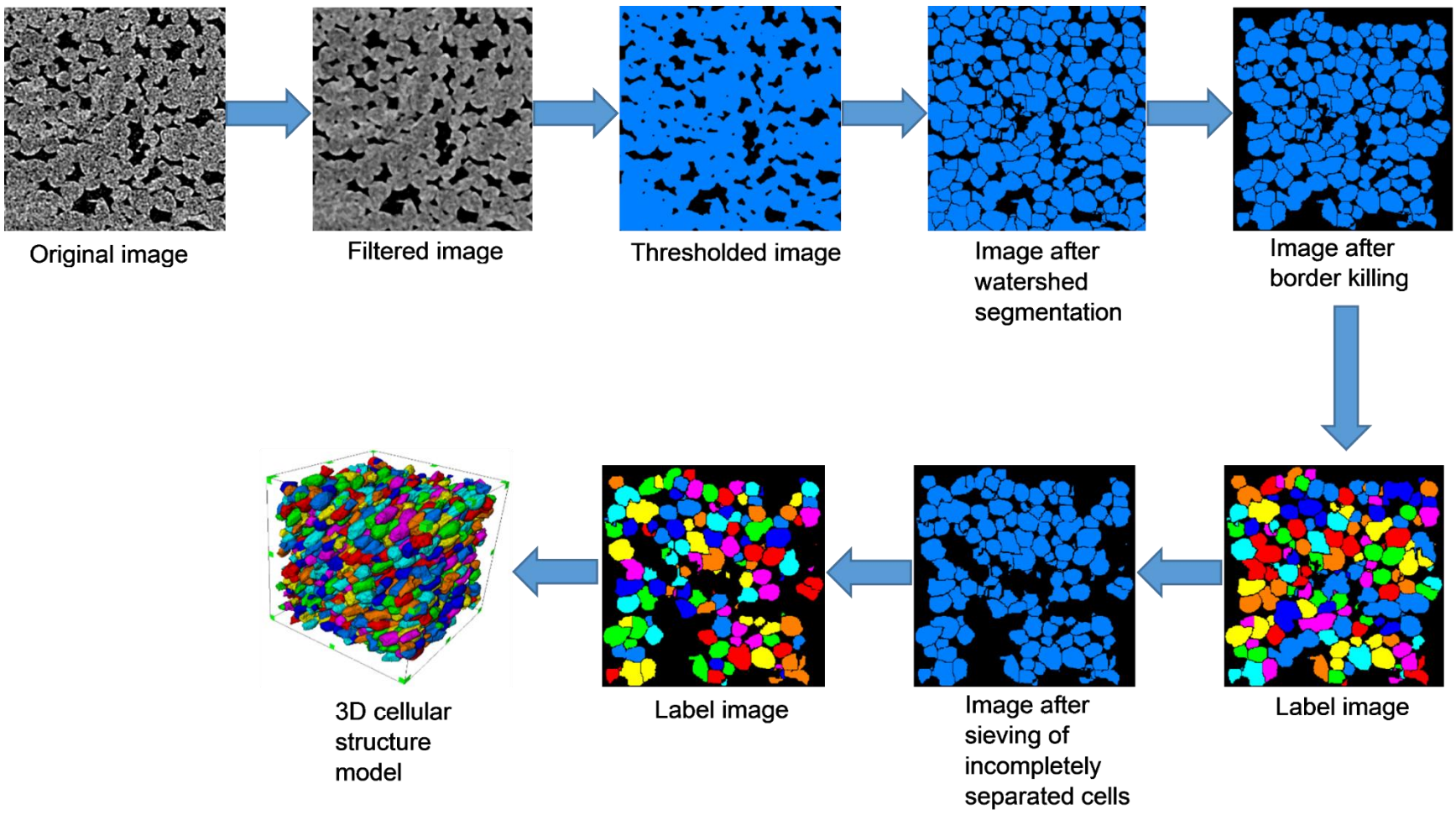


**Fig. 3.** Schematic representation of the procedure followed in isolation of individual cells and measurement of individual cell parameters using Avizo 2019.1.

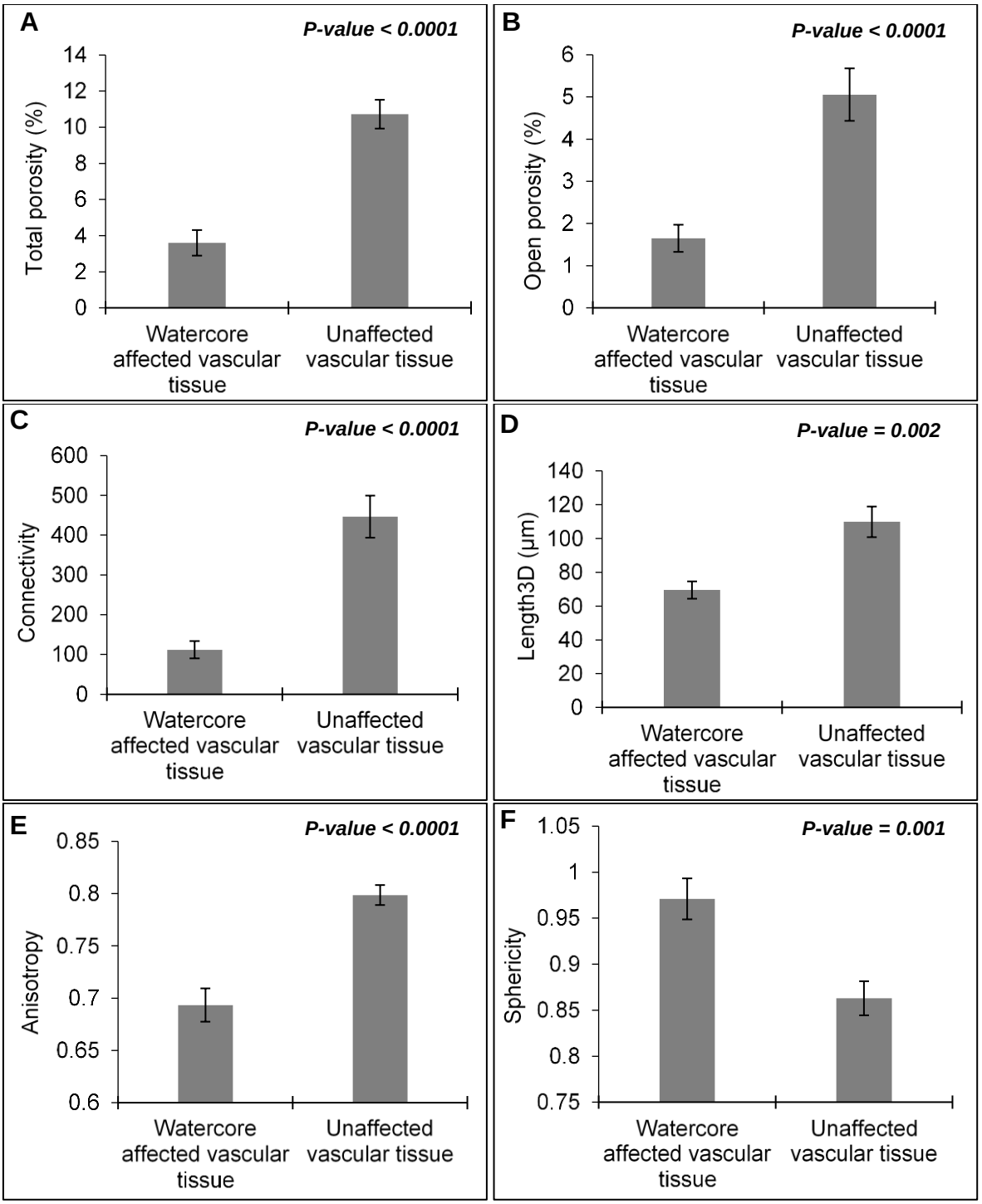


Fig. 4. Bar graphs and corresponding standard error bars for the following 3D pore parameters of fruit vascular tissue samples with watercore and unaffected fruit vascular tissue A) Total porosity B) Open porosity C) Connectivity D) Length3D E) Anisotropy and F) Sphericity. Error bars indicate standard error of 15 independent measurements.

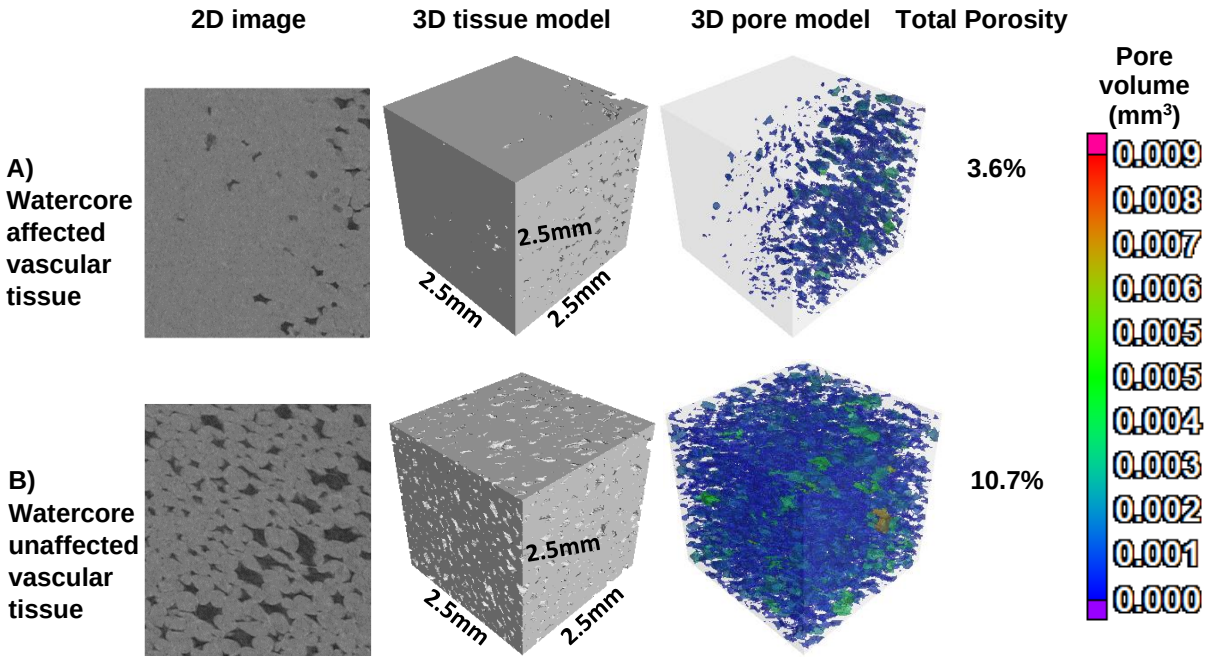


**Fig. 5.** 2D images, accompanying 3D tissue models and 3D pore models for regions of interests from A (watercore affected) and (B) unaffected vascular tissue. 2D images show pores in dark grey and fruit vascular tissue in light grey. Different colours in the 3D pore models represent different individual pore volumes as defined in the scale.

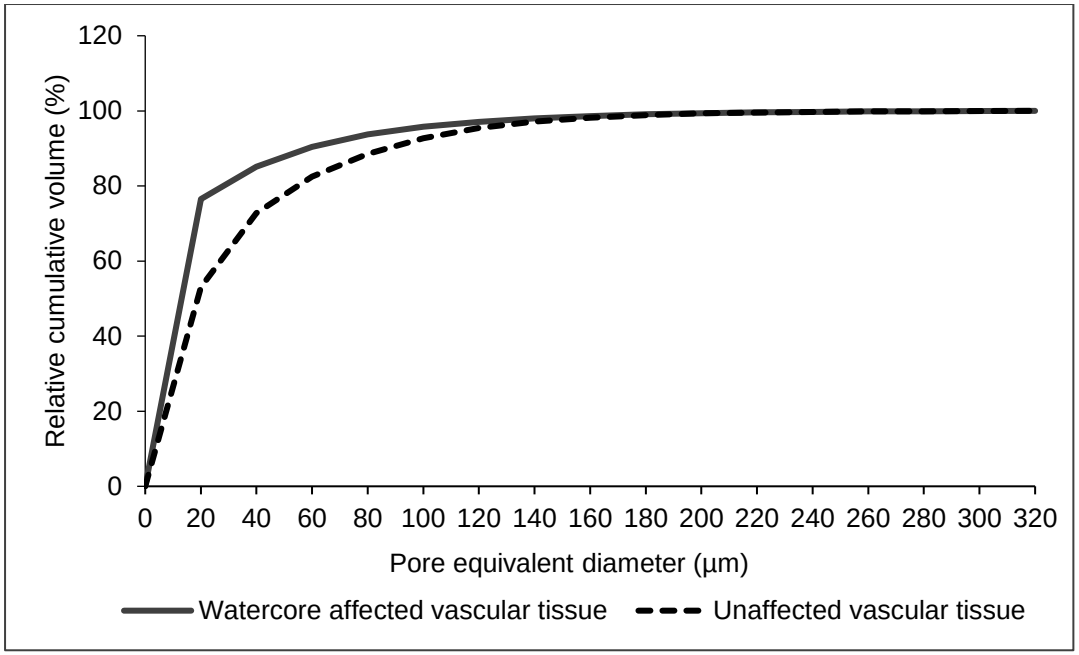


**Fig. 6.** Pore space distributions expressed as cumulative volume fractions of individual pores in function of its equivalent diameter (µm) for watercore affected and unaffected fruit vascular tissue.

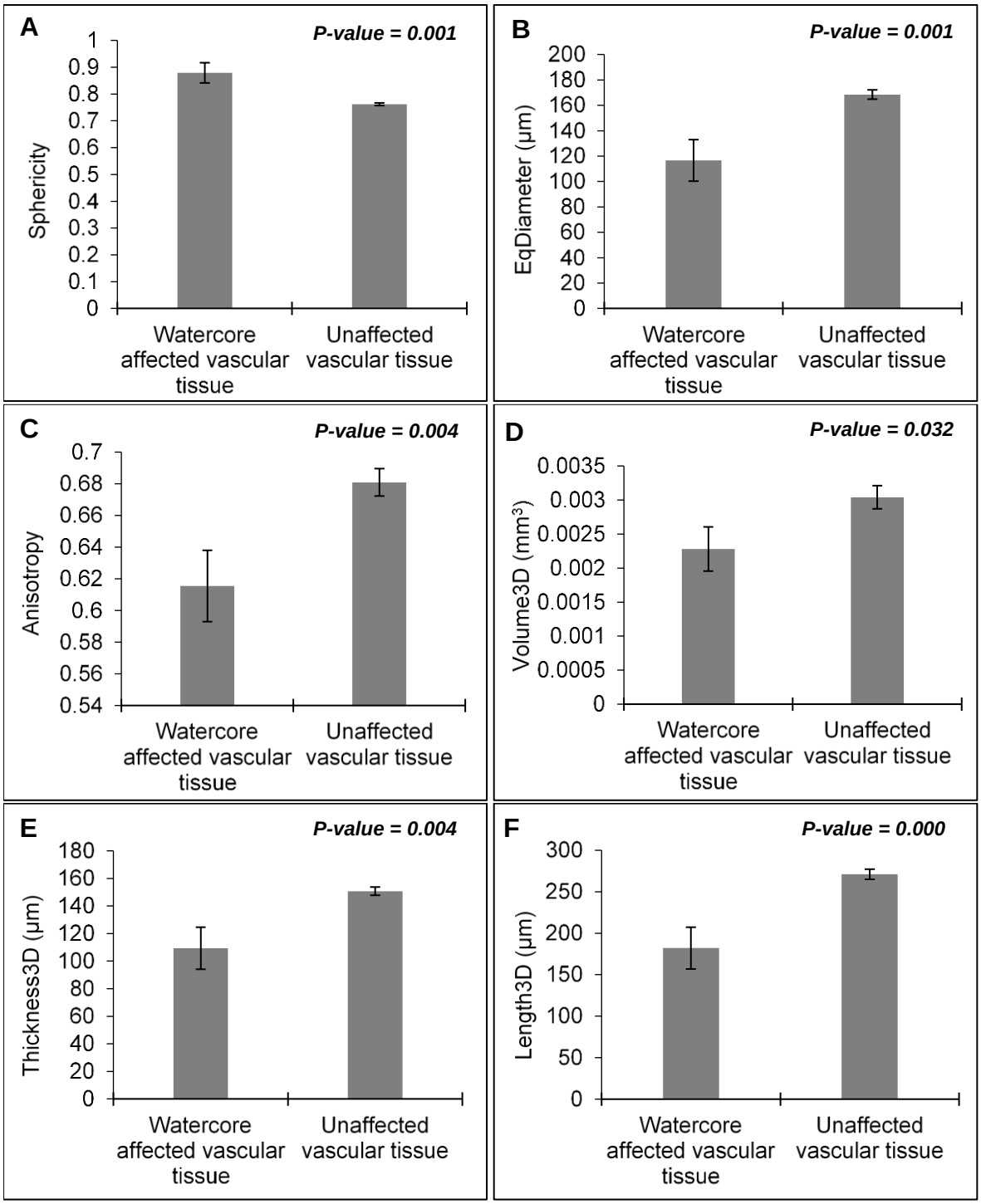


**Fig. 7.** Bar graphs and corresponding standard error bars for the following 3D cell parameters of fruit vascular tissue with watercore and unaffected fruit vascular tissue A) Sphericity B) EqDiameter C) Anisotropy D) Volume3D E) Thickness3D and F) Length3D. Error bars indicate standard error of 15 independent measurements.

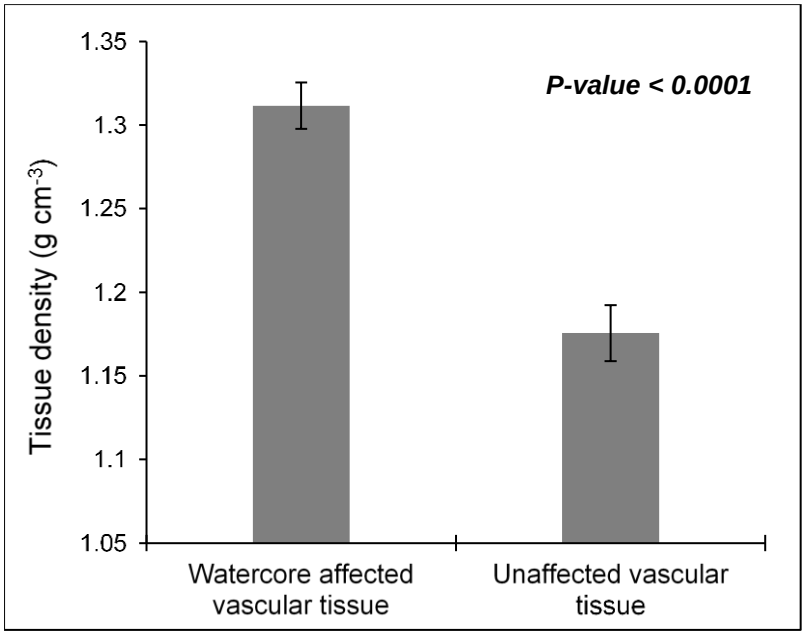


**Fig. 8.** Tissue density of fruit vascular tissue with watercore and unaffected regions. Density measurements were done on low-resolution X-ray CT images. Error bars indicate standard error of 15 independent measurements.


**Fig. 9.** Greyscale image (A) obtained from low-resolution scanning at 60 µm and corresponding original image of the same fruit with radial watercore (B).

**PAPER 4**

# X-ray computed tomography and 3D image analysis to characterize the aeration and cell properties of different browning types observed after long-term storage of 'Fuji' apples


## Abstract

The storage potential of 'Fuji' apples is limited by the incidence of internal browning (IB) disorders such as core-flush, radial browning and $CO_2$ damage. The objectives of this study were to i) determine which storage regime is most effective in maintaining quality and reducing IB incidence in 'Fuji' apples ii) use high-resolution X-ray computed tomography (CT) and 3D image analysis in quantifying microstructural properties of fruit tissue affected by the different IB types identified from the storage experiments. Fruit were stored in regular atmosphere (RA), controlled atmosphere (CA) and delayed controlled atmosphere (delayed CA) storage. Fruit were subjected to a storage period of 6 months at -0.5 °C, simulated shipment period 4 weeks in RA at -0.5 °C and shelf-life period of 7 days at 20 °C. There was a high incidence of core-flush browning in RA stored fruit at the end of the simulated shipping period. Although CA and delayed CA were effective in reducing core-flush incidence, they also resulted in a higher incidence of radial browning. X-ray CT scanning showed that all browning types evaluated were a result of cell collapse and damage which caused an increased tissue porosity and higher pore sphericity, anisotropy and pore size distribution. Contrasting structures of browning affected tissue and healthy tissue were observed, showing that browning disorders in 'Fuji' apples affect fruit at a microstructural level.


**Keywords**: Controlled atmosphere, radial browning, core-flush, high-resolution X-ray CT, porosity

## 1. Introduction

'Fuji' is an important apple variety and is the sixth most cultivated apple cultivar in South Africa (HORTGRO, 2019). It is mainly grown in the apple production regions around the Western Cape Province in South Africa. The popularity of 'Fuji' apples in South Africa and globally can be attributed to its distinctive juiciness, crispness and sweetness (Kweon et al., 2013). However, to achieve optimum quality characteristics such as maximum red colouration and high total soluble solutes, 'Fuji' in some cases may be harvested at an advanced maturity, especially in warmer production regions when waiting for cooler weather conditions, conducive to anthocyanin development (Kweon et al., 2013; Moggia et al., 2015, Honda and Moriya, 2018). Harvesting 'Fuji' apples at an advanced maturity increases susceptibility of fruit to storage disorders such as internal browning (IB; Argenta et al., 2000).

To ensure all year-round availability and off-season marketing, fruit must be stored for extended periods under controlled environments such as controlled atmosphere (CA) storage (Kweon et al., 1998; Moggia et al., 2015). CA storage utilises a slightly elevated $CO_2$ and low $O_2$ concentration to suppress fruit respiration, thereby increasing the storage life of the fruit (Gonzalez et al., 2001). Although beneficial in many aspects, CA storage may result in fruit developing physiological disorders during cold storage. One of the most problematic physiological disorders that develop in 'Fuji' apples is IB (Volz and Mitcham, 1997; Gonzalez et al., 2001). Several researchers have highlighted the susceptibility of 'Fuji' apples to IB disorders (Grant et al., 1996; Kweon et al., 1998; Argenta et al., 2001; Gonzalez et al., 2001; Kweon et al., 2013). Delaying the establishment of CA storage for a few weeks after harvest has been found to be helpful in reducing incidence of IB disorders in 'Fuji' apples (Argenta et al., 2000).

Different IB types occur in apples and they vary depending on their severity and location within the apple tissue. Radial and diffuse browning have been identified in 'Cripps' Pink' apples, radial browning has been reported to be a senescence related disorder that occurs

due to fractured cell walls in vascular tissue cells while diffuse browning is reported to follow the collapse of cortical cells (de Castro et al., 2007; James and Jobling, 2009; Moggia et al., 2015). Both of these browning types have been shown to increase with increasing storage time and $CO_2$ concentration within the storage atmosphere (James and Jobling, 2009). Core-flush browning has also been identified in 'Fuji' apples and it is characterized by diffuse browning around the core of the apple (Fan et al., 1999; Argenta et al., 2001). The causes of core-flush in apples have been attributed to senescence (Argenta et al., 2001) and chilling injury (Fan et al., 1999). Carbon dioxide injury/damage is another common browning type that occurs in apples during long-term CA storage and is characterized by a deep brown discolouration usually accompanied by pits and cavities in the cortex and core region of the fruit (James and Jobling, 2009). It is a result of high $CO_2$ concentration within the fruit and is aggravated by elevated $CO_2$ levels in the storage atmosphere (Lau, 1998).

To get more insight into the different browning types in 'Fuji' apples, it is necessary to evaluate the fruit microstructure. Fruit contains microstructural features such as intercellular spaces (pores), cells and cell walls which are only manifested in the sub-micrometre range (Herremans et al., 2014). Fruit microstructure affects the behaviour and quality of fruit during long-term storage, highly connected pores may facilitate better movement and exchange of metabolic gases as compared to poorly connected pores (Herremans et al., 2014). High-resolution imaging techniques that are non-destructive in nature are useful in evaluating fruit microstructure. Traditionally, light and confocal microscopy have been used to evaluate fruit microstructure (Khan and Vincent, 1990; Schotsmans et al., 2004; Pieczywek and Zdunek, 2012; Herremans et al., 2013). However, these methods are limited in their penetration depth and they rely on destructive analysis of thin 2D sections to estimate volumetric parameters of 3D structures (Herremans et al., 2013). A method for isolating and measuring shape and size of apple cells was proposed by McAtee et al. (2009), however, this method still does not provide sufficient 3D geometric information. Xray CT is an imaging technique that can be utilised in the acquisition of 3D spatial data from intact fruit samples

(Ting et al., 2013). Xray CT has been gaining popularity due to its non-destructive nature, high penetration depth and non-reliance on tedious sample preparation (Herremans et al., 2013; Vicent et al., 2017). The use of Xray CT in apple fruit microstructure evaluations has been explored by different researchers. Through the use of Xray CT, Ting et al. (2013) evaluated porosity and microstructural properties of four different apple cultivars (Braeburn, Fuji, Golden Delicious, Jazz) stored under similar conditions (2 °C in RA conditions) for 100 days, Herremans et al. (2013) characterized 'Braeburn' browning disorder while Diels et al. (2017) assessed bruise volumes in apples. Chigwaya et al. (2021) used X-ray CT to characterize the microstructure of 'Fuji' apple tissue after exposure to high $CO_2$/low $O_2$ stress conditions.

The objectives of this study were to i) determine which storage regime is most effective in maintaining quality and reducing IB incidence in 'Fuji' apples ii) use high-resolution X-ray computed tomography (CT) and 3D image analysis in quantifying microstructural properties of fruit tissue affected by the different IB types identified from the storage experiments. The quantitative and qualitative assessment of microstructural properties of fruit tissue with IB is expected to shed more light on how to better store 'Fuji' apples in a way that will minimize incidence of these disorders.

## 2. Materials and methods

### *2.1. Fruit material*

Fruit were harvested on the 3rd of April 2018 from Wakkerstroom farm (33°17'47.1"S 19°14'54.8"E) located in the Koue Bokkeveld area in Western Cape Province, South Africa. The fruit were harvested at shoulder height from each tree, from either side of the canopy. Harvesting was done during the commercial harvest window for 'Fuji' in South Africa. Fruit were transported to the fruit evaluation laboratory at the Department of Horticultural Sciences, Stellenbosch University, South Africa. Maturity indexing was done on 400 fruit on arrival at the lab to determine the maturity status of the fruit at harvest. The rest of the fruit were then stored

under different storage regimes. The schematic presentation of the procedures followed in this study is shown in Fig. 1.

*2.2. Storage regimes*

Fruit were subjected to three different storage regimes to determine the efficacy of maintaining quality and reducing IB incidence. The first storage regime was RA storage in which fruit were stored for 6 months in a cold room with normal air at a temperature of -0.5 °C. The second storage regime was a CA regime in which fruit were stored for 6 months at -0.5 °C in airtight containers with an $O_2$ concentration of 1.5% and a $CO_2$ concentration of 0.5%. The third storage regime was delayed CA in which fruit were first stored for 3 weeks at -0.5 °C in RA storage before being transferred to CA storage (1.5% $O_2$ and 0.5% $CO_2$) for 5 months. After the cold storage period had lapsed, all fruit were stored for 4 weeks in a RA at -0.5 °C to simulate the shipping period from South Africa to overseas markets. After the 4 weeks had lapsed, fruit were subjected to a 7 day shelf-life period at 20 °C. Fruit evaluations were done at harvest, after 6 months cold storage, after the 4 weeks simulated shipping period and after shelf-life.

*2.3. Fruit quality evaluations*

To get a clear indication of the maturity status of the fruit at harvest, a sample of fruit were used to determine diameter, mass, height, background peel colour, blush percentage, flesh firmness, titratable acidity (TA), total soluble solutes (TSS) and starch breakdown. TA and TSS were measured on pooled samples of 20 fruit whereas the other parameters were done on single fruit at harvest. Subsequent fruit evaluations were done at the end of cold storage, simulated shipping period and shelf-life. Each of the three treatments consisted of eight replicates of 60 fruit each. The parameters measured were fruit diameter, background peel colour, mass, hue angle, firmness, TSS and TA and internal disorders. Fruit diameter, mass and height were measured using a Cranston gauge and electronic balance, both fitted

to the fruit texture analyser (FTA 2007, Güss, Strand, South Africa). Background colour of fruit were rated from 0.5 (green) to 5 (yellow), using the South African Industry colour chart for apples and pears (Unifruco Research Services, Bellville, South Africa). Hue angle was determined on both cheeks of a fruit using a calibrated colorimeter (Minolta colour recorder DR-10, Konica Minolta, Inc., Japan). The blush percentage was determined by trained reviewers who estimated the percentage of the fruit surface covered by a red blush (0% for no red blush and 100% for full red blush). Fruit firmness was measured equatorially, on a peeled surface on opposite sides of the fruit, using a universal fruit texture analyser, fitted with a 7.9 mm diameter probe (FTA 2007, Güss, Strand, South Africa). TSS content was measured on a drop of expressed juice from a pooled sample of 20 fruit per replicate using a hand-held digital refractometer (Atago Digital-Refractometer PR-32, Tokyo, Japan). TA was measured by titration of individual fruit juice from a pooled sample of 20 fruit per replicate using an automated titrator (Metrohm AG 760. Harison, Switzerland). Percentage starch conversion was estimated using the iodine test with a starch conversion chart (Unifruco Research Services, Bellville, South Africa) with a scale of 0% to 100%, where 0% was totally stained and 100% was totally unstained. Fruit were also evaluated for the incidence of IB disorders and core-rot.

*2.4. Browning types identified*

The browning types identified are shown in Fig. 2. Carbon dioxide damage was identified as the formation of a brown discolouration accompanied by pits and cavities in the apple flesh (James and Jobling, 2009). Radial browning was identified as browning of the vascular tissue adjacent to the vascular bundles (Tong et al., 2016). However, the radial browning observed was light and not very dark and apparent. Core-flush browning was identified as a brown discolouration around the core region of the apple. Due to the limited browning types identified in our storage experiments, ‘Fuji’ fruit (subjected to the same storage period as in our experiments) with $CO_2$ damage and cavities had to be sourced from a local pack-house. The

fruit with $CO_2$ damage were identified after sorting with non-destructive hyperspectral imaging used at the pack-house.

*2.5. Sampling for high-resolution X-ray CT scanning*

Cylindrical samples for high-resolution X-ray CT were obtained using a cork-borer of 5 mm inside diameter from different regions of the apple tissue (Fig. 3 and Fig. 4). For apples with $CO_2$ damage and radial browning, two samples were taken from each fruit, one from a brown area and one from the non-brown area of the same fruit (Fig. 5). In fruit with radial browning, a sample was taken on the vascular tissue surrounding the vascular bundles in the cortex region of each fruit. For apples with core-flush browning, one sample was taken from an affected region in the core of each apple. For apples without any form of browning, 2 samples were taken from each apple, one from the core and one from the cortex region (Fig. 5). The cylindrical tissue samples were cut on either end to about 15 mm long and wrapped in parafilm to avoid dehydration during scanning.

*2.6. High-resolution X-ray CT*

The samples were then loaded individually onto the Phoenix Nanotom S instrument (GE Sensing & Inspection Technologies GmbH, Wunstorf, Germany) at the Stellenbosch University Central Analytical Facility for scanning (du Plessis et al., 2016). Various system settings were tested to optimize the scan quality. A series of projection images were obtained as the sample was rotated 360° and 2600 projection images were captured. The samples were scanned at a voltage of 60 kV, current of 240 µA, and a pixel size of 3 µm. The average scan time was 45 min per sample. A series of 2D X-ray images were obtained, and these were reconstructed using reconstruction software Datos|x®2.1 (GE Sensing & Inspection Technologies GmbH, Wunstorf, Germany) to generate virtual 3D images (du Plessis et al., 2016).

*2.7. Image analysis*

To extract suitable quantitative information from X-ray CT images, it is necessary to do 3D image analysis. The projection (2D) images produced during scanning were reconstructed into 3D volumes using Datos|x®2.1 (GE Sensing & Inspection Technologies GmbH, Wunstorf, Germany). The Polychromacity of the X-ray beam gives rise to the beam hardening effect. As a result of this, beam hardening correction had to be applied to correct this artefact. A beam hardening correction of level 2 (software specific value) was used. Analysing the whole image in its entirety can be a very arduous and time-consuming exercise, hence it was necessary to select a region of interest (ROI) from the original image (Schoeman et al., 2016). Although a ROI is smaller in size compared to the original image, it is important to ensure that the selected ROI is large enough to be statistically representative of the whole sample. In this study a ROI measuring 2 x 2 x 1.5 mm was used. This representative volume of 6 $mm^3$ was large enough to give sufficient microstructural information that is representative of the whole sample and was larger than the lower limit for a representative volume element of 1.3 $mm^3$ that was suggested by Mendoza et al. (2007).

After this, it was necessary to remove random noise that occurs during scanning, filtering was done using a median filter for cell analysis in Avizo 2019.1 (VSG, Bordeaux, France) and an adaptive gauss filter for pore analysis in VGStudio Max 3.2 (Volume Graphics, GmbH, Germany). After the image was filtered, the next step was to segment the image into the constituent cells and pores so that subsequent analysis procedures could be carried out. Automatic thresholding using Otsu's method was done to create a binary image consisting of only cells and pores. Otsu's thresholding involves the defining of a single grey value to separate regions of the image based on analysis of the image histogram (Otsu, 1979; Zhang et al., 2017). Voxels containing grey values lower than this threshold value are regarded as background (pores) while those with grey values higher than the threshold value are regarded as sample material (cells; Schoeman et al., 2016). Segmentation of X-ray CT images using Otsu method has been used by Herremans et al. (2013) in Braeburn apples, Muziri et al.

(2016) in ‘Forelle’ pears and Ting et al. (2013) in the determination of differences in microstructural properties of different apple cultivars. After image thresholding, 3D image analysis was done, and various microstructural properties were determined (Table 1). 3D image analysis was done using Avizo 2019.1, CTAn 1.18.0.0 (Bruker microCT, Kontich, Belgium) and VGStudio Max 3.2.

*2.8. Cell isolation*

Automatic segmentation of individual cells was not possible due to insufficient contrast between cytoplasm and cell wall (Cantre et al., 2014). The 3D region that was identified as cells after segmentation needed to be further segmented into individual cells to allow for the quantification of individual cell properties. To differentiate neighbouring cells in the binary image, a technique known as watershed separation was used (Meyer and Beucher, 1990). This was implemented using the separate objects module in Avizo 2019.1. The watershed algorithm works by calculating the Chamfer distance map of the binary image, in which greyscales represent the distance from that pixel to the nearest black (background) pixel, regardless of direction. The chamfer distance map which computes the distance as a discrete approximation is a height chart, producing a mountain peak at the centre of each of the cells. In this study, the Separate objects/Chamfer Conservative module in Avizo 2019.1 was used to compute watershed lines on the segmented binary image. All cells that intersected the dataset borders after watershed separation were removed to exclude incomplete individual cells from the cell measurements. After watershed separation, some cells were not fully separated, such cells had to be excluded from the image since they will give rise to inaccurate results. A virtual sieve was used to remove incorrectly segmented cells and unseparated clumps of cells. Based on literature, all individual objects with a length larger than 400 µm and a sphericity index lower than 0.75 were removed from the 3D model (Herremans et al., 2015b; Wang et al., 2020). This allowed the 3D model of the image to comprise of only the correctly segmented cells (Fig. 6). This protocol was validated by Herremans et al. (2015b) by manually

segmenting individual cells and they found no significant differences in this method and manually segmented individual cells.

*2.9. Statistical analysis*

The data for different storage regimes was analysed by using a completely randomized design (CRD) with a factorial arrangement having two factors (storage regime and evaluation time), each factor having three levels. The analysis was done at a 95% confidence level using STATISTICA Version 13.1 (StatSoft Inc., Tulsa, USA). To quantify differences in the pore and cell properties differences amongst the different tissue types from fruit with $CO_2$ damage, ANOVA was done using STATISTICA. Fisher's LSD was used for mean separations at a confidence level of 95%. A completely randomised design was used. To quantify differences in pore and cell properties in fruit with radial browning and core-flush, independent t-tests were done at a 95% confidence level using STATISTICA.

## 3. Results

*3.1. Fruit maturity at harvest*

Table 2 presents the maturity parameters of 'Fuji' apples that were used in this study. Maturity at harvest is a very important factor that affects the quality and storage potential of apples. The quality and storage potential can be affected by either early pre-optimum harvest or late post-optimum harvest especially when the fruit are intended for long-term storage. The apples used in this study were harvested during the commercial harvest period in 2018 and the maturity indices show that the apples were relatively over-mature at the time of harvest as shown by the very high starch breakdown (81 ± 19.5%), low flesh firmness (7.7 ± 0.6kg) and low TA (0.31 ± 0.02%; Table 2). Different degrees of radial browning were found in 63% of the fruit that were evaluated at harvest (Table 2).

*3.2. Long-term storage*

Table 3 presents fruit quality parameters as influenced by storage regime, evaluation time and the interaction thereof. Diameter did not significantly differ for the interaction as well as for the storage regime. However, the different evaluation times had significant differences in diameter with 6 months having the largest diameter (75.4 mm). The interaction between storage regime and evaluation time as well as storage regime were not significant for fruit mass. However, the fruit mass was different for evaluation time *(P < 0.0001)* and the mass was highest at the end of 6 months cold storage. The fruit mass at the end of the 4 weeks simulated shipping period and end of 7 days shelf-life were not significantly different from each other. Background peel colour was significantly affected *(P = 0.0001)* by the interaction between storage regime and evaluation time and was the most yellow (5.0) in RA stored fruit at the end of the 7 days shelf-life while it was the greenest (3.2) in CA stored fruit at the end of 6 months cold storage. The interaction did not have a significant effect *(P = 0.5884)* on hue angle. However, storage regime had a significant effect *(P = 0.0169)* on hue angle, and it was the highest in CA stored fruit (71.1°) and lowest in RA stored fruit (69.9°).

There was no interaction *(P = 0.0677)* between storage regime and evaluation time for flesh firmness. However, both storage regime *(P = 0.0037)* and evaluation time *(P < 0.0001)* had a significant effect on fruit firmness. Fruit from the delayed CA treatment had a significantly higher firmness (6.3 kg) as compared to fruit from RA and CA. Fruit firmness was lowest (5.5 kg) at the end of the 7 days shelf-life period and highest (6.8 kg) at the end of 6 months cold storage. The interaction between storage regime and evaluation time was not significant *(P = 0.1365)* for TSS, storage regime was also not significant *(P = 0.9832)* for TSS. Evaluation time had a significant effect *(P < 0.0001)* on TSS, which were significantly higher (14.3%) at evaluations at the end of 6 months cold storage, TSS levels at the end of the 4 weeks simulated shipping period and 7 days shelf-life period were not significantly different. The interaction between storage regime and evaluation time had a significant effect *(P < 0.0001)* on TA and it was highest (0.28%) in delayed CA stored fruit at the end of 6 months cold storage and lowest (0.08%) in RA stored fruit at the end of shelf-life. The interaction between storage

regime and evaluation time had a significant effect *(P < 0.0001)* on core-flush incidence. Core-flush was significantly highest (43%) in RA stored fruit at the end of the 4 weeks simulated shipping period. The incidence of core-flush at the end of shelf-life in RA stored fruit was also high (30%). Fruit from all treatments did not have any core-flush incidence at the end of 6 months cold storage. The interaction did not significantly influence *(P = 0.2073)* the incidence of radial browning. However, both storage regime *(P < 0.0001)* and evaluation time *(P < 0.0001)* had a significant effect on the incidence of radial browning. Radial browning was significantly lower (6.0%) in RA stored fruit and highest in CA stored fruit (16%), but the latter did not differ significantly to delayed CA fruit (11%). Radial browning incidence was significantly the highest (16%) after 6 months cold storage. The interaction between storage regime and evaluation time did not significantly affect *(P = 0.3293)* core-rot incidence. Storage regime also did not significantly affect *(P = 0.2448)* core-rot incidence. However, evaluation time had a significant effect *(P = 0.0070)* on the incidence of core-rot. Core-rot was significantly the highest (3%) at the end of shelf-life and the lowest (2%) at the end of 6 months cold storage and the end of the simulated shipping period.

### *3.3. High-resolution X-ray CT scanning*

#### *3.3.1. Pore properties of fruit tissue with core-flush browning*

The closed porosity (1.6%) of fruit tissue with core-flush browning was significantly lower (*P < 0.0001*) as compared to that of unaffected core tissue (4.5%; Fig. 7A). Fruit tissue with core-flush browning had an open porosity of 17.4%, which was significantly higher (*P < 0.0001*) than that of unaffected core samples (6.4%; Fig. 7B). The total porosity of 18.8% found in fruit tissue affected by core-flush browning was significantly higher (*P = 0.0001*) as compared to the total porosity in unaffected core tissue (10.5%; Fig. 7C). Connectivity of pores was significantly higher (*P = 0.013*) in fruit tissue with core-flush (connectivity = 401) as compared to unaffected core tissue (connectivity = 290; Fig. 7D). The pore equivalent diameter was significantly lower (*P = 0.048*) in fruit tissue with core-flush as compared to unaffected core tissue (Fig. 7E). The sphericity of pores in fruit tissue with core-flush and

unaffected core tissue was not significantly different (*P = 0.071*; Fig. 7F). Large openings in the flesh of fruit tissue affected by core-flush browning are evident (Fig. 8). Unaffected core tissue samples generally had smaller pores with an average individual pore volume of 0.002 $mm^3$, while core-flush affected tissue samples had an average individual pore volume of 0.008 $mm^3$ (Fig. 8 A, B).

### *3.3.2. Pore properties of fruit tissue with radial browning*

The closed porosity was significantly lower *(P < 0.0001)* in vascular tissue with radial browning (1.4%) compared to unaffected vascular tissue (4.5%; Fig. 9A). Open porosity was significantly higher *(P < 0.0001)* in vascular tissue with radial browning (29.6%) as compared to unaffected vascular tissue (6.3%; Fig. 9B) while the total porosity was significantly higher *(P < 0.0001)* in vascular tissue with radial browning (30.6%) compared to unaffected vascular tissue (10.5%; Fig. 9C). Connectivity of pores did not differ significantly *(P = 0.096)* between vascular tissue with radial browning and unaffected vascular tissue (Fig. 9D). The pores from vascular tissue with radial browning had an equivalent diameter of 63.3 µm and was significantly higher than that of unaffected vascular tissue (EqDiameter = 44.43 µm; Fig. 9E). The sphericity of pores did not differ significantly *(P = 0.208)* between vascular tissue with radial browning and unaffected vascular tissue (Fig. 9F). The 2D and 3D images of radial browning show huge openings in the vascular tissue samples with radial browning compared to tissue without radial browning (Fig. 10 A, B).

### *3.3.3. Pore properties for fruit with $CO_2$ damage*

Table 4 presents the pore properties of $CO_2$ damaged brown tissue, $CO_2$ damaged white tissue (unaffected tissue from fruit with $CO_2$ damage) and unaffected cortex tissue (unaffected tissue from fruit without $CO_2$ damage). The closed porosity was significantly higher *(P = 0.001)* in fruit tissue affected by $CO_2$ damage (6.2%) compared to the unaffected fruit tissue in fruit affected by $CO_2$ damage which was lowest (2.9%). The unaffected fruit cortex tissue did,

however, not differ in closed porosity compared to the affected $CO_2$ damaged brown cortex tissue. The open porosity did not differ significantly *(P = 0.237)* between the affected (brown) and unaffected (white) tissue of $CO_2$ injured fruit and unaffected tissue from fruit without any $CO_2$ damage. The total porosity was significantly higher *(P = 0.034)* in brown fruit tissue samples (28.6%) compared to white tissue samples from $CO_2$ damaged fruit. However, the total porosity of brown fruit tissue samples with $CO_2$ damage was not significantly different from the total porosity of unaffected cortex tissue samples (23.4%). The total porosity in $CO_2$ damaged white tissue was also not significantly different from that of the unaffected cortex tissue. The connectivity of pores did not differ significantly *(P = 0.919)* amongst the different tissue types that were scanned. The equivalent diameter also did not differ significantly *(P = 0.418)* amongst the different tissue types. The length of the pores differed significantly *(P = 0.001)* amongst the different tissue types, the pores in fruit tissue with $CO_2$ damage had the smallest length (length3D = 164.38 µm) whilst the pores from unaffected fruit cortical tissue had the longest length (length3D = 229.92 µm) and was not significantly different from that of $CO_2$ damaged white tissue (length3D = 221.58). Fruit tissue with $CO_2$ damage had a significantly lower *(P < 0.0001)* anisotropy (0.769) as compared to $CO_2$ damaged fruit, white tissue (0.822) and unaffected fruit, cortex tissue (0.830). Pores from $CO_2$ damaged fruit brown tissue were significantly *(P < 0.0001)* more spherical with a sphericity of 0.831, as compared to $CO_2$ damaged fruit white tissue (sphericity = 0.753) and unaffected fruit, cortex tissue (sphericity = 0.752). The 2D and 3D images shown in Fig.11 (A-C) show clear differences in the shape and structure of pores between $CO_2$ damaged brown tissue, $CO_2$ damaged fruit's white tissue and unaffected fruit tissue.

### *3.3.4. Cell properties of fruit tissue with core-flush browning*

The equivalent diameter of cells from fruit tissue with core-flush browning was significantly higher (EqDiameter = 178.69 µm) as compared to that of cells from unaffected core tissue (EqDiameter = 160.57 µm; Fig. 12A). The degree of anisotropy did not differ significantly *(P = 0.966)* between cells from core-flush affected tissue and cells from unaffected

core tissue (Fig. 12B). Cells from core-flush affected tissue had a significantly larger volume (volume3D = 0.0035 $mm^3$) as compared to cells from unaffected core tissue (volume3D = 0.0026 $mm^3$; Fig. 12C). The width of cells from core-flush affected tissue was significantly *(P = 0.007)* larger as compared to the cells from unaffected core tissue (Fig. 12D). The sphericity of cells from core-flush affected tissue and cells from unaffected core tissue did not differ significantly *(P = 0.531;* Fig. 12E). In terms of length, the cells from core-flush affected tissue were significantly longer (length3D = 288.42 µm) as compared to cells from unaffected core (length3D = 262.30 µm; Fig. 12F).

### *3.3.5. Cell properties of fruit tissue with radial browning*

Vascular tissue cells with radial browning had a significantly higher *(P < 0.0001)* equivalent diameter as compared to unaffected vascular tissue cells (Fig. 13A). The degree of anisotropy was also significantly different with cells from radial brown vascular tissue being less anisotropic (anisotropy = 0.63) compared to cells from unaffected vascular tissue (anisotropy = 0.68; Fig. 13B). The volume of cells from radial brown vascular tissue was significantly larger (volume3D = 0.0046 $mm^3$) as compared to cells from unaffected vascular tissue (volume3D = 0.0030 $mm^3$; Fig. 13C). Cells from vascular tissue with radial browning had a significantly higher width (width3D = 181.12) as compared to cells from unaffected vascular tissue (width3D = 153.75; Fig. 13D) while cells from vascular tissue with radial browning were significantly more spherical (sphericity = 0.81) compared to cells from unaffected vascular tissue (sphericity = 0.76; Fig. 13E). In terms of length, cells from vascular tissue with radial browning had a significantly longer length (length3D = 298.73 µm) as compared to cells from unaffected vascular tissue (length3D = 271.09 µm; Fig. 13F).

### *3.3.6. Cell properties of fruit tissue with $CO_2$ damage*

Table 5 presents the cell properties of $CO_2$ damaged brown tissue, $CO_2$ damaged white tissue (unaffected tissue samples from fruit with $CO_2$ damage) and unaffected cortex tissue

(unaffected tissue samples from fruit without $CO_2$ damage). Cells from $CO_2$ damaged white tissue were significantly larger compared to cells from $CO_2$ damaged brown tissue and unaffected cortex tissue in terms of length, thickness, width, area, equivalent diameter and volume. Cells from $CO_2$ damaged brown tissue had the smallest cells in terms of the measured cell parameters. Cells in $CO_2$ damaged brown tissue were significantly *($P < 0.0001$)* less spherical as compared to $CO_2$ damaged white tissue and unaffected cortex tissue. The anisotropy of the cells did not differ significantly *($P = 0.240$)* among the different tissue types.

## 4. Discussion

The results of this study show that core-flush browning was significantly higher in fruit from RA storage plus the 4 weeks simulated shipping period while CA and delayed CA significantly reduced core-flush incidence at the end of both simulated shipping and shelf-life periods. There was an inverese relationship between core-flush incidence and TA levels, treatment combinations with high core-flush incidence had low TA levels, possibly due to the usage of acids in senescent related metabolic procceses. According to Argenta et al. (2001), coreflush is a physiological disorder that occurs during long-term RA and CA storage and is characterized by a brown discolouration in the core of the apple. Core-flush is a result of the interaction between senescence and chilling injury and is induced by low temperatures during fruit storage (Fan et al., 1999; Argenta et al., 2000; Franck et al., 2007). Both senescence and chilling injury have an effect on the structure and integrity of the membrane bilayer. Chilling injury is a result of loss of fluidity of the plasma membrane resulting from irreversible bulk lipid phase changes following the separation of the membrane lipid bi-layer (James and Jobling, 2009). Fan et al. (1999) described core-flush as the development of diffuse browning in the core region of the fruit as a result of improper temperature management during fruit storage. The susceptibility of ‘Fuji’ apples to core-flush has been highlighted by Kweon et al. (2013) and Argenta et al. (2000).

Both delayed CA and CA storage were effective in significantly reducing the incidence of core-flush at the end of the shelf-life period. Similar results were also obtained by Argenta et al. (2000) and they attributed the effectiveness of delayed CA to the concept that fruit are more susceptible to browning development during the first few weeks of storage and therefore delaying CA establishment can help to reduce browning disorders. The effectiveness of CA storage in reducing core-flush shows that core-flush incidence may be a senescence related disorder. Previously, Fan et al. (1999) highlighted that core-flush appears as fruit ripens during storage and is likely associated with senescence. The effectiveness of delayed CA in reducing core-flush in 'Fuji' can be attributed to the energy status of the fruit and it's role in maintaining membrane integrity during long-term storage (Saquet et al., 2003). 'Conference' pears subjected to delayed CA had a higher respiration activity and ethylene production which led to increased adenosine triphosphate (ATP) concentration in the fruit tissue (Saquet et al., 2003). This high energy status is beneficial in providing additional energy to maintain membrane integrity, this helps reduce IB disorders which normally occur as a result of disruption of the plasma membrane (Saquet et al., 2003). Delaying the establishment of CA storage for 2 months was also found to be effective in reducing core browning in 'Empire' apples (DeEll and Ehsani-Moghaddam, 2012).

High-resolution X-ray CT scans done in this study showed that the total porosity of fruit tissue affected by core-flush was significantly higher as compared to the porosity of fruit tissue without core-flush. This finding confirms results from other studies which provided that core-flush may be a senescent related disorder characterized by the collapse of cells which leaves open voids in the apple flesh (Fan et al., 1999). These large open pores are often reffered to as lysigenous pores and are formed when complete cells disintergrate leading to the formation of large voids (Schotsmans et al., 2004; Muziri et al., 2016). The increase in the size of intercellular spaces as a result of the dissolution of the middle lamellae has also been highlighted by Schotsmans et al. (2004). The shape and size of the cells was also affected by core-flush, the size of cells from core-flush affected tissue was significantly larger as compared

to cells from unaffected tissue. Cell structure changes during senescence have also been highlighted by James and Jobling (2009), they found that the cells changed from their regular round shape to an irregular shape. This results in altering of the shape and distribution of pores, negatively impacting fruit gas diffusion kinetics which are highly dependant on pore structure.

The incidence of radial browning was highest in fruit stored in CA and delayed CA and was lowest in fruit from RA storage. Radial browning involves browning of the vascular tissue sorrounding the vascular bundles while the rest of the cortical tissue remains unaffected (James et al., 2008; James and Jobling, 2009). The fruit used in this study had a high incidence of radial watercore and this may have contributed to the incidence of radial browning. Radial browning sometimes occurs when fruit is harvested at advanced maturity, in this study the fruit were relatively over-mature with a firmness of 7.7 kg, which is less than the recommended 8.5 kg and a TA level of 0.31% which is less than the recommended 0.45% (Findlay and Combrink, 2013). Watercore results in the flooding of intercellular spaces in the vascular tissue with a sorbitol rich fluid and this affects the efficacy of the pores to efficiently transport respiratory gases (Argenta et al., 2002). This may result in anoxic conditions in vascular tissue cells and incidence of radial browning (Argenta et al., 2002). The incidence and severity of radial browning has been found to be related to increased storage time and reduction in the $O_2$ concentration of the storage atmosphere (James and Jobling, 2009). This finding confirms the results of this current study in which fruit from CA storage had the highest incidence of radial browning. CA storage utilises an elevated $CO_2$ concentration and reduced $O_2$ to reduce respiration rates and maintain quality during long-term storage (Argenta et al., 2002). The origin of flesh browning disorders in apples can be traced back to chilling injury, senescent breakdown or $CO_2$ damage (James and Jobling, 2009). However, chilling injury and senescence are more likely to interact with each other since both of them affect the integrity of the cell membrane.

In contrast, $CO_2$ damage is a result of high $CO_2$ concentration within the fruit and is affected by the rate of $CO_2$ diffusion within the fruit and the $CO_2$ concentration in the storage atmosphere (Lau, 1998). $CO_2$ damage in apples is identified as the presence of brown discolouration which is normally accompanied by pits and cavities within the apple flesh (Lau, 1998; Saquet et al., 2003). High levels of $CO_2$ have a negative effect on the $O_2$ consumption of a number of fruit and vegetables (Peppelenbos and van't Leven, 1996). This is due to competitive inhibiton which causes both the inhibitor ($CO_2$) and substrate ($O_2$) compete for the same active site of the enzyme (Peppelenbos and van't Leven, 1996). Therefore, the elevated $CO_2$ concentration in the CA storage atmosphere and within the apple tissue causes a reduced uptake of $O_2$. Low $O_2$ uptake by the cells causes a change from normal metabolism to the less efficient anaerobic respiration resulting in reduced energy being available to maintain membrane structure and integrity (Herremans et al., 2013). This will result in the membrane damage by reactive oxygen species leading to decompartmentalisation and mixing of polyphenol oxidase and phenolic substrates, triggering a series of oxidation reactions which will produce brown coloured polymers which are ultimately responsible for IB (de Castro et al., 2008; Lee et al., 2012; Herremans et al., 2014; Ma et al., 2015). In addition, high $CO_2$ levels can cause the pH to drop due to dissociation of carbonic acid to bicarbonate and hydrogen ions (Mathooko, 1996). Such $CO_2$ mediated drop in pH may have a significant impact on various enzymes and enzymatic intermediates in fruit metabolic pathways (Mathooko, 1996). The cellular fluids that are produced from cell damage and leakage will momentarily flood the intercellular spaces resulting in reduced porosity (Chigwaya et al., 2018). However, these cellular fluids will diffuse out of the fruit as storage time progresses leaving cavities within the fruit (Herremans et al., 2013).

High-resolution X-ray CT scans carried out in this study showed that vascular tissue affected by radial browning had a significantly high porosity as compared to unaffected vascular tissue. James and Jobling (2009) used the scanning electron microscope (SEM) to evaluate the microstructure of 'Cripps' Pink' apples and found that radial flesh browning was

characterized by fracturing of cell walls in vascular tissue with no damage being observed in the rest of the cortical tissue. The fracturing of cell walls in fruit tissue affected by radial browning has been attributed to senescence, which causes the breakdown of cells and leakage of cellular fluids into the intercellular spaces (James and Jobling, 2009). Flooding of intercellular spaces with cellular fluids reduces the diffusion of gases within the fruit and this leads to the build up of toxic levels of $CO_2$, aggravating the browning disorder (James and Jobling, 2009). The breakdown and dissociation of cells as a result of senescence can help explain the large porosity of fruit tissue affected by radial browning. The cellular structure of vascular tissue with radial browning was significantly different from the cellular structure of unaffected vascular tissue.

High-resolution X-ray CT scans done on fruit with $CO_2$ damage showed an increase in porosity and sphericity in fruit tissue affected by $CO_2$ damage. An increase in pore size and distribution during long-term storage was also observed by Herremans et al. (2013) in ‘Braeburn’ apples affected by ‘Braeburn’ browning disorder, they attributed this increase in pore size to the connection of neighbouring smaller pores to form single larger pores as a result of loss in cell to cell adhesion. According to Herremans et al. (2013), cellular breakdown was apparent in ‘Braeburn’ browning disorder which is a form of $CO_2$ damage. The breakdown and collapse of cells caused by high internal $CO_2$ levels cause the flooding of intercellular spaces with cellular constituents and this momentarily reduces the total porosity. However, when these cellular constituents are redistributed and moisture diffuses out of the fruit, large voids or cavities are left in the apple tissue and this increases the overall porosity of the affected tissue.

In a previous study, we found that the short-term exposure of ‘Fuji’ apples to a storage atmosphere enriched with 50% $CO_2$ led to decompartmentalisation, flooding of intercellular spaces and a reduction of porosity in affected tissue (Chigwaya et al., 2018). This finding suggests that flooding of intercellular spaces with cellular fluids is one of the initial stages of $CO_2$ induced IB, this is then followed by diffusion of cellular fluids from the fruit leaving behind

voids and cavities within the fruit. In terms of cell properties, 'Fuji' apple tissue affected by $CO_2$ damage had smaller cells by volume as compared to normal 'Fuji' apple tissue. This shows that the cells were affected by the hypoxic/anoxic conditions and this subsequently affected the sphericity and other properties of the pores. The pores in $CO_2$ damaged fruit tissue were more spherical and this is due to the changes in cell structure. Pores in normal apple tissue are randomly shaped and do not assume any particular shape. Changes in structure and shape of pores affects the effectiveness of the pores in their role of efficiently facilitating gas diffusion within the apple tissue, this will further aggravate the IB disorders discussed in this paper (core-flush, radial browning and $CO_2$ damage).

## 5. Conclusions

The results of this study showed that both delayed CA and CA storage were able to significantly reduce the incidence of core-flush in 'Fuji' apples and they were not significantly different from each other in their efficacy. However, they both resulted in a significantly higher incidence of radial browning. The benefits of delaying the establishment of CA storage after harvest were not seen in this study as the delayed CA treatment did not significantly reduce the incidence of both core-flush and radial browning when compared to CA storage. The incidence of browning disorders in this study can be attributed to the advanced maturity of fruit and watercore incidence. High-resolution X-ray CT scans done in this study showed that both core-flush and radial browning may be senescence related disorders since they were both associated with collapse and damage of cells, leaving voids within the fruit. This drastically increased the porosity of fruit tissue with core-flush and radial browning, affecting the quality and texture of fruit. Radial watercore may promote the incidence of radial browning in 'Fuji' by restricting respiratory gas movements in the affected vascular tissue. Core-flush affected fruit tissue as well as $CO_2$ damaged brown tissue had a significantly higher porosity, showing that these browning disorders generally result from collapse of cells leaving open spaces within the fruit tissue. While this finding seems to counter the findings of the first two research papers

of this dissertation (i.e. IB affected tissue having lower porosity), this can be attributed to the long storage duration which allowed sufficient time for cellular fluids released from damaged cells into the pores to diffuse out of the fruit leaving voids (high porosity) within the fruit tissue. In the first two research papers, the short storage duration of only three days may not have been long enough to allow cellular fluids to diffuse out of the fruit tissue and hence affected tissue had low porosity due to flooding of intercellular spaces. Additionally, the relationship between IB incidence and low porosity reported in Paper 1 and 2 was not observed in this paper as some of the IB types (radial browning and $CO_2$ damage) occurred in the cortex region which has a higher porosity. Only core-flush occurred in the core region which has a lower porosity. This shows the complex nature of IB and associated factors, which results in IB symptoms occuring in different regions of the fruit. It is important to ensure that 'Fuji' apples are harvested at the prescribed maturity levels so as to reduce the risk of IB disorders during storage. Furthermore, it is important to implement measures such as dynamic CA to carefully control $CO_2$ and $O_2$ levels in the storage environment.

## Acknowledgements

This study was made possible by the financial support from the South African Apple and Pear Producer's Association and HORTGRO Science.

## References

Argenta, L., Fan, X., Mattheis, J., 2000. Delaying establishment of controlled atmosphere or $CO_2$ exposure reduces 'Fuji' apple $CO_2$ injury without excessive fruit quality loss. Postharvest Biol. Technol. 20, 221–229. https://doi.org/10.1016/S0925-5214(00)00134-4.

Argenta, L., Fan, X., Mattheis, J., 2001. Development of internal browning in 'Fuji' apples during storage, in: Washington Tree Fruit Postharvest Conference. Wenatchee, WA, pp. 1–4. http://ucce.ucdavis.edu/files/datastore/234-56.pdf.

Argenta, L., Fan, X., Mattheis, J., 2002. Impact of watercore on gas permeance and incidence of internal disorders in 'Fuji' apples. Postharvest Biol. Technol. 24, 113–122. https://doi.org/10.1016/S0925-5214(01)00137-5.

Cantre, D., Herremans, E., Verboven, P., Ampofo-Asiama, J., Nicolaï, B., 2014. Characterization of the 3-D microstructure of mango (*Mangifera indica* L. cv. Carabao) during ripening using X-ray computed microtomography. Innov. Food Sci. Emerg. Technol. 24, 28–39. https://doi.org/10.1016/j.ifset.2013.12.008.

Chigwaya, K., Schoeman, L., Fourie, W.J., Crouch, I., Viljoen, D. and Crouch, E.M., 2018. 'Fuji' apple internal browning explored via X-ray computed tomography (CT). Acta Hortic. 1201, 309-316. https://doi.org/10.17660/ActaHortic.2018.1201.42.

Chigwaya, K., du Plessis, A., Viljoen, D.W., Crouch, I.J., Crouch, E.M., 2021. Use of X-ray computed tomography and 3D image analysis to characterize internal browning in 'Fuji' apples after exposure to $CO_2$ stress. Sci. Hortic. 277, 1–10. https://doi.org/10.1016/j.scienta.2020.109840.

de Castro, E., Barrett, D.M., Jobling, J., Mitcham, E.J., 2008. Biochemical factors associated with a $CO_2$-induced flesh browning disorder of Pink Lady apples. Postharvest Biol. Technol. 48, 182–191. https://doi.org/10.1016/j.postharvbio.2007.09.027.

de Castro, E., Biasi, B., Mitcham, E., Tustin, S., Tanner, D., Jobling, J., 2007. Carbon dioxide-induced flesh browning in Pink Lady apples. Am. Soc. Hortic. 132, 713–719. https://doi.org/10.21273/JASHS.132.5.713.

DeEll, J.R., Ehsani-Moghaddam, B., 2012. Delayed controlled atmosphere storage affects storage disorders of 'Empire' apples. Postharvest Biol. Technol. 67, 167–171. https://doi.org/10.1016/j.postharvbio.2012.01.004.

Diels, E., van Dael, M., Keresztes, J., Vanmaercke, S., Verboven, P., Nicolaï, B., Saeys, W., Ramon, H., Smeets, B., 2017. Assessment of bruise volumes in apples using X-ray computed tomography. Postharvest Biol. Technol. 128, 24–32. https://doi.org/10.1016/j.postharvbio.2017.01.013.

du Plessis, A., le Roux, S.G., Guelpa, A., 2016. The CT Scanner Facility at Stellenbosch

University: An open access X-ray computed tomography laboratory. Nucl. Instruments Methods Phys. Res. Sect. B Beam Interact. with Mater. Atoms 384, 42–49. https://doi.org/10.1016/j.nimb.2016.08.005.

Fan, X., Mattheis, J.P., Blankenship, S., 1999. Development of apple superficial scald, soft scald, core flush, and greasiness is reduced by MCP. J. Agric. Food Chem. 47, 3063–3068. https://doi.org/10.1021/jf981176b.

Franck, C., Lammertyn, J., Ho, Q.T., Verboven, P., Verlinden, B., Nicolaï, B.M., 2007. Browning disorders in pear fruit. Postharvest Biol. Technol. 43, 1–13. https://doi.org/10.1016/j.postharvbio.2006.08.008

Findlay, J.S., Combrink, J.C., 2013. South African controlled atmosphere storage operator's manual. SA Apple and Pear Producers' Association. Paarl, South Africa.

Gonzalez, J.J., Valle, R.C., Bobroff, S., Biasi, W. V, Mitcham, E.J., McCarthy, M.J., 2001. Detection and monitoring of internal browning development in 'Fuji' apples using MRI. Postharvest Biol. Technol. 22, 179–188. https://doi.org/10.1016/S0925-5214(00)00183-6.

Grant, J., Mitcham, B., Biasi, B., Chinchiolo, S., 1996. Late harvest, high $CO_2$ storage increase internal browning of Fuji apples. Calif. Agric. 50, 26–29. https://doi.org/10.3733/ca.v050n03p26

Herremans, E., Verboven, P., Bongaers, E., Estrade, P., Verlinden, B.E., Wevers, M., Hertog, M.L.A.T.M., Nicolaï, B.M., 2013. Characterisation of 'Braeburn' browning disorder by means of X-ray micro-CT. Postharvest Biol. Technol. 75, 114–124. https://doi.org/10.1016/j.postharvbio.2012.08.008

Herremans, E., Verboven, P., Defraeye, T., Rogge, S., Ho, Q.T., Hertog, M.L.A.T.M., Verlinden, B.E., Bongaers, E., Wevers, M., Nicolaï, B.M., 2014. X-ray CT for quantitative food microstructure engineering: The apple case. Nucl. Instruments Methods Phys. Res. Sect. B Beam Interact. with Mater. Atoms 324, 88–94. https://doi.org/10.1016/j.nimb.2013.07.035.

Herremans, E., Verboven, P., Hertog, M.L.A.T.M., Cantre, D., van Dael, M., De Schryver, T.,

Van Hoorebeke, L., Nicolaï, B.M., 2015a. Spatial development of transport structures in apple (*Malus* × *domestica* Borkh.) fruit. Front. Plant Sci. 6, 1–14. https://doi.org/10.3389/fpls.2015.00679.

Herremans, E., Verboven, P., Verlinden, B.E., Cantre, D., Abera, M., Wevers, M., Nicolaï, B.M., 2015b. Automatic analysis of the 3-D microstructure of fruit parenchyma tissue using X-ray micro-CT explains differences in aeration. BMC Plant Biol. 15, 1–14. https://doi.org/10.1186/s12870-015-0650-y.

Honda, C., Moriya, S., 2018. Anthocyanin Biosynthesis in Apple Fruit. Hortic. J. 87, 305–314. https://doi.org/10.2503/hortj.OKD-R01

HORTGRO, 2019. Key Deciduous Fruit Statistics. Accessed 8 September 2020. https://www.hortgro.co.za/wp-content/uploads/docs/2020/07/key-deciduous-fruit-statistics-2019-1.pdf

James, H., Jobling, J. and Tanner, D., 2008. Investigating structural and physiological differences between radial and diffuse types of flesh browning in Cripps Pink apples. Acta Hortic. 768, 77-84 https://doi.org/10.17660/ActaHortic.2008.768.8.

James, H.J., 2007. Understanding the flesh browning disorder of 'Cripps Pink' apples. PhD dissertation, Faculty of Agriculture, Food and Natural Resources, The University of Sydney, New South Wales, Australia.

James, H.J., Jobling, J.J., 2009. Contrasting the structure and morphology of the radial and diffuse flesh browning disorders and $CO_2$ injury of 'Cripps Pink' apples. Postharvest Biol. Technol. 53, 36–42. https://doi.org/10.1016/j.postharvbio.2009.02.001.

Khan, A.A., Vincent, J.F.V., 1990. Anisotropy of apple parenchyma. J. Sci. Food Agric. 52, 455–466. https://doi.org/10.1002/jsfa.2740520404.

Kweon, H.J., Kang, I.K., Kim, M.J., Lee, J., Moon, Y.S., Choi, C., Choi, D.G., Watkins, C.B., 2013. Fruit maturity, controlled atmosphere delays and storage temperature affect fruit quality and incidence of storage disorders of 'Fuji' apples. Sci. Hortic. 157, 60–64. https://doi.org/10.1016/j.scienta.2013.04.013.

Kweon, H.J., Kim, H.Y., Ryu, O.H., Park, Y.M., 1998. Effects of CA Storage Procedures and Storage Factors on the Quality and the Incidence of Physiological Disorders of 'Fuji' Apples. Hortic. Environ. Biotechnol. 39, 35–39.

Lau, O.L., 1998. Effect of growing season, harvest maturity, waxing, low $O_2$ and elevated $CO_2$ on flesh browning disorders in 'Braeburn' apples. Postharvest Biol. Technol. 14, 131–141. https://doi.org/10.1016/S0925-5214(98)00035-0.

Lee, J., Mattheis, J.P., Rudell, D.R., 2012. Antioxidant treatment alters metabolism associated with internal browning in 'Braeburn' apples during controlled atmosphere storage. Postharvest Biol. Technol. 68, 32–42. https://doi.org/10.1016/j.postharvbio.2012.01.009.

Ma, Y., Lu, X., Nock, J.F., Watkins, C.B., 2015. Peroxidase and polyphenoloxidase activities in relation to flesh browning of stem-end and calyx-end tissues of 'Empire' apples during controlled atmosphere storage. Postharvest Biol. Technol. 108, 1–7. https://doi.org/10.1016/j.postharvbio.2015.05.002.

Mathooko, F.M., 1996. Regulation of respiratory metabolism in fruits and vegetables by carbon dioxide. Postharvest Biol. Technol. 9, 247–264. https://doi.org/10.1016/S0925-5214(96)00019-1.

McAtee, P.A., Hallett, I.C., Johnston, J.W., Schaffer, R.J., 2009. A rapid method of fruit cell isolation for cell size and shape measurements. Plant Methods 5, 1–7. https://doi.org/10.1186/1746-4811-5-5.

Mendoza, F., Verboven, P., Mebatsion, H.K., Kerckhofs, G., Wevers, M., Nicolaï, B., 2007. Three-dimensional pore space quantification of apple tissue using X-ray computed microtomography. Planta 226, 559–570. https://doi.org/10.1007/s00425-007-0504-4.

Meyer, F., Beucher, S., 1990. Morphological segmentation. J. Vis. Commun. Image Represent. 1, 21–46. https://doi.org/10.1016/1047-3203(90)90014-M.

Moggia, C., Pereira, M., Yuri, J.A., Torres, C.A., Hernández, O., Icaza, M.G., Lobos, G.A., 2015. Preharvest factors that affect the development of internal browning in apples cv. Cripps Pink: Six-years compiled data. Postharvest Biol. Technol. 101, 49–57. https://doi.org/10.1016/j.postharvbio.2014.11.005.

Muziri, T., Theron, K.I., Cantre, D., Wang, Z., Verboven, P., Nicolaï, B.M., Crouch, E.M., 2016. Microstructure analysis and detection of mealiness in 'Forelle' pear (*Pyrus communis* L.) by means of X-ray computed tomography. Postharvest Biol. Technol. 120, 145–156. https://doi.org/10.1016/j.postharvbio.2016.06.006.

Otsu, N., 1979. A threshold selection method from gray-level histograms. IEEE Trans. Syst. Man Cybern. 9, 62–66.

Peppelenbos, H.W., van't Leven, J., 1996. Evaluation of four types of inhibition for modelling the influence of carbon dioxide on oxygen consumption of fruits and vegetables. Postharvest Biol. Technol. 7, 27–40.

Pieczywek, P.M., Zdunek, A., 2012. Automatic classification of cells and intercellular spaces of apple tissue. Comput. Electron. Agric. 81, 72–78. https://doi.org/10.1016/j.compag.2011.11.006.

Saquet, A.A., Streif, J., Bangerth, F., 2003. Energy metabolism and membrane lipid alterations in relation to brown heart development in 'Conference' pears during delayed controlled atmosphere storage. Postharvest Biol. Technol. 30, 123–132. https://doi.org/10.1016/S0925-5214(03)00099-1.

Schoeman, L., Williams, P., du Plessis, A., Manley, M., 2016. X-ray micro-computed tomography (μCT) for non-destructive characterisation of food microstructure. Trends Food Sci. Technol. 47, 10-24. https://doi.org/10.1016/j.tifs.2015.10.016.

Schotsmans, W., Verlinden, B.E., Lammertyn, J., Nicolaï, B.M., 2004. The relationship between gas transport properties and the histology of apple. J. Sci. Food Agric. 84, 1131–1140. https://doi.org/10.1002/jsfa.1768.

Ting, V.J.L., Silcock, P., Bremer, P.J., Biasioli, F., 2013. X-ray micro-computer tomographic method to visualize the microstructure of different apple cultivars. J. Food Sci. 78, E1735–E1742. https://doi.org/10.1111/1750-3841.12290

Tong, C.B.S., Chang, H.Y., Boldt, J.K., Ma, Y.B., DeEll, J.R., Moran, R.E., Bourgeois, G., Plouffe, D., 2016. Diffuse flesh browning in 'Honeycrisp' apple fruit is associated with low temperatures during fruit growth. HortScience 51, 1256–1264.

https://doi.org/10.21273/HORTSCI11179-16.

Vicent, V., Verboven, P., Ndoye, F.T., Alvarez, G., Nicolaï, B., 2017. A new method developed to characterize the 3D microstructure of frozen apple using X-ray micro-CT. J. Food Eng. 212, 154–164. https://doi.org/10.1016/j.jfoodeng.2017.05.028.

Volz, R., Mitcham, B., 1997. Internal browning in 'Fuji' Apples. Perish. Handl. Newsl. 6. Accessed 2 December 2019. http://ucce.ucdavis.edu/files/datastore/234-56.pdf.

Wang, Z., Van Beers, R., Aernouts, B., Watté, R., Verboven, P., Nicolaï, B., Saeys, W., 2020. Microstructure affects light scattering in apples. Postharvest Biol. Technol. 159, 110996. https://doi.org/10.1016/j.postharvbio.2019.110996.

Zhang, P, Lu, S., Li, J., Zhang, P, Xie, L., Xue, H., Zhang, J., 2017. Multi-component segmentation of X-ray computed tomography (CT) image using multi-Otsu thresholding algorithm and scanning electron microscopy. Energy Explor. Exploit. 35, 281–294. https://doi.org/10.1177/0144598717690090.

**Table 1**

Morphometric parameters used to describe 3D high-resolution X-ray CT images, based on Herremans et al. (2013), with modifications.

| **Microstructural parameter** | **Unit** | **Description** |
|---|---|---|
| Volume | $mm^3$ | Volume of object |
| Area | $mm^2$ | Area of the object boundary |
| Length | µm | Maximum of the ferret diameters used over a range of angles |
| Width | µm | Minimum of the ferret diameters used over a range of angles |
| Equivalent diameter | µm | The diameter of a sphere of equivalent volume as the irregularly shaped object |
| Anisotropy | - | Measure of preferential alignment of structures. This value is scaled from 0 for total isotropy to 1 for total anisotropy |
| Euler number | - | It gives information about the connectivity of a 3D structure. Higher values indicate poorly connected structures and lower values for better connected structures |
| Connectivity | - | The number of connections between matrix structures per unit volume, based on Euler number |
| Total Porosity | % | Pore volume divided by the total volume |
| Closed porosity | % | The connected assemblage of space (black) voxels that is fully surrounded in 3D by solid (white) voxels. |
| Open porosity | % | Any space located within a solid object or between solid objects with connection in 3D space with outside space. |
| Sphericity | - | measures the ratio of the surface area of a sphere with the same volume as the cell/pore to its surface area |

**Table 2**

Physiochemical properties (± standard deviation) of 'Fuji' apples used in this study at harvest.

| Parameter | Value |
|---|---|
| Diameter (mm) | 71.7 ± 6.1 |
| Mass (g) | 166.1 ± 27.0 |
| Height (mm) | 61.9 ± 4.6 |
| Background peel colour (Chart value) | 3.3 ± 0.3 |
| Blush percentage (%) | 48 ± 19.0 |
| Firmness (kg) | 7.7 ± 0.6 |
| #TA (%) | 0.31 ± 0.02 |
| ^TSS (%) | 13.6 ± 0.8 |
| Starch breakdown (%) | 81.0 ± 19.5 |
| *Radial watercore (%) | 63.0 |

#Titratable acidity
^Total soluble solutes
*Radial watercore percentage represents the number of fruit that had radial watercore expressed as a percentage of the total number of fruit evaluated and standard deviation cannot be calculated.

**Table 3**

Physiochemical properties and internal disorders of 'Fuji' apples as influenced by two factors i.e. storage regime (regular atmosphere (RA), controlled atmosphere (CA) and delayed controlled atmosphere (delayed CA) ), evaluation time (6 months cold storage at -0.5 °C (6 m), 6 months cold storage at -0.5 °C + 4 weeks RA at -0.5 °C (6 m + 4 w), 6 months cold storage at -0.5 °C + 4 weeks RA at -0.5 °C + 7 days shelf-life at 20 °C (6 m + 4 w + 7 d) and their interaction thereof. CA storage conditions comprised of 1.5% $O_2$ and 0.5% $CO_2$. Different letters indicate differences at the 0.05 level.

| Storage regime | Evaluation time | Diameter (mm) | Mass (g) | Background peel colour (Chart value) | Hue angle | Firmness (kg) | TSS^ (%) | TA& (%) | Core-flush# (%) | Radial Browning# (%) | Core-rot # (%) |
|---|---|---|---|---|---|---|---|---|---|---|---|
| **Main effects:** | | | | | | | | | | | |
| **RA** | - | 75.0 ns | 13.7 ns | 4.4 | 69.9 b | 6.1 b | 13.7 ns | 0.11 | 25 | 6 b | 2 ns |
| **CA** | - | 74.8 | 13.7 | 3.9 | 71.1 a | 6.1 b | 13.7 | 0.19 | 8 | 16 a | 3 |
| **delayed CA** | - | 74.5 | 13.8 | 4.0 | 70.7 ab | 6.3 a | 13.8 | 0.19 | 12 | 11 a | 1 |
| - | **6 m** | 75.4 a | 14.3 a | 3.6 | 70.2 ns | 6.8 a | 14.3 a | 0.21 | 0 | 16 a | 2 a |
| - | **6 m+4 w** | 74.6 b | 13.4 b | 4.4 | 70.9 | 5.6 b | 13.4 b | 0.13 | 2 | 9 b | 2 a |
| - | **6 m+4 w+7 d** | 74.1 b | 13.3 b | 4.6 | 70.2 | 5.5 c | 13.3 b | 0.12 | 2 | 6 b | 3 b |
| **Interaction:** | | | | | | | | | | | |
| **RA** | **6 m** | 76.3 ns | 14.1 ns | 3.9 c | 69.2 ns | 6.7 ns | 14.1 ns | 0.13 d | 0 e | 6 ns | 1 ns |
| | **6 m+4 w** | 74.7 | 13.4 | 4.5 b | 70.0 | 5.6 | 13.4 | 0.09 e | 43 a | 5 | 2 |
| | **6 m+4 w+7 d** | 73.6 | 13.4 | 5.0 a | 70.5 | 5.5 | 13.4 | 0.08 e | 30 b | 7 | 5 |
| **CA** | **6 m** | 75.4 | 14.1 | 3.2 d | 71.6 | 6.8 | 14.1 | 0.26 b | 0 e | 18 | 3 |
| | **6 m+4 w** | 74.5 | 13.6 | 4.4 b | 71.4 | 5.6 | 13.6 | 0.15 c | 4 e | 20 | 2 |
| | **6 m+4 w+7 d** | 74.3 | 13.2 | 4.4 b | 70.2 | 5.4 | 13.2 | 0.14 cd | 15 cd | 11 | 4 |
| **delayed CA** | **6 m** | 74.6 | 14.4 | 3.7 c | 70.1 | 7.0 | 14.4 | 0.28 a | 0 e | 19 | 0 |
| | **6 m+4 w** | 74.6 | 13.2 | 4.3 b | 71.7 | 5.7 | 13.2 | 0.15 cd | 13 d | 4 | 4 |
| | **6 m+4 w+7 d** | 74.3 | 13.3 | 4.4 b | 70.2 | 5.7 | 13.3 | 0.14 cd | 18 c | 5 | 3 |
| **Source of variation** | | | | | | **Pr > F** | | | | | |
| Storage regime | | *0.6248* | *0.9832* | *<0.0001* | ***0.0169*** | ***0.0037*** | *0.9832* | *<0.0001* | *<0.0001* | ***<0.0001*** | *0.2448* |
| Evaluation time | | ***0.0014*** | ***<0.0001*** | *<0.0001* | ***0.0487*** | ***<0.0001*** | ***<0.0001*** | *<0.0001* | *<0.0001* | ***<0.0001*** | ***0.0070*** |
| Storage regime x Evaluation time | | *0.1021* | *0.1365* | ***0.0001*** | *0.5884* | *0.0677* | *0.1365* | ***<0.0001*** | ***<0.0001*** | *0.2073* | *0.3293* |

*Values with different letters are significantly different according to Fisher's LSD (*P<0.05*)

^Total soluble solutes

#Logit transformation was used for radial browning, core-flush and core-rot

&Titratable acidity

**Table 4**

Pore properties of 'Fuji' fruit tissue affected by $CO_2$ damage and unaffected fruit tissue obtained from X-ray CT scanning of fruit tissue cylindrical samples. Pore properties were determined on 6 $mm^3$ volume regions of interest obtained from fruit tissue analysis using VGStudio Max 3.2 and Avizo 2019.1. 3D means that the measurements were done on 3D volumes. Different letters indicate differences at the 0.05 level.

| | **Closed porosity (%)** | **Open porosity (%)** | **Total porosity (%)** | **Connectivity** | **EqDiameter (µm)** | **Length3D (µm)** | **Anisotropy** | **Sphericity** |
|---|---|---|---|---|---|---|---|---|
| $CO_2$ damaged brown tissue | 6.2 a | 23.7 ns | 28.6 a | 231 ns | 79.8 ns | 164.38 b | 0.769 b | 0.831 a |
| $CO_2$ damaged white tissue | 2.9 b | 18.3 | 20.6 b | 223 | 81.1 | 221.58 a | 0.822 a | 0.753 b |
| Unaffected cortex tissue | 4.8 a | 19.5 | 23.4 ab | 213 | 88.0 | 229.92 a | 0.830 a | 0.752 b |
| *Pr > F(Model)* | *0.001* | *0.237* | *0.034* | *0.919* | *0.418* | *0.001* | *< 0.0001* | *< 0.0001* |
| *LSD-value* | *1.624* | *6.643* | *5.903* | *85.306* | *13.357* | *35.359* | *0.027* | *0.034* |

**Table 5**

Cell properties of 'Fuji' fruit tissue affected by $CO_2$ damage and unaffected fruit tissue obtained from X-ray CT scanning of fruit tissue cylindrical samples. Cell properties were determined on 6 $mm^3$ volume regions of interest obtained from fruit tissue using the watershed separation algorithm which was applied in Avizo 2019.1. 3D means that the measurements were done on 3D volume. Different letters indicate differences at the 0.05 level.

| | **Length3D (µm)** | **Thickness3D (µm)** | **Width3D (µm)** | **Area3D ($mm^2$)** | **Volume3D ($mm^3$)** | **Anisotropy** | **EqDiameter (µm)** | **Sphericity** |
|---|---|---|---|---|---|---|---|---|
| $CO_2$ damaged brown tissue | 278.86 c | 166.56 b | 170.76 b | 0.14 b | 0.0033 c | 0.650 ns | 174.10 c | 0.71 b |
| $CO_2$ damaged white tissue | 310.98 a | 185.65 a | 187.58 a | 0.17 a | 0.0052 a | 0.633 | 206.64 a | 0.82 a |
| Unaffected cortex tissue | 290.80 b | 173.15 b | 174.88 b | 0.15 b | 0.0041 b | 0.634 | 191.19 b | 0.80 a |
| *Pr > F(Model)* | *< 0.0001* | *< 0.0001* | *< 0.0001* | *< 0.0001* | *< 0.0001* | *0.240* | *< 0.0001* | *< 0.0001* |
| *LSD-value* | *10.115* | *7.395* | *7.139* | *0.010* | *0.00045* | *0.023* | *7.755* | *0.018* |

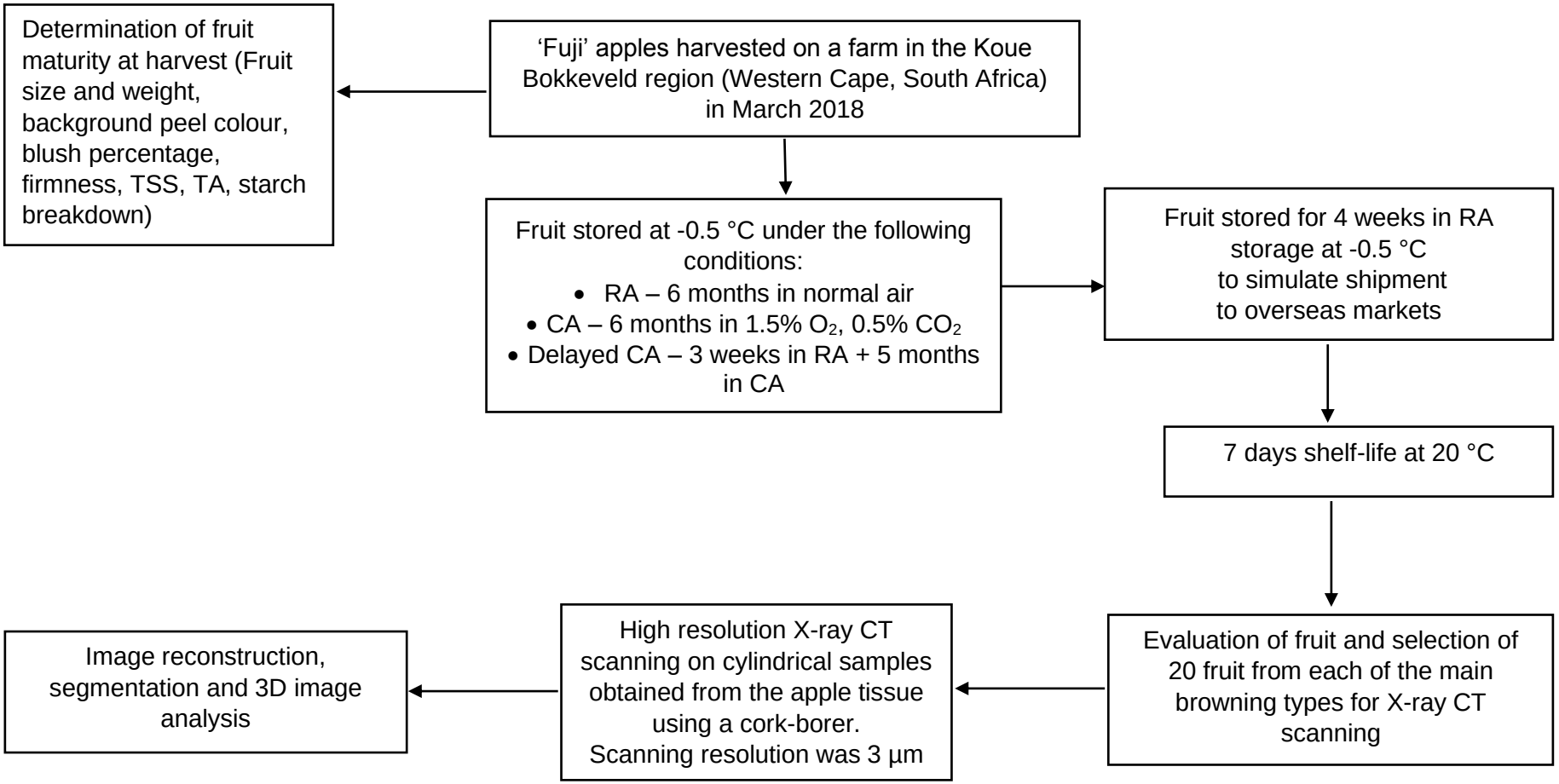


**Fig. 1.** Schematic presentation of fruit harvest, maturity indexing, fruit storage, fruit evaluations and X-ray CT scanning (TSS – total soluble solutes, TA – titratable acidity).


**Fig. 2.** Different browning types of ‘Fuji’ apples that were evaluated in this study, A – $CO_2$ damage, B – Core-flush and C – Radial browning.

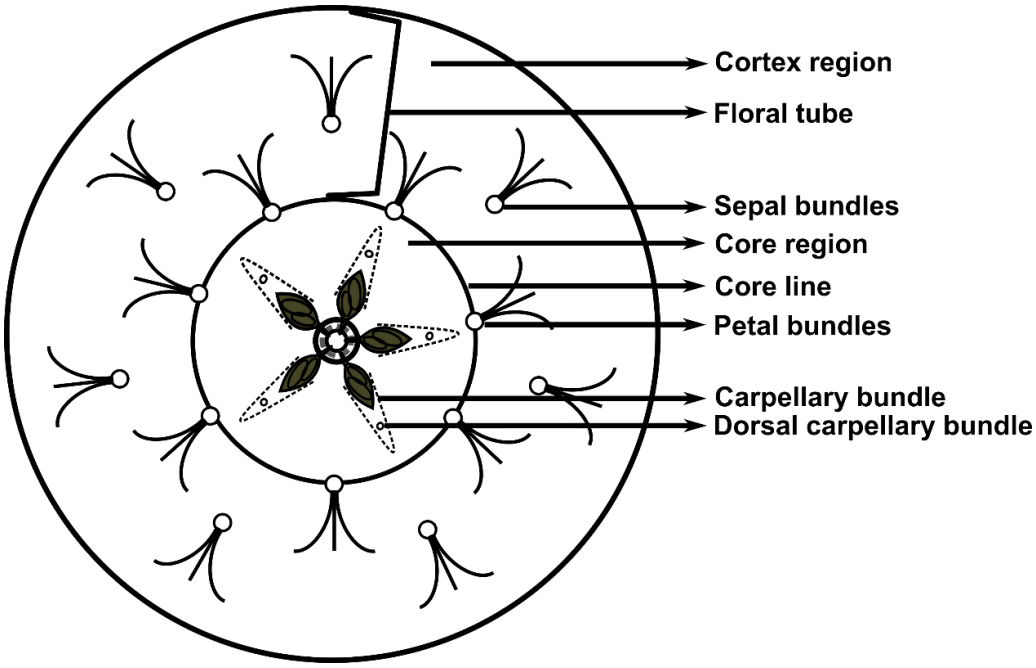


**Fig. 3.** Diagram of apple fruit in transverse section showing gross morphology of apple fruit. Based on Herremans et al. (2015a).

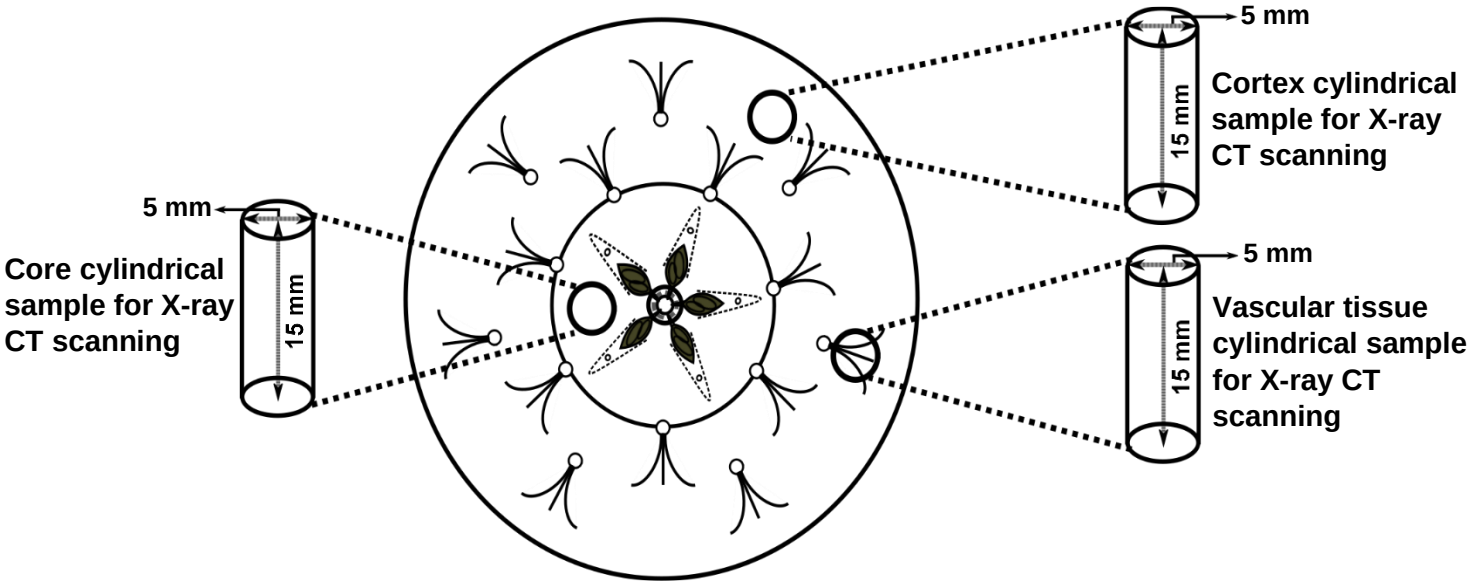


**Fig. 4.** Sampling positions from the vascular tissue, the cortex region and core region of the fruit. Cortex samples were obtained using a 5 mm diameter cork-borer from the cortex region, vascular tissue samples were obtained using a 5 mm diameter cork-borer from the tissue adjacent to the vascular bundles and core cylindrical samples were obtained from the core region using a using a 5 mm diameter cork-borer. X-ray CT scanning was done on these cylindrical samples.

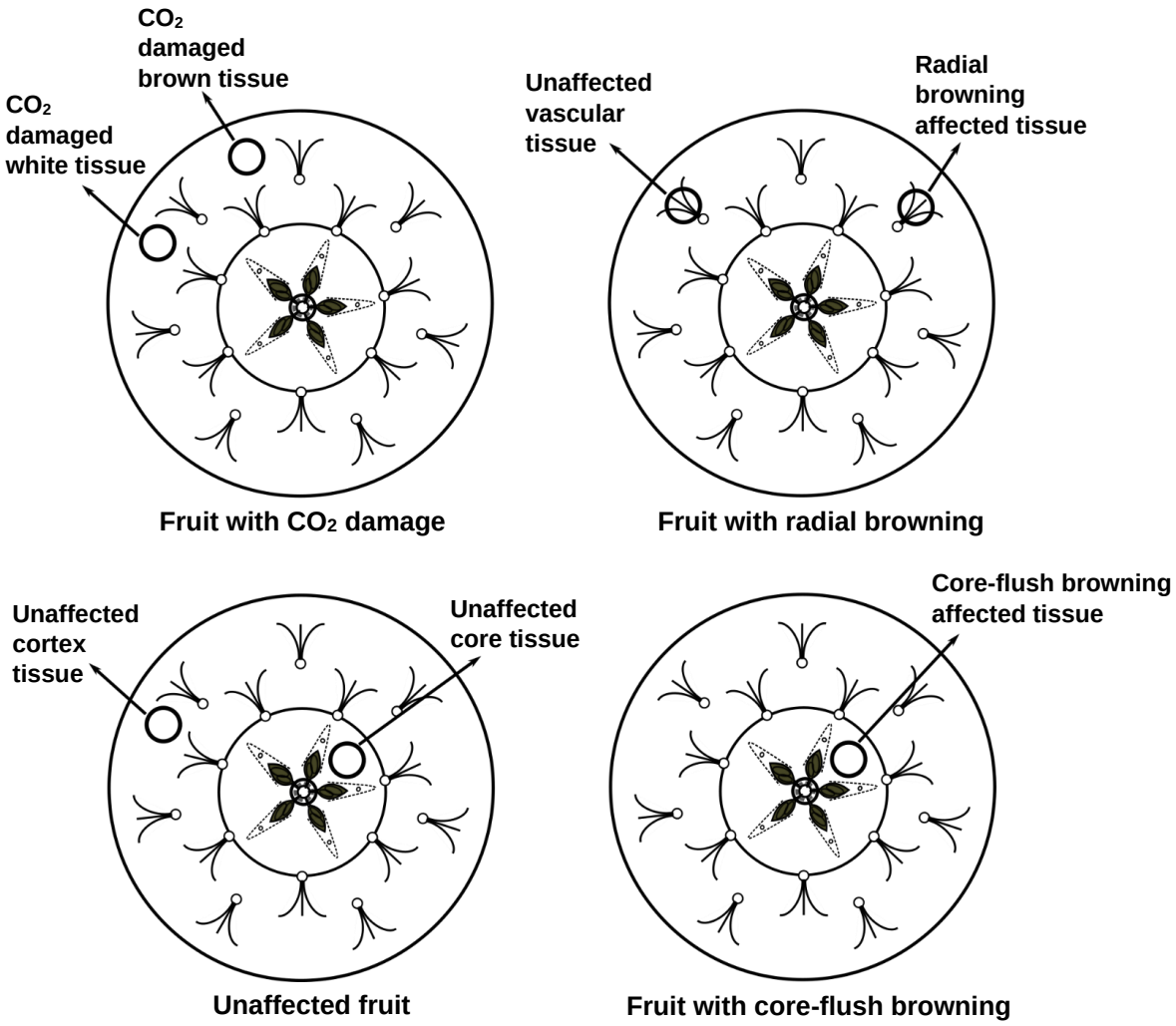


**Fig. 5.** Schematic presentation for the sampling positions from 'Fuji' fruit with $CO_2$ damage, radial browning, unaffected fruit and core-flush. Samples for X-ray CT were obtained from the fruit tissue using a cork-borer with a 5 mm inside diameter.

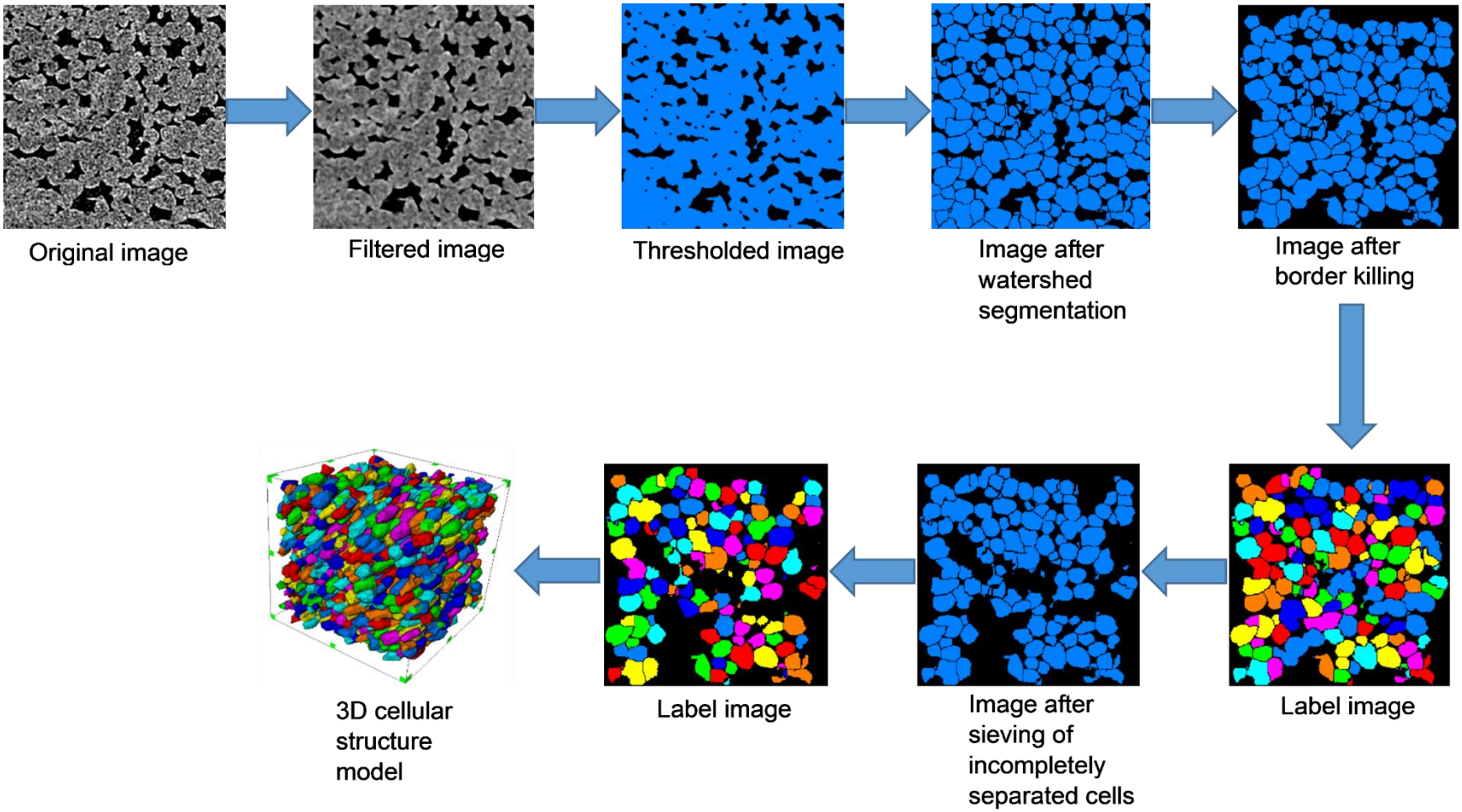


**Fig. 6.** Schematic representation of the procedure followed in isolation of individual cells and measurement of individual cell parameters using Avizo 2019.1.

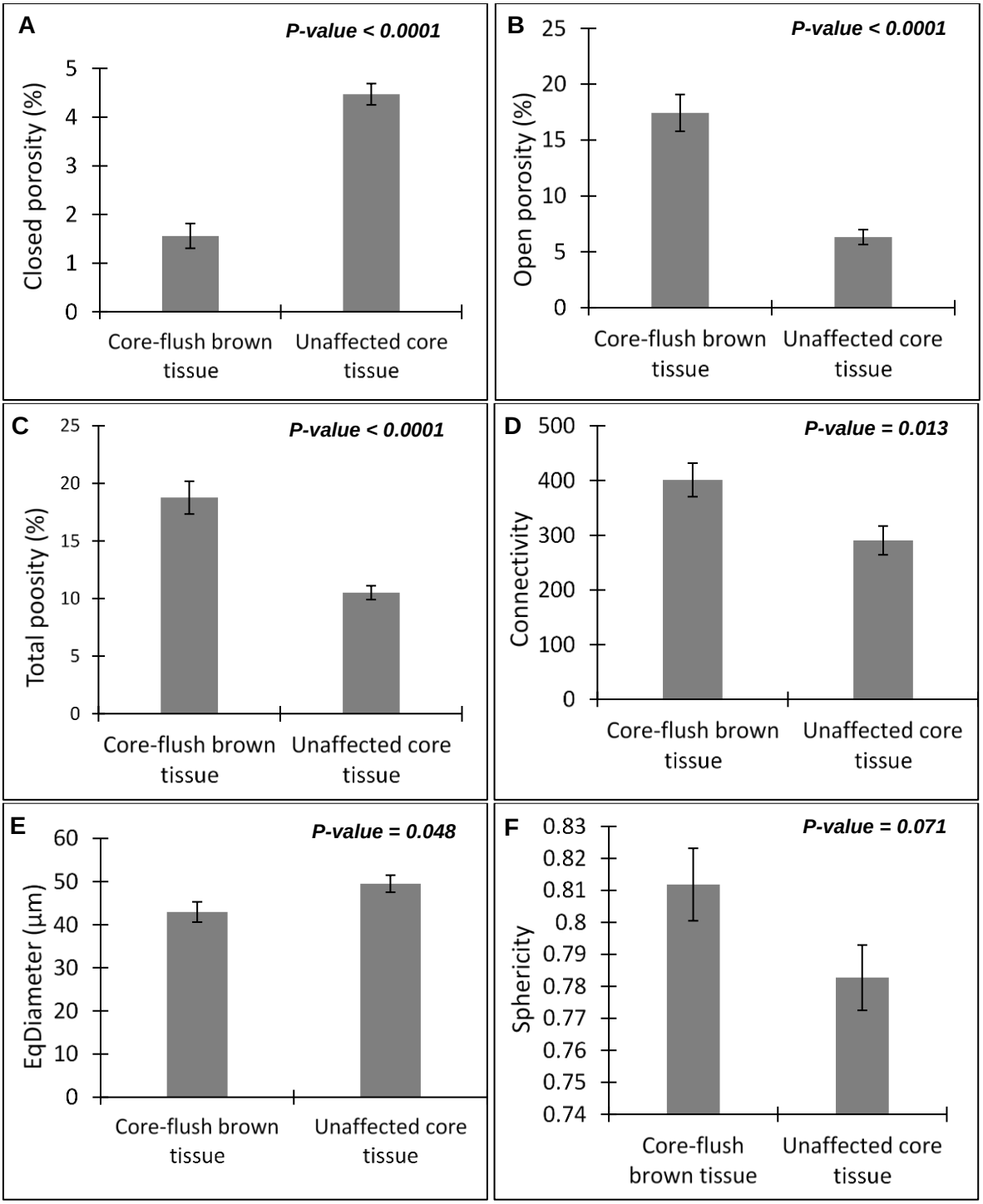


**Fig. 7.** Bar graphs and corresponding standard error bars for the following 3D pore parameters of 'Fuji' fruit tissue with core-flush browning and unaffected core tissue A) Closed porosity B) Open porosity C) Total porosity D) Connectivity E) EqDiameter and F) Sphericity. Measurements were done on 6 $mm^3$ regions of interest from core-flush browning affected tissue and unaffected core tissue images obtained after X-ray CT scanning.

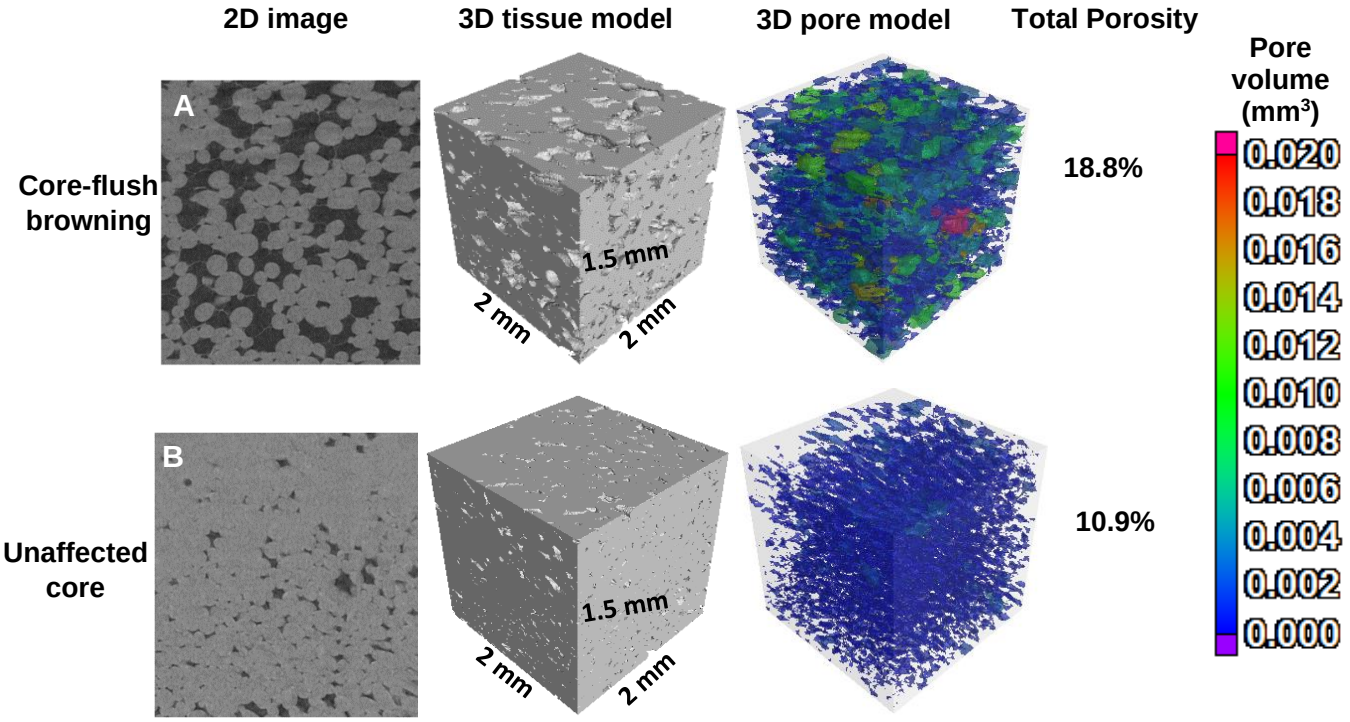


**Fig. 8**. 2D images,3D tissue models and 3D pore models for regions of interests from A – the core of fruit with core-flush browning and B – the core of 'Fuji' fruit without core-flush browning. 2D images show pores in dark grey and cells in light grey. Different colours in the 3D pore models represent different individual pore volumes as defined in the scale. The total volume for the 3D models is 6 $mm^3$ (2 x 2 x 1.5 mm).

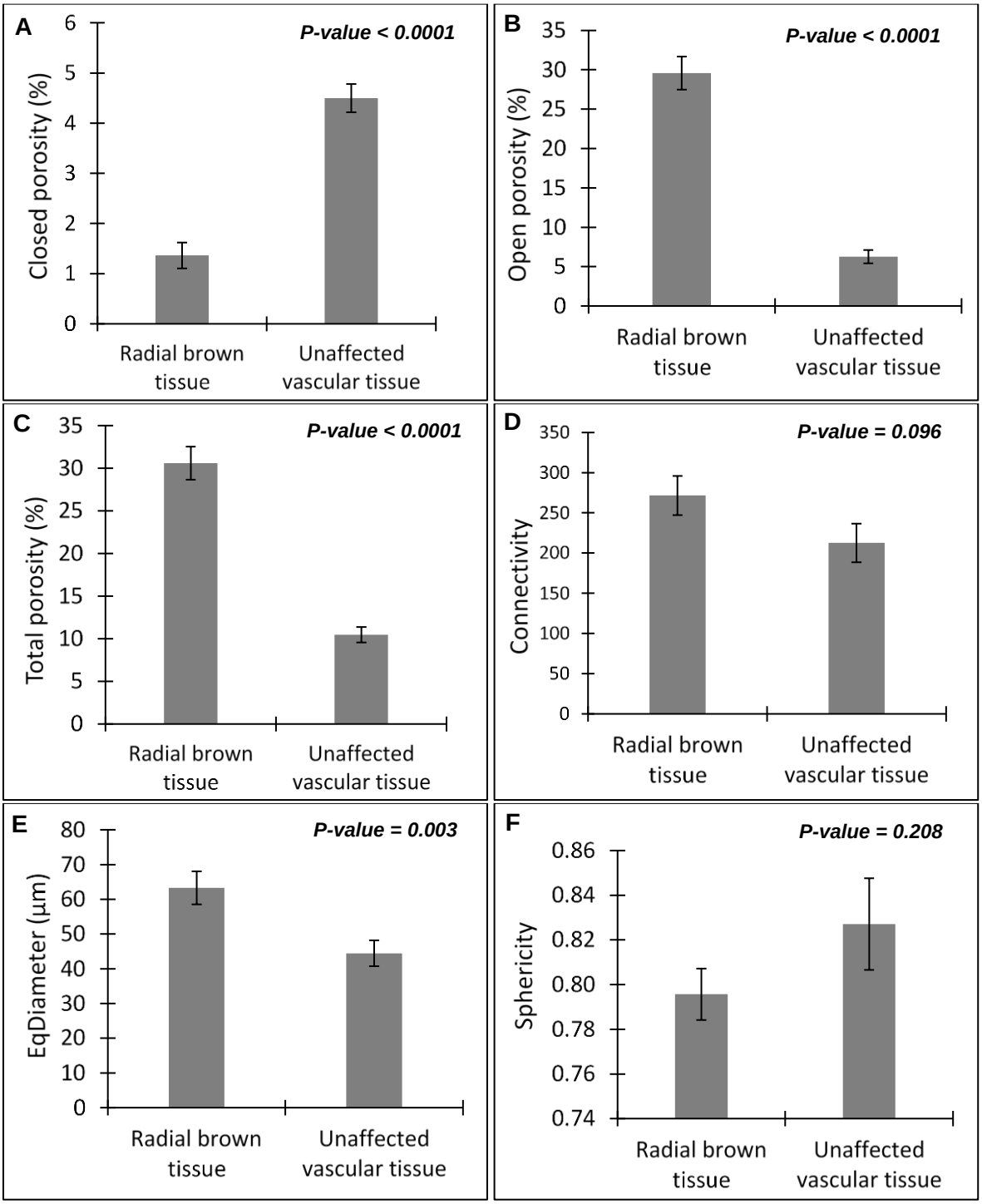


**Fig. 9.** Bar graphs and corresponding standard error bars for the following 3D pore parameters of 'Fuji' fruit tissue with radial browning and unaffected vascular tissue A) Closed porosity B) Open porosity C) Total porosity D) Connectivity E) EqDiameter and F) Sphericity. Measurements were done on 6 $mm^3$ regions of interest from radial browning affected tissue and unaffected vascular tissue images obtained after X-ray CT scanning.

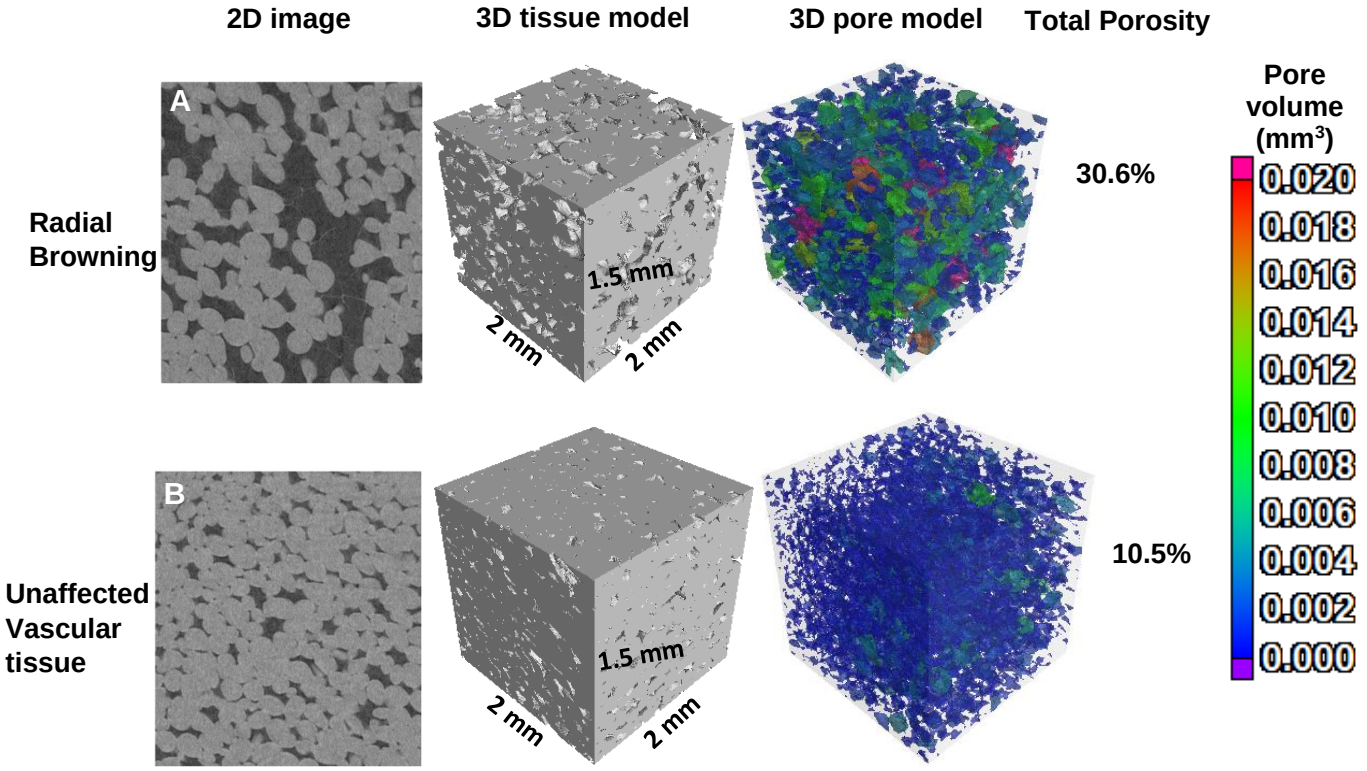


**Fig. 10.** 2D images, accompanying 3D tissue models and 3D pore models for regions of interests from A – Radial browning affected tissue, B – Unaffected vascular tissue. Pores are in dark grey and cells are in light grey. 2D images show pores in dark grey and cells in light grey. Different colours in the 3D pore models represent different individual pore volumes as defined in the scale. The total volume for the 3D models is 6 $mm^3$ (2 x 2 x 1.5 mm).

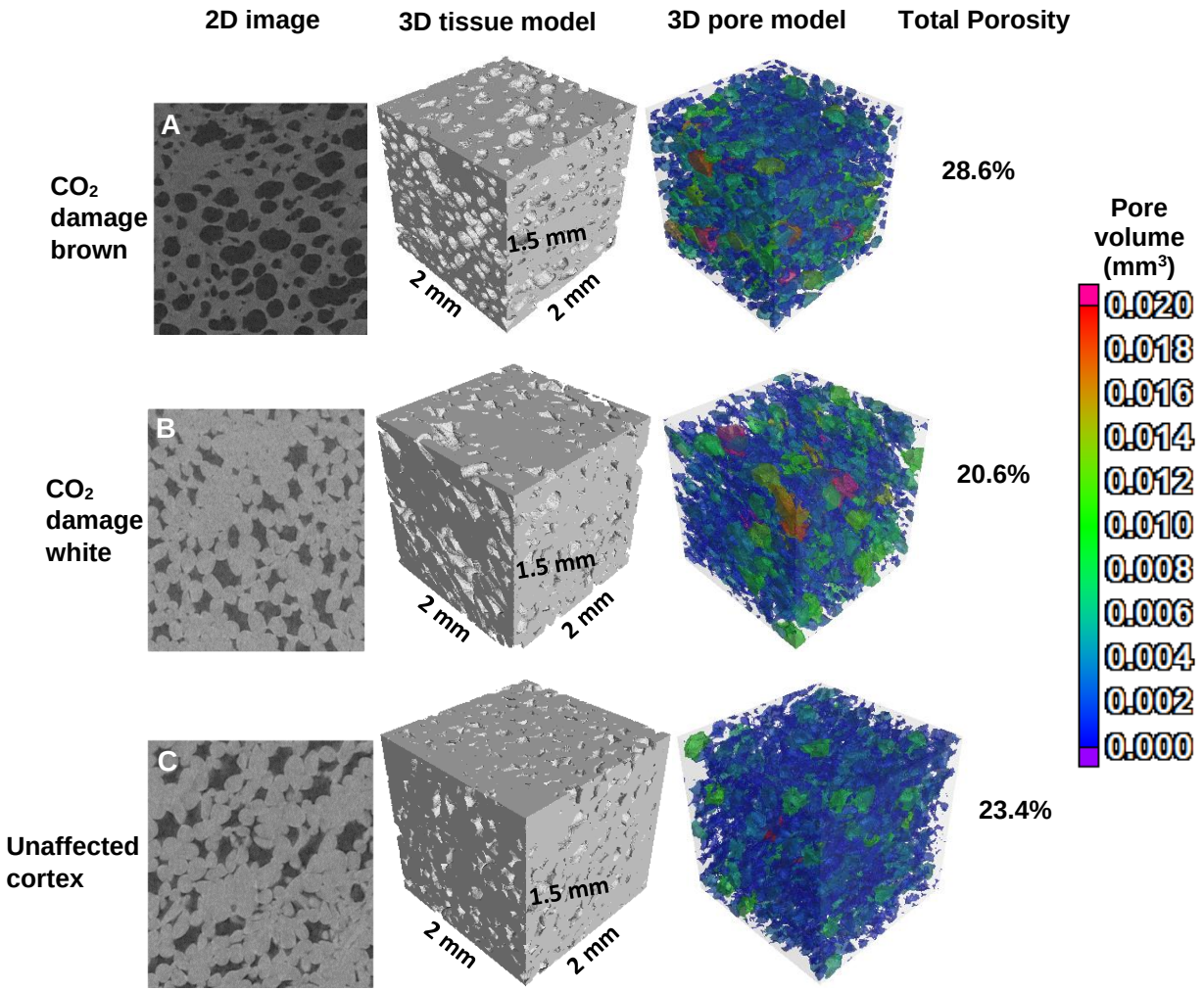


**Fig. 11.** 2D images, accompanying 3D tissue models and 3D pore models for regions of interests from A – $CO_2$ damaged brown tissue, B – $CO_2$ damaged white tissue, C – Unaffected cortex. 2D images show pores in dark grey and cells in light grey. Different colours in the 3D pore models represent different individual pore volumes as defined in the scale. The total volume for the 3D models is 6 $mm^3$ (2 x 2 x 1.5 mm).

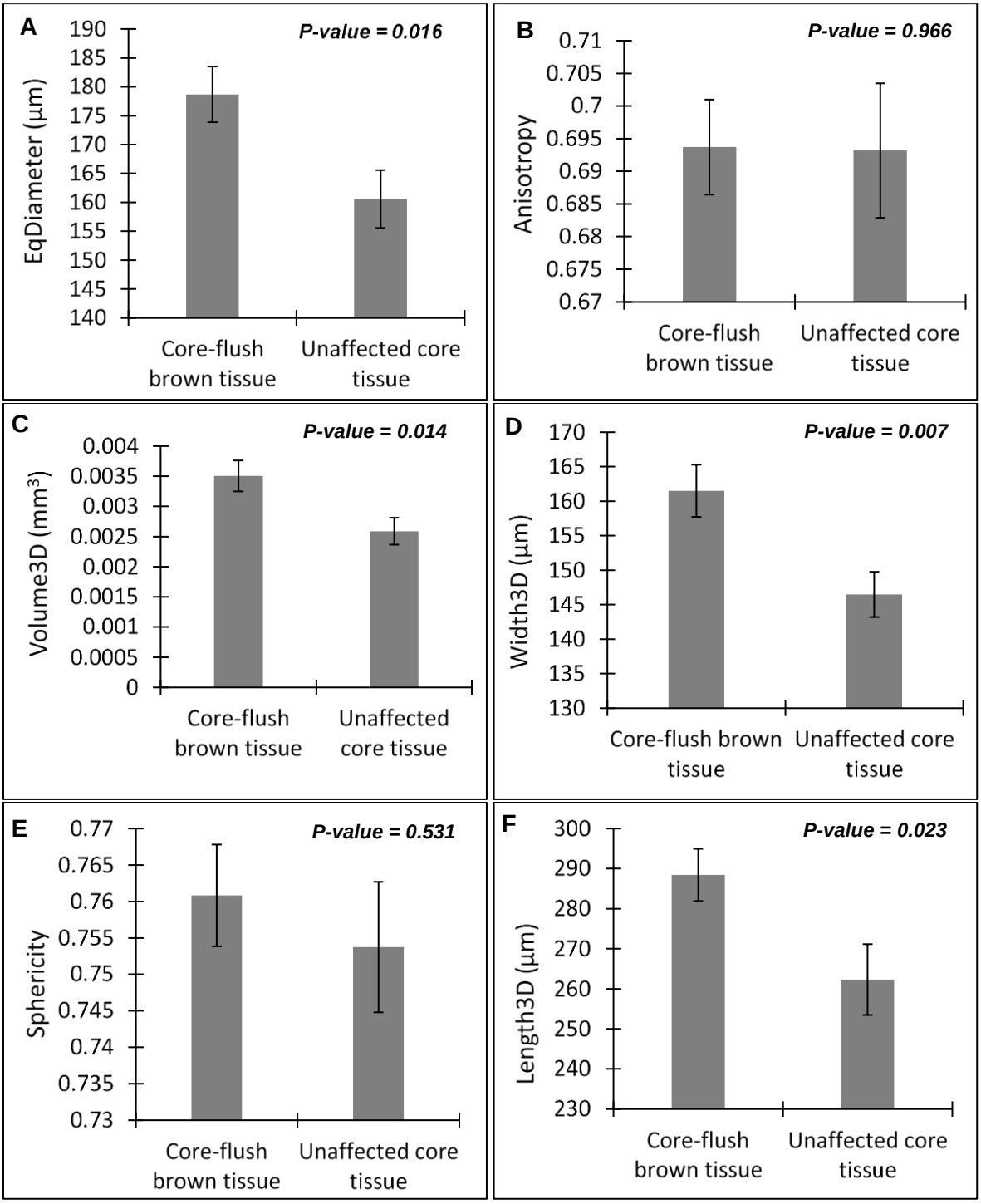


**Fig. 12.** Bar graphs and corresponding standard error bars for the following 3D cell parameters of fruit tissue with core-flush browning and unaffected core tissue A) EqDiameter B) Anisotropy C) Volume3D D) Width3D E) Sphericity and F) Length3D. Measurements were done on 6 $mm^3$ regions of interest from core-flush browning affected tissue and unaffected core tissue images obtained after X-ray CT scanning.

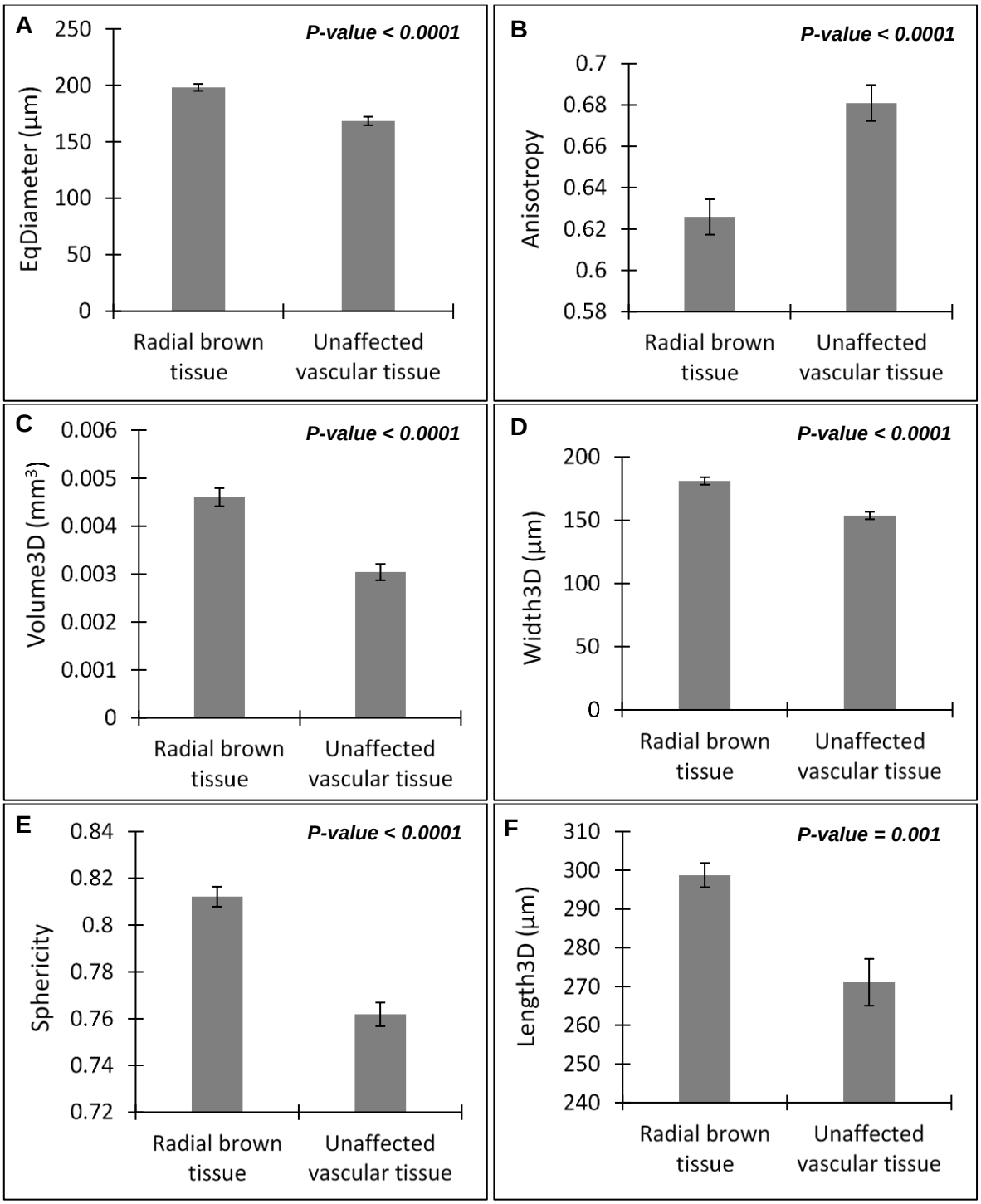


**Fig. 13.** Bar graphs and corresponding standard error bars for the following 3D cell parameters of fruit tissue with radial browning and unaffected vascular tissue A) EqDiameter B) Anisotropy C) Volume3D D) Width3D E) Sphericity and F) Length3D. Measurements were done on 6 $mm^3$ regions of interest from radial browning affected tissue and unaffected vascular tissue images obtained after X-ray CT scanning.

# GENERAL DISCUSSION AND CONCLUSIONS

Apple fruit production and export activities are of major economic importance to the South African economy. 'Fuji' apples occupy 9% of all the land under apple production in South Africa (HORTGRO, 2019). In terms of export volumes, 4.7 million 'Fuji' apple cartons were passed for export in 2019, predominantly to Far Eastern and Asian markets (HORTGRO, 2019). Therefore, Fuji is an important cultivar in South Africa, and it is important to ensure that only fruit of high quality are delivered to markets. However, 'Fuji' apples sometimes develop internal browning (IB) disorders during long-term storage, and this causes significant losses to producers and exporters (Argenta et al., 2001; Volz et al., 1998). In 2015, up to 80% of South African 'Fuji' apples exported to the Far East developed IB, this led to many claims against fruit exporters as well as significant financial losses (Crouch, 2016). The exact reasons behind the high incidence of IB in 2015 are still unclear and therefore it is important to carry out research to identify factors that can mitigate similar occurrences in future.

In South Africa, the recommended storage conditions for 'Fuji' apples are -0.5 °C, 1.5% $O_2$ and 0.5% $CO_2$ for a duration of 7 - 8 months (Findlay and Combrink, 2013). Previous research has highlighted the importance of avoiding the harvest of over-mature fruit as well as delaying the establishment of controlled atmosphere (CA) conditions to reduce browning incidence in apples (Argenta et al., 2000, 2001; de Castro et al., 2007, 2008; Kweon et al., 2012). Different browning types that have been identified in apples include radial and diffuse browning in 'Cripps' Pink' apples (James and Jobling, 2009), 'Braeburn' browning disorder in 'Braeburn' (Herremans et al., 2013), $CO_2$ induced browning in 'Cripps' Pink' (de Castro et al., 2007), $CO_2$ injury/damage in 'Fuji' (Argenta et al., 2002) and core flush in 'Fuji' (Argenta et al., 2000).

IB affects fruit microstructure and techniques that elucidate microstructural properties can help identify the reasons behind IB incidence (Herremans et al., 2013). Traditionally, techniques such as light, confocal and electron microscopy have been used to investigate fruit

microstructure (Schotsmans et al., 2004; Parker and Guerra, 2008; James and Jobling, 2009). Microstructural changes in relation to browning of 'Cripps' Pink' apples were investigated using scanning electron microscopy by James and Jobling (2009) while Parker and Guerra (2008) evaluated the occurrence of intercellular callus hairs in 'Fuji' apples using light microscopy. However, these methods have a limited penetration depth and do not provide sufficient 3-dimensional (3D) geometric information. In addition, these methods normally require destructive sample preparation, meaning that samples cannot be studied in their natural states at atmospheric conditions. X-ray computed tomography (CT) is an innovative imaging technique that provides sufficient 3D geometric information of a scanned object and requires minimal sample preparation, allowing samples to be studied in their natural states. Several studies have been done to characterize apple fruit microstructure using X-ray CT (Ting et al., 2013; Herremans et al., 2013, 2014; Chigwaya et al., 2018; Poles et al., 2020). However, exploration of 'Fuji' browning types using X-ray CT still needs to be investigated further. Numerous X-ray CT studies have provided possible explanations on why 'Fuji' is susceptible to IB during storage, Ting et al. (2013) found that Fuji apples contain a higher proportion of smaller pores compared to other cultivars and this may reduce efficient gas transport causing higher susceptibility to IB. Recently, the presence of a higher fraction of smaller pores in 'Fuji' was also highlighted by Poles et al. (2020). The current study was therefore carried out to further investigate IB disorders in 'Fuji' apples using X-ray CT.

In summary, this dissertation was an integrated study of IB in 'Fuji' apples based on five major hypotheses, namely: (i) short-term exposure of 'Fuji' apples to an elevated level of $CO_2$ has a significant effect on IB incidence and fruit tissue microstructure (Paper 1) (ii) different fruit morphological and microstructural properties influence the susceptibility of 'Fuji' apples to $CO_2$ stress-induced IB (Paper 2) (iii) watercore has a significant impact on the microstructural properties and susceptibility of 'Fuji' apples to IB during long-term storage (Paper 3) (iv) storage regime has a significant effect on the incidence of different IB types in 'Fuji' apples (Paper 4) and (v) different browning types observed after long-term storage of 'Fuji' apples

have a significant effect on microstructural properties of fruit tissue (Paper 4). The experimental studies were preceded by two comprehensive literature review chapters, the first literature review evaluated X-ray CT and its application in fruit microstructure evaluation while the second literature review looked at factors influencing the incidence of IB in apples.

In general, this study added to the existing knowledge of 'Fuji' IB and how fruit microstructure is related to IB incidence. $CO_2$ stress studies showed that high $CO_2$ has a negative impact on 'Fuji' quality resulting from IB incidence in the core region. The core region is characterized by low porosity and was preferentially affected by IB after short-term exposure to high $CO_2$/low $O_2$ levels (Paper 1 and 2) compared to the cortex region which has a higher porosity. Because the data from this study does not directly link low porosity to IB susceptibility, it can be suggested that there is a possible connection between low porosity and IB (developing after short-term exposure to high $CO_2$/low $O_2$ levels) incidence. The difficulty in conducting controlled experiments to manipulate porosity means that all work linking IB incidence to low porosity has not been able to conclusively ascertain the relationship. Other factors such as the environment during fruit growth and development may also play a role in susceptibility to IB incidence. To fully ascertain the link between low porosity and IB, it is important to find methods that can quantitatively and directly address the question. The relationship between low porosity and IB incidence in Paper 1 and 2 was not observed in Paper 4 in which fruit were stored for a longer duration. In Paper 4, some of the IB types evaluated (radial browning and $CO_2$ damage) occurred in the cortex region which has a higher porosity, a finding that is in contrast to the findings of Paper 1 and 2. This finding seems to suggest that the factors behind IB incidence after short-term exposure to high $CO_2$/low $O_2$ levels may be different from the factors and processes behind IB incidence after long-term storage at normal CA conditions (1.5% $O_2$ and 0.5% $CO_2$). This shows that IB disorders are highly complex for each apple cultivar affected and there is no guarantee that similar symptoms are caused by similar mechanisms. The complexity of the IB disorders may arise

from factors induced during fruit growth and development, fruit maturity, duration of the stress and the combined impacts of atmosphere and temperature.

$CO_2$ damage observed in commercially stored South African 'Fuji' apples is not only limited to the core region of the fruit but occurs in different regions of the fruit tissue. More research is therefore needed to determine why browning due to short-term exposure occurs in a different pattern to IB observed commercially. Fruit size was a significant factor affecting susceptibility of 'Fuji' to $CO_2$ stress-induced IB. Larger sized fruit were significantly more susceptible and therefore it is recommended to avoid the long-term storage of large over-matured fruit to reduce likeliness of IB incidence during storage. Carefully controlling pre-harvest factors such as crop load, nutrition and irrigation, which ultimately influence the final fruit size is recommended. Harvesting of over-matured fruit also increases the probability of watercore development. This current study showed that the microstructure of watercore affected fruit tissue may increase the risk of IB development during storage and so the long-term storage of fruit with watercore should be avoided. Both CA and delayed CA were effective in reducing core-flush incidence, however both these storage regimes did not significantly reduce radial browning incidence. The benefits of delaying the establishment of CA storage after harvest were not seen in this study, as the delayed CA treatment did not significantly reduce the incidence of both core-flush and radial browning when compared to CA storage.

Future work on evaluation of IB and fruit microstructure using X-ray CT should be done together with gas diffusion modelling studies. While such modelling studies have been done on other apple cultivars, they have not been fully applied to 'Fuji' apples, especially those of South African origin. This will help to further explain how the different fruit microstructural properties affect movement of respiratory gases within the fruit tissue, allowing the optimization of storage conditions for 'Fuji' apples based on microstructural and gas diffusion properties. In addition, future studies should also systematically look at variation in fruit microstructural properties due to pre-harvest factors such as thinning, irrigation, fertilisation

and age of the spurs on which fruit grows. This investment in time and resources is needed because fruit microstructure at harvest may affect subsequent quality and storability of fruit. Therefore, identifying and controlling pre-harvest factors that influence fruit microstructure will help achieve better quality fruit with less susceptibility to disorders such as IB. Microstructural properties of fruit such as tissue density and porosity are climate dependant. The variation in IB incidence between warmer and cooler seasons shows that fruit tissue density and porosity may be factors in determining IB incidence and should therefore studied further and in more detail. Porosity mapping can be used in future studies to screen fruit for porosity differences, segregate and treat them with IB-inducing storage conditions to further ascertain the relationship between porosity and IB.

With advancing technology, it will become possible to produce larger X-ray detectors as well as X-ray tubes with smaller focal spots and high current, this will allow scanning of larger fruit types at high resolutions and lower integration times, paving way for more in depth X-ray CT and fruit quality studies. Biochemical analysis can also be incorporated in future studies to further describe the expression of different IB types. The current study added to international knowledge through the novel work of mapping the porosity and determining porosity profiles of South African grown ‘Fuji’ apples. This allowed for the determination of porosity changes before and after disorder development. To our knowledge this has not been published internationally before. In addition, this study also identified browning types not previously described in ‘Fuji’ and described the conditions leading to these disorders. This study quantified properties of these different browning types in ‘Fuji’ apples using X-ray CT, an area of study that has not been explored previously. Although this study has shown that X-ray CT can evaluate and characterize fruit internal quality, more research and development still needs to be done to market X-ray CT technology as an on-line sensor of fruit internal quality. Issues such as acquisition speed, image processing speed and safety regulations still need to be evaluated. Additionally, an economic evaluation to determine the financial benefits of commercially using X-ray CT sorting devices is needed.

## References

Argenta, L., Fan, X., Mattheis, J., 2000. Delaying establishment of controlled atmosphere or $CO_2$ exposure reduces 'Fuji' apple $CO_2$ injury without excessive fruit quality loss. Postharvest Biol. Technol. 20, 221–229. https://doi.org/10.1016/S0925-5214(00)00134-4

Argenta, L., Fan, X., Mattheis, J., 2001. Development of internal browning in Fuji apples during storage, in: Washington Tree Fruit Postharvest Conference. Wenatchee, WA, pp. 1–4. http://ucce.ucdavis.edu/files/datastore/234-56.pdf.

Argenta, L.C., Fan, X., Mattheis, J.P., 2002. Responses of 'Fuji' apples to short and long duration exposure to elevated $CO_2$ concentration. Postharvest Biol. Technol. 24, 13–24. https://doi.org/10.1016/S0925-5214(01)00120-X.

Chigwaya, K., Schoeman, L., Fourie, W.J., Crouch, I., Viljoen, D. and Crouch, E.M., 2018. 'Fuji' apple internal browning explored via X-ray computed tomography (CT). Acta Hortic. 1201, 309-316. https://doi.org/10.17660/ActaHortic.2018.1201.42.

Crouch, I., 2016. Mitigating the Risk of Internal Browning in Fuji. HORTGRO Science fresh notes. Accessed 9 July 2020. https://pdfs.semanticscholar.org/9431/ae2f5b39f8056c737444a8e80ae72d996c2f.pdf.

de Castro, E., Barrett, D.M., Jobling, J., Mitcham, E.J., 2008. Biochemical factors associated with a $CO_2$-induced flesh browning disorder of Pink Lady apples. Postharvest Biol. Technol. 48, 182–191. https://doi.org/10.1016/j.postharvbio.2007.09.027.

de Castro, E., Biasi, B., Mitcham, E., Tustin, S., Tanner, D., Jobling, J., 2007. Carbon dioxide-induced flesh browning in Pink Lady apples. Am. Soc. Hortic. 132, 713–719. https://doi.org/10.21273/JASHS.132.5.713.

Findlay, J.S., Combrink, J.C., 2013. South African controlled atmosphere storage operator's manual. SA Apple and Pear Producers' Association. Paarl, South Africa.

Herremans, E., Verboven, P., Bongaers, E., Estrade, P., Verlinden, B.E., Wevers, M., Hertog, M.L.A.T.M., Nicolaï, B.M., 2013. Characterisation of 'Braeburn' browning disorder by

means of X-ray micro-CT. Postharvest Biol. Technol. 75, 114–124. https://doi.org/10.1016/j.postharvbio.2012.08.008.

Herremans, E., Melado-Herreros, A., Defraeye, T., Verlinden, B., Hertog, M., Verboven, P., Val, J., Fernández-Valle, M.E., Bongaers, E., Estrade, P., Wevers, M., Barreiro, P., Nicolaï, B.M., 2014. Comparison of X-ray CT and MRI of watercore disorder of different apple cultivars. Postharvest Biol. Technol. 87, 42–50. https://doi.org/10.1016/j.postharvbio.2013.08.008.

HORTGRO, 2019. Key Deciduous Fruit Statistics. Accessed 8 September 2020. https://www.hortgro.co.za/wp-content/uploads/docs/2020/07/key-deciduous-fruit-statistics-2019-1.pdf

James, H.J., Jobling, J.J., 2009. Contrasting the structure and morphology of the radial and diffuse flesh browning disorders and $CO_2$ injury of 'Cripps Pink' apples. Postharvest Biol. Technol. 53, 36–42. https://doi.org/10.1016/j.postharvbio.2009.02.001.

Kweon, H.J., Kim, M.J., Moon, Y.S., Lee, J., Choi, C., Choi, D.G., Lee, D.H., Kang, I.K., 2012. Relationship between Preharvest Factors and the Incidence of Storage Disorders in 'Fuji' Apples during CA Storage. Korean J. Hortic. Sci. Technol. 30, 50–55.

Parker, M.L., Guerra, W., 2008. Occurrence and implications for postharvest quality of intercellular callus hair growth in the outer cortex of apples of 'Fuji' and 'Fuji' sports. Postharvest Biol. Technol. 48, 192–198. https://doi.org/10.1016/j.postharvbio.2007.10.007.

Poles, L., Gentile, A., Giuffrida, A., Valentini, L., Endrizzi, I., Aprea, E., Gasperi, F., Distefano, G., Artioli, G., La Malfa, S., Costa, F., Lovatti, L., Di Guardo, M., 2020. Role of fruit flesh cell morphology and MdPG1 allelotype in influencing juiciness and texture properties in apple. Postharvest Biol. Technol. 164, 111161. https://doi.org/10.1016/j.postharvbio.2020.111161.

Schotsmans, W., Verlinden, B.E., Lammertyn, J., Nicolaï, B.M., 2004. The relationship between gas transport properties and the histology of apple. J. Sci. Food Agric. 84, 1131–1140. https://doi.org/10.1002/jsfa.1768.

Ting, V.J.L., Silcock, P., Bremer, P.J., Biasioli, F., 2013. X-ray micro-computer tomographic method to visualize the microstructure of different apple cultivars. J. Food Sci. 78, E1735–E1742. https://doi.org/10.1111/1750-3841.12290.

Volz, R.K., Biasi, W. V., Grant, J.A., Mitcham, E.J., 1998. Prediction of controlled atmosphere-induced flesh browning in 'Fuji' apple. Postharvest Biol. Technol. 13, 97–107. https://doi.org/10.1016/S0925-5214(97)00080-X.